Cultural Heritage Science

David Scott
Roland Schwab

Metallography in Archaeology and Art

Springer

Cultural Heritage Science

The preservation and interpretation of our cultural heritage is one of the major challenges of today's society. Cultural Heritage Science is a highly interdisciplinary book series covering all aspects of conservation, analysis and interpretation of artworks, objects and materials from our collective cultural heritage. The series focuses on science and conservation in three main fields

- Art technology
- Active conservation and restoration
- Preventive conservation and risk management

The series addresses conservators and conservation scientists at museums, institutes, universities and heritage organizations. It also provides valuable information for curators and decision makers at museums and heritage organizations. Cultural Heritage Science comprises two subseries, one focusing on advanced methods and technology for conservation experts, the second presenting the latest developments in conservation science. All titles in the book series will be peer reviewed. Titles will be published as printed books and as eBooks, opening up the opportunity to include electronic supplementary material (videos, high-resolution figures, special data formats, and access to databases).

More information about this series at http://www.springer.com/series/13104

David A. Scott • Roland Schwab

Metallography in Archaeology and Art

Springer

David A. Scott
Department of Art History
University of California
Los Angeles, CA, USA

Roland Schwab
Curt Engelhorn Centre for Archaeometry
Mannheim, Germany

ISSN 2366-6226 ISSN 2366-6234 (electronic)
Cultural Heritage Science
ISBN 978-3-030-11264-6 ISBN 978-3-030-11265-3 (eBook)
https://doi.org/10.1007/978-3-030-11265-3

Cover illustration: Bronze Age bronze belt plate from Svenstrup, Denmark with precipitation of an intermetallic phase within a matrix of annealed and reworked α_{Cu} solid solution.

This Springer imprint is published by the registered company Springer Nature Switzerland AG.
The registered company address is: Gewerbestrasse 11, 6330 Cham, Switzerland

Acknowledgments

The authors would like to thank Jackie Burns, Registrar's Department, The Getty Center, Brentwood, for processing copyright requests for image reproduction from the collections of the J. Paul Getty Museum; Dr. Marion True, formerly Curator of Antiquities, Department of Antiquities Conservation, J. Paul Getty Museum, Malibu; the late Dr. Frank Preusser, formerly Head, Scientific Department, The Getty Conservation Institute, Marina del Rey; Dr. Pieter Meyers, formerly Head, Conservation Department, Los Angeles County Museum of Art; Professor Emeritus Gerhard Eggert, Academy of Fine Arts, Stuttgart; the late Dr. Nigel J. Seeley, formerly Senior Lecturer, Department of Conservation and Materials Science, Institute of Archaeology, University College London; Dr. Brian Gilmore, formerly of the Royal Armouries and now independent researcher; and the late Thelma Lowe of Berkeley, California. We are grateful to Dr. Laurie Palasse and Markus Ehmer from Bruker Nano GmbH in Berlin who offered the possibility to perform electron backscatter diffraction (EBSD) measurements.

We thankfully acknowledge the permissions of various institutions all over the world for sampling and analyzing their material.

Thanks are due to the following publishers or organizations for permission to reproduce a number of images in the text and to the J. Paul Getty Trust for permission to reproduce several images mentioned in the text from previous work of one of the authors (Scott 1991). Special thanks are due to Macmillan Company Inc., 175 5th Avenue, New York, 10010, for permission to reproduce several images from *Metallic Materials in Engineering*, by Carl H. Samans (1963); to Prentice Hall, Inc., Upper Saddle River, New Jersey, 07458, for permission to reproduce some images from *The Science of Engineering Materials* (1969) by Charles O. Smith; and to the MIT Press, Cambridge, Massachusetts, for one graph from the compendium of papers by Cyril Stanley Smith, *A Search for Structure* (1981). Finally, we owe a debt to Springer for suggesting the book as a volume in "Cultural Heritage Science" series.

All drawings are by the authors unless otherwise captioned. All photomicrographs are by the authors unless otherwise noted in the text.

Technical Information

All objects presented in this book have been examined over the years with varying instruments at different facilities, where the authors were employed.

All percentages are weight percent unless otherwise specified as atomic percent. All temperatures are in degrees centigrade unless degrees absolute, or degrees Fahrenheit, are specified in the chart concerned. Etchants used for the samples are derived from the Appendix given at the end of the text. X-ray fluorescence analyses were carried out with a Kevex 0750A, a Thermo Scientific ARL QUANT'X, and Fischerscope XAN 150 energy-dispersive X-ray fluorescence spectrometers. Electron microprobe analyses were carried out at the Getty Conservation Institute using a Jeol Superprobe and a Cameca Electron Microprobe operated by Dr. Eric Doehne; a Jeol Superprobe at the Department of Geology, UCLA, operated by Dr. Frank Kyte; and a Jeol JXA 8900 RL at the Institute of Physical Metallurgy at the University of Freiberg, operated by Dr. Dietrich Heger. The chemical compositions of precious metals have been analyzed with laser ablation inductively coupled plasma mass spectrometry (LA-ICP-MS) using a Resonetics solid-state laser (ArF, 193 nm) and a Thermo Scientific XS II quadrupole mass analyzer (QICP-MS) at the Curt-Engelhorn-Zentrum Archäometrie (CEZA) by various persons. Scanning electron microscope images and microanalyses have been performed in an EVO 60 MA 25 scanning electron microscope with a Bruker QUANTAX EDS system with SD-detector at CEZA. Dr. Laurie Palasse carried out EBSD measurements with Bruker's ARGUS™ forescattered/backscattered electron imaging system in a Zeiss Gemini field emission scanning electron microscope at Bruker's application center in Berlin. Dr. Volker Klemm has recorded selected area electron diffraction (ED) pattern of an ion-thinned specimen in a Philips CM30 transmission electron microscope with the DITABIS image plate system at the Institute of Physical Metallurgy at the University of Freiberg.

Photomicrographs were taken by David A. Scott with a Nikon D300 camera on a Nikon Epiphot inverted metallurgical microscope or with a Canon EOS-80D DSLR camera with adaptor to enable capture on the Nikon Epiphot. Roland Schwab uses a Zeiss Axioskop 40 A Pol with digital imaging system Zeiss AxioVision, and some images have been taken with a Zeiss Neophot 32 inverted metallurgical microscope at the Institute of Physical Metallurgy at the University of Freiberg.

Microhardness measurements were obtained by Martens (HM) and Vickers (HV) hardness testing, using different test forces.

The emphasis of this book is on metallography; it is not meant to be a comprehensive account of the ancient metallurgy of the world, as this task is obviously beyond the authors' capacity, but it is supposed to provide a broad sweep across this issue, without being able to paint in too many of the fine details.

Department of Art History David A. Scott
University of California
Los Angeles, CA, USA
Curt Engelhorn Centre for Archaeometry Roland Schwab
Mannheim, Germany

Contents

List of Figures

Chapter 1
Introduction to Metallography

Metallography is essentially the science of the internal structure of metallic materials, broadly understood to include the examination and identification of grains, phases or interfaces and crystal orientations of a metal, as well as its non-metallic inclusions and voids, corrosion crusts and patinas. The technique traditionally relies on the sampling of an object to remove a representative sample, which is then mounted, ground, polished and etched for examination of the microstructure under the optical microscope. This principle procedural method is still valid, but there has been a drastic change over the decades from exclusively optically microscopical examination of microstructure to methods based on electron and ion beams or X-rays. In recent years, we have seen the emergence of new powerful techniques such as electron backscatter diffraction (EBSD), which are capable of identifying and characterizing quantitatively all microstructural components by automated high-speed pattern acquisition (see Chap. 3). Hence, metallography is not confined merely to microscopical examination but also comprises methods to reveal structure and mechanical properties of metals and alloys.

The increased resolution and importance of bulk structure accompanies a new concept of classification of structure into macro-, micro- and nanostructure, depending on the size ranges of structures and according to the measurement methods. The scale of macrostructure can be fairly large ranging from millimetres to the infinite, while microstructure is relevant for micro-devices having sizes typically of 1–1000 micrometres, while nanostructures have dimensions of about 1–100 nanometres [15]. Nanoscale magnification and three-dimensional microscopy have become common tools in modern metallography, and it is symptomatic that the chapter about "Microstructure" of the last edition of *Physical Metallurgy* that first published in 1965 does not refer to classical two-dimensional examination of surfaces anymore but to three-dimensional characterization by X-ray tomography or serial sectioning techniques and subsequent computer-simulated modelling of microstructure to replicate the microstructural features [53].

Nevertheless, "classical" metallography and the morphology of metals have been an important aspect of our understanding of metallic phases, bonding and the

D. A. Scott, R. Schwab, *Metallography in Archaeology and Art*, Cultural Heritage Science, https://doi.org/10.1007/978-3-030-11265-3_1

techniques that are used to manipulate properties and attributes such as hardness and colour. Many of these choices are culturally determined: they represent decisions made about the nature of materials and how they are to be used. Three of the metallic materials of antiquity have given their names to phases of societal development which we recognize as the Chalcolithic, the Bronze Age and the Iron Age, a lens through which we can view the past and discern the sometimes illusory nature of the concept of continual progress, of the aggregation of technological development as one generation builds upon the achievements of the former [5, 6], and the different paths which the development of metallurgy took in Africa and the New World; see, for example, Kusimba and Killick [27], Lechtman [28] and Scott [49].

The study of metals by means of simple optical devices dates back to the seventeenth century [50], but the science of metallography really began with the work of Henry Clifton Sorby (1826–1909), who made seminal advances in the field of the petrological examination of rocks and minerals and developed an incident-light microscope. Following that, Sorby realized that reflected light microscopy could be of essential application to the study of the microstructure of metals, particularly iron and steel [50]. The development and concepts of early metallography have been well-described by Cyril Stanley Smith in his book *A History of Metallography* (1960), which the reader interested in further historical information is referred to.

As applied to archaeological studies, metallography came into use in the first few decades of the twentieth century and has been of great importance to archaeologists, corrosion scientists, conservators, metallurgists and engineers ever since. The scientific examination of ancient metals had already started in the late eighteenth century with the determination of their chemical compositions (see Caley [3]) and was systematically extended during the 1930s, when instrumental analytical techniques such as optical emission spectroscopy became available [36]. Indeed metallography of ancient metals can be used to check on the results of analytical determinations, which may be affected by non-metallic inclusions, heterogeneity of the alloy or internal or external corrosion. The only way to gauge these effects on the analysis is by metallographic examination. Metallographic studies are an integral part of a comprehensive investigation of the elemental composition, isotopic data, surface binocular examination, X-ray macrostructure analysis and microstructure of the artefacts in question.

Pioneering works revealing the microstructure of metals had already been published by the early 1900s, and, in a few papers, the microstructures of ferrous and nonferrous objects from all over the world have been published and illustrated, albeit with quite (in)different quality (e.g. [1, 20, 24–26, 30, 45, 46]).

The principal difficulty in creating better research tools for metallography was the limitations on the kind of microscopy available and the quality of the illumination and photography in the early 1900s (see Sect. 3.3.1).

Comparatively few studies were published between the First and Second World Wars (e.g. [2, 4, 32, 33]), a dearth of young researchers meant that meagre advances occurred in conservation science or the metallurgy of ancient metals during this period. We recommend Édouard Salin's and Albert France-Lanord's [48] book *Le fer à l'époque mérovingienne*, which not only illustrates early medieval iron

technology utilizing photographs, drawings, micrographs and radiographs but also documents the metallographical and analytical equipment of that time. This book also includes a discussion of the methodologies for the conservation and restoration of archaeological iron objects.

During the late 1950s and early 1960s, the situation began to improve and has continued to go from strength to strength since that period. For archaeological metals, some of the authors in English who began to have an impact were Herbert H. Coghlan [7–14]), Ronald F. Tylecote [58–60] and Cyril Stanley Smith [50–52]. CS Smith was an exceptionally creative metallurgist who developed theoretical models and methods for deriving the three-dimensional shapes of the crystalline structures of metals from the two-dimensional microscope images, but he is also one of the pre-eminent metallurgists of ancient metals, whose research forms a body of work brought together in the seminal volume published in 1981, which deserves to be better known.

Important writers in the metallographic field of ancient metals emerged in many countries from the 1950 to 1960 period onwards, with seminal contributions by Jerzy Piaskowski [37–39] in Poland, Carlo Panseri and Massimo Leoni [34, 35] in Italy, Albert France-Lanord [21–23] and Eduard Salin [47] in France, Robert Thomsen [56, 57] in Denmark and Erik Tholander [54, 55] in Sweden, Joachim Emmerling [16–19] in Germany and of course Radomìr Pleiner [40–44]) in the former Czechoslovakia, who published several volumes concerning ancient iron technology.

Advances in optical techniques and the application of the scanning electron microscope (SEM) and electron probe microanalyser (EPMA) have continued to make metallography more accessible to a wider array of researchers across the globe and now form part of many investigations of ancient metals (Chap. 3). Metallography continues to be an important method for the understanding of how metals were smelted, cast, worked, plated, alloyed or corroded. Metal objects may be plated or coated with other metals, which limits the extent to which non-destructive analysis can be used to provide a definitive answer to the question of their identity. Precious metal alloys such as gold-silver, silver-copper and gold-copper alloys are often finished by surface enrichment or depletion gilding or some other form of surface treatment or coating (Chap. 6). In such cases, metallography has to be used to gain further information and can determine, in conjunction with analyses of the polished cross-section, the nature of the surface coating. The primary distinction to be made in a great number of initial studies is whether the metal or alloy has been cast to shape, or whether it has been worked and annealed to shape, and the extent of corrosion has important implications for authenticity studies of ancient metals.

Metallography can help to inform us about the past use of metallic materials as well as aspects of their extraction, the use of sulphide or oxide ores in the smelting of copper, and to answer quite sophisticated questions concerning the fabrication of ancient iron, steel and cast irons. As the methodology is also applied to waste products, furnace linings, technical ceramics and metallurgical slag, the latter often

includes tiny prills of metallic materials along with the silicate minerals that constitute the slag.

Numerous problems relating to the authentic nature of ancient metallic artefacts, particularly silver and copper alloys, as well as iron and steel artefacts, can be addressed by metallography. In cases of authenticity questions, it is often possible to adduce enough information from the metallographic section to avoid the need for further studies, particularly in the case of ancient bronzes, where the extent of patina penetration and the type of patina may be crucial and sufficient evidence may exist to condemn the artefact as a modern reproduction. Some of these achievements are illustrated through the metals and alloy discussed in this book, which we hope will be a reliable guide for the understanding of microstructures of ancient metals, as well as an introduction to principal practices of metallography.

There are numerous standard textbooks available in many languages concerning metallography in the wider context; to the English reader, we refer to further work detailed in Chap. 3, and these textbooks should be consulted for further reading. Many of them have become obsolete because of substantial changes in materials, preparation methodology and especially digital imaging but still give valuable information about materials and practices used for previous metallographic investigations. In modern metallography large samples may be ample and often easily replaced, but samples of ancient metals are of important historical value, are often unique and should be stored safely.

Some textbooks deal exclusively with preparation procedures or selected applications, while others are concerned with etching principles, or they introduce basic concepts and practical application of quantitative methods for characterizing the microstructure. Some textbooks, such as the *ASM Handbooks* (Lyman [29]; Mills [31; Vander Voort [61]), offer theoretical metallographic background information and individual practical application, both of which are essential for the examination and interpretation of metallographic structures.

Nevertheless, there are major differences between the constitutions and the examination of modern metals and ancient artefacts, which will be discussed in this book in greater detail so that the reader can form an appreciation of the excitement and curiosity that ancient metals can arouse as well as inform us of some of the achievements of cultures long since dead.

References

1. Bell, H.: Notes on a bloom of roman iron found at corstopitum (Corbridge). J. Iron Steel Inst. **85**, 118–128 (1912)
2. Calbiani, G.: Esame di ferri Romani ricuperati dalle navi del Lago di Nemi. La Metallurgia Italiana. **31**(6), 359–370 (1939)
3. Caley, E.R.: Analysis of Ancient Metals. International Series of Monographs on Analytical Chemistry 19. Pergamon, Oxford/London/Edinburgh/New York/Paris/Frankfurt (1964)
4. Carpenter, H.C.H., Robertson, J.M.: The metallography of some ancient Egyptian implements. J. Iron Steel Inst. **121**, 417–454 (1930)
5. Childe, V.G.: The Bronze Age. Cambridge University Press, Cambridge (1930)

6. Childe, V.G.: The Dawn of European Civilization. Kegan Paul, London (2003)
7. Coghlan, H.H.: Notes on Prehistoric and Early Iron in the Old World. Occasional papers on technology 8. Pitt Rivers Museum, Oxford (1956)
8. Coghlan, H.H.: Metallurgical examination of eleven palstaves. Bull. Hist. Metall. Group. **1**, 7–21 (1967)
9. Coghlan, H.H.: Metallurgical examination of a bronze sword found in the Thames at Battersea. Bull. Hist. Metall. Group. **5**, 71–73 (1971)
10. Coghlan, H.H.: Copper artefacts from Tutankhamen's tomb. J. Hist. Metall. Soc. **9**, 64–67 (1975a)
11. Coghlan, H.H.: Notes on the Prehistoric Metallurgy of Copper and Bronze in the Old World. Pitt Rivers Occasional Papers on Technology 4. Pitt Rivers Museum, Oxford (1975b)
12. Coghlan, H.H.: Medieval iron artifacts from the Newbury area of Berkshire: metallurgical examination. J. Hist. Metall. Soc. **12**, p12–p19 (1978)
13. Coghlan, H.H.: Analysis of bronze age artifacts from Irish museums. J. Hist. Metall. Soc. **13**, 98–106 (1979)
14. Coghlan, H.H.: Examination of some continental Bronze Age decorative objects. J. Hist. Metall. Soc. **14**, 80–93 (1980)
15. Czichos, H., Saito, T., Smith, L. (eds.): Springer Handbook of Materials Measurement Methods. Springer, Berlin/Heidelberg (2006)
16. Emmerling, J.: Technologische Untersuchungen an dem Schwert von Hornweiler. Forschungungen und Berichte der Staatlichen Museen zu Berlin. 8, pp. 120–123 (1967a)
17. Emmerling, J.: Die metallographische Untersuchung der Schwertklingen aus Münsingen. Jahrbuch des Bernischen Historischen Museums in Bern. **47/48**, 147–190 (1967b/1968)
18. Emmerling, J.: Technologische Untersuchungen an eisernen Bodenfunden. Alt-Thüringen. **12**, 267–319 (1972)
19. Emmerling, J.: Zur Technologie zweier Schwerter und einer Lanzenspitze aus Wolkow. Alt -Thüringen. **16**, 120–126 (1979)
20. Foote, H.W., Buell, W.H.: Composition, structure, and hardness of some Peruvian bronze axes. Am. J. Sci. **34**, 128–132 (1912)
21. France-Lanord, A.: La fabrication des épées damassées aux époques mérovingienne et carolingienne. Pays gaumais. **10**(1–3), 19–45 (1949)
22. France-Lanord, A.: Reconstruction des techniques: le métal. In: Laming, A. (ed.) La Découverte du passé: progrès récents et techniques nouvelles en préhistoire et en archéologie, pp. 281–297. Picard, Paris (1952)
23. France-Lanord, A.: La fabrication des épées de fer gauloises. Revue d'histoire de la sidérurgie. **5**(4), 315–327 (1964)
24. Garland, H.: Metallographical researches on Egyptian metal antiquities. J. Inst. Met. **10**, 329–343 (1912)
25. Hadfield, R.: Sinhalese iron and steel of ancient origin. J. Iron Steel Inst. **85**, 134–186 (1912)
26. Hanemann, H.: Metallographische Untersuchung einiger altkeltischer und antiker Eisenfunde. Internationale Zeitschrift für Metallographie. **4**, 248–256 (1913)
27. Kusimba, C.M., Killick, D.: Ironworking on the Swahili coast of Kenya. In: Kusimba, C.M., Kusimba, S.B. (eds.) East African Archaeology: Foragers, Potters, Smiths and Traders, pp. 100–123. University of Pennsylvania Press, Pennsylvania (2011)
28. Lechtman, H.N.: Andean value systems and the development of prehistoric metallurgy. Technol. Cult. **25**, 1–36 (1984)
29. Lyman, T. (ed.): ASM Handbook 8th edition Volume 8: Metallography, Structures and Phase Diagrams. Metals Park, American Society for Metals (1973)
30. Mathewson, C.H.: A metallographic description of some ancient Peruvian bronzes from Machu Picchu. Am. J. Sci. **190**(240), 525–616 (1915)
31. Mills, K. (ed.): ASM Handbook 9th edition Volume 9: Metallography and Microstructure. Materials Park, American Society for Metals (1985)
32. Neumann, B.: Römisches Eisen. Z. Elektrochem. Angew. Phys. Chem. **29**, 175–179 (1923)
33. Neumann, B.: Römischer Damaststahl. Archiv für das Eisenhüttenwesen. **1**, 241–244 (1927/28)

34. Panseri, C., Leoni, M.: Esame metallographico di alcune lame di spade galliche del II secolo a.C. La metallurgia italiana. **51**(1), 5–12 (1959)
35. Panseri, C., Leoni, M.: Advanced methods for the metallurgical examination of archaeological metal objects. In: Thomson, G. (ed.) Recent Advances in Conservation, pp. 101–103. Butterworths, London (1963)
36. Pernicka, E.: Trace element fingerprinting of ancient copper: a guide to technology or provenance? In: Young, S.M.M., Pollard, A.M., Budd, P., Ixer, R.A. (eds.) Metals in Antiquity. British Archaeological Reports international series 792, pp. 163–171. Archaeopress, Oxford (1999)
37. Piaskowski, J.: An interesting Example of Early Technology: A Socketed Axe from Wietrzno-Bóbraka in the Carpathians. J. Iron Steel Inst. **194**, 336–340 (1960)
38. Piaskowski, J.: Metallographic Investigations of Ancient Iron Objects from the Territory between the Oder and the Basin of the Vistula River. J. Iron Steel Inst. **198**, 263–282 (1961)
39. Piaskowski, J.: The manufacture of medival damscened knives. J. Iron Steel Inst. **202**, 561–568 (1964)
40. Pleiner, R.: Staré evropské kovárství. Nakl. Československé akademie věd, Prague (1962)
41. Pleiner, R. (ed.): Archaeometallurgy of Iron. Archaeological Institute ČSAV, Prague (1989)
42. Pleiner, R.: The Celtic Sword. Clarendon, Oxford (1993)
43. Pleiner, R.: Iron in Archaeology. The European Bloomery Smelters. Archeologicky Ústav Avcr, Prague (2000)
44. Pleiner, R.: Iron in Archaeology. Early European Blacksmiths. Archeologicky Ústav Avcr, Prague (2006)
45. Rupe, H.: Notitz über die chemische Untersuchung prähistorischer Gräberfunde von Castraneda. Verhandlungen der Naturforschenden Gesellschaft in Basel. **18**(1), 1–13 (1905)
46. Rupe, H., Müller, F.: Chemische und metallographische Untersuchungen prähistorischer Eisenfunde. Verhandlungen der Naturforschenden Gesellschaft in Basel. 27, pp. 108–148 (1916)
47. Salin, É.: Sur les techniques de la métallurgie du fer de la préhistoire au temps des grandes invasions. Revue de Métallurgie. **49**(3), 165–176 (1952)
48. Salin, É., France-Lanord, A.: Le fer à l'époque mérovingienne. Geuthner, Paris (1943)
49. Scott, D.A.: Gold and Platinum Metallurgy of Ancient Colombia and Ecuador. CSP Press, Los Angeles (2012)
50. Smith, C.S.: A History of Metallography. University of Chicago Press, Chicago (1960)
51. Smith, C.S.: The Interpretation of Microstructures of Metallic Artefacts, Application of Science in the Examination of Works of Art, pp. 20–52. Laboratory of Museum of Fine Arts, Boston (1965)
52. Smith, C.S.: A Search for Structure: Selected Essays on Science, Art and History. MIT, Cambridge, MA (1981)
53. Spanos, G., Reynolds, W.T.: Microstructure of metals and alloys. In: Laughlin, D.E., Hono, K. (eds.) Physical Metallurgy II, 5th edn, pp. 1073–1112. Elsevier, Amsterdam (2015)
54. Tholander, E.: Evidence of the use of carburized steel and quench hardening in late Bronze Age Cyprus. Opuscula Atheniensia. **10**(3), 15–22 (1971)
55. Tholander, E.: Comments on medieval Swedish Osmond iron. J. Hist. Metall. Soc. **9**, 68–70 (1975)
56. Thomsen, R.: Metallographic studies of an axe from the Migration Age. J. Iron Steel Inst. **204**, 905–909 (1966)
57. Thomsen, R.: Et meget maerkeligt metl: En beretning fra jernets barndom. Varde, Denmark (1975)
58. Tylecote, R.F.: Metallurgy in Archaeology. Edward Arnold LTD, London (1962)
59. Tylecote, R.F.: A history of metallurgy. The Metals Society, Lety, London (1976)
60. Tylecote, R.F.: The Early History of Metallurgy in Europe. Longman, London/New York (1987)
61. Vander Voort, G.F. (ed.): ASM Handbook Volume 9: Metallography and Microstructure. Materials Park, American Society for Metals (2004)

Chapter 2
The Historical Development of Metallurgy

The utilization of metals and the development of metallurgy has been an important societal progress for mankind: the introduction of metallurgy was fundamental to the evolution of complex and almost hierarchical society systems. The evaluation of the real impact of metallurgy on ancient societies has been quite an intellectual challenge to archaeologists and historians without substantial data of metallurgical processes and innovations, properties of metals and alloys, information about mines and the distribution of raw material.

Forbes [11], a historian of technology, has introduced his book *Metallurgy in Antiquity* with the sentence "…facts which can be gathered from archaeological, historical, philological and technical documents and books are not sufficient to form a continuous story". Nonetheless, he wrote the book "with fancy as the woof of the story".

Indeed the research into ancient metallurgy is not a new discipline, but systematic interdisciplinary investigations during the last half-century generated a wide range of perspectives on that field called archaeometallurgy (see Craddock [8]; Roberts and Thornton [37]; Timberlake [46]). Archaeometallurgical research is not only based on the chemical, structural and technological characterization of metals themselves but includes the investigation of all pyrotechnical debris such as slag and technical ceramics: crucibles, moulds or furnace linings to reconstruct ancient metallurgical processes (see, e.g. Craddock [6]; Roberts and Thornton [37]). The characterization of ore deposits and their minerals is also an important task to correlate artefacts with their provenance and to reveal trade and social relations of the past. Mining archaeology has achieved sustained success in rediscovering and dating ancient mines, in the reconstruction of the mining technology, the quantitative output and the interaction with the surroundings (e.g. Domergue [10]; O'Brien [27]; Tripcevich and Vaughn [47]). Finally, the continuous (re-)evaluation of written sources and of historic graphic material in the view of new research is still an important task. There have always been some key issues, such as the beginning of metallurgy within certain regions, the earliest use of metals and alloys or the transition from one technology to another. Nevertheless, the march of historical usage often

D. A. Scott, R. Schwab, *Metallography in Archaeology and Art*, Cultural Heritage Science, https://doi.org/10.1007/978-3-030-11265-3_2

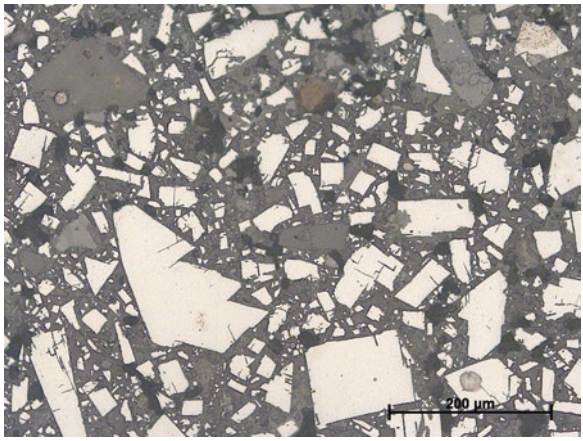

Fig. 2.1 Polished section of a so-called lead bead from Neolithic Tell Halula (Syria) viewed in bright field showing high reflecting cubic galena (PbS) crystals with cleavage within lead carbonate

exposes the lack of knowledge concerning properties of individual alloys and their deliberate use or production in different regions during specific periods.

The use of metals goes back some 7000–8000 years. In the Old World, we move from a premetallic phase where minerals were used for gemstones to a Chalcolithic copper phase. Copper was the first metal used by humans and not lead, as far as we can see today. Some incorrectly labelled lead minerals from Çatalhöyük [34, 43] and some other places (Fig. 2.1) have introduced much confusion into this discussion, which is not finally closed (see Craddock [6, p. 125]). Indeed Moorey ([25, p. 295]) maintains that lead was one of the first metals to be used by man, although he used to say that it was *the* first!

It is usually an easy task to distinguish between minerals and metals by metallography, whereas field analytics, for example, with portable X-ray fluorescence devices (p-XRF), which are very popular today and generally helpful, can be quite misleading, because it is not possible to detect many light elements which are essential components of mineral compounds. Indeed, with increasing sophistication and the use of portable vacuum or flushing techniques, even sodium and magnesium can now be seen, even if not easily quantified.

Arsenical copper was the first alloy deliberately used by man, but bronze has most probably been the first alloy that has been deliberately produced. The archaeological period known as the Iron Age is different in its technical stages, in which we are still enmeshed, although steel itself is giving way to new composites, polymers and high-performance and nano-engineered materials. It is an interesting fact that iron and steel production by direct smelting, the so-called bloomery process, has been a valued technology in most parts of the world, which hasn't changed much for more than 2000 years. Whereas in Europe the introduction period of the indirect process, the blast furnace, in medieval times had quite a few teething troubles until the seminal improvements in the nineteenth century. In ancient China these concerns were obviated by the introduction of white and grey cast iron long before the west began to make use of it.

The concept of continual progression and societal development is firmly entrenched in this series of transitions from the hammering of small pieces of native copper to the production of alloyed steels and beyond. It is a linear view that disguises a number of truths about metallurgical development in different continents and different societies, connecting style, systems of belief and technological choices (see Lechtman [21]).

In the local development of different metallurgical traditions, independent inventions, skills introduced by diffusion and local experimentation are the reality of the complex mix of events, which make up the metallurgical past. There is most probably not just one story but many intertwined stories with different origins at different times. This, surely, should be an obvious facet of human history, but some archaeologists, in applying broad concepts to the development of metallurgy, have tried to simplify this complexity, arguing against the "diffusionist" hypothesis of an earlier generation of archaeologists to expand on the theme of "independent invention", which does not explain the complex tapestry of the metallurgical past.

Childe [4] puts forward the idea that metallurgy originated in the Near East and was adopted in Eurasia by diffusion, whereas Renfrew [35] argued for the independent invention of metallurgy at different places such as southern Iberia in the fourth millennium BC. This is a view which has been thought to lack evidence but which is also still in dispute because of more recent scientific evidence from Europe. The discussion about diffusion versus independent invention is reviewed by several authors in *Archaeometallurgy in Global Perspectives* [37]. Clearly, the *ex oriente lux* theory is an oversimplification of the complex societal events involved in the inception of metallurgy. The transubstantiation of minerals to copper metal and the early use of native copper have long been a source of fascination in attempts to unravel this mystery: Childe [5] talked of "homotaxis", or modes of development, with this primary period of copper use corresponding to "mode zero" of our development over time, while Daniel [9] talked of an "eochalcic episode". These neologisms, which now seem rather artificial, have faded into obscurity. More colloquially, and meaningfully, a whole age of humanity's past has been designated the Bronze Age, signifying the great importance of copper and copper alloys in a crucial stage of our development from hunting-and-gathering communities to settled villages and the rise of agriculture.

There are complexities regarding the early use of metals in the Old World, problems regarding the validity of the independent invention model, the transmission of metal objects, metallurgical practices and the role of metallic artefacts [44]. New discoveries are continually shifting the picture that we have of the earliest use of copper (Chap. 5). The earliest evidence for native copper and copper oxide use for beads, hooks and needles in Europe is now thought to date from the mid-sixth millennium BC, from sites such as Divostin and Rudna Glava in Serbia [1]. Rudna Glava itself is most probably an enigmatic example of error or of misinterpretation in the research into ancient metallurgy. Rudna Glava is without doubt one of the oldest copper mines in Europe, with dates that show that the mine was in use from the late sixth millennium BC [1, 27, pp. 40–7], and it has been assumed that this mine has been the major source for Eneolithic copper of the Balkans (e.g. Jovanović

[15]). Indeed copper oxide minerals such as malachite were won, but as of 2019, perhaps only one single Neolithic copper artefact from the Balkans has been shown by lead isotopic analysis and chemical analysis to derive from the ore minerals of Rudna Glava [12, 29, 30, 33, 38]. It might be possible that further analyses could indicate the use of ore minerals from Rudna Glava for early copper smelting, as Gale and his co-workers [12, p. 169] have already suggested, but at the moment it seems more likely to be a misinterpretation of archaeological evidence for copper mineral winning.

However, the contemporary settlement of Belovode, also in Serbia, provides the earliest documented proof of pyrometallurgical copper extraction in Europe [33], which is at a comparable date to sites in Anatolia (Chap. 5). In other areas of Europe and the central Mediterranean, there is increasing evidence of copper mining and smelting from the late fifth millennium BC onwards [2, 27].

It is obvious from many lines of research that smelting of the copper ores would have been initially small scale, operating at relatively low temperatures, carried out under poorly reducing conditions using oxide or roasted sulphide ores in small stone or clay structures or crucibles without intentional flux additions, creating relatively little slag [2, 7]. Smelting of this kind usually creates prills of copper which have to be further refined (Fig. 2.2), often by remelting in a crucible. Some of these prills, which are usually totally transformed to oxide compounds, are sometimes found in settlements, and there is again a serious confusion in terms of natural copper mineral compounds or corroded copper.

Our ability to provenance early copper sources is limited, because many old mines have been eradicated by modern mining or not yet identified. The general approaches and their benefits or failures to link ore to metal have been controversial

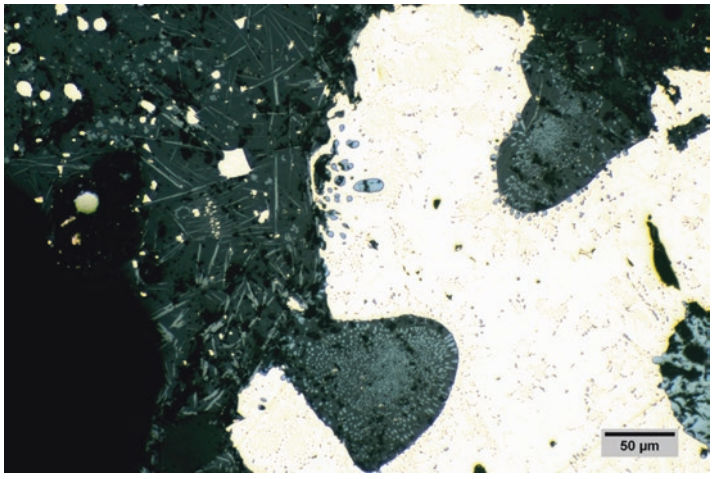

Fig. 2.2 Experimental smelt of copper from high-quality malachite, smelted using a simple clay mini-furnace and charcoal with hand-held bellows used for heating. The result was prills of copper entrapped in a tenacious slag. The slag incorporates some fayalite in a glassy matrix

and have been discussed many times elsewhere (for references see Pernicka [28]; Pollard and Bray [32]), but thorough case studies, such as those from the Balkans, the Mediterranean and other regions have clearly demonstrated the successful application of scientific methods to such questions.

A good example of trial and error, combined with basic research in archaeometallurgy, is the question of the origin of Eneolithic material in the British Isles and continental Western Europe termed Bell Beaker metal. More recently Roberts [36, p. 433] has referred to the general problems of source definition of the Beaker metal, which remains a problem. A case study focuses on the British Isles: Junghans and his co-workers [13, pp. 128–138], part of the so-called SAM group (see Pernicka [28]), have selected a group of arsenical coppers, which is prevalent on Ireland and in some regions of Central Europe during the third millennium BC. Due to the lack of knowledge concerning contemporary copper mines on Ireland and maybe due to the continental influences on the Beaker culture, they suggested an import of metal from Central Europe. Further analysis could show that some of the material also reached Britain, but now Ireland has been proposed to be the main source, which has also been questioned (see Northover et al. [26]). With the discovery of the arsenic-bearing copper mines on Ross Island, it has become clear that it was one of the major sources for copper for the British Isles in the late Chalcolithic and the Early Bronze Age [26, 27]. The SAM group has misinterpreted their data, because of the lacking knowledge, but as a result of their work, they had predicted the Ross Island material through their basic research, several decades before the discovery of the mine itself.

By the second millennium BC, when tin-bronze became common across much of the Old World, there is a significant rise of copper mining and metallurgy, even on quite different scales. Small-scale mining sites such as Copa Hill in Wales, dated 2100–1600 BC, show that advances in this kind of technological process had reached quite far-flung locations with many logistical problems [27, 45]. Most of these early mines were run by open-cast mining to extract weathered secondary copper minerals, but some mines show a complex series of vast underground tunneling [3, 6, pp. 23–92, 10, 27]. The shafting of Kargaly in the southern Ural has reached around 40 metres depths, but the tunnel system embraces a territory of nearly 500 km^2 [3]. The Mitterberg area in the Tyrol is one of the largest Bronze Age mining fields in Europe and shows mining galleries with nearly 200 m depth [31]. With increasing demand and more underground mining, a drastic change in ore choice from oxidized secondary to sulphidic minerals occurred, which involved more complex technologies for ore processing and smelting.

Most Continental European Early Bronze Age artefacts clearly show fahlore impurity patterns (see, e.g. Krause [20]), whereas Middle Bronze Age metal generally has lower concentrations of impurity elements like antimony, silver and bismuth [31]. The Mitterberg mining area lodes are dominated by some Ni-As minerals and chalcopyrite, which is connected with a three-step matte smelting process to remove sulphur and iron by roasting and slagging, before the copper can be reduced. Iron-rich slag containing matte prills is the common metallurgical relicts of this eastern alpine process [19], but similar debris can be found from many sites all over

the Old World (e.g. Hauptmann [14]; Kassianidou [16]; Zwicker et al. [52]), albeit they are not necessarily evidence for a deliberate matte smelting.

Early iron smelting may originate from the smelting of iron-bearing copper ores or from the addition of iron-containing fluxing materials under highly reducing conditions in the smelt. However this remains uncertain, although it is a convenient model to explain the advent of iron, with quite a lot of indications from the archaeological material as to the likelihood of this (Chaps. 4 and 5).

The transition from bronze to iron in the different parts of the world is actually an interesting topic for many economic and technological reasons (Chap. 5). Nonetheless, innovations do not follow a simple logic, and the triumphal procession of iron has undergone many vicissitudes in different parts of the world, from the appearance of the first iron implements to full-fledged iron using societies (see Wertime and Muhly [50]). Cast iron technology first emerged in China from the ninth century BC and has been transferred to other Asian countries many centuries later, but it took around 2000 years until European bloomery smelters changed to this technology, while African iron smelters never did.

Each continent has its own especial creations or metallurgical developments depending on the culture and the geography, the ores available in the region concerned and how these ores are utilised or processed. Thus, early metallurgical development in Africa encompassed around 11,000 km of distance from Egypt to the Cape and nearly five millennia [17], with the principal metal produced being iron. The advent of copper and iron metallurgy on the African continent is an interesting topic, and especially in sub-Saharan Africa, the beginning of the use of iron is one of the most debated features of the metallurgy, as there is no bronze metallurgy preceding this important development, essential for so much of African agricultural development (see Van der Merwe [49]). Some practices extend through time remarkably, for example, isolated human finger bones were buried beneath prehistoric furnace bases in the Lowveld of eastern South Africa to ensure a successful smelt, and the same practice is recorded by the early twentieth century ethnographers in the same region.

For various reasons, not much is currently known of early Egyptian iron smelting compared with sub-Saharan Africa, perhaps because excavations are more focused in these areas on iron metallurgy and more readily accessed. Copper objects first appeared in the Maadi culture near the Nile delta between 4000 and 3200 BC. Copper and gold artefacts first appeared in lower Nubia and are dated from 3600 to 3300 BC, the increased use of metals being a long slow process. Surprisingly, there was no tin or bronze, no silver, no gold and no lead in southern Africa before the beginning of trade with the Islamic world [17]. The lack of these developments may have a bearing on the discussion concerning the independent development of metallurgy in Africa, which could well prove to be an indigenous technology as was the entire metallurgical technology of South America. As far as ferrous metals are concerned, their origin in Africa has been something of a mystery. There are several very old radiocarbon dates in the literature, and recently Zangato and Holl [51] have suggested that iron production activities have taken place in Central Africa as early as

3000–2500 BC, which would be the earliest iron working in the world (see comments in the same issue of the journal) which is further discussed by Killick [18].

In the New World, metallurgical development had not yet reached the stage of the extraction of iron by the fifteenth century AD, but given the parallels between human inventiveness in the Old and the New, there is no reason to think that iron metallurgy would not have come sometime after 1500 AD, when the continent was invaded by the Europeans and the native cultures destroyed.

In broader terms there is "independent invention" of metallurgy in the New World, which shows that metallurgy can be developed without contact with cultures which already have discovered metallurgical processes. The necessary materials required, ceramics, clay, charcoal, stone, wood and fire, are universally available. These materials needed to come first, especially ceramics and the ability to shape and fire large ceramic structures or make refractory crucibles in which metals can be manipulated or smelted.

Extractive metallurgy in the New World began in the Southern Andes, where the mineral resources are rich in copper, tin, lead and silver (see Tripcevich and Vaughn [47]). Extractive metallurgy developed strongly in this region and "diffused" up towards the North, with the dates for metallurgical activity in Costa Rica, being later than those in Colombia, which are later than those in Ecuador and Peru. The separation between different cultures in the New World resulted in the smelting of sulphide ores being prevalent in Peru but absent in Colombia [22, 23, 39, 41]. The pre-eminent metallurgy of Colombia, Panama and Costa Rica is that of gold-copper alloys often with depletion gilding and a variety of different coloured gold alloys, especially during the period from the early centuries AD onwards (Chap. 6). Silver was not extracted in this region and occurs in the gold alloys as a result of its inclusion in the native gold but was extracted in Peru and Chile, for example, where extensive use was made of silver.

Copper may have been smelted from oxide ores, but not from sulphide ores in the Colombian area, while in Peru, complex metallurgical extraction processes had been developed for the cupellation and scorification of silver, the alloying of silver-copper alloys, the fabrication of silver-gold-copper alloys with extracted silver and the extensive use of copper-arsenic alloys. One of the remarkable alloys made for decorative purposes is an extensive range of silver-copper alloys, which extends into Ecuador, but only crosses the Colombian border as far as the extreme south, in the Nariño region. These alloys are often surface depleted in copper, resulting in heavily debased silver-copper alloys which appear to be made of silver. This decorative use of metals is an important one: metals were not primarily instruments of war, in the same way that they were in the Old World. Bronze Age peoples made extensive of tin bronze for arrowheads, swords, daggers and knives. Copper alloy maceheads are the most well-known South American war-like metallic implement, which we associate with the Inca Empire, but in earlier cultures in South America, the extensive use of metals for this purpose was practically unknown.

Many unique metallurgical achievements took place in South America. Perhaps the most impressive is the development of electrochemical replacement plating in Peru to deposit very thin coatings of gold or silver onto copper [24]. The other is the

use of platinum plating or cladding in the La Tolita-Tumaco culture of Ecuador, which before the birth of Christ had already made use of platinum to produce platinum-gold composite artefacts, at a time when platinum was totally unknown in Europe [39, 40]. Native platinum from South America first entered the European market during the eighteenth century as "white gold" and attracted considerable interest because of its difficulties in working or casting to shape [48, p. 152]. From the eighteenth to the nineteenth centuries, the number of metals known increased significantly, but many others such as arsenic, antimony, nickel or zinc have not been known in metallic form before modern times or only sporadically in their native forms, but some of their alloys enjoyed great popularity from prehistory (Chap. 5). Indeed metallic zinc has been used in Asia from the thirteenth century AD onwards, but it has not been produced in Europe before the eighteenth century; nevertheless brass has been the most popular copper alloy from the first century BC until today (Chap. 5). Actually, we do not know if brass making has been developed independently in the Old World or has been transferred from Asia or vice versa. Certainly, we can say that the indigenous people in the New World did not undertake the production of brass and therefore have not used it before the first Europeans entered the continent.

We have seen remarkable progress in understanding ancient metallurgy, but there are many gaps in terms of knowledge and comprehension about individual metallurgical practices and developments. Metallography has been an essential part of the unravelling of the story of these metallurgical developments. The identity of an excavated artefact, even if heavily corroded, can usually be determined by metallographic examination. The mounted section can then be used for further, detailed studies to determine precise compositional data. Determining whether an artefact has been cast or worked to shape is most important for the history of metallurgy, and this kind of information has been slowly assembled through thousands of studies carried out over the past 100 years. During that time, the fine achievements of pattern-welded swords and damascened iron were unravelled; the Chinese story of grey and white cast iron and the history of the utilization of copper, arsenical bronze and tin bronze elaborated; the subtleties of the extraction of silver and the use of silver alloys defined; and the use of tin, gold, silver, bronze and platinum as plating or cladding materials investigated, and numerous site reports have been issued, containing metallographic images and reports which are essential for our understanding of the archaeological past. The chapters which follow provide a brief overview of some of the important developments in the field of metallography of ancient metals.

References

1. Borić, D.: Absolute dating of metallurgical innovations in the Vinča culture of the Balkans. In: Kienlin, T.L., Roberts, B.W. (eds.) Metals and Societies. Studies in Honour of Barbara S. Ottaway Universitätsforschungen zur Prähistorischen Archäologie 169, pp. 191–245. Rudolf Habelt, Bonn (2009)

2. Bourgarit, D.: Chalcolithic copper smelting. In: LaNiece, S., Hook, D., Craddock, P. (eds.) Metals and Mines: Studies in Archaeometallurgy, pp. 3–14. Archetype Publications in association with the British Museum, London (2007)
3. Chernykh, E.N.: Kargaly: the largest and most ancient metallurgical complex on the border of Europe and Asia. In: Linduff, K.M. (ed.) Metallurgy in Ancient Eastern Eurasia from the Urals to the Yellow River. Chinese Studies 31, pp. 223–237. E. Mellen Press, New York (2004)
4. Childe, V.G.: The Bronze Age. Biblio and Tannen, New York (1930)
5. Childe, V.G.: The Story of Tools. Cobett, London (1944)
6. Craddock, P.T.: Early Metal Mining and Production. Edinburgh University Press, Edinburgh (1995)
7. Craddock, P.T.: Paradigms of metallurgical innovation in pre-historic Europe. In: Hauptmann, A., Pernicka, E., Rehren, T., Yalçın, Ü. (eds.) The Beginnings of Metallurgy. Der Anschnitt Beiheft 9, pp. 175–192. Deutsches Bergbau-Museum, Bochum (1999)
8. Craddock, P.T.: Archaeometallurgy 1962–2013: the establishment of a discipline. Hist. Metall. **47**, 1–12 (2013)
9. Daniel, G.: The Idea of Prehistory. World Publishing Company (1963). http://archive.org/details/ideaofprehistory/006990mbp
10. Domergue, C.: Les mines antiques. La production des métaux aux époques grecque et romaine. Picard, Paris (2008)
11. Forbes, R.J.: Metallurgy in Antiquity: a Notebook for Archaeologists and Technologists. Brill, Leiden (1950)
12. Gale, N.H., Stos-Gale, Z., Raduncheva, A., Panayotov, I., Ivanov, I., Lilov, P., Todorov, T.: Early metallurgy in Bulgaria. In: Craddock, P., Lang, J. (eds.) Mining and Metal Production through the Ages, pp. 122–173. The British Museum Press, London (2003)
13. Junghans, S., Sangmeister, E., Schröder, M.: Kupfer und Bronze in der fühen Metallzeit Europas Studien zu den Anfängen der Metallurgie 2.1. Gebr. Mann, Berlin (1968)
14. Hauptmann, A.: The Archaeometallurgy of Copper. Evidence from Faynan, Jordan, Natural Science in Archaeology. Springer, Berlin (2007)
15. Jovanović, B.: Primary copper mining and the production of copper. In: Craddock, P.T. (ed.) Scientific Studies in Early Mining and Extractive Metallurgy. British Museum Occasional Paper No. 20, pp. 31–40. British Museum, London (1980)
16. Kassianidou, V.: The formative years of the Cypriot copper industry. In: Tzachili, I. (ed.) Aegean Metallurgy in the Bronze Age, pp. 249–267. Ta Pragmata Corp, Athens (2008)
17. Killick, D.: Cairo to cape: the spread of metallurgy through eastern and southern Africa. In: Roberts, B.W., Thornton, C. (eds.) Archaeometallurgy in Global Perspective, pp. 507–527. Springer, New York (2014)
18. Killick, D.: Invention and innovation in African iron-smelting technologies. Camb. Archaeol. J. **25**(1), 307–319 (2015)
19. Kraus, S., Schröder, C., Klemm, S., Pernicka, E.: Archaeometallurgical studies on the slags of the Middle Bronze Age copper smelting site S1, Styria, Austria. In: Hauptmann, A., Modaressi-Tehrani, D. (eds.) Archaeometallurgy in Europe III. Der Anschnitt Beiheft 26, pp. 301–308. Deutsches Bergbau-Museum, Bochum (2015)
20. Krause, R.: Studien zur kupfer- und frühbronzezeitlichen Metallurgie zwischen Karpatenbecken und Ostsee Vorgeschichtliche Forschungen 24. Verlag Marie Leidorf GmbH, Rahden (2003)
21. Lechtman, H.: Style in technology, some early thoughts. In: Lechtman, H., Merrill, R.S. (eds.) Material Culture: Styles, Organization, and Dynamics of Technology, pp. 3–20. West Publishing Company, St. Paul (1977)
22. Lechtman, H.: Andean value systems and the development of prehistoric metallurgy. Technol. Cult. **25**, 1–36 (1984)
23. Lechtman, H.: The production of copper-arsenic alloys in the Central Andes. Highland ores and coastal smelters? J. Field Archaeol. **18**, 43–76 (1991)
24. Lechtman, H., Erlij, A., Barry, E.J.: New perspectives on Moche metallurgy: techniques of gilding copper at Loma Negra, Northern Peru. Am. Antiq. **47**(1), 3–30 (1982)

25. Moorey, P.R.S.: Ancient Mesopotamian Materials and Industries: the Archaeological Evidence. Eisenbrauns, Winona Lake, Ind (1999)
26. Northover, J.P.N., O'Brien, W., Stos, S.: Lead isotopes and metal circulation in beaker/early bronze age Ireland. J. Ir. Archaeol. **10**, 25–47 (2001)
27. O'Brien, W.: Prehistoric Copper Mining in Europe. 5500–500 BC. Oxford University Press, Oxford (2015)
28. Pernicka, E.: Provenance determination of archaeological metal objects. In: Roberts, B.W., Thornton, J. (eds.) Archaeometallurgy in Global Perspective, pp. 239–268. Springer, New York (2014)
29. Pernicka, E., Begemann, F., Schmitt-Strecker, S., Wagner, G.A.: Eneolithic and Early Bronze Age copper artefacts from the Balkans and their relation to Serbian copper ores. Prähistorische Zeitschrift. **68**(1), 1–54 (1993)
30. Pernicka, E., Begemann, F., Schmitt-Strecker, S., Todorova, H.: Prehistoric copper in Bulgaria: its composition and provenance. Eurasia Antiqua. **3**, 41–180 (1997)
31. Pernicka, E., Lutz, J., Stöllner, T.: Bronze Age copper produced at Mitterberg, Austria, and its distribution. Archaeol. Aust. **100**, 19–55 (2016)
32. Pollard, A.M., Bray, P.: Chemical and isotopic studies of ancient metals. In: Roberts, B.W., Thornton, J. (eds.) Archaeometallurgy in Global Perspective, pp. 217–238. Springer, New York (2014)
33. Radivojević, M., Rehren, T., Pernicka, E., Šljivar, D., Brauns, M., Borić, D.: On the origins of extractive metallurgy: new evidence from Europe. J. Archaeol. Sci. **37**(11), 2775–2787 (2010)
34. Radivojević, M., Rehren, T., Shahina Farid, S., Pernicka, E., Camurcuoğlu, D.: Repealing the Çatalhöyük extractive metallurgy: the green, the fire and the 'slag'. J. Archaeol. Sci. **86**, 101–122 (2017)
35. Renfrew: Cycladic metallurgy and the Aegean Early Bronze Age. Am. J. Archaeol. **71**, 1–20 (1967)
36. Roberts, B.W.: Production networks and consumer choice in the earliest metal of Western Europe. In: Roberts, B.W., Thornton, C. (eds.) Archaeometallurgy in Global Perspective Methods and Syntheses, pp. 423–446. Springer, New York (2014)
37. Roberts, B.W., Thornton, J. (eds.): Archaeometallurgy in Global Perspective. Springer, New York (2014)
38. Schmitt-Strecker, S., Begemann, F.: Kupfer- und bronzezeitliche Metallartefakte vom Westbalkan: Zur Frage nach den Quellen ihres Kupfers. Praehistorische Zeitschrift. **80**(1), 49–64 (2005)
39. Scott DA: Pre-Hispanic Colombian metallurgy: studies of some gold and platinum alloys. PhD thesis, Institute of Archaeology, University of London (1982)
40. Scott, D.A.: The LaTolita-Tumaco culture: master metalsmiths in gold and platinum. Lat. Am. Antiq. **22**(1), 65–95 (2011)
41. Scott, D.A.: Ancient Metals: Microstructure and Metallurgy 3: Catalogue of Ancient Colombian Data, Los Angeles, California (2012)
42. Scott, D.A., Bray, W.: Ancient platinum technology in South America. Platin. Met. Rev. **24**, 147–157 (1980)
43. Sperl, G.: Zur Urgeschichte des Bleis. Z. Met. **81**(11), 799–801 (1990)
44. Thornton, J.: Archaeometallurgy: evidence of a paradigm shift? In: Kienlin, T.L., Roberts, B.W. (eds.) Metals and Societies, Studies in Honour of Barbara S. Ottaway. Universitätsforschungen zur prähistorischen Archäologie 169, pp. 25–33. Rudolf Habelt, Bonn (2009)
45. Timberlake, S.: Excavations on Copa Hill, Cwmystwyth (1986–1999): An Early Bronze Age Copper Mine within the Uplands of Central Wales. British Archaeological Reports British Series 348. Archaeopress, Oxford (2003)
46. Timberlake, S.: The use of experimental archaeology/archaeometallurgy for the understanding and reconstruction of Early Bronze Age mining and smelting technologies. In: LaNiece, S., Hook, D., Craddock, P.T. (eds.) Metals and Mines: Studies in Archaeometallurgy, pp. 124–128. Archetype Publications, London (2009)

47. Tripcevich, N., Vaughn, K.J. (eds.): Mining and Quarrying in the Ancient Andes: Sociopolitical, Economic, and Symbolic Dimensions. Springer, Boston (2013)
48. Tylecote, R.F.: A History of Metallurgy. The Metals Society, London (1976)
49. Van der Merwe, N.J.: The advent of Iron in Africa. In: Wertime, T.A., Muhly, J.D. (eds.) The Coming of the Age of Iron, pp. 463–506. Yale University Press, New Haven/London (1980)
50. Wertime, T.A., Muhly, J.D. (eds.): The Coming of the Age of Iron. Yale University Press, New Haven/London (1980)
51. Zangato, É., Holl, A.F.C.: On the Iron front: new evidence from North-Central Africa. J. Afr. Archaeol. **8**(1), 7–23 (2010)
52. Zwicker, U., Virdis, P., Ceruti, M.L.: Investigations on copper ore, prehistoric copper slag and copper ingots from Sardinia. In: Craddock, P.T. (ed.) Scientific Studies in Early Mining and Extractive Metallurgy. British Museum Occasional Paper 20, pp. 135–164. British Museum, London (1980)

Chapter 3
Principles and Practice of Metallography

3.1 Sampling and Specimen Preparation

3.1.1 Sampling

One of the principal differences between metallography in modern material sciences or industrial quality control is that the taking of samples from objects of cultural heritage is usually a one-time procedure with very limited scope as regards sample size or position. When rare or valuable objects are permitted to be sampled for analysis, small samples can only be taken from inconspicuous locations. Therefore, there are a number of criteria that should be considered before any sampling is undertaken:

A. The microstructure of the samples should not be altered in the process of removal.
B. The sample should be representative of the object as a whole or of a selected feature or area of the object.
C. The orientation of the sample in its dimensional relationship to the object concerned should be marked on a photograph or a drawing of the object.
D. If it is not obvious from where the sample was taken, the position on the object concerned should be marked on a photograph or a drawing of the object.
E. The sample should be assigned a laboratory number together with sufficient documentation to enable its identity to be preserved.
F. The object should be photographed or drawn before the sample is taken. This is especially important if the dimensions of the object are fundamentally altered by the material removed.

Metallographic studies should be integrated as far as possible with archaeological data, such as date and geographical and cultural provenance. The chemical composition and technology of manufacture to extract the maximum benefit from the removal of a small sample from the object remains the most important. There are

D. A. Scott, R. Schwab, *Metallography in Archaeology and Art*, Cultural Heritage Science, https://doi.org/10.1007/978-3-030-11265-3_3

still far too many metallic artefacts lacking detailed provenance information because they were obtained from dealers, museum collections, private donors, etc., which lack documentation, or from uncontrolled excavations.

It is generally possible to undertake metallographic examination on whole objects without sampling, if a small area of the artefact can be polished, which is normally used on components that are too large for the laboratory and where sampling is not permissible (see Bramfitt and Lawrence [10]). Alternatively the whole object is mounted with a resolvable moulding material like acrylic resin and then ground and polished at the position of interest, analysed at this location and finally removed from the redissolved resin (see Blet-Lemarquand et al. [8]). This technique is especially useful for gold items, because of the high reflectivity of gold; the polished spots are invisible to the naked eye, and for small items like coins, which cannot be sectioned. However, the predominant methodology is to remove a small sample with the use of a jeweller's saw, or a scalpel, a vibro-tool cutter, hand-held micro-diamond wheel or a diamond cut-off machine, which is cooled ensuring that no microstructural alteration takes place during removal. Careful cutting with a fine jewellers saw is often the only choice in the field or in museum storage areas and care must be taken to avoid undue damage to the sample itself. For example, cutting away a tiny sample with a scalpel blade may create too much mechanical deformation, ruining the true microstructure of the object.

Figure 3.1 shows the deformation zone of a sample, which was taken by pliers. The advent of hand-held drills with small diamond wafering blades has made sampling much easier, as removal of a small sample with a jewellers saw from a hard material, such as medium-carbon steel, can take a considerable period of time by comparison. Very hard bronzes are also best cut using a miniature diamond tip in the field, while high-speed cut-off saws with diamond-impregnated blades are available in the laboratory.

Laboratory sampling of archaeological or art material has much in common with industrial practice if the object is large enough to be held in the diamond

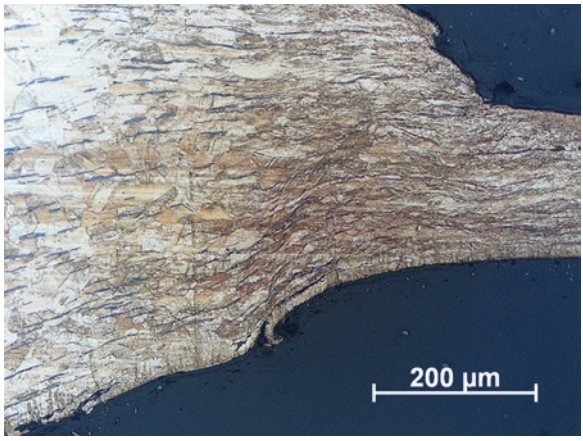

Fig. 3.1 Fragment from a Bronze Age shield (type "Nipperwiese") from Schiphorst, Schleswig-Holstein, Germany, which has been taken by pliers. Thickness reduction and slip lines are still visible at several hundred of micrometres away from the real cut surface (etched with acid ferric chloride)

blade cut-off saw, which is oil or water cooled, and with varying weights. Normal specimen holders offered by the manufactures are often not suitable for fragile, non-uniform and tiny samples from art and archaeology contexts. Pragmatism and creativity are therefore needed to convert commercial specimen holders or design suitable new ones. Speed of rotation and cutting weight exerted on the object can be varied to suit the material, producing a clean cut with no deformation or thermal damage to the sample whatever. A proper sectioning by a diamond blade cut-off saw offers a high-quality surface where a first grinding step with rough grinding paper can be omitted (see Aliya [1, pp. 233–35]; Geels [20, pp. 14–45]; Vander Voort [75, pp. 62–69]). If samples are big enough, an accurate cut into halves by a thin wafering blade and using the other part for other investigations can be a good strategy.

It might be surprising to some readers that we have to point out the following basic principle, but interdisciplinary working should be based on mutual understanding, though it is often connected with confusion in terms – especially when cultural scientists have to work together with different scientific disciplines. There is a fundamental difference between the microscopical examination of metals and biological or geological samples. This difference is due to the fact that all metals are opaque to optical light. This means that they do not allow light to pass through them, even the thinnest foils, although the greenish light which can be seen in thin gold foils is light transmitted through the grain boundaries. Therefore, metallic samples have to be prepared as polished sections and not as thin sections, and they are observed by reflected light rather than transmitted light.

3.1.2 Mounting

Specimens are usually too small to be handled in the preparation process and must be mounted in a suitable mounting material. Specimens were once mounted in molten sulphur, waxes, dental plasters, low-melting-point alloys and others (see Kehl [28]), so the reinvestigation of "old" samples sometimes produces some oddities and unpleasant surprises. These materials have caused much trouble, due to degradation, varying hardness, sensitivity to solvents, increased brittleness over time and difficulties in polishing and preparing a scratch-free surface and are nowadays replaced by polymeric materials such as epoxy, acrylic or phenolic resins (see Geels [20]). The criteria for the choice of a specific mounting material are dependent on the constitution of the sample and the scheduled analysis. Factors such as porosity, thermal sensitivity or hardness of the sampled material as well as the viscosity, the polymerization conditions and the hardness of the mounting material must be traded off (see Bousfield [9]; Geels [20]; Samuels [59]). Otherwise, mounting may negatively affect the preparation, damage the specimen or create trouble in subsequent examinations. The orientation of the sample in the mounting mould has to be carefully considered, and there is a danger that small fragments will float or otherwise be disturbed when resin is poured over them. To obviate these problems, the sample

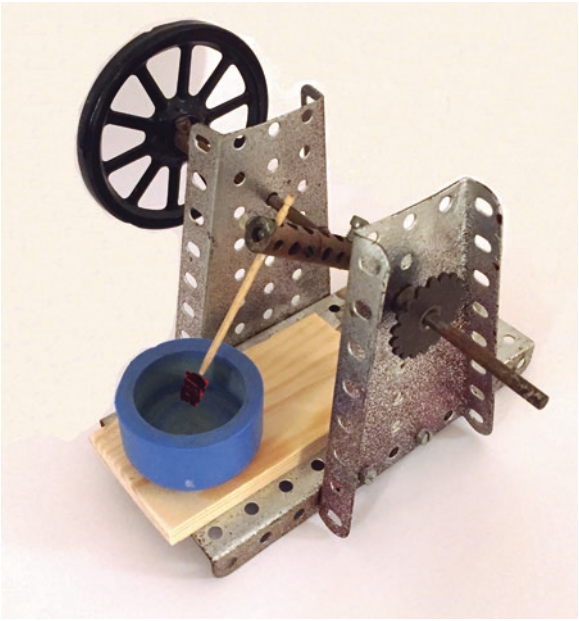

Fig. 3.2 Mounting jig for small samples attached on the end of a cocktail stick with adhesive

can be held in place on the bottom of the mould with a thin plastic strip, available from metallographic supply companies, or can be held on the end of a cocktail stick by a tiny blob of cellulose nitrate adhesive, with the stick held upright in a small clamp. Scott [67] has described devices of this type, and one of them is illustrated in Fig. 3.2. Dr. Shugar (personal communication) has used small silicon carbide discs mounted on wooden sticks, followed by small circles of felt with diamond polish for the preparation of small areas of large objects which cannot be cut and mounted, with some success. This obviates the need to cut and remove a sample from some types of artefacts which could be suitable for this approach.

If scanning electron microscope examination (SEM) or electron microprobe analysis (WDS-EPMA) is planned, where samples have to be electrically conductive, it can be useful to use a copper wire instead of the cocktail stick, and a conductive adhesive to fix the sample. Samuels [59] shows some helpful proposals for methods to make electrical contact with the back of a specimen mounted in non-conducting materials. Electrical conductivity is essential to scanning electron microscope examination or electron microprobe analysis (WDS-EPMA) to avoid electrostatic charging. Conductive mounting resins as well as fillers such as graphite, nickel or copper powders are commercially available. However, it should be pointed out that the high-count rate necessary for EPMA analysis requires specific mounting techniques and materials, because many polymers suffer deterioration under the impact of the electron beam. In addition, many mounting materials react with X-rays, used for X-ray diffraction or X-ray fluorescence analysis.

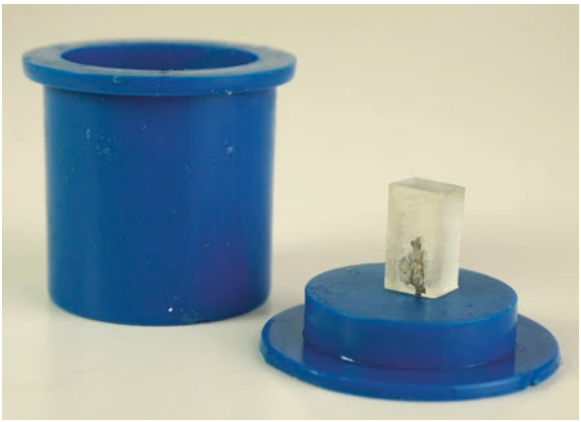

Fig. 3.3 Fragile tin sheet from a Roman tinned statuette from Trier, Germany, fixed on a small block of epoxy resin to stabilize sample position before embedding. (Photo by E. Duberow)

Many archaeological materials are heavily corroded and are therefore porous and mechanical unstable. The disadvantage of using the plastic or metal clip technique for archaeological material is that some of these materials are so fragile and corroded that they cannot be held in place because the force exerted by the plastic or metal may even be too much for the fragile sample, especially if it is an exceptionally thin piece of sheet. In this case, some small blocks of acryl glass or epoxy resin can be used to stabilize and to position the sample, as shown in Fig. 3.3. The samples can be fixed on the block with instant adhesive and then both embedded with resin. The porosity of those samples makes them difficult to prepare and to investigate. Their fragility and porosity causes pull-outs during polishing, and the cracks and pores can store air and humidity, which is troublesome for scanning electron microscope examination, as well as for light microscope examination, as alcohol, water or remaining acids can vaporize during the investigation. It is therefore profitable to infiltrate those samples, as well as ceramics or slag. Special low-viscosity resins are available from different providers, but impregnation is best done in vacuum.

Vacuum impregnation is the only satisfactory procedure and can be performed in homemade apparatus (Fig. 3.4) or if more regularly used, in equipment specially designed for metallographic purposes, shown in Fig. 3.5. The basic principle is the same, but commercially available apparatuses are more timesaving, as they allow the impregnation of several samples in one step. The samples must be placed in moulds, and then the moulds can be placed in a vacuum chamber. A vacuum pump has to pump out all the air from the pores, and then resin is sucked into the chamber, replacing the vacuum within the pores. After curing all voids should be covered and filled by the mounting material, and the specimens should be suitable for preparation and examination. The cups which are used for embedding the sample are made from silicon rubber or high-density polyethylene. Even with the use of a mould release agent on the surface of these embedding cups, they eventually degrade on contact with the epoxy mounting resin.

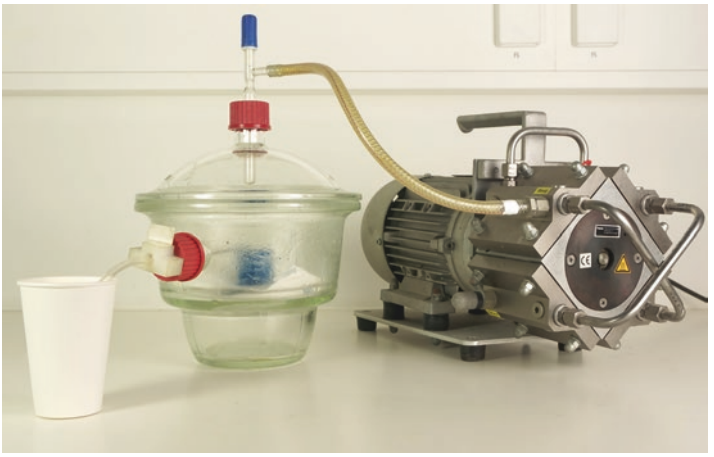

Fig. 3.4 Self-made apparatus for impregnation of single moulds, consisting of a desiccator, a vacuum pump and a tube to suck the resin in. (Photo by E. Duberow)

Fig. 3.5 Commercial vacuum impregnation system with a turntable, suitable for the impregnation of up to 14 moulds within one step and user-defined programmes for cycle time and levels of vacuum for different materials. (Photo by E. Duberow)

Silicon rubber cups are more readily degraded and eventually discolour and stick irreversibly to the epoxy resin used for the mounting. The resin itself is part of the problem, as these are subject to continual chemical remodification over the years, producing casting resins which have different mechanical and chemical properties. Regular use of a mould release agent will ensure that these moulds can be used for

many years. With the polyethylene cups, the authors have found that a thin smearing of butter or Vaseline around the inner surfaces of the mould is sufficient to avoid adhesion of the resin to the cup!

3.1.3 Grinding and Polishing

The preparation methods have changed over time, and some practices have been abandoned, and others have been modified. Grinding and polishing are elemental steps in the metallographic specimen procedure, even though the techniques applied have altered significantly. Advances have been made in terms of polishing compounds, and there are now available a number of different polishing materials for the modern metallographer.

Commercial providers for material preparation have designed consumables and especially equipment for fully automated grinding and polishing, electrolytic and vibratory polishing, which are usually not standard in archaeometric laboratories. Apart from that, electrolytic polishing of archaeological materials should be avoided, because electropolishing does not only completely remove all traces of mechanical grinding and polishing operations but also all non-metallic compounds, as Fig. 3.6 illustrates, which would have provided valuable information.

We refer to more or less traditional standard preparation practices which have wide applicability and which can be modified according to the requirements of the

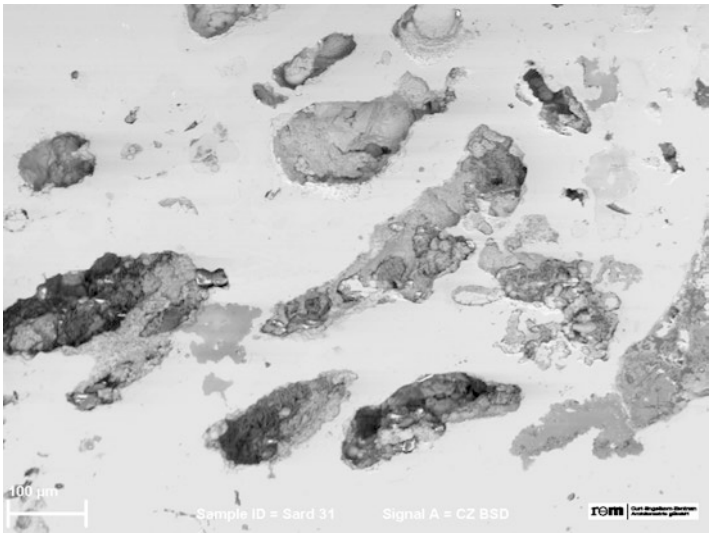

Fig. 3.6 SEM image of the surface of an oxhide ingot from Sardinia (original sampled by U. Zwicker). The sample has once been electro polished for EMPA, which removed all non-metallic components and left deep craters

materials. The standard literature provides many examples for automated or manual preparation procedures for nearly every specific material and can be consulted for further information [20, 34, pp. 61–142; 46, 59, 75, pp. 127–266; 76]. Although care has to be taken in applying standard industrial metallographic practice to ancient metals, as often several minutes of grinding of samples are recommended for industrial alloys, which would be impractical for ancient specimens, whose size frequently precludes such thorough preparation techniques, there would simply be no sample left to study! The smaller the sample is, the greater the degree of care which has to be exercised in its preparation.

The mounted sample is ground on wet silicon carbide papers or diamond grinding discs. Abrasive material is also available as powders in suspensions. Grinding hard materials requires a different type of surface than grinding softer materials; also, the size of the sample and the roughness of the surface influence the choice of grinding material and grit size. Grinding must remove surface damage and eliminate every roughness, using progressively finer abrasive grits. Plane grinding by coarse grit size paper is the first step in the grinding process to ensure a uniform plane surface. Coarser grit size papers (<P 240) are usually not necessary for ancient metals. Such papers are often used in belt grinders, which have widely been used in metallographic laboratories to produce a flat surface of the specimen before embedding [28, pp. 3–4 ; 75, p. 98], but these are best avoided for most ancient and archaeological samples as there is a danger of too much surface damage to the material. The succeeding paper should be one or two grit sizes smaller than that used before and employed to erase all previous grinding scratches. The grit size numbering systems of silicon carbide papers are stated according to the American ANSI standard (American National Standards Institute) or the European FEPA standard (Federation of European Producers of Abrasives), which differs as to how they designate the size of the silicon carbide grit. For example, the FEPA paper grit number P1200 has nearly the same grain size (≈ 15 μm) as ANSI grit number 600 (see Vander Voort [76, p. 1093]). These different standards must be kept in mind by the following recommendations for preparation from the literature. The final grinding step should finish with the finest grit size that is necessary to leave a flat and uniform surface. All grinding should be done wet to wash away all grinding debris and to keep the specimen cool. Specimens should be cleaned after each grinding step to remove grinding debris to avoid contamination during the next preparation step. A jet of water, compressed air and especially a final cleaning in an ultrasonic bath are effective cleaning methods [59, p. 260; 75, p. 72]. Wiping clean with cotton wool under flowing water can only be done for harder materials, whereas silver, gold or unalloyed copper can easily be scratched by natural cotton wool (see below). Washing in ethanol or methanol from a wash bottle followed by drying is recommended.

Polishing on synthetic napped cloth wheels using diamond powder suspension in water as the polishing agents with a compatible lubricant is the final step in producing scratch-free surfaces. Diamond suspensions are usually 6 micron diamond to 1 micron diamond. If required, a finer finish can be obtained using colloidal silica or 0.25-micron diamond in water or oil suspension, but for many purposes, polishing down to 1 micron is sufficient. Silicon oxide suspensions have been well proven

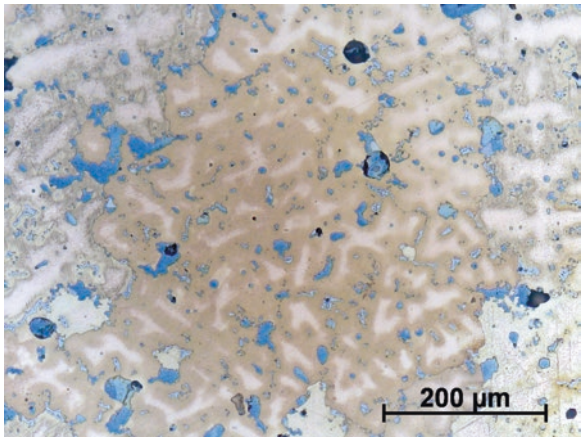

Fig. 3.7 Casting waste from the Late Iron Age oppidum of Manching, Germany, with 7.2% Pb and 9.5% Sn. Micro segregation is revealed, and lead inclusions have lost the typical black smearing and turned to blue-grey after a final attack polish step with aluminium oxide and ammonium hydroxide

over the years in producing almost perfectly polished surfaces. Colloidal silica is useful for the removal of scratches from the diamond stage of polishing if they cannot be otherwise eradicated but can also form a film on the polished surface of the sample, which must be removed with water. As colloidal silica has a tendency to coagulate, the supernatant liquid should always be used for final polishing. Aluminium oxide or other abrasives (see Petzow [46], table 1.5) have become less important and have been widely replaced by diamond suspensions, because of its universal application and the high removal rates. Indeed in certain cases, an aluminium oxide polishing on a suitable cloth such as matted wool with or without a little neutral liquid soap can achieve excellent results, shown in Fig. 3.7 as soft metals like tin or lead are not effectively polished with diamonds.

Particularly scratch-free surfaces of soft materials such as copper or silver alloys can be achieved by so-called attack or etch polishing, when chemical polishing is combined with mechanical polishing by the addition of a dilute etchant to the abrasive. The combination of chemical activity and mechanical abrasion produces scratch-free and deformation-free specimens, although the process is hard to control due to the great variation in properties and composition of ancient and historic metals. Some sellers provide alkaline, with a pH of about 10, or acidic, colloidal oxide suspensions, which are ready to use or are suitable for mixing with chemical reagents for attack polishing. Some attack polishing additives are listed in the literature [20, 59, tab. 9.1; 75, pp. 543–551; 76, pp. 1107–1110]. By reducing the dilution of the etchant and an extension of the polishing time, a small but noticeable relief between the grains can be achieved, which can be useful for special microscopy techniques such as differential interference contrast (DIC), orientation contrast in the SEM or colour etching.

All grinding and polishing can be done manually by hand, or using automated grinding and polishing equipment, but many samples from cultural heritage are so tiny that only careful manual preparation is possible. In any case, the correct amount of pressure applied must be determined by experience since some materials quickly

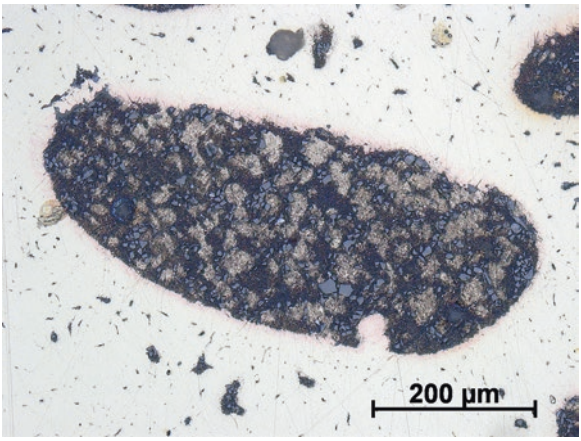

Fig. 3.8 High-leaded bronze belt ring from the Late Iron Age oppidum from the Martberg (Germany), with embedded abrasive fragments in the lead globules, because of too high polishing force

become deformed and annealed, producing false structures, or abrasives get easily embedded on the surface, as shown in Fig. 3.8.

Especially soft metals such as lead and tin are difficult to prepare, and papers should be waxed with paraffin to prevent embedding of particles. They are also prone to the introduction of false structure due to high polishing pressures producing a pseudo structure by twining and spontaneous recrystallization. Scott [65] has published an etch-polish technique for ancient lead which gave good results. Hard phases like intermetallics can crack, especially by automated polishing with too high pressure. On the other hand, if the pressure is too low, scratches will retain until the end of the final polishing step.

The quality of the preparation can significantly influence the response of the sample to the etching process. Specimens to be colour etched or examined with polarized light require a high-quality surface and should be polished with particular care, while techniques like EBSD are extremely sensitive to surface disturbance and need special procedures for preparation. After final polishing, the specimen surface must be cleaned carefully with alcohol and sufficiently dried before any investigation. Care must be taken at this stage to avoid drying marks on the surface of the sample. This may require careful attention with archaeological materials to avoid difficulties in the etching or visual examination of the specimen surface.

3.1.4 Etching

When mounted samples are studied, the surface of the metallic specimen should be examined first in the freshly polished state (see Sect. 3.2), followed by etching with a suitable chemical solution. Very important samples where the interface between the corrosion crust and the metal may be reserved for examination in the polished condition only, as etching may attack and remove the corrosion crust and non-metallic inclusions. Etching reveals metallic structure, but the importance of the

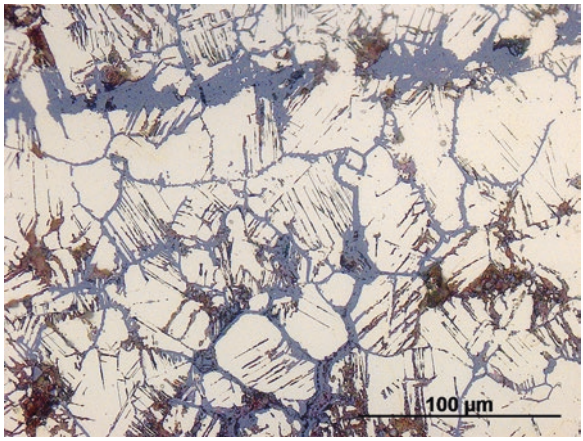

Fig. 3.9 Microstructure of a brass jug with 17% zinc and 1.4% lead from Khorasan region in Central Asia, dated to the second half of the twelfth century AD. Slip planes and grain boundaries are outlined by selective corrosion during burial

corrosion interface may be paramount, especially in authenticity studies, frequently required in the case of ancient bronze and silver artefacts. Microstructural features may be selectively etched or pseudomorphically preserved on metallic surfaces, which allows this technique to reveal micromorphology directly, as Fig. 3.9 illustrates.

A list of suitable etchants is given in the Appendix. A very comprehensive list of different etchants for all purposes is given by G.F. Vander Voort [75], whereas most conventional etchants and their applications are described in all the standard literature (see, e.g. Geels [20]; Lyman [34]; Petzow [46]; Vander Voort [76]). A useful online source of scores of different etchants is that provided by the Etchant's Database (http://www.steeldata.info/etch/html/overview.htm).

Etching must reveal microstructural characteristics, which are not yet evident in the as-polished condition and must produce contrast between the features of interest and the other microstructural components. Contrasting only by optical techniques will be reviewed in Sect. 3.2. Etching is a controlled selective corrosive attack, affecting preferentially a specific phase, by using a chemical solution, which is called the etchant. An etchant is a combination of either an acid or base with an oxidizing or reducing agent in a solute such as water or alcohol, but also glycerine or glycol or other media can be used. Aqueous solutions usually etch more rapidly than alcoholic solutions. By chemical etching, a surface relief is produced by local redox reactions, whose actual process and extent are based on the different local electrochemical potential of the microstructural constituents [46, pp. 40–43]. The local dissolution of some microstructural features changes the reflectivity of the surface by roughening or even staining it by the deposition of a thin surface film. The incident light then is reflected, diffracts or gets absorbed, or topography gives grey scale values by shadowing, producing an optical contrast. Colour contrast can best be achieved by the interference layer technique, which is based on coating the surface with interference layers by evaporation, sputtering or chemical deposition (see Bühler and Hougardy [12]). The latter is called immersion colour etching or tint etching, which can be performed without the need for additional technical

equipment (see Vander Voort [77]). Many of these colour etchants, also used extensively in this volume, were originally devised by Klemm [29, 30], Beraha [5, 6]; Beraha and Shpigler [7] and Vilella and Kindle [80]. Frequently, copper alloys etch rather quickly, especially in alcoholic ferric chloride, and dilution of some etchants with additions of alcohol may be necessary to prevent too rapid etching.

Contrast enhancement by etching is due to inhomogeneity within microstructures, and therefore the rates of surface-etchant interaction vary locally and temporally. Differences in phase compositions, but also large differences in lattice orientation and crystal imperfections, are contrasting features revealed by etching. Composition and physical condition of the specimen are factors that influence the time of etching. Two-phased or multiphased alloys generally etch more rapidly than single-phased alloys, because of the local difference in electrochemical potential of the phases, forming a corrosion cell with anodic and cathodic regions [46, pp. 40–43].

Displacements by cold working in certain regions are also readily attacked and produce a high contrast because of the differences in orientation of the reflected light, shown in Fig. 3.10, but also grain boundaries are nothing else than lattice defects and retain internal energy. This is why grain boundaries have a higher dissolution potential than the grains themselves and some etchants – usually strong oxidizing agents – reveal grain boundaries, whereas other etchants produce more uniform surfaces and reveal the different crystallographic orientation of grains, which are randomly sectioned in the polishing plane of the sample.

It should be noted that etching reagents can be used to produce very particular effects, which can introduce errors in the interpretation of microstructure, due to selective attack that some etchants may cause. Oberhoffer's reagent, for example, which is used to reveal segregation in ferrous metals, deposits copper from the solution on the phosphorous-rich regions of the sample and prevents any further attack to these parts, while segregation-free regions are deeply etched without bringing out the structure fully. Reagents which are based on sodium thiosulphate or potassium metabisulphite solutions such as Klemm's or Beraha's reagents form sulphide films on metal surfaces which show affinity to sulphur but only slightly affect regions

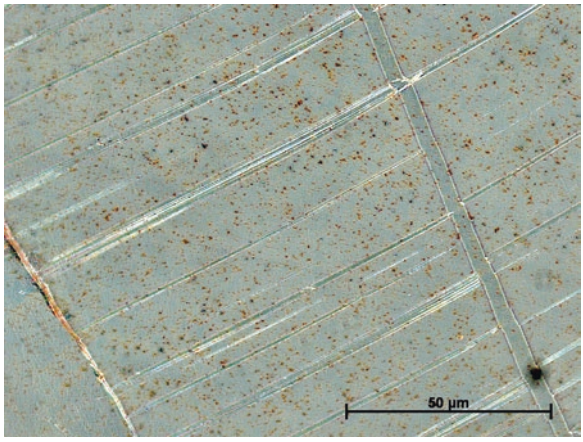

Fig. 3.10 Slip lines in gilded silver phalera from Uročišče Kruglik, Ukraine, dated to the end of the second century BC. The parallel steps on the surface become visible after etching with acidified potassium dichromate viewed with polarized light

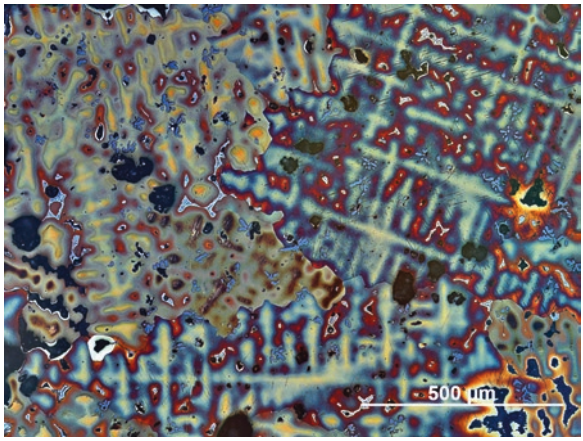

Fig. 3.11 Coarse crystallites of solid solution in the bronze part of a bracelet from the Royal tomb of Lori Berd, Armenia, containing dendritic micro segregations. Interdendritic tin segregation and $\alpha + \delta$ between primary α_{Cu}-solid solution is clearly revealed by etching with Klemm's reagent III

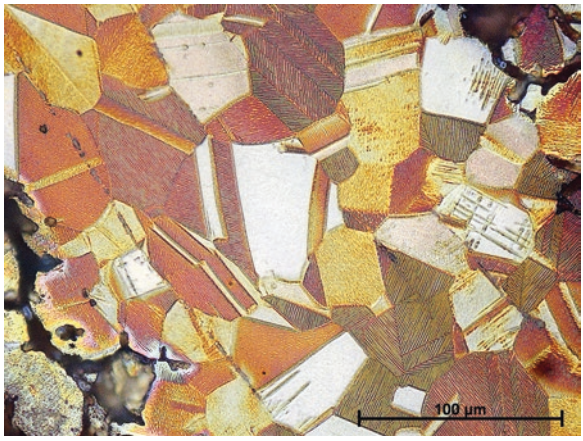

Fig. 3.12 Recrystallized α-brass of a gladiator helmet from Herculaneum (see also Figs. 3.21 and 5.17). Klemm's reagent II has produced pattern of parallel lines on the individual twins and grains which are related to their crystallographic orientations

with elements with low affinity to sulphur. For this reason, these etchants are very sensitive to the concentration gradients caused by segregation of alloying elements, as shown in Fig. 3.11, but also to crystallographic texture, revealing preferred orientations as can be seen in Fig. 3.12.

Indeed many standard etchants have been developed to evaluate the overall structure, but as this general requirement is not always achieved satisfactorily, double or multiple etching are sometimes employed, by using different etchants sequentially – mostly grain contrast etchants combined with grain boundary etchants. Colour etching procedures sometimes recommend attack polishing, some slight relief polishing or pre-etching with standard general-purpose etchants to achieve good results (see Beraha and Shpigler [7]; Vander Voort [77]). Increasingly, the authors have become aware of the advantages of colour etching in the preparation of archaeological material [68]. The reasons for this are, firstly, that grains can be delineated without deeply etching the sample, as in conventional etching, and that corrosion crusts are not necessarily disrupted by this technique. Secondly, the presence of casting segre-

gation is very sensitive to colour etching, and since many alloys retain some aspect of this, it is clearly visible in the etched sections. Care should, however, be taken to repolish the sample before long-term storage as corrosion may still occur in storage. Some samples with incipient bronze disease must be stored at relative humidity's less than 30%; otherwise, continued slow corrosion of them will occur. With fragile ironwork suffering from akaganeite corrosion, storage at less than 19% relative humidity may be necessary.

Most conventional etchants work by immersing the specimen in a suitable reagent, while others will not work without swabbing a cotton wool swab saturated with the reagent over the surface. At this point, it might be helpful to proffer some advice that there is a danger of scratching soft metals such as unalloyed copper, gold or silver, by swabbing with natural cotton, and therefore semi-synthetic viscose wool should be used instead. Some etchants have to be heated or even boiled, but most etching can be performed at room temperature. Heavily strained bronze sheet may etch in alcoholic ferric chloride, one of the standard etchants at a very fast rate, so some experience has to be gained in the length of time; a sample is submerged in an etching solution. The best course is often to immerse for a few seconds only and then gauge the result. If further etching is required, the sample can then be reimmersed for a further few seconds. Dilution of some of the standard etchants may be advisable in certain cases. Some colour etching processes take many minutes rather than seconds, and this has to be gauged carefully by the investigator depending on the alloying system involved.

A final instruction must be given concerning safety precautions, especially with the handling and storing of etchants. Most etchants are dilute chemicals with one or more active ingredients in a solute, and many etchants can be quite safely handled for specimen preparation. Indeed the single ingredients can already be dangerous, as highly concentrated acids or bases are needed to mix the reagents. Some ingredients are hazardous to the health, some are toxic, some are flammable, and some are strong oxidizing agents, while others are reducing, and mixing them together can result in violent or even explosive reactions. It is therefore essential to consult the Material Safety Data Sheets of the ingredients and the literature (e.g. Geels [20]; Petzow [46]; Vander Voort [76]). Some etchants like Beraha's colour etchants form hydrofluoric acid (HF) when ammonium difluoride (NH_4HF_2) dissolves and must be used and stored in plastic containers. Used etchants should not be disposed of except in specialized containers for safe disposal of laboratory waste.

3.2 Light and Electron Microscopy

3.2.1 Light Optical Microscopy (LOM)

Having created a flat and highly reflective surface, examination of the section can utilize the optical light microscope, preferably a metallograph, and samples can also be placed in the electron microprobe (EPMA), in the scanning electron microscope

(SEM), or analysed with X-rays such as X-ray fluorescence (XRF) or X-ray diffraction (XRD) techniques, all of which are invaluable in a comprehensive study of metallographic sections. All chemical and structural analysis should be done before etching the surface. Electron beam or X-ray analysis is non-destructive, and the specimens are kept ready for microstructural analysis, whereas all laser ablation (LA-ICP-MS or LA-ICP-OES) and especially glow discharge techniques (GDOES or GDMS) leave veritable craters on the surface and the specimen must be prepared again. Therefore, the first and basic procedure is to start with optical light microscopy (LOM) using incident bright-field illumination to get an overview of the section. For reflected light microscopy, the light passes directly onto the specimen surface and reflects back through the objectives to the eyepiece. By the absorption of some wavelengths of the incident white light, their complementary colours are reflected back, for which reason metals such as copper or gold appear coloured, whereas most metallic phases have a very high reflectivity over the entire range of the visible light and cannot be distinguished from each other. Therefore, phase contrast of opaque materials is very poor under bright-field illumination, but topographical features that are at an angle to the incident light reflect the light outside the objective lens and appear dark. Most metallic microstructural constituents show reflection differences which are too low in contrast and are not yet evident in the as-polished condition viewed in bright field, but pores and cracks, non-metallic inclusions, corrosion products and also many intermetallic compounds are already detectable by their lesser or greater reflectivity. They can be documented and quantified only by distinguishing them by their general optical characteristics, with no general necessity of exact identification (see Sect. 3.3.2). To enhance the optical contrast to reveal further microstructural details, the reflection capacity of the surface of the specimen must be increased by etching or by changing the illumination mode. Dark-field illumination or polarized light is an optical method to enhance the contrast without any alteration of the surface and should be used for further evaluation of microstructure [68]. The contrast produced by dark-field illumination is negative to that viewed in bright field as dark fractions appear bright and vice versa. Its application is useful for the identification of some non-metallic inclusions and for improving contrast to surface irregularities. Much more revealing than dark field is the use of polarized light, as many non-metallic compounds such as inclusions or corrosion products, but also some metals and alloys, are optical anisotropic. Most crystals except the cubic system are optical anisotropic and show double refraction of the polarized light from the surface. This birefringence produces manifold local colour effects without the need for additional etching, which can be intensified by tint etchants (Fig. 3.13). Crystals with a cubic symmetry or amorphous materials are normally optical isotropic, which means that their optical properties are the same and do not change the state of polarization by reflecting the light uniformly in all directions.

Optical isotropic materials do not respond to polarized light and remain dark. Anisotropy of non-metallic inclusions and isotropy of most metals have predestined polarized light microscopy for the identification of non-metallic inclusions in metals and alloys.

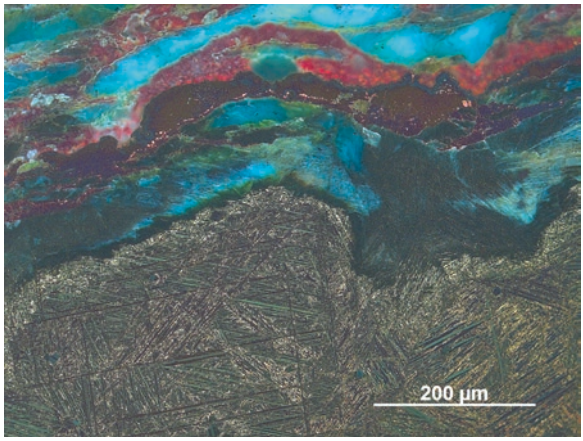

Fig. 3.13 Corrosion layer and microstructure of a high-tin (29% Sn) bracelet from Southeast Asia. The acicular β-phase needles are best viewed under bright-field illumination after tint etched with Klemm's reagent III, but viewed with polarized light, the β-phase is still observable and the alternate bands of the corrosion layers are revealed

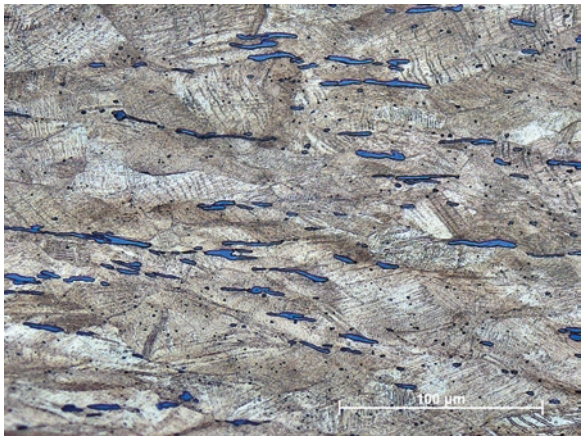

Fig. 3.14 Elongated copper sulphide inclusions within a cold-worked metal matrix of an Urnfield bronze cup appear blue-grey under bright-field illumination. Their mean volume fraction has been determined by area analysis A_A to be 1.5%

The best known application for ancient and modern alloys is to distinguish between cuprous oxide and copper sulphide inclusions, which both appear bluish-grey under bright-field illumination (Fig. 3.14). These two minerals can already be distinguished in the bright field with some experience, but they can be clearly differentiated by viewing in dark field or in polarized light (Fig. 3.15). Cuprite (Cu_2O) has a cubic structure and should appear dark, but it shows a strong anomalous anisotropy effect and gleams bright ruby red under dark-field illumination or polarized light, shown in Fig. 3.16.

The colour variation can be from yellow-red to pale reddish. Authenticity studies tend to take the axiomatic view that bright red crystalline cuprite is a good indication of the authenticity of the bronze or copper alloy concerned and is a distinction with a long pedigree and a general consensus. Cuprite is also one of the most common corrosion products of ancient copper alloys, which immediately overlays the original metallic surface [66]. Scott [64] and Piccardo and co-workers [48] have shown the colour change of cuprite from ruby red to orange and finally to yellow to

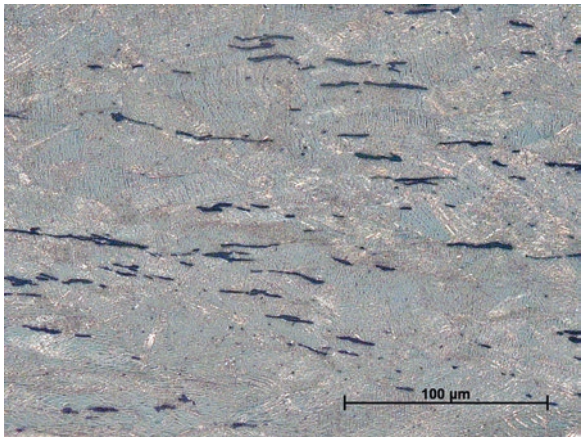

Fig. 3.15 Same as Fig. 3.14 viewed under polarized light. Copper sulphide inclusions and metal matrix are optically isotropic and appear dark

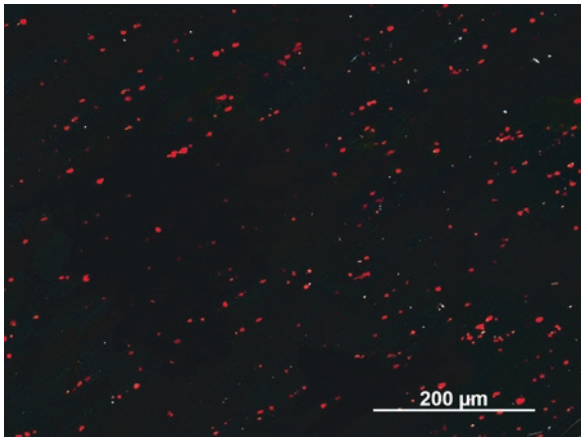

Fig. 3.16 Copper oxide inclusions in the Eneolithic copper disc from Hornstaad viewed under polarized light. Their volume fraction V_V has been determined by area analysis A_A to be 0.29% in total

be influenced by the increased presence of tin oxides in the corrosion layers of bronze, and an example is shown in Fig. 3.17.

A similar effect can be observed for brasses. Multiphase corrosion layers containing miscellaneous anisotropic phases may be differentiated and identified under polarized light, but also grain or dendritic structure and twins of some metals and alloys are revealed by polarized light due to their different crystallographic orientations. Ancient and historic metals which are known to be active to polarized light are antimony, arsenic, tin or zinc, but also some of their alloys [45], Tab. III). Figure 3.18 shows the grain structure of an Early Bronze Age tin bead from Southern Germany, revealed by polarized light.

Copper is an isotropic metal and inactive to polarized light, but arsenic is anisotropic, and von Schwarz [81] found anisotropy in high arsenical copper alloys. Figure 3.19 shows the microstructure a hypereutectic arsenical bronze viewed under polarized light. The position of this image is identical to Fig. 5.9, which has been recorded in

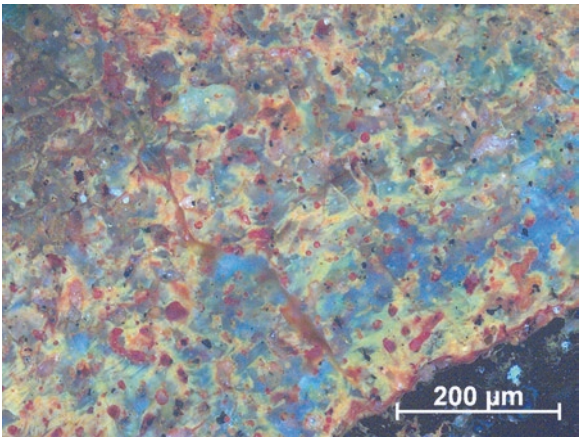

Fig. 3.17 Corroded surface of a life-sized Greek statue, so-called Agon, from a shipwreck found near Mahdia, Tunisia, viewed under polarized light. The alloy is tin-rich and the mineralized surface contains mainly of tin (hydro-) oxides with some relicts of cuprite

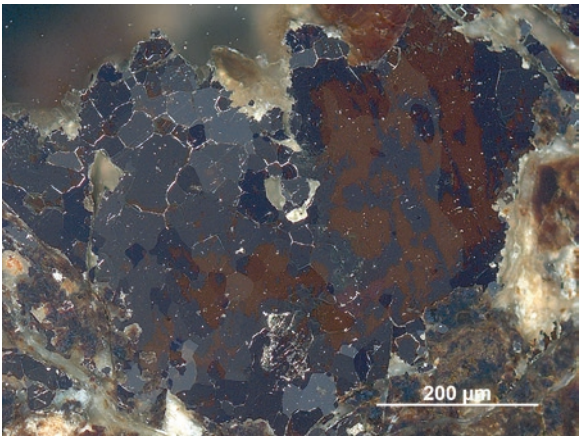

Fig. 3.18 Badly corroded Bronze Age tin-bead viewed under polarized light reveals grain structure of the metallic parts without etching

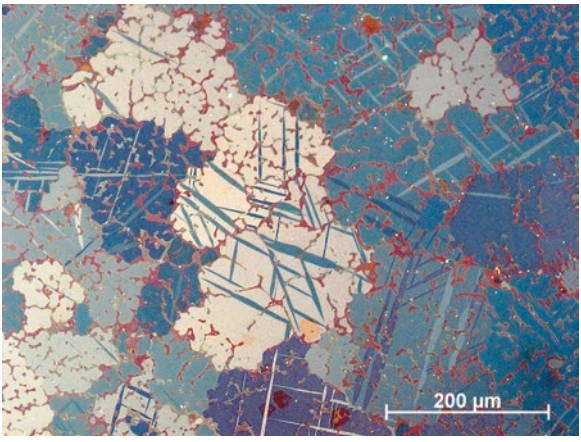

Fig. 3.19 Cross section of the arsenic rich part of the bracelet from Lori Berd, Armenia, viewed under polarized light, revealing coarse-grained aggregates of twinned α_{Cu}-Cu_3As eutectic

bright-field illumination, showing a dendritic as-cast microstructure. Viewed under polarized light, the equiaxed grains with twin bands appear, and EBSD measurement has revealed that it has a pseudo-hexagonal structure, corresponding to the mineral Domeykite, which is identical to the intermetallic γ-phase ($Cu_{3-x}As$) of the Cu-As equilibrium diagram (Fig. 5.7). Cubic α-Domeykite, shown in Fig. 4.18, does not respond to polarized light. Isotropic metals that are inactive to polarized light must be treated to create an optical effect by adequate etching procedures (Sect. 3.1.4).

3.2.2 Scanning Electron Microscopy (SEM)

Here we refer exclusively to scanning electron microscopy (SEM), as other electron microscope techniques such as transmission electron microscopy (TEM) need special specimen preparation, whereas specimens ready for light optical microscopical examination can directly be studied with high-resolution imaging and microstructural and microchemical analysis in the SEM. In the latter case, the specimen must be electronically conductive (Sect. 3.1.2) but can be examined in an etched or unetched condition, although usually the unetched state is preferred.

SEM and electron microprobe analysis have become common tools in material sciences as well as in the study of nearly all ancient materials over many decades (see Olsen [43]; Meeks et al. [36]). Cameca (Compagnie des Applications Mécaniques et Electroniques au Cinéma et à l'Atomistique) launched the first commercial electron probe microanalyser (EPMA) in 1958 [52, p. 2], and the Research Laboratory for Archaeology and the History of Art in Oxford has been engaged in the development of a microanalyser for archaeological applications nearly simultaneously [54]. The first commercial scanning electron microscope was produced by Cambridge Scientific Instruments in 1965 [52, p. 2], and a secondary electron image of an ancient granulation work appeared already in the same year [41, p. 226]. Schaaber [60] demonstrated practical application of the microprobe to metallography of ancient metals by analysing slag inclusions in Celtic and Roman iron finds, while Panseri and Leoni [44] examined nickel-cobalt segregation bands in an Etruscan spearhead. It is possible that Darling and Healy [13] published one of the earliest backscattered electron images of the microstructure of a Greek coin. Today many metallographic examinations of archaeological metals are totally based on SEM examination without any support of optical microscopy. Indeed, the SEM is one of the most versatile instruments for investigating ancient metals, but in our opinion, SEM cannot be regarded as a complete substitute for LOM. SEM offers several major advantages over the optical microscope such as much higher resolution, higher magnification, better depth of field and most of all its chemical- and structural analysis ability, but it provides no real colour differentiation, and many contrasts are more distinctly viewed with optical light. A skilled metallographer can identify and outline the phases and their distribution quickly and comparatively easy by the application of LOM. Another, but less objective reason is the aesthetics of well-prepared and proper etched microstructure viewed under an optical micro-

scope. An Instagram site by one of the author (Scott) called *Davidscottmetals* is a good illustration of the aesthetic approach to metallographic imagery.

There are numerous excellent standard textbooks devoted to principles of scanning electron microscopy and microanalysis, which should be consulted for further information and the deep knowledge they possess (see, e.g. Goldstein et al. [22]; Heinrich [25]; Reed [52]; Reimer [53]), but it is essential to the application of SEM in metallography to briefly introduce its basic function and mode of operation.

In the SEM a finely focused electron beam scans across the surface of the specimen and forms a two-dimensional raster of various signals point-by-point. These signals are based on the interaction of the beam with the target material, producing imaging signals and X-rays, which must be collected by an appropriate detector. For most conventional metallographic applications, the microscope column and the chamber must operate under vacuum conditions (10^{-3}–10^{-5} Pa) to avoid scattering of the accelerated electrons by gas molecules. Lang [32] showed that it can be useful to work at low vacuum (50 Pa) without conductive carbon coating to analyse carbon-nitride precipitations in Early Iron Age falcatae. These instruments operate with retained vacuum in the column, but with low vacuum in the chamber. The operator can vary the pressure – 10 Pa to 2700 Pa are possible in modern instruments – or must reduce the accelerating voltage to balance the charge of non-conductive substances for investigation without coating or other preparation techniques (see Goldstein et al. [22]; Stokes [71]). General terms for such an instrument are variable pressure SEM (VP-SEM), extended pressure SEM (EP-SEM) or environmental SEM (ESEM), but there also some other acronyms such as natural or atmospheric SEM (ASEM), which the latter is a little bit misleading, considering that average atmospheric pressure is more than 100,000 Pa. Working with low vacuum means that gas is present in the chamber and the beam electrons interact with gas and form a so-called skirt of scattered electrons. The skirt radius depends on working distance, pressure, beam energy and property of the gas (see Goldstein et al. [22]; Stokes [71]). For practical application of X-ray microanalysis in the VP mode, it should be clear that with increasing skirt radius, X-rays may be generated hundreds of microns away from the impact point of the beam and elements begin to appear in the spectrum which shouldn't be there according to the corresponding SE/BSE image (see Goldstein et al. [22]; Stokes [71]).

Again, in conventional metallographic work with the SEM, the sample must be conductive because the irradiated specimen is negatively charged by the beam. It must be vacuum resistant and stable against electron bombardment. In an electron microscope, an electron gun (thermionic W or LaB_6, or field emission cathode) emits a beam of electrons, which is accelerated towards the specimen and focused by electromagnetic lenses. The electrons of the beam collide with the atoms present in the sample so that the speed and direction of the incident electrons change; they are scattered both elastically and inelastically. Inelastic scattering means that the incident electrons lose energy during the penetration of the specimen surface. This energy may be transferred to electrons of the specimen atoms, generating an image and an analytical signal, or emitted as continuous X-rays, the so-called Bremsstrahlung, which is the main background of every primary X-ray emission

spectrum with energies from nearly zero to the maximum energy of the electron beam. If the transferred energy is high enough for a loosely bound valence electron to escape from the atomic shell and the kinetics are still high enough to get through the solid and leave the surface, it can be gathered by a positive biased collector as so-called secondary electrons (SE). Their exit energy is very low, and therefore only those that are generated at shallow depths of the order of a few nanometres are released from the surface. The intensity of secondary electrons is therefore dependent on the surface topography, where protruding positions emit more electrons than fissures and holes, where most electrons lose all of their energy and are reabsorbed. Secondary electron mode can be compared to the incident bright-field illumination in the LOM, as topographical features can be viewed with a very large depth of focus, whereas flat specimen in the as-polished condition do not show much contrast. SE mode is useful in examining the surfaces of objects, as shown in Fig. 3.20, fracture surfaces as shown in Fig. 3.21 and etched specimens, illustrated in Fig. 3.22.

The analytical signal is due to inelastic scattering by more tightly bound inner shell electrons, having the greatest binding energy, which requires higher energies to remove them from their orbitals and which is a less frequent event. When an electron in an inner atomic shell is ejected by an incident electron, leaving the atom ionized with an electron vacancy in its inner shell, it gets replaced by the transition of an orbital electron from a higher energy level. During this internal rearrangement, X-rays are produced, as the energy difference between the two levels is emitted. Therefore, each transition of electrons is characteristic for a certain energy level within the atomic union and the energy emitted as X-rays is characteristic for a

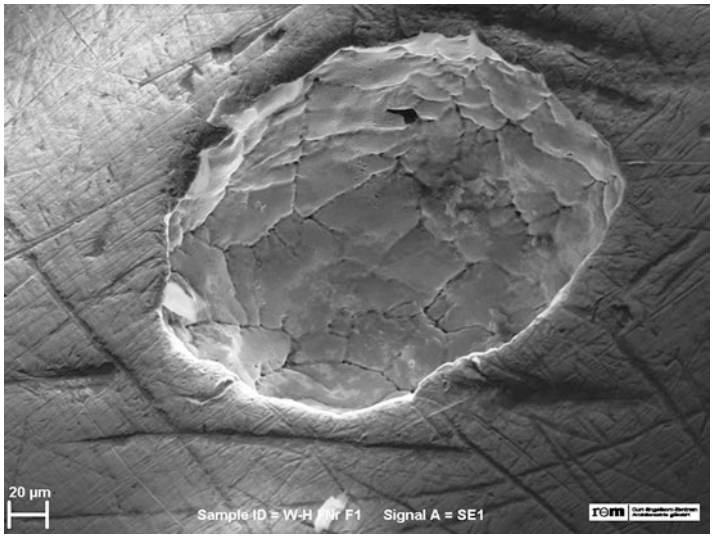

Fig. 3.20 Secondary electron image of the surface of an Early Iron Age gold ring from Worms-Herrnsheim burial showing deep blowholes

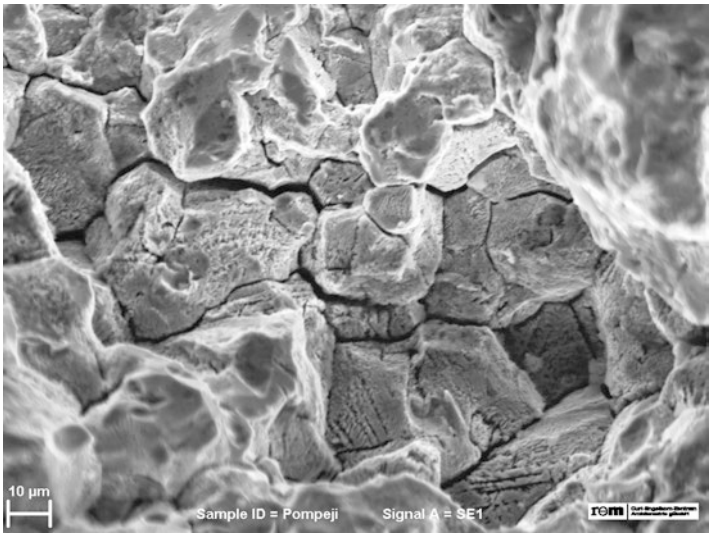

Fig. 3.21 Stress corrosion cracked brass alloy of a Roman gladiator helmet from Herculaneum, Italy (first century AD). Intergranular corrosion and some slip lines are visible in the fracture (SE image)

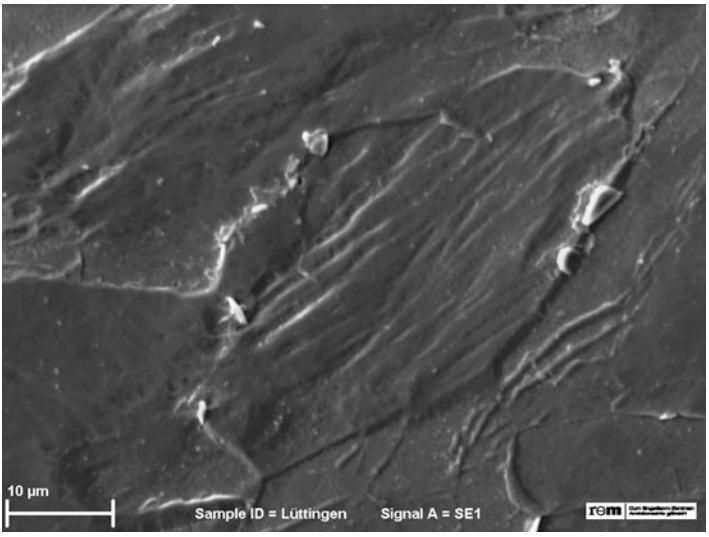

Fig. 3.22 Surface of a cold-worked iron chain link from a Roman mail shirt after etching with nital. Secondary electron image reveals spheroidal carbides at the grain boundaries

specific element. Notation K, L and M, which are used for X-ray emission lines, refer to the shell initially ionized, while Greek letters indicate the shell from which an electron originates to fill the vacancy, usually with a numerical subscript to denote the particular line of a series. Thus, when an electron is removed from the K orbital, being the innermost shell, and this electron vacancy is filled by an electron from an L level, the X-ray emission line is notated Kα, whereas if the electron is filled by an electron from an M level, the line is notated Kβ, or by filling other shells Lα, Lβ, Mα, etc., respectively (see Heinrich [25]; Reed [52]). The probability of the transition from L → K is always greater than that of the transition from M → K, but the binding energy increases from the outer to the inner shells as well as with increasing atomic number. Therefore the choice of accelerating voltage is depending on elements present within the target and must be balanced between the excitation energy needed and the background produced (see below). Measurement of the emitted X-ray signals can be performed by energy-dispersive (EDS) or wavelength-dispersive spectrometers (WDS), which instruments with the latter are traditionally called electron probe microanalysers (EPMA) with a much better spectral resolution and better detection limits, whereas energy-dispersive X-ray spectrometers (EDS or EDX) are commonly attached to conventional SEMs. It is possible to attach both EDS and WDS to a SEM, but the focusing geometry in an EPMA is designed for best angular and distance relationship between specimen, analysing crystals and detector to optimize analytical tasks, which is usually at the expense of the optical systems. A SEM is arranged for versatile applications and optimized to imaging methods.

Qualitative information can be obtained quickly by energy-dispersive X-ray spectrometry, but nevertheless quantitative chemical information is a basic task for electron microanalysis as it is generally to all X-ray spectrometry-based methods. Quantification can be achieved by different methods, but a correction of the matrix effects is essential, which is commonly applied in electron microanalysis by the so-called *ZAF* correction method (*Z* = atomic number differences influences the deceleration of electrons and background intensity; *A* = absorption of primary emitted characteristic X-rays; *F* = (secondary) X-ray fluorescence generated by characteristic and continuous X-rays). *ZAF* matrix correction procedures are nowadays software based, using tabulated values of constants. There are other approaches for correction procedures around, and again, standard literature should be consulted for basic knowledge and further reading (see Goldstein et al. [22]; Heinrich [25]; Reed [52]).

Standard-based methods are generally considered to be more accurate than so-called standard-less analysis but also more time-consuming, as sample and standard must be measured with the same parameters. Traditional standard reference methods usually calculate the concentrations *C* from the so-called *k* ratio of the matrix corrected intensities *I* of sample and standard after subtracting the background:

$$C_{\text{Sample}} = \frac{I_{\text{Sample}}}{I_{\text{Standard}}} \frac{(ZAF)}{(ZAF)}.$$

Standard-less methods have become more popular with computer-aided systems and high efficient silicon drift detectors (SDD), which are capable of processing high counting rates with comparatively high-energy resolution (≤121 eV for Mn-Kα are available at the moment). Most commercial EDX systems nowadays are installed with standard-less quantification software according to different mathematical and physical models, computer deconvolution of peak overlaps or stored standard references to compute concentrations. There is an ongoing progress in hardware and software technology to increase accuracy and precision of EDX analysis, and manufacturers have developed suitable user interfaces to make convenient handling available. The operators are therefore obliged to regularly control their results by measurements of appropriate standards under defined and reproducible conditions to ensure the accuracy of their analyses.

In contrast to most other analytical methods, the analytical data from X-ray microanalysis are highly space-resolved and provide direct information about compositional heterogeneity. Due to the finely focused electron beam and controlled scanning over the surface, the X-ray signals can be recorded in different ways. Micrometre-sized volumes of phases and particles can be analysed by point analysis, while line scans reveal the variation of selected elements along a line, which is, e.g. suitable to measure concentration gradients. A powerful application possibility is the two-dimensional mapping of X-ray intensities, which provides information on the spatial distribution of constituents within a selected area of interest (Fig. 3.23). After proper quantitative elemental map acquisition, modern EDX systems offer software tools that turn individual distributions of elements representing a chemically defined component of a complex multiphase material into a so-called phase image (Fig. 3.24), which is calculated by the spatial variability of specific X-ray intensity ranges at each pixel in the map (see Kotula et al. [31]).

Elastic scattering of the incident beam electrons is due to the retardation in the Coulomb field associated with atomic nuclei and implies almost no transfer of energy to the specimen electrons. When charged particles pass through the Coulomb field of a nucleus, they change direction, and the beam expands due to magnitude of

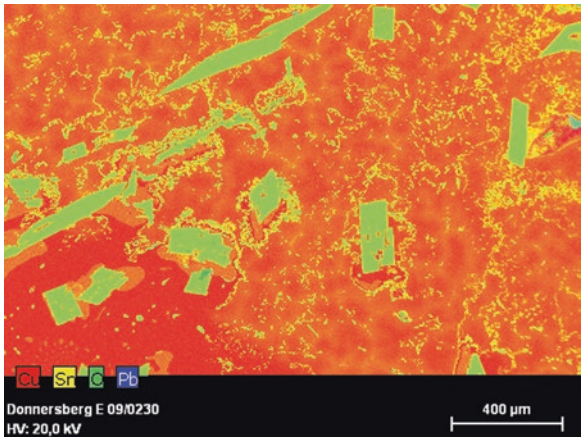

Fig. 3.23 Quantitative element map of a bronze casting waste from the oppidum on the Donnersberg in the Palatine Forest, Germany, showing the inhomogeneous distribution of tin and the presence of oxide phases

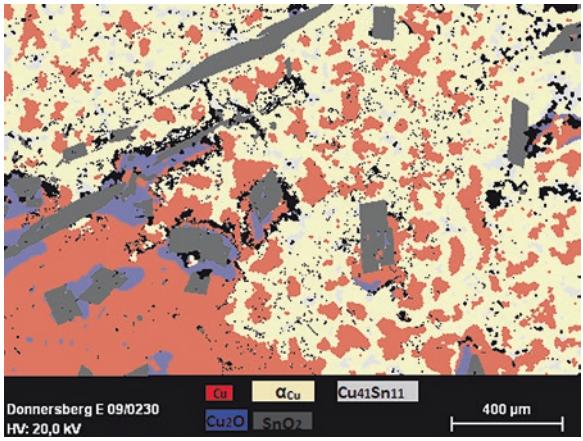

Fig. 3.24 Phase image created from quantitative element map (Fig. 3.23) showing selective internal oxidation of tin from a bronze alloy with precipitations of SnO_2 and formation of Cu_2O within the de-alloyed areas

the Coulomb force. Accumulated elastic scattering events that deviate the primary electrons' trajectory by an angle greater than 90° lead to an escape of so-called backscattered electrons (BSE) back out of the specimen's surface with nearly an equal energy (Heinrich [25], pp. 241–53). The deceleration of accelerated electrons and the amount of shift in direction depends on the Coulomb interaction between the positive field of the nucleus and the negative bound electrons. Coulomb force is proportional to atomic number of elements, for which reason the so-called backscattering coefficient, which is the ratio of backscattered to primary electrons incident normal to the flat surface, increases with increasing atomic number of the elements of the specimen.

Therefore, the image created by BSE signals is called compositional or atomic number contrast, which reflects differences in atomic number of elements or average atomic number for alloys and compounds (Fig. 3.25). BSE imaging is a very effective tool for metallography combined with X-ray microanalysis, but X-ray microanalysis should only be acquired together with a corresponding BSE image which shows a much better resolution than can be achieved by X-ray elemental map (see Goldstein et al. [22]). Indeed the backscattered electron image contains two types of information: compositional and topographic. In order to form an image with backscattered electrons, a semiconductor detector that has ring geometry is usually placed in their path above the sample to increase the angle of collection. The detectors have the capabilities of summing the segment's output signal eliminating topographic information and producing a pure compositional signal. Operating the BSE segments in pairs and then subtracting the segments' output signal yields topographic images (Fig. 3.26).

The backscattered signal in particular carries information about the crystal lattice and its orientation relative to the primary beam. Similar to optical isotropy and anisotropy, the proportion of backscattered electrons also depends on crystallographic isotropy or anisotropy which is associated with orientation and crystal properties. Lattice planes vertical to the surface allow electrons of a normal incident beam to penetrate more deeply into the lattice where they get absorbed, whereas

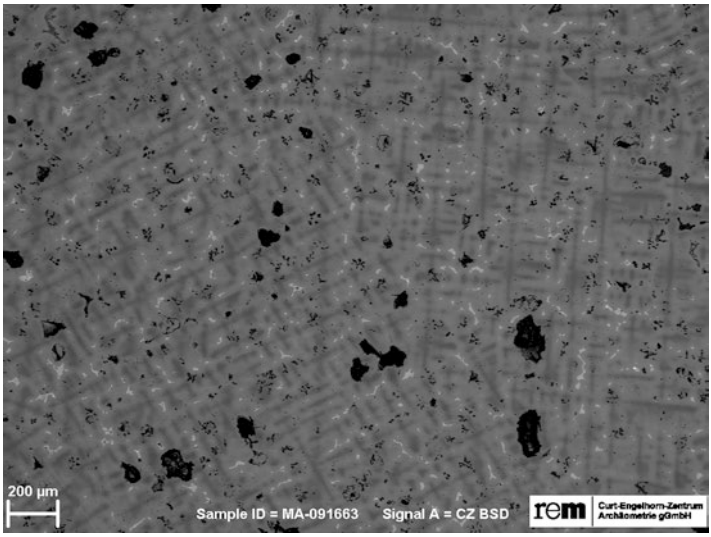

Fig. 3.25 Backscattered electron image of the bronze part of a bracelet from the Royal tomb of Lori Berd, Armenia. Compositional contrast reveals dendritic micro segregation (see Fig. 3.11). The α + δ shows the highest backscattering coefficient, whereas copper sulphides and pores are black

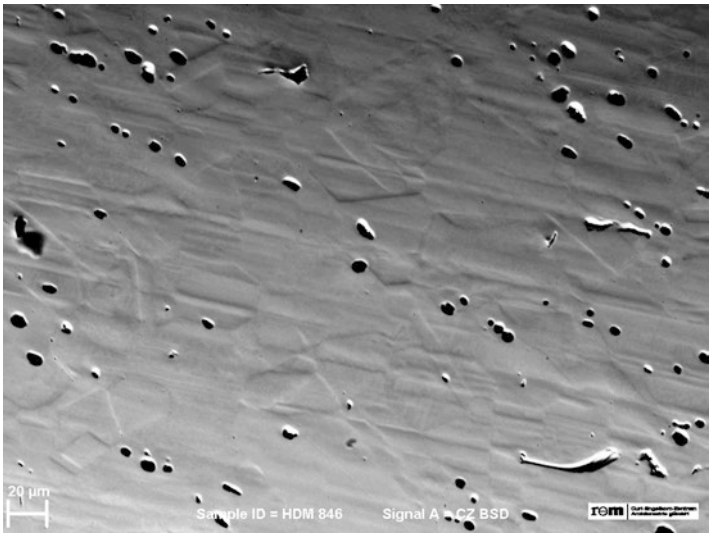

Fig. 3.26 Surface topography of the copper disc from Hornstaad with equiaxed twinned grains. The specimen is attack polished and imaged with two positively biased and two passive segments of the BSE detector

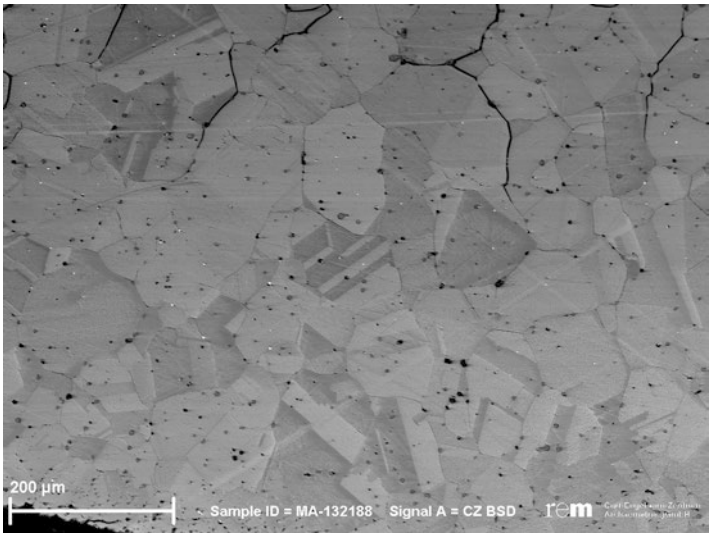

Fig. 3.27 Electron channelling contrast from a copper alloy belt sheet from Boğazköy, Turkey, showing grain boundaries and annealing twins. The specimen is attack polished, tilted and imaged with a positively biased BSE detector

planes parallel to the surface show a higher backscattering coefficient. The contrast resulting from crystallographic anisotropy is called orientation or channelling contrast. This contrast is usually weak, but by increasing the beam current and tilting the sample, grain boundaries, for example, can be visualized by BSE without etching, because of the different crystallographic orientation of the grains resulting in different grey levels shown in Fig. 3.27.

Channelling contrast by backscattered electrons is a subtle effect, and the evaluation of channelling patterns, which correspond to the lattice diffracting crystal planes, has been a useful application but on an academic level only. Crystallographic surface orientation evaluation by electron backscatter diffraction (EBSD) has become an additional and powerful standard characterization technique to scanning electron microscopy in metallography within the past two decades (see Rollett and Barmak [55]; Schwartz et al. [63]). The application of this technique to ancient metals has been very limited so far (e.g. Northover and Northover [40]). EBSD is performed by tilting the sample at a large angle of incidence of 70° to maximize the backscattering coefficient. Most systems use a forescatter geometry where diodes are mounted front of the sample near the phosphor screen to capture electrons with lower incidence scattered in a forward direction, called forescatter electrons (FSE). Fully automated commercial EBSD systems are readily available and can give extensive crystallographic orientation information of large areas in a sort time. EBSD is suitable for phase identification and for determination of orientation, size and shape of individual crystals quantitatively (see Schwartz et al. [63]).

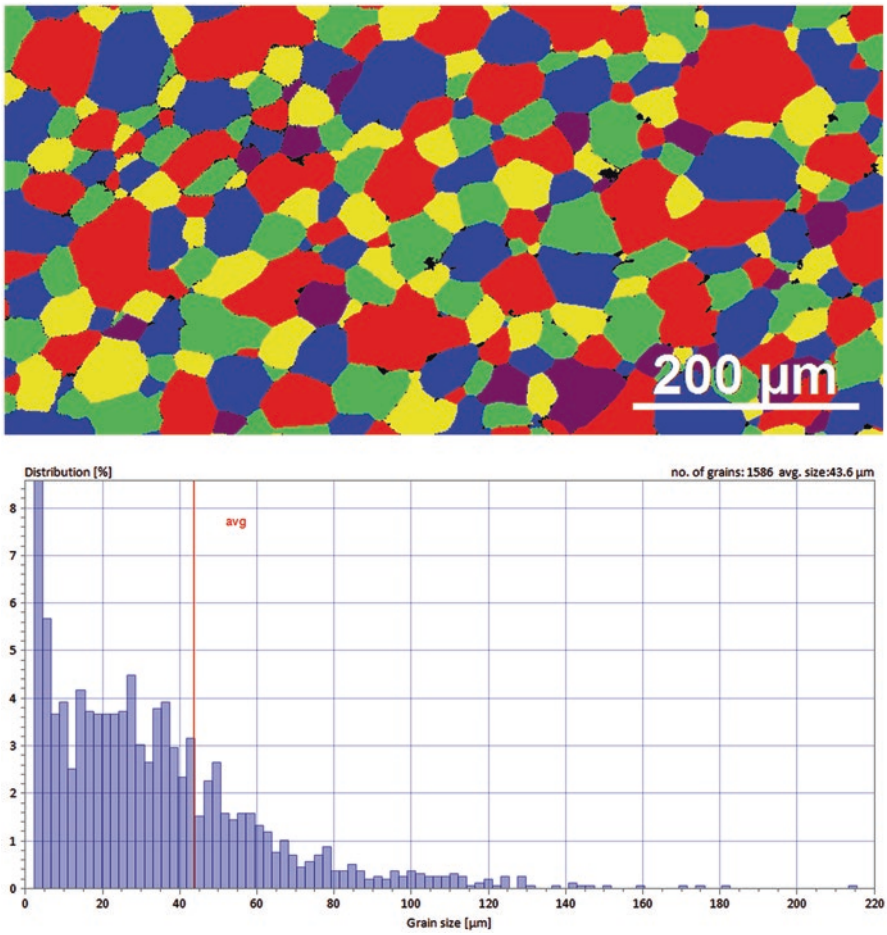

Fig. 3.28 EBSD grain size map with randomly coloured grains and grain size histogram of the recrystallized bronze alloy (11.7% Sn) of a belt plate from the Early Iron Age hoard from Fliess in Tyrol. (Image L. Palasse, Bruker Nano GmbH)

Figures 3.28 and 3.29 show EBSD pattern of a fully annealed Early Iron Age (HaC) bronze belt plate from the hoard of Fliess in Tyrol (Austria), with grain size distribution. It should be noted that grain size and orientation have been quantitatively acquired within one map in 20 min. EBSD pattern quality is extremely sensitive to surface disturbance, since the signals are generated from a layer about a few nanometres from the surface [55]. Any deformation or surface layer will disturb the diffraction bands and results in a loss of intensity and contrast, for which reason an accurate sample preparation is especially required, more so than for any other microscopical technique (see, e.g. Vander Voort [78, 79]; Witt and Nowell [83]).

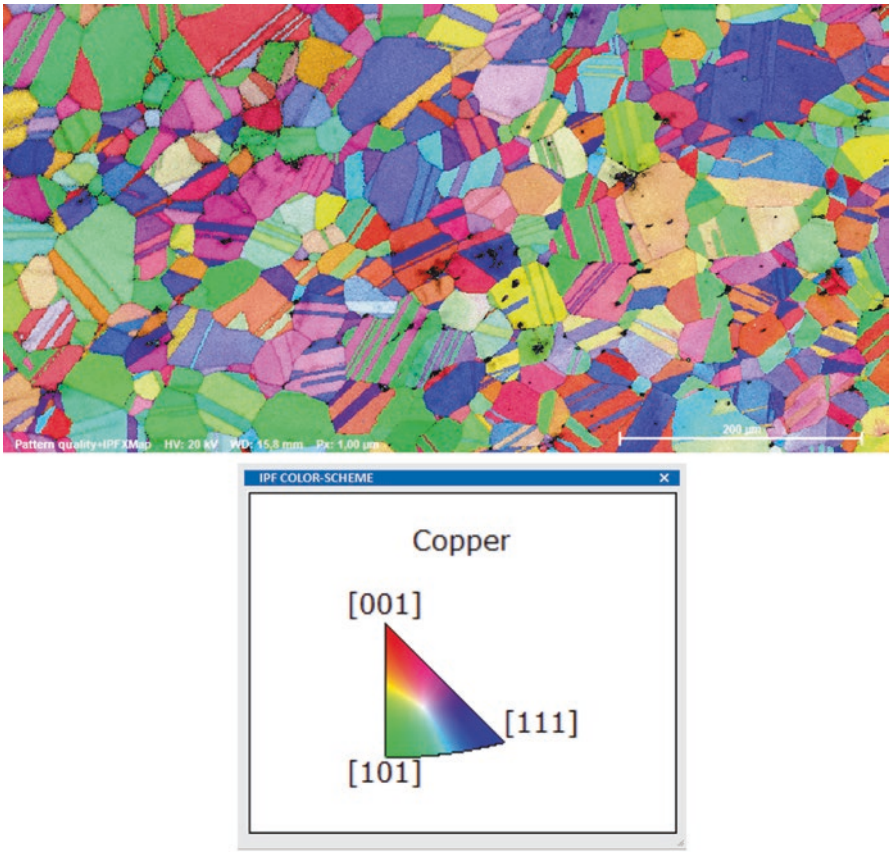

Fig. 3.29 RGB colour-coded EBSD orientation image with inverse pole figure (IPF) for the cubic class showing recrystallized α_{Cu}-solid solution grains with twins. Intermediate orientations are coloured by a mixture of the primary components red, green end blue. (Image L. Palasse, Bruker Nano GmbH)

The combined application of LOM and SEM is a powerful tool in the investigation of ancient metals, because the same specimen can be used without additional sampling.

For relocating regions of interest from light microscope to scanning electron microscopy, a significant microstructural feature is needed, which is not always the case, or hardness indentations can be used to mark the area of interest. For small samples from archaeological materials with some individualistic corrosion pattern, the relocation is usually not such a problem, but with increasing sample size, it can become quite time-consuming. Therefore, some microscope producers have developed a combined hardware and software solution, which is called correlative light electron microscopy (CLEM). It allows the flexible transfer of specimens from one microscope system to another without intermediate preparation steps.

3.3 Image Analysis and Quantitative Metallography

3.3.1 Image Analysis

After proper specimen preparation, the components of microstructure have to be revealed, identified, quantified and finally documented. Documenting important points in the microstructure at suitable magnifications is an essential task in the metallography of ancient metals. As mentioned before, sampling and analysing rare and valuable objects are very limited in scope, and the examination often cannot be repeated. Tiny and corroded samples are prone to be extruded by polishing and must be treated with care. Non-metallic inclusions or corrosion products that are present when the section is examined in the polished condition should be noted and evaluated before etching. Otherwise, they will either be dissolved or partially obliterated by etching. Especially the identification and quantification of non-metallic inclusions are tasks of increased significance for understanding ore sources, metallurgical processes and the history of implements (Sect. 4.4).

The early metallographers had to sketch their observations graphically by hand or make imprints directly from the etched surface, as Alois von Widmanstätten and others did with meteorites and wrought iron [69]. The adoption of photography to microscopic observation to document microstructure directly took place in the second half of the nineteenth century, which has been part of Henry Clifton Sorby's pioneering work [69]. Early metallographic microscopes had to use external cameras with additional oblique illumination, because of the low intensity of the illumination sources available [69]. Later microscopes had electric illuminations integrated and special attachments for a camera above the eyepiece. Professional metallographic microscopes, so-called metallographs, have been large instruments with integrated illumination source but with a separate attachment for the camera to permit permanent recording of the microstructure during microscopical observation [28, 58]. Today the illumination system is mounted beneath the specimen stage, and the camera is usually attached to the binocular head with a side port as a built-in integral part of the construction, connected directly to a display monitor of a computer with digital image software.

It is obvious that the documentation by photography is important in metallography to reproduce microstructural features observed and to make them comprehensible to others. Indeed, the earliest metallographic observations on prehistoric metals have still been recorded only through drawings (e.g. Rupe [56]); albeit further publications about metallographic studies of different ancient metal objects appeared, a few years later do already show micrographs on a respectable level [18, 19, 23, 24, 35].

Quantitative data of microstructures have been manually acquired by visual comparison, direct measurements at the microscope using inserted graticules in the ocular, or by grids applied to micrographs [14, 73, 75]. Scanning machines and television-equipped image analysers have been developed from the 1960s to 1980s [14, 17]. Nowadays, digital image acquisition has more or less totally replaced

analogue photographic techniques, and quantification is performed by computer-based digital image analysers [20, 57, 84]. As a basic principle, the digital image and the analogue photomicrograph are both two-dimensional reports from a two-dimensional view of a three-dimensional structure (see below). Indeed the major difference between digital and analogue imaging is that digital data are already stored as discrete picture elements (pixels) arranged in a regular two-dimensional grid. The digital image is therefore a function of two coordinates, meaning that each point P is at a specific location within a defined area A, each representing a different level of intensity. Therefore, all points or pixels forming an image with spatial arraignment of different intensities, grey levels or full colour, which characterize phases, interphases or pores, are captured. The fraction of all pixels with a specific intensity or colour represents the area fraction of each constituent of interest in the image. These defined positions of microstructural constituents render the image ready for automatic or semi-automatic measurements of size, geometry and fraction of microstructural constituents (see below).

3.3.2 Quantitative Metallography

Interpretation of microstructure under the microscope involves a high degree of empirical deduction. The identification of constituents is a common problem, but with skill and experience, it is possible to gain a detailed understanding. The application of electron microscope with its chemical and structural analysis ability has become a common tool in metallography, and it is suitable for identifying unknown phases by its variety of analytical techniques of characterization (Sect. 3.2). Finally, phase identification, indication of deformation, annealing or transformation processes and solidification structures still require a qualitative description of microstructure, though a micrograph is no description of condition of isolatable features but an experimental measurement of a system of interacting parts. Therefore, structure and mechanical properties of materials are strictly correlated. The determination of the relative quantity of constituents, whether it is a single-, two-phase or multiphase system; the presence and morphology of inclusions, pores and precipitations; or the relative specification of size of grains, such as descriptors of coarse or fine, would be another qualitative visual judgement. Indeed metallographers realized quite early that composition connects linearly with percentages of constituents and that there must be correlation of the microstructure with mechanical properties of materials [69, pp. 240–2].

Structurally, metals are made up of different phases, inclusions and pores, whose volume percentages, distribution, size, shape and orientation affect their properties. Therefore, the quantification of features visible in metallographic sections is essential for the understanding of relationships in microstructure. The quantitative characterization of this microstructural geometry is usually called stereology or quantitative metallography [14, 73].

It is beyond the scope of this chapter to cover the whole range of this topic, and standard monographs should be consulted whenever a quantitative evaluation is attempted (e.g. DeHoff and Rhines [14]; Exner and Hougardy [17]; Ohser and Mücklich [42]; Russ and DeHoff [57]; Underwood [73]). The application of stereological principles involves understanding the fundamental nature of microstructure and metallographic principles: firstly, traditional metallographic specimens are two-dimensional sections through three-dimensional solid bodies with spatial distributions and shapes of phases. From this two-dimensional view of a three-dimensional structure, planar data are obtained, which must be translated to spatial estimates of structure. To characterize microstructural features, a number of symbols and notations are advised by the International Society for Stereology ([20], tab. 17.1; [73], tab. 1.1; [75], tab. 6-1). Each notation is usually a combined term, which represents a geometrical element within a specific dimension. Conventionally, ratios are written as subscripts instead of fractions, in which the subscript indicates the unit of interest. So, for example, the notation N_A for number density is equivalent to $\frac{N}{A}$, which indicates the number N of a feature of interest per unit test area A [17, 73]. The basic notations and equations used throughout the book will be introduced in this chapter.

A planar section of a microstructure consists of areas, lines and points, which are in fact sections through particles, grains or interfaces, shown in Fig. 3.30. The area occupied by each constituent in a two-dimensional section is proportional to its three-dimensional volume, the line correspond to surface and point to a line in a solid body. Therefore, volume fraction V_v is considered to correspond to area fraction A_A or lineal fraction L_L or point count P_P (see below). Thus, the basic and simplest stereological equation is $V_v = A_A = L_L = P_P$ (e.g. Exner and Hougardy [17]). In practice are all microstructural components given in volume fractions, which are referred to as the unit volume of the microstructure. Therefore, the sum of the volume fractions

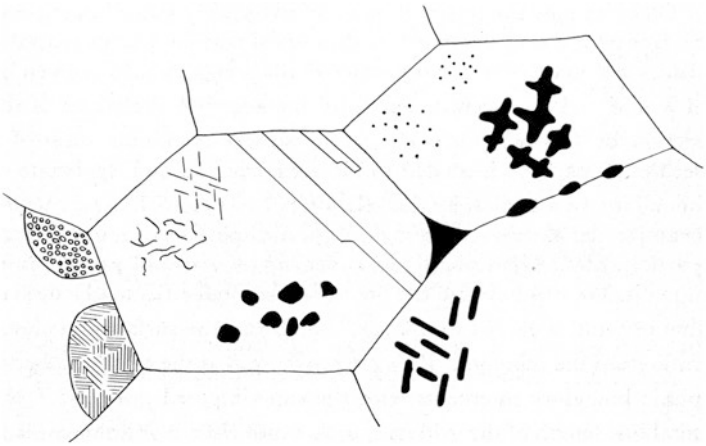

Fig. 3.30 Schematic illustration of a plane section through a polycrystalline body containing isolated microstructural features. (After Brandon [11])

of all phases in the test unit must be equal to one or, given in percentages, equal to 100%. Consequently, the volume fraction of a microstructural component must be in the range $0 \leq V_V \leq 1$ [21, p. 429]. Pores are by definition hollow, but in stereological practice, they are space filling volumetric elements like particles and must be treated as a microstructural component of equal value like a real spatial phase.

Furthermore, a metallographic section is a more or less arbitrary sectional view through the geometry of a particular microstructure. This implies that geometric shapes and quantities of constituents in the microstructure cannot be uniform or regular, and no constituents are exactly alike. Therefore, the problem of characterizing of a three-dimensional microstructure must rely on simplifying assumptions. Thus, any measurement of size, distribution or arrangement must be based on the general assumption that there is a certain probability of occurrence of events and that where the number of items is large, their distribution should be commonly described as Gaussian, even if the latter in many practical cases is not applicable. It becomes obvious that quantitative microstructure characterization can only be determined in statistical terms, so that the measurements must always be processed using an appropriate statistical procedure. Consequently, a metallographic specimen must be representative of the material, which is hundreds or thousands of times larger than the microstructure viewed under a microscope. Furthermore, the measured results should be comparable and the measurement reproducible. Representativeness and reproducibility are rarely given in studies concerning samples from objects of high cultural value. It is easy to understand that the application of stereological principles to archaeological and historical metals is limited and actually not regularly performed; nevertheless, it is useful to take the idea on-board and develop it for the future.

Before evaluating the practicality of quantitative methods to ancient metals, some general and historical aspects should be reviewed. According to Smith [69] scientists already realized the correlation between temperature and grain size in the eighteenth century by experiments and macroscopic observations of fractures. It is said that the first quantitative measurement using a microscope had already been performed by the French geologist A. Delesse, in 1848. Delesse demonstrated the proportional relation of area and volume in a random cross section [14, pp. 1–2]; 73, pp. 25–6], even though the relationship between grain size and mechanical properties, such as cold workability, had not been studied systematically by microscopy until the end of the nineteenth century [69, p. 241].

The relationship between heat treatment and microstructural geometry has been studied by measurements of lamellar spacing of pearlite or average grain intercept upon random sections [14]. Grain size estimation and the determination of volume fractions of particular constituents have been the oldest and are still the most common performed stereological measurements. To make a sound quantitative study of a metallographic specimen, several basic stereological measurement procedures and devices for quantitative analysis have been developed and improved, whereas many of these are now made obsolete by digital imaging technology. Nevertheless, it is useful to know the different methods, as some partly corroded samples do not allow standard quantitative digital image analysis, but for example, grain size or

volume fractions of specific microstructural constituents can be determined by manual measurements of microstructural images.

3.3.2.1 Methods of Measuring

3.3.2.1.1 Comparison Methods

Indeed, stereological measurements were laborious and time-consuming before the introduction of digital imaging technologies. Therefore, metallographers, especially in industrial quality control, wanted quick and easy methods for characterization of microstructures. Standard chart methods were introduced in the 1920s and were extensively used to estimate grain sizes, volume fractions and shapes of inclusions, pores or particles [75, p. 414]. Comparison charts are most simply used as wall charts or for direct comparison with the microscopical field in view, employing a recommended magnification, to select the most representative chart compared to the microstructure under investigation. Chart comparison ratings are generally semi-quantitative, subjective and not reproducible but sufficiently accurate for most commercial purposes. For research work, they should be replaced by stereological methods [17, pp. 83–87; 75, pp. 440–445, 502]. In spite of this, they are still in use, because they are fast and convenient to employ.

Grain sizes on worked objects can be measured using a grain size comparator eyepiece such as the graticule shown in Fig. 3.31 or compared standards given as wall charts. The most commonly used scale is that of the American Society for Testing of Materials (ASTM). By direct visual comparison at various magnifications, the ASTM number can be determined (see below). The ASTM has prepared a set of

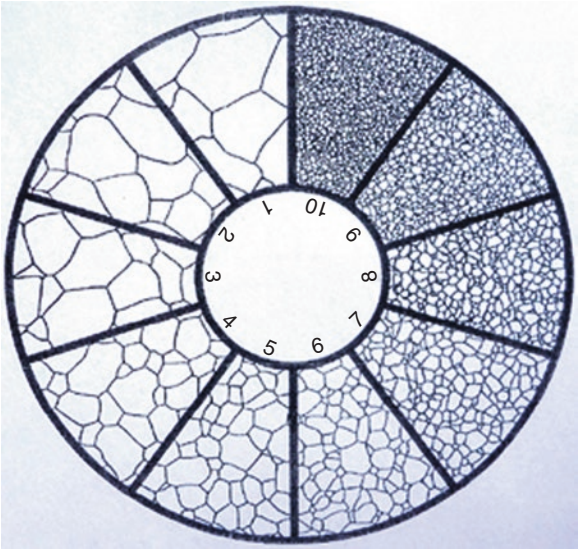

Fig. 3.31 Grain size eyepiece reticule for untwinned grains. For use with a 10x objective lens

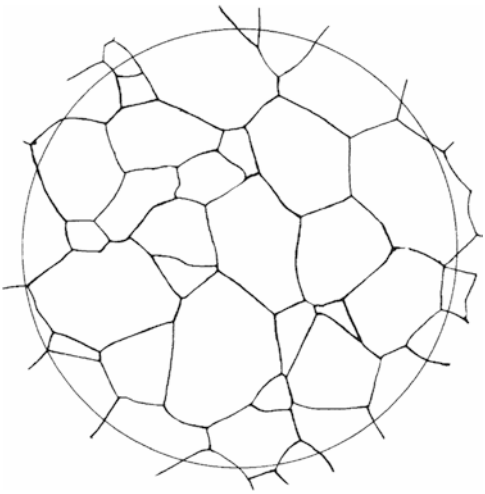

Fig. 3.32 ASTM grain size number 3 from Plate I for untwinned grains after flat etch at 100x magnification. (From ASTM E-112)

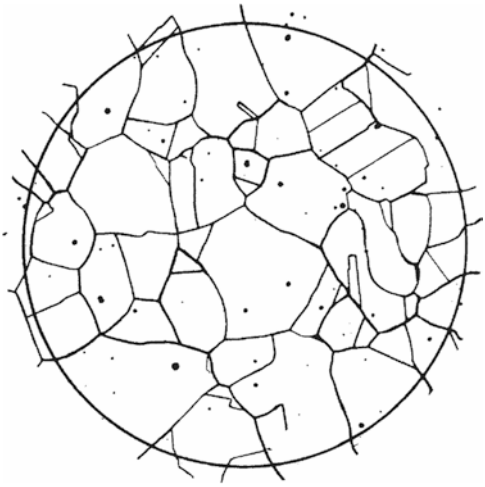

Fig. 3.33 ASTM grain size number 3 from Plate II for twinned grains after flat etch at 100x magnification. (From ASTM E-112)

standard charts for ferrous and non-ferrous materials, classified in four categories according to the appearance after etching and the absence or presence of twins, for which two examples are reproduced here in Figs. 3.32 and 3.33.

Great accuracy in this type of measurement is seldom required; what is useful is the approximation to an ASTM number that can readily be compared by another investigator. On the other side, it must be pointed out that great accuracy in this type of measurement cannot be achieved and bias will be introduced, which is usually 0.5–1 grain size number lower (ASTM E112-10). ASTM scale has been frequently used for the classification of grain sizes of archaeological iron objects (e.g. Piaskowski [47]; Pleiner [49]). The comparison chart method has also been the traditional approach for rating the inclusion content of steels. Vander Voort [74] has

given a detailed review about different charts and their application to the rating of non-metallic inclusions in modern steels. Comparison charts, such as the Swedish Jernkontoret or the German DIN 50602, have regularly been used to rate slag inclusions in archaeological wrought iron (e.g. Eichert et al. [15]; Hošek et al. [27]; Pleiner [49, 50]). Most of these charts were designed to categorize specific inclusions of steels, others to cover a wider range of ferrous alloys, but all of them have been developed using modern indirectly smelted iron, whose non-metallic inclusions originate from other metallurgical processes than ancient bloomery iron and do not adequately reflect the appearance of inclusions in ancient steels.

3.3.2.1.2 Feature Count

One basic stereological measurement is based on counting numbers N of individual features within a certain unit of interest, which can be a line L, an area A or a volume V, to obtain a representative average value. The number N of a specific microstructural constituent x is a fraction of the counted number of constituents of interest and the test unit. Therefore, N_L is the mean number per unit length (mm^{-1}), while N_A is the mean number per unit area (mm^{-2}) and N_V is the mean number per unit volume (mm^{-3}).

3.3.2.1.3 Point Counting

The point count method refers to the number of test points that fall in the unit of interest. The point fraction P_P is the ratio of the number of points in microstructural components of interest x to the total number of test points P_T in the test unit: $P_P = \frac{P_x}{P_T}$. This unit can be a certain test line, where the line intercept count P_L is the number of point intersections of this line (mm^{-1}), whereas P_A is the number of point intercepts in an area with regularly arrayed points (mm^{-2}). Again, this method is based on the general assumption that there is a certain probability that a randomly chosen point will include the microstructural component of interest. There can be confusion between number counting and point counting as they can be the same in certain cases, such as single-phase structures, so $P_L = N_L$. In a two-phase or multiphase microstructure, $P_L = 2\,N_L$.

3.3.2.1.4 Lineal Analysis

The lineal intercept method is employed randomly, or better using uniformly parallel arranged straight lines across the microstructure. The lineal fraction L_L is the ratio of the sum of individual lengths intercepted by microstructural constituent of interest L_X, divided by the total line length L_T: $L_L = \frac{\Sigma L_x}{L_T}$.

3.3.2.1.5 Areal Analysis

Area fraction A_A is the ratio of the sum of areas of microstructural constituent of interest A_x per total test unit area A_T: $A_A = L_L = \frac{\Sigma A}{A_T}$. Areal analysis is a planimetric method and can nowadays be performed with computer-aided digital image analysis. Before, manual area analysis must have been a troublesome undertaking, which involved the measurement with a planimeter, or cutting out the areas of interest from a photograph and comparing the weights of the pieces with the total weight of the photograph [73]. Area fraction has generally rarely been used, but Emmerling [16] applied this technique by cutting photographs to determining the volume fraction of pearlite and ferrite in prehistoric steel, which is now of historical interest.

The introduction of computer-based digital image analysis enabled high-speed (semi-) automatic image data acquisition. Automatic image processing techniques are usually based on image segmentation, which separates a digital image into sets of pixels sharing certain characteristics. These clusters of pixels should ideally correspond to a certain microstructural component, which can be characterized by contrast differences. For quantitative digital measurements, most basic stereological equations are still valid, but many classical stereological methods have become superfluous. Volume fraction V_v still equals area fraction A_A, which still equals point fraction P_P. The point fraction P_P would theoretically best denote the ratio of the pixel of interest to the total number of pixels of an image, but pixels are no points, which are dimensionless. Pixels have a finite area and are therefore generally thought to represent the smallest single components of a digital image. Therefore, area fraction A_A is now the quotient of N_p, the number of pixels of a determined phase and N_0 the total number of pixels in an image: $V_V = A_A = \frac{N_p}{N_0}$ [84].

3.3.2.2 Practical Application to Prehistoric and Historic Metals

Theoretically all stereological measurements can be used for ancient metals too, but quantitative characterization of microstructure is not often used for the metallographic investigation of ancient metals. Therefore, the real additional benefit of adopting every current practice in obtaining meaningful stereological data is not in sight at the moment, because of the lacking of statistical relevant data. Hence, we refer to the most regularly used measurements, their practical application and their values.

A general restriction to make a sound and representative quantitative study is often the small sample size or the condition. Surface corrosion and deep pitting corrosion sometimes do only allow the investigation of selected areas at high magnification, but increasing the magnification means reducing the observation area. Therefore, sizes and distribution of microstructural features are biased and require a higher number of areas observed to reduce the standard deviation, if possible.

A very important task for quantitative metallography is the quantification of volume fraction V_V of non-metallic inclusions (NMI) in modern as well as in ancient metals. Non-metallic inclusions are nearly always present in ancient metals, and in Sect. 4.3, the diversity and origin of them in the different alloys will be explained. Size, amount and composition of NMIs have a significant influence to mechanical properties of metals, but especially in ancient metals, they are a useful information source for metallurgical process applied (Sect. 4.3). The orientation of the plane-of-polish influences significantly inclusion rating, as orientation change, shape, number and distribution of the inclusions change [74, p. 13]. The amount of inclusions can be directly correlated to results of chemical analysis, as some elements have only very limited solid solubility, while others can partition between metallic and non-metallic phases (Chap. 5). Usually volume fraction V_V can immediately be measured from the image by area fraction A_A without great difficulty (Fig. 3.34).

If there are different inclusions within one sample, or the inclusions are multi-phased, it can be useful to define all phases as a single phase to get the total volume fraction of the inclusions and separate them in a second step. In the case of partly corroded microstructures, this method can be difficult or impossible, because of the possibly optical similarity of corrosion products and inclusions. For such samples, point or feature counting usually is the best and sometimes only solution, shown in Fig. 3.35.

One of the first things that we notice about ancient worked metals is how much the size of the individual grains vary, often even within the same object. Grain size has a significant effect to mechanical properties of alloys, such as hardness, yield strength or fatigue resistance, and most mechanical properties are improved as the size of the grains decrease. One of the functions of modern metallurgy is therefore

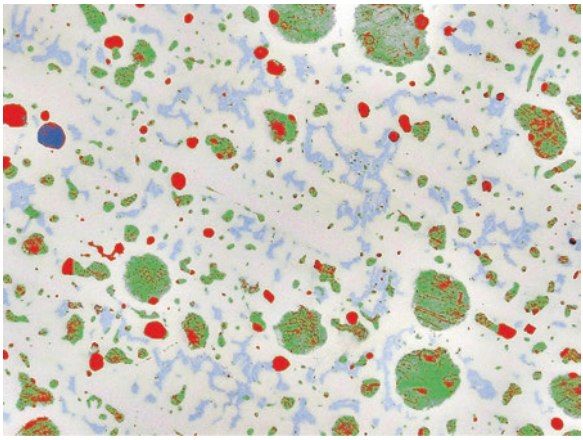

Fig. 3.34 Microstructure of a leaded high-tin bronze bracelet (28% Sn, 16.5% Pb) containing α + δ, lead globules, copper sulphide and copper oxide inclusions in α_{Cu} solid solution. Determination of V_V of non-metallic inclusions by digital area analysis is quick performed and oxide (not colour coded), and sulphide inclusions (red) can be separated. Lead content ($V_V = 11.9\%$) is underestimated, because of scratches and unsuccessful polishing

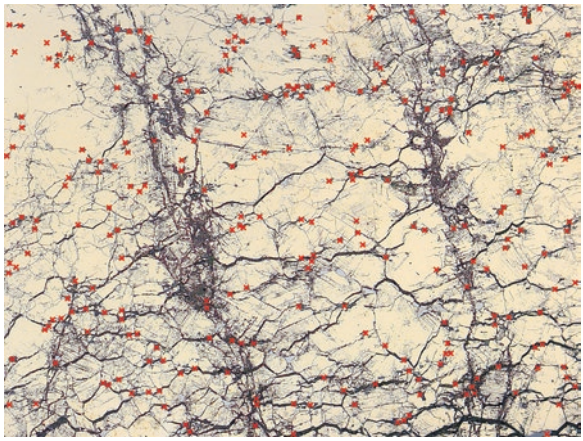

Fig. 3.35 Determination of V_V of non-metallic inclusions by feature count N_A within the corroded microstructure of a bronze belt from Denmark. The count of non-metallic inclusions is normalized by dividing by the area of the image. Volume fraction has been over estimated by digital area analysis A_A, because of the optical similarity of inclusions and corroded phases

to make the size of the metallic grains consistent across the alloy, depending on the engineering application that it is intended to be used for. Grain size measuring has thus to be adopted, and the most commonly used scale is the ASTM average grain size number *G,* whereas a wide variety of international standards exists. Grain size number represents the average planar grain size, and the relationship between ASTM grain size number and grain size depends on the measurement method, which are usually based on grain area or intercept length. Widely used is the planimetric method, known as the Jeffries method, which determines the grain size by calculating the number of grains *N* per unit area *A,* N_A. ASTM grain size number *G* is based on the formula: $N_{AE} = 2^{G-1}$, where N_{AE} represents the number of grains per square inch of at a magnification of 100x and N_A the number of grains per square millimetres by multiplying N_{AE} with 15.50 at a magnification of 1x (see ASTM E112-10; Geels [20]). Grain size measurement by the lineal intercept method has been developed by Emil Heyn, where grain boundary intersections *P* or the number *N* of intercepted grains are counted. The mean linear intercept length $\bar{L}$ is defined by $\bar{L} = \frac{1}{N_L} = \frac{1}{P_L}$ for space filling grains ($V_v = 1$), where *N* or *P* is divided by the total line length. The mean lineal intercept is related to ASTM grain size number *G* by the following empirical equation:

$$G = \left(-6.646 \log \bar{L}\right) - 3.298 \quad \left(\text{see Vander Voort}[75]\right).$$

With automatic or semi-automatic digital image analysis, grain size can be directly evaluated by measuring grain boundary lengths, shown in Fig. 3.36, which would be a fast and convenient method, but in practice lineal intercept methods are more suitable to non-uniform, intergranular corroded and twinned or slipped microstructures of ancient metals (Fig. 3.37).

For accuracy and precision, 50 grains in each of minimum three areas are required for modern alloys (ASTM E112-10), which is hard to realize for archaeological

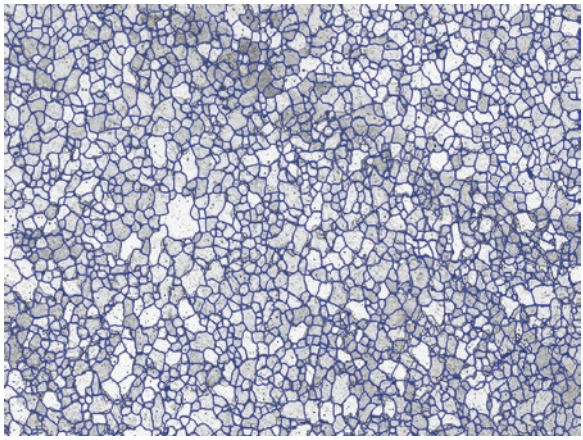

Fig. 3.36 Automatic measurement of grain boundaries of a ferritic mid-nineteenth century puddled iron from the fence of the church of Warburg-Dössel, Germany

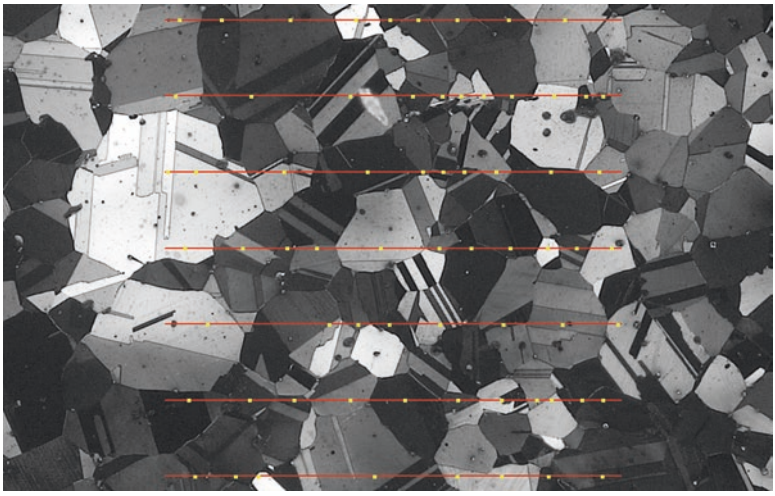

Fig. 3.37 Lineal intercept measurement $\bar{L} = \frac{1}{N_L}$ of grain diameters of a bronze belt from the hoard of Fliess, Austria, with twinned grains (see Fig. 3.29)

specimens. Figure 3.38 shows the typical mean grain sizes of ancient copper alloys, while Fig. 3.28 shows the grain size distribution within a single object.

When metals are as-cast and a dendritic structure remains, the mechanical properties of casting can be characterized by the distance between the dendrites, which is called dendrite arm spacing (DAS) or secondary dendrite arm spacing (SDAS). The DAS is best approximated by the dendrite cell intervals (centre-to-centre distance between two cells). The DAS can be measured by classical stereological

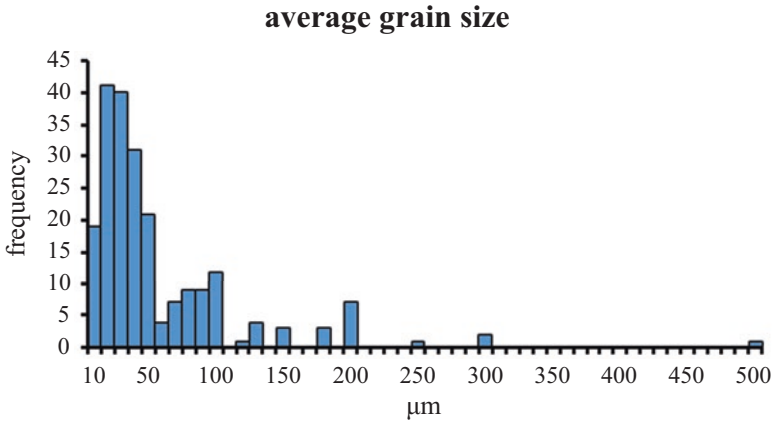

Fig. 3.38 Mean grain size distribution of ancient copper alloys (data taken from Northover [37–39] and own measurements)

intercept method, following this equation: $DAS = \frac{L}{n}$, where L is the length of the measured line and n number of arms intersected across a line traverse, or by areal analysis. Modern image analysing systems enable calibrated images so that the DAS can immediately be measured from the image. The DAS is the bigger, the slower the material solidifies (i.e. fewer but thicker dendrite arms at the same measuring length develop). Large, coarse dendrites generally mean that the cooling rate of the alloy in the mould was fairly slow, usually implying that heated or well-insulated moulds were employed. Finer dendrite arm spacing usually imply faster cooling rates.

3.3.3 Mechanical Properties

Actually, the testing of mechanical properties is no real development of modern material science. In modern material science, such tests are made to obtain information on elastic and plastic properties of an alloy, but the knowledge about plasticity of metals must have been already essential to prehistoric metalworkers. Literary evidence is given by Pliny (34, 94), who refers to malleable and castable bronze, which the latter would break by hammering or by the late medieval Islamic "Ayn-i-Akhbari" document, which reports the different qualities of brass (Sect. 5.1). Best archaeological evidence of mechanical testing of metals comes mainly from coins and of scrap metal depots. Coins with chisel cuts on the surface to expose forgeries are known from all periods [86, p. 237]. Such cutting or punching tests were not primarily focused to get information about the mechanical properties of the coins

but revealing their constitutions. Plated coins could have been easily detected by this ancestor of the modern notch impact test, and finally the revealed impact strength could also give information about the composition. Metallic deposits from Bronze Age to Roman times contain a variety of items crushed to pieces. Apart from ritual destruction or the antique practice for punishment "*damnatio memoriae*", the principal purpose for this destruction is a practical one, having the right size for melting down. Indeed some items show intensive bending and impacts from different tools. It seems as if the destruction should also reveal the mechanical properties such as hardness and tensile strength, to avoid the melting of unsuitable material. Like modern recycling, pre-industrial recovery of metals from scrap might have caused trouble without proper handling and separation.

3.3.3.1 Hardness Testing

Modern tensile testing is controlled tension until fracture, while hardness is a feature that is characterized by a measure of a metal's resistance to plastic deformation. The hardness test for bronze cannons developed in 1874 by Franz von Uchatius, an Austrian artillery general, for example, was nothing else than a falling chisel from a defined height of 25 cm [26, p. 2]. A related early approach to the problem was the scleroscope, which utilized graded steel balls that were dropped onto a metallic surface from a defined height (again 25 cm). Scleroscope hardness test is a dynamic measurement, at which the extent of rebound of the steel sphere was a measure of the hardness of the metal [26, pp. 76–78]. The main difference between modern mechanical testing of materials compared to empirical individual tests is to measure the behaviour of metals when subjected to certain reproducible conditions. Friedrich Mohs, a German mineralogist, developed one of the earliest reliable diagnostic hardness tests in 1812. The Mohs hardness test compares the resistance of a mineral to being scratched by ten reference minerals with different hardness. The Mohs scale is not suitable for metals, as it is strongly nonlinear and the hardness differentiation is too low. Scratching indeed had been adapted to metals but has been nearly totally replaced by methods in which indenters of different size and form are forced into the surface of a material by means of an applied load. Rockwell hardness testing machines use conical diamond or steel ball penetrators, equally to Brinell hardness testers, which also use a ball intender, while Knoop and Vickers hardness tests are performed by diamond pyramids. The test force (nowadays given in N or kgf) presses the intender into the surface of the specimen (in mm^2) for a specific loading time (in s), after which the intender is pulled back and the shape of intention can be measured: the smaller the indentation, the harder the material. Generally, the hardness values are based on applied test force F divided by the intended surface area A ($H = \frac{F}{A}$) and can be given in kilogrammes-force per square millimetre (Kgf/mm^2) or kilopond per square millimetre (Kp/mm^2). Hardness values can also be converted to SI units and given in Newton per square millimetre (N/mm^2) by multiplying with the standard gravity 9.80665 m/s^2. Indeed hardness is not a single fundamental

property, as the shape of the intenders influences the extend of elastic and plastic deformation of the surface, for which reason the general relationship of hardness values equates the test force per indentation size and must be calculated individually for each testing method by their specific equations (see Geels [20, pp. 626–39]; Vander Voort [75, pp. 339–66]). Therefore, hardness values are usually given without units in hardness numbers, using abbreviations for the method applied, the load used in kgf and ideally also the loading time (time is specified for modern hardness testing machines). So Knoop (HK) and Vickers hardness (HV), in the Anglo-Saxon language area also Diamond Pyramid Hardness (DPH) or Diamond Pyramid Number (DPN), are clearly characterized by this nomenclature, while Brinell hardness number (HB) must give the material of the ball intender, like HBS for steel or HBW for a tungsten carbide intender, just as Rockwell hardness (HR) must supply a scale symbol which gives form and force of the intender. For example, HRB would be a steel ball with 100 Kgf, while HRA and HRC would be a diamond cone (see Geels [20], tab. 21.2; Herrmann [26], pp. 29 tab. 1).

Hardness values achieved by different methods are not directly comparable but can be converted by the use of conversion charts (ASTM E140). These tables are based on empirical data, so that the accuracy of the conversion depends on the accuracy of the provided data and the resulting curve fits. For a quick comparison of hardness values, some simple hardness conversation equations are available giving approximate equivalents [20, p. 643].

All these conventional indentation hardness testing methods ignore the elastic deformation, and hardness is exclusively determined by the plastic indentation depth. To include the plastic as well as the elastic response of the tested material, Martens hardness testing (HM), formerly known as Universal hardness (HU), has been developed. Martens hardness uses mostly a Vickers indenter and is determined by instrumented measurement during application of a test force. Test force and the depth of indentation are recorded during the penetration, which makes it suitable for materials with low modulus of elasticity and composites [26, p. 186-; 61]. Martens hardness values are related to the sum of plastic and elastic indentation depths and are given in N/mm^2. Hardness values given in SI units but determined by conventional indentation hardness testing are not identical to Martens hardness values by the reason mentioned before.

3.3.3.2 Practical Application to Prehistoric and Historic Metals

Most modern mechanical test procedures like tensile test are not suitable for cultural objects, as it implies the total destruction of the sample, albeit it has been sporadically applied (e.g. Hadfield [23]; Salin and France-Lanord [58]; Zwicker [85]). Hardness testing is the only reasonable method combined with the metallography of ancient metals, as it leaves a small indentation and other mechanical properties may be estimated from hardness data. As tensile strength and hardness are both indicators of the resistance of a metal to plastic deformation, they correlate roughly linearly for several metals.

Dynamic measurements like those that scleroscopic hardness has only been sporadically applied to archaeological metals (e.g. Mathewson [35]), while static indentation tests are usual. The test forces for standard Rockwell method are very high (>10 Kgf) and therefore not suitable for testing ancient metals, because of the low sample sizes. Therefore, Rockwell hardness testing has hardly been performed but then converted to Brinell and Vickers hardness values (e.g. Anteins [2]; Arrhenius [3]). Brinell hardness test is the oldest of modern indentation tests and has been widely used in industry and research [75, p. 339], but it has been less applied to ancient metals (e.g. Hadfield [23]; Sperl [70]). In practice for small-sized samples, the microhardness tests with Knoop (e.g. Panseri and Leoni [44]) and most of all Vickers intenders have been proven successfully and are commonly used. The advantages of the microhardness tests are that only a very small sample of material is required and that it is valid for a wide range of test forces. Martens hardness (HM) testers are not yet widely distributed, and therefore the application to ancient metals is still quite rare (e.g. Schwab [62]). It should be noticed that some older publications also use the abbreviations MH, HM or Hm (e.g. Pleiner [49]; Thomsen [72]). These abbreviations only refers to hardness measurement with a microhardness tester after Hanemann, which is based on a Vickers diamond pyramid with small test loads where the area of the indentation may be directly measured instead of measuring the lengths of the diagonals.

The application of hardness testing to ancient metals offers valuable information about mechanical properties and completes characterization without great effort. The inhomogeneity in composition and the effects of plastic deformation, quenching or annealing can be illustrated by mapping hardness distributions in correspondence to overview images or drawings, as it is used for iron objects (e.g. Eichert et al. [15]; Pleiner [50]). The carbon contents of quench-hardened steels, for example, can be roughly estimated by microhardness testing without any need of chemical analysis. Precision and accuracy of hardness tests must be checked regularly by reference test blocks having different levels of hardness.

In a similar manner, quantitative methods can be applied to microstructural studies of prehistoric metals. It is reasonable to discuss the usefulness of bulk hardness or representativeness of mean values of microhardness. Measuring macrohardness with larger forces is usually not possible because of the mostly small sample size. So loads of 1 kgf or less must be used, which raise measurement errors, material influences and load dependence. At least five to ten hardness readings are required for a representative bulk hardness value of a relatively homogeneous material. For the determination of a significant mean hardness of inhomogeneous material, statistical methods are recommended.

The mean value of this heavily leaded alloy was determined 78 HV 0.1 ± 4 after 30 hardness indentations with 100 gf test force. The same result has been achieved after 20 hardness indentations, and after 10 indentations, the result diverts only 2% relative. Indeed a divergent hardness of 62 HV 1 ± 3 has been achieved after 20 hardness indentations with 1 kgf test force. This result has already achieved after 10 indentations. Between 10 and 20 microhardness, indentation seems to be enough for characterizing the mean hardness of leaded cast bronze, but the load dependence clearly becomes obvious. The microhardness with low test force represents the

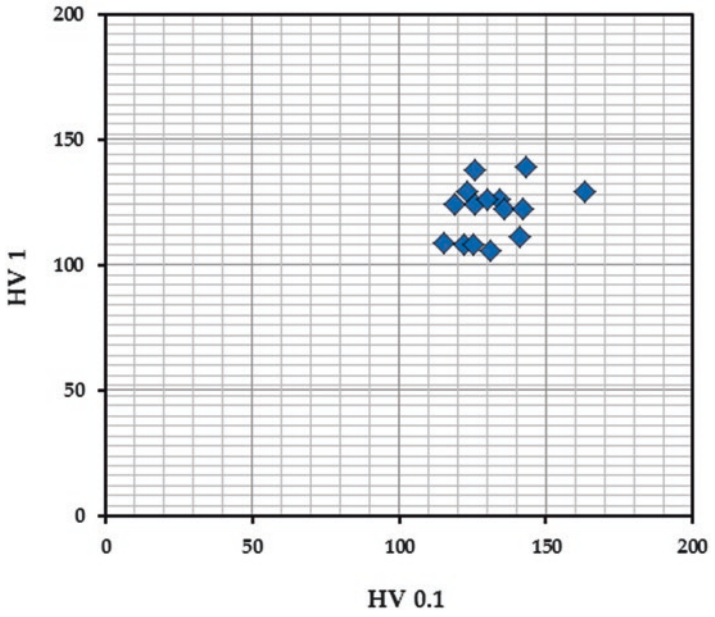

Fig. 3.39 Hardness distribution within one sample from a worked and partly annealed bronze situla from the Late Iron Age oppidum of Manching, Bavaria. Hardness testing has been performed at 0.1 kgf with a mean of 132 HV 0.1 and at 1 kgf with a mean of 121 HV 1, at which microhardness is biased by local inhomogeneity of microstructure

α_{Cu}-solid solution, whereas the hardness with heavier test forces is affected by the irregular distributed lead particles. Mean values of life-sized statues vary between 70 HV 0.1 and 120 HV 0.1, whereas typical mean values measured with higher test forces is 40–80 HV (see Leoni [33, p. 192]; Raub [51, p. 352]; Willer et al. [82], tab. 1).

Comparison between single-phased wrought copper and silver alloys have shown that there is usually not much deviation between mean values of different test force, but the precision of a lower test force is naturally more influenced by microstructural inhomogeneity (Fig. 3.39). The precision is usually between 10% and 20% relative for inhomogeneous worked and annealed objects, while the precision for mean hardness values of fully annealed objects is usually between 1% and 10% relative.

The hardness, obtained on a microscale using tiny indenters and microscopes to measure the size of the indentation, do not give large differences between the Brinell and Vickers numbers, but there are systematic variations in the two numbers that are addressed in the comparison charts shown in Fig. 3.40.

These charts will be useful in further comparison of data related to microhardness discussed later in the volume or given as data for individual alloying systems. Hardness is usually inversely proportional to brittleness. As alloys are cold-worked, dislocations pile up, and the ability of the alloy to be cold-worked further drops. The hardness increases until the alloy may become too brittle to actually be used in

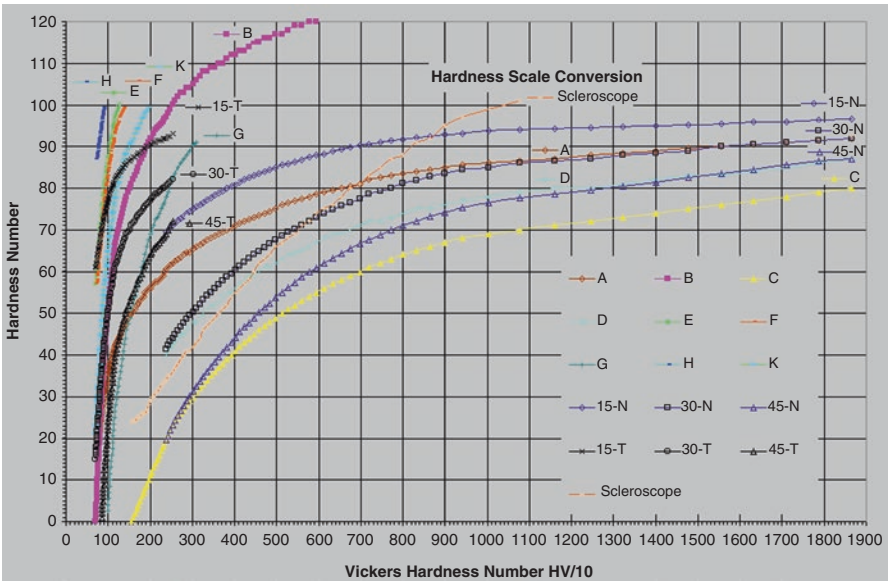

Fig. 3.40 Comparison of the Vickers hardness with 10 kgf compared with Hardness values in a number of different scales. For example, a Vickers hardness of 110 HV 10 gives a Brinell hardness of about 70 HB. From http://www.gordonengland.co.uk (2018)

practice without cracking. Annealing of the alloy will reform the grain structure and allow the dislocation density to be relieved. The effects of annealing in different alloy systems will be discussed later in relation to individual alloys.

References

1. Aliya, D.: Metallographic sectioning and specimen extraction. In: Vander Voort, G.F. (ed.) Metallography and Microstructure ASM handbook 9, pp. 229–241. ASM International, Materials Park (2004)
2. Anteins, A.K.: The structure and manufacturing techniques of pattern-welded objects found in the Baltic States. J. Iron Steel Inst. **206**, 563–571 (1968)
3. Arrhenius, B.: Technische Analysen der Schwerter von Elvran und Gravråk, Norwegen. In: Müller-Wille, M. (ed.) Zwei karolingische Schwerter aus Mittelnorwegen. Studien zur Sachsenforschung, vol. 3, pp. 155–167. Lax, Hildesheim (1982)
4. ASTM E112-10: Standard Test Methods for Determining Average Grain Size. ASTM International, West Conshohocken (2010)
5. Beraha, E.: New metallographic reagents for stainless steel and heat-resisting alloys. J. Iron Steel Inst. Jpn. **204**, 248–252 (1966)
6. Beraha, E.: Metallographic reagents based on Sulphide films. Pract. Metallogr. **7**(5), 242–248 (1970)
7. Beraha, E., Shpigler, B.: Color Metallography. American Society for Metals, Metals Park (1977)

8. Blet-Lemarquand, M., Da Mota, H., Gratuze, B., Leusch, V., Schwab, R.: Material sciences applied to West Hallstatt Gold. In: Schwab, R., Milcent, P.-Y., Armbruster, B., Pernicka, E. (eds.) Early Iron Age Gold in Celtic Europe. Forschungen zur Archäometrie und Altertumswissenschaft 6.1, pp. 101–132. Verlag Marie Leidorf GmbH, Rahden/Westf (2018)
9. Bousfield, B.: Surface Preparation and Microscopy of Materials. Wiley, Chichester (1992)
10. Bramfitt, B.L., Lawrence, S.J.: Field metallography techniques. In: Vander Voort, G.F. (ed.) ASM Handbook Volume 9: Metallography and microstructure, pp. 478–492. ASM International, Materials Park (2004)
11. Brandon, D.G.: Modern Techniques in Metallography. Butterworth, London (1966)
12. Bühler, H.-E., and Hougardy H.P.: Atlas of interference layer metallography. Deutsche Gesellschaft für Metallkunde, Oberursel (1980)
13. Darling, A.S., Healy, J.F.: Micro-probe analysis and the study of Greek gold-silver-copper alloys. Nature. **231**, 443–444 (1971)
14. DeHoff, R.T., Rhines, F.N. (eds.): Quantitative Microscopy. McGraw-Hill, New York (1968)
15. Eichert, S., Mehofer, M., Baier, R.: Archäologische und archäometallurgische Untersuchungen an einer karolingerzeitlichen Flügellanzenspitze aus dem Längsee in Kärnten/Österreich. Archäologisches Korrespondenzblatt. **41**, 139–154 (2011)
16. Emmerling, J.: Technologische Untersuchungen an eisernen Bodenfunden. Alt-Thüringen. **12**, 267–319 (1972)
17. Exner, H.E., Hougardy, H.P.: Quantitative Image Analysis of Microstructures: A Practical Guide to Techniques, Instrumentation and Assessment of Materials. DGM, Oberursel (1988)
18. Foote, H.W., Buell, W.H.: Composition, structure, and hardness of some Peruvian bronze axes. Am. J. Sci. **34**, 128–132 (1912)
19. Garland, H.: Metallographical researches on Egyptian metal antiquities. J. Inst. Met. **10**, 329–343 (1912)
20. Geels, K.: Metallographic and Materialographic Specimen Preparation, Light Microscopy, Image Analysis and Hardness Testing. ASTM International, West Conshohocken (2007)
21. Gokhale, A.M.: Quantitative Characterization and Representation of Global Micreostructural Geometry. In: Vander Voort, G.F. (ed.) Metallography and Microstructure ASM Handbook 9, pp. 428–447. ASM International, Materials Park (2004)
22. Goldstein, J.I., Newbury, D.E., Joy, D.C., Lyman, C.E., Echlin, P., Lifshin, E., Sawyer, L., Michael, J.R.: Scanning Electron Microscopy and X-Ray Microanalysis. Springer, New York (2003)
23. Hadfield, R.: Sinhalese Iron and steel of ancient origin. J. Iron Steel Inst. **85**, 134–186 (1912)
24. Hanemann, H.: Metallographische Untersuchung einiger altkeltischer und antiker Eisenfunde. Internationale Zeitschrift für Metallographie. **4**, 248–256 (1913)
25. Heinrich, K.F.J.: Electron Beam X-Ray Microanalysis. Van Nostrand Reinhold Company, New York (1981)
26. Herrmann, K. (ed.): Hardness Testing: Principles and Applications. ASM International, Materials Park (2011)
27. Hošek, J., Bárta, P., Šmerda, J.: Metallographic examination and reconstruction of the 6th century lombardic sword from Kyjov. Mater. Manuf. Process. **32**(7–8), 885–899 (2017)
28. Kehl, G.L.: The Principles of Metallographic Laboratory Practice. McGraw-Hill, New York/London (1939)
29. Klemm, H.: Farbenätzungen des Feingefüges der Metalle mit Natriumthiosulfat. Metallkundliche Berichte 45. Verlag Technik, Berlin (1952)
30. Klemm, H.: Anwendungsmöglichkeiten des Natriumthiosulfat-Verfahrens. Prakt. Metallogr. **5**, 163–167 (1968)
31. Kotula, P.G., Keenan, M.R., Michael, J.R.: Automated analysis of SEM X-ray spectral images: a powerful new microanalysis tool. Microsc. Microanal. **9**(1), 1–17 (2003)
32. Lang, J.: Iberian Falcata in the British museum. In: Pernicka, E., Schwab, R. (eds.) Under the volcano. Forschungen zur Archäometrie und Altertumswissenschaft 5, pp. 49–57. Marie Leidorf, Rahden/Westf (2014)

33. Leoni, M.: Metallographic investigation of the horses of san Marco. In: Perocco, G. (ed.) The Horses of San Marco. Venice, pp. 191–199. Olivetti, Milano (1979)
34. Lyman, T. (ed.): Metallography, Structures and Phase Diagrams ASM handbook 8. American Society for Metals, Metals Park (1973)
35. Mathewson, C.H.: A metallographic description of some ancient Peruvian bronzes from Machu Picchu. Am. J. Sci. **190**(240), 525–616 (1915)
36. Meeks, N., Cartwright, C., Meek, A., Mongiatti, A. (eds.): Historical Technology, Materials and Conservation: SEM and Microanalysis. Archetype, London (2012)
37. Northover, J.P.: Metal analysis and metallography of early metal objects. In: Vandkilde, H. (ed.) From Stone to Bronze. The Metalwork of the Late Neolithic and Earliest Bronze Age in Denmark, Jutland. Archaeological Society Publications 32, pp. 321–358. Jutland Archaeological Society, Aarhus (1996)
38. Northover, J.P.: Analysis of copper alloy metalwork from Arbedo TI. In: Schindler, M.P. (ed.) Der Depotfund von Arbedo TI und die Bronzedepotfunde des Alpenraums vom 6. bis zum Beginn des 4. Jh. v.Chr.. Antiqua 30, pp. 289–315. Schweizerische Ges. für Ur-und Frügeschichte, Basel (1998)
39. Northover, J.P.: Analysis and metallography of copper alloy metalwork. In: Lippert, A., Stadler, P. (eds.) Das spätbronze- und früheisenzeitliche Gräberfeld von Bischofshofen-Pestfriedhof. Universitätsforschungen zur prähistorischen Archäologie 168, pp. 351–384. R. Habelt, Bonn (2009)
40. Northover, S., Northover, P.: Applications of electron backscatter diffraction in archaeology. In: Meeks, N., Cartwright, C., Meek, A., Mongiatti, A. (eds.) Historical Technology, Materials and Conservation: SEM and Microanalysis, pp. 76–85. Archetype, London (2012)
41. Ogilvie, R.E.: Electron microanalysis of paint samples from the Bersheh sarco-phagus. In: Application of Science in the Examination of Works of Art, pp. 223–228. Museum of Fine Arts, Boston (1965)
42. Ohser, J., Mücklich, F.: Statistical Analysis of Microstructures in Materials Science Statistics in Practice. Wiley, Chichester (2000)
43. Olsen, S.L. (ed.): Scanning Electron Microscopy in Archaeology. BAR international series 452. BAR, Oxford (1988)
44. Panseri, C., Leoni, M.: Research on an Iron spearhead from the Etruscan sanctuary of Fanum Voltumnae, fourth to third centuries B.C. In: Levey, M. (ed.) Archaeological Chemistry. A Symposium, pp. 205–229, Philadelphia (1967)
45. Perryman, E.C.W.: The examination of metal surfaces. In: GKT, Conn., Bradshaw, F.J. (eds.) Polarized Light in Metallography, pp. 70–87. Butterworths Scientific Publications, London (1952)
46. Petzow, G.: Metallographic Etching: Techniques for Metallography, Ceramography, Plastography. ASM International, Materials Park (1999)
47. Piaskowski, J.: Metallographic investigations of ancient Iron objects from the territory between the Oder and the basin of the Vistula River. J. Iron Steel Inst. **198**, 263–282 (1961)
48. Piccardo, P., Mille, B., Robbiola, L.: Tin and copper oxides in corroded archaeological bronzes. In: Dillmann, P., Beranger, G., Piccardo, P., Matthiesen, H. (eds.) Corrosion of Metallic Heritage Artefacts. Investigation, Conservation and Prediction for Long-Term Behaviour. European Federation of Corrosion Publications 48, pp. 239–262. Woodhead Publishing, Cambridge (2007)
49. Pleiner, R.: Die Technologie des Schmiedes in der Großmährischen Kultur. Slovenská Archeológia. **15**(1), 77–188 (1967)
50. Pleiner, R.: Zur Schmiedetechnik im römerzeitlichen Bayern. Bayerische Vorgeschichtsblätter. **35**, 113–140 (1970)
51. Raub, C.J.: Was kann der Archäologe von der Metallkunde erwarten? Fundberichte aus Baden-Württemberg. **10**, 345–365 (1985)
52. Reed, S.J.B.: Electron Microprobe Analysis, 2nd edn. Cambridge University Press, Cambridge (1993)

53. Reimer, L.: Scanning Electron Microscopy: Physics of Image Formation and Microanalysis. Springer series in optical sciences 45, 2nd edn. Springer, Berlin/Heidelberg (1998)
54. Roberts, G.: X-ray microanalyser. Archaeometry. **3**(1), 36–37 (1960)
55. Rollett, A.D., Barmak, K.: Orientation mapping. In: Laughlin, D.E., Hono, K. (eds.) Physical Metallurgy II, 5th edn, pp. 1113–1140. Elsevier, Amsterdam (2014)
56. Rupe, H.: Notitz über die chemische Untersuchung prähistorischer Gräberfunde von Castraneda. Verhandlungen der Naturforschenden Gesellschaft in Basel. **18**(1), 1–13 (1905)
57. Russ, J.C., DeHoff, R.T.: Practical Stereology, 2nd edn. Kluwer Academic, New York (2000)
58. Salin, É., France-Lanord, A.: Le fer à l'époque mérovingienne. Geuthner, Paris (1943)
59. Samuels, L.E.: Metallographic Polishing by Mechanical Methods, 3rd edn. ASM International, Materials Park (1982)
60. Schaaber, O.: Beiträge zur Frage des Norischen Eisens. Metallkundliche Grundlagen und Untersuchungen an Funden vom Magdalensberg. Carinthia I. **153**, 129–279 (1963)
61. Schadewald, I., Heermant, C., Dengel, D.: Martenshärteprüfung. Härterei-technische Mitteilungen. **56**(4), 236–241 (2000)
62. Schwab, R.: Evidence for carburized steel and quench-hardening in the 'Celtic' oppidum of Manching. Hist. Metall. **36**(1), 6–16 (2002)
63. Schwartz, A.J., Kumar, M., Adams, B.L., Field, D.P.: Electron Backscatter Diffraction in Materials Science, 2nd edn. Springer, New York (2009)
64. Scott, D.A.: Pre-Hispanic Colombian metallurgy: studies of some gold and platinum alloys. Ph.D. diss. University of London, London (1982)
65. Scott, D.A.: The metallographic preparation of ancient lead. Stud Conserv. **41**, 60–62 (1996)
66. Scott, D. A.: Copper and Bronze in Art: Corrosion, Colorants, Conservation. J. Paul Getty Press, Los Angeles (2002)
67. Scott, D.A.: Laboratory notes homemade equipment aids for metallographic sample preparation. The Conservator. **31**, 87–91 (2008)
68. Scott, D.A.: Colour metallography in the examination of ancient metals. Stud. Conserv. **59**, 113–122 (2014)
69. Smith, C.S.: A History of Metallography. The University of Chicago Press, Chicago (1960)
70. Sperl, G.: Zur Urgeschichte des Bleis. Z Met. **81**(11), 799–801 (1990)
71. Stokes, D.J.: Principles and Practice of Variable Pressure/Environmental Scanning Electron Microscopy (VP-ESEM). Wiley, Chichester (2008)
72. Thomsen, R.: Metallographic studies of an axe from the migration age. J. Iron Steel Inst. **204**, 905–909 (1966)
73. Underwood, E.E.: Quantitative Stereology. Addison-Wesley, Reading (1970)
74. Vander Voort, G.F.: Inclusion measurement. In: JL, McCall., French, P.M. (eds.) Metallography as a Quality Control Tool, pp. 1–88. Plenum Press, New York/London (1980)
75. Vander Voort, G.F.: Metallography, Principles and Practice. McGraw-Hill, New York (1984)
76. Vander Voort, G.F. (ed.): Metallography and Microstructure ASM handbook 9. ASM International, Materials Park (2004a)
77. Vander Voort, G.F.: Color metallography. In: Vander Voort, G.F. (ed.) Metallography and Microstructure ASM handbook 9, pp. 493–512. ASM International, Materials Park (2004b)
78. Vander Voort, G.F.: Metallographic specimen preparation for Electron backscattered diffraction part I. Pract. Metallogr. **48**(9), 454–473 (2011a)
79. Vander Voort, G.F.: Metallographic specimen preparation for electron backscattered diffraction part II. Pract. Metallogr. **48**(10), 527–543 (2011b)
80. Vilella, J.R., Kindle, W.F.: Sodium Bisulphite as an etchant for steel. Metal Progress. **76**(6), 99–100 (1959)
81. von Schwarz, M., Die Anwendung des Polarisationsmikroskopes bei der Untersuchung von Kupferlegierungen. Z. Met. **24**(5), 97–103 (1932)
82. Willer, F., Schwab, R., Mirschenz, M.: Römische Bronzestatuen am Limes: Archäometrische Untersuchungen zur Herstellungstechnik. Bonner Jahrbücher. **216**, 57–208 (2017)
83. Witt, R., Nowell, M.: Specimen preparation of difficult materials for EBSD characterization. Microsc. Microanal. **17**(S2), 414–415 (2011)

84. Wojnar, L., Kurzdłowski, K.J., Szala, J.: Quantitative image analysis. In: Vander Voort, G.F. (ed.) Metallography and Microstructure ASM handbook 9, pp. 403–427. ASM International, Materials Park (2004)
85. Zwicker, U.: Untersuchungen an einem Eisenbarren aus dem Depotfund von Renningen (Kr. Leonberg). Fundberichte aus Schwaben. **18**(1), 282–283 (1967)
86. Zwicker, U., Oddy, A., La Niece, S.: Roman techniques of manufacturing silver-plated coins. In: La Niece, S., Craddock, P. (eds.) Metal Plating and Patination, pp. 223–246. Elsevier, London (1993)

Chapter 4
The Structure of Metals and Alloys

4.1 The World of Microstructure and Phase Diagrams

The properties of metals and alloys are dependent on their atomic structure. Metals are an aggregation of atoms that, apart from mercury, are solid at room temperature. These atoms are held together by "metallic bonds" that result from sharing available electrons. A negative electron bond pervades the structure, and heat and electricity can be conducted through the metal by the free movement of electrons. The atoms are regularly arranged, forming a symmetrical three-dimensional group, which repeats itself periodically and which is called a unit cell. Unit cells of identical characteristics form a crystal with regular spatial distribution of atoms, which can be defined by a space lattice. Atoms can be stacked in different ways to create a variety of simple lattice types. There are three common types of lattice structure that most metals belong to (Fig. 4.1): face-centred cubic (fcc), body-centred cubic (bcc) and close-packed hexagonal (cph).

In the face-centred cubic (fcc) lattice, layers of atoms can be built up, which can be modelled in spheres, so that the third row of spheres does not occupy the same position as the spheres in the first row; the structure then repeats every third layer (ABCABCABC…). In the close-packed hexagonal structure (cph), a model can be made up of spheres stacked in layers as well, but in the hexagonal structure, the spheres repeat the pattern every second layer (ABABABAB…). In the body-centred cubic metals (bcc), the atoms are arranged at the corners of a cube with one atom in the centre of the cube.

This arrangement is strong but allows substitution of solvent atoms by atoms of a solute or other atoms to enter the cube if they have small radii, such as carbon or nitrogen in steels. The latter are called interstitials, because they fit between the interstices of the lattice of a solvent and expand the unit cell of the solvent. There are only a few elements such as hydrogen, carbon, nitrogen or boron, with radii small enough, capable to locate between the atoms of a solvent (H = 0.037 nm; B = 0.082 nm, C = 0.077 nm; N = 0.071 nm). The ability of carbon, in particular, to

D. A. Scott, R. Schwab, *Metallography in Archaeology and Art*, Cultural Heritage Science, https://doi.org/10.1007/978-3-030-11265-3_4

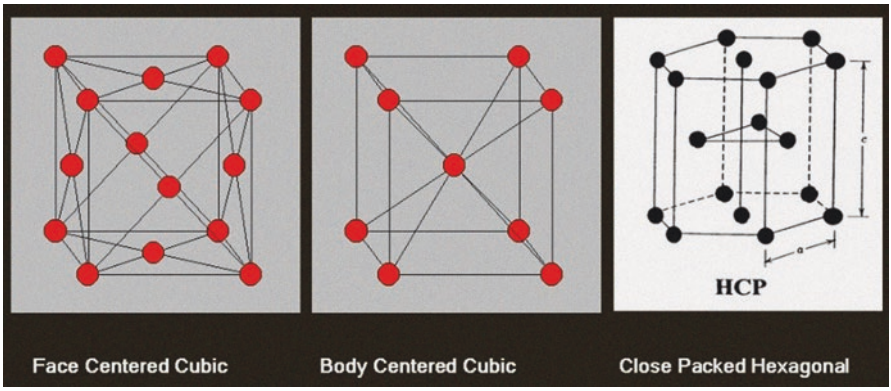

Fig. 4.1 Unit cells of the three common space lattices in ancient metals and their arrangement of atoms

fit into the iron lattice produces steels, which have considerable strength, compared with pure iron.

More important and more common is the replacement (substitution) of solvent atoms by those of the solute, which has been regarded by the traditional chemical view of early researchers as a solid solution of one metal in the other. The term solid solution is used when atoms of different elements are able to share the same phase together, that is, when solute atoms are soluble within the crystal lattice of a solvent without changing the type of structure of the host metal. Atomic size, crystal structure and lattice parameters, chemical affinity and electron concentration are the factors governing solid solubility, whereas binding energy and specific gravity affect liquid miscibility or immiscibility. Actually, the degree of substitutional solid solubility of metal compounds, formed by different metals, is dependent on general factors that Hume-Rothery and co-workers determined by their experimental work on several metallic systems (see, e.g. Hume-Rothery and Raynor [41]). Those "Hume-Rothery Rules" predict that metals must have the same type of lattice structure for complete solid solubility, that the difference between atomic sizes of alloying elements must not exceed 15%, that the chemical affinity should not be high and when the ratios of valence electrons to atoms are different and that the lower valance metals have better solubility than vice versa. Deviation from Hume-Rothery's Rules leads to a decrease in the maximum solid solubility and finally to immiscibility or to a tendency to form other compounds, such as intermetallic phases, rather than solid solutions. The atomic size difference between solvent and solute is generally always a parameter of the extent of solid solution strengthening. In fact, there exist several aberrations from these rules, and we recommend the reader who is interested to consult some of the original work for evaluating the general concepts (e.g. Hume-Rothery and Raynor [41]) and some critical interpretations (e.g. Barrett and Massalski [5]; Mizutani et al. [72]; Zhang et al. [131]).

One of the most useful theoretical aids to the study of the microstructure of ancient metals is the equilibrium diagram, also called the phase diagram or consti-

tutional diagram. Since many alloys are mixtures of two, three or more different components, phase diagrams are used to plot temperature against composition and to map out the areas of the different phases, which occur at different compositions or temperatures in the system concerned.

All standard phase diagrams refer to a fixed pressure of constant atmosphere. Phase diagrams provide information about melting and freezing temperatures, solubility limits and phase stability under conditions of equilibrium. The emphasis is on equilibrium conditions, which is an important parameter to remember. Phase diagrams are valid only when components achieve equilibrium conditions, which almost never occurs completely in ancient metals. This means that the interpretation of the microstructure of some metallic systems has to be carried out with care and with an awareness that the system might not be in equilibrium.

If there is some reason why this ideal state cannot be reached, then the actual microstructure which is observed in ancient artefacts will be potentially different from that predicted by the phase diagram. The phase diagram is, however, the essential skeleton on which the details of the appearance of the system hang, even if the ancient alloys in question are far removed from an equilibrated state. Nevertheless it is possible to predict phases that are present in the microstructure with their chemical composition and their amounts in alloys approximately to the compositions shown in the diagrams in many instances, especially in worked and annealed alloys. It is in cast alloys that the general relationship between phase diagrams and the proportion and composition of the phases predicted by them tends to break down.

A phase is a component of an alloy system whose composition can vary within certain limits or have a fixed stoichiometric ratio of different kinds of atoms. As a result, phases can be of rather variable elemental composition, for example, the alpha phase in the copper-tin system, which is the copper-rich primary solid solution (α_{Cu}), could have less than 1% of tin or up to a maximum of 15.8% of tin dissolved. It could not have 20% of tin, because that is outside of the stability limits of the alpha phase and another phase will replace the alpha phase. The delta phase in the copper-tin system, which is an intermetallic compound, has a fixed stoichiometric ratio of $Cu_{41}Sn_{11}$ with 32.55% tin instead [98]. Indeed several earlier researchers found that the delta phase would be of slightly variable composition at different temperatures but corresponding to the formula $Cu_{31}Sn_8$, which has been the long-established stoichiometric formula (see Hansen and Anderko [35] for critical evaluations of the literature).

More recent compilations of the data and thermodynamic assessment indicate that the ideal formula would be $Cu_{41}Sn_{11}$ [98, 107]. The delta phase would have a very limited thermodynamic stability under equilibrium conditions, but the cooling rate is the most decisive factor that affects the decomposition of the delta phase, and in practice, the delta phase is stable and persists for thousands of years without change.

As a result, the copper-tin system can be redrawn at lower tin concentrations to create phase diagrams, which actually relate to empirical conditions rather than thermodynamic theory that will be given later in Chap. 5.

Alloys do not have a particular melting point. They soften and pass through a pasty stage between temperature zones shown on the phase diagram as solidus and liquidus curves. The solidus is the line in the phase diagram that separates the pasty stage of the alloy, usually a mixture of solid and liquid, from the completely solid alloy below the temperature of the solidus line. The liquidus is the line on a phase diagram that shows the temperature at which solidification begins on cooling from the melt.

The boundary region between these lines can be narrow or broad. In some alloys of importance in antiquity, such as copper-tin, gold-copper-silver or copper-arsenic, there is considerable separation between liquidus and solidus curves, which exacerbates the difficulties of attaining equilibrium cooling conditions from the melt and enhances the segregation effects that can be observed in these alloys. This is because the alloy has a longer period of time in a semi-solid region of partial solidification in which time for segregation to become fixed in the solid is accentuated compared with alloys with a narrow separation between liquidus and solidus. It is especially prevalent in copper-arsenic alloys, which have a steep and broad incline in the liquidus area at low arsenic concentrations, and consequently segregation can be severe.

Conventional binary phase diagrams are two-dimensional plots of the two components on each end of the horizontal axe versus the temperature on the vertical axe. The compositions of the solute and the solvent are given in atomic percent and in weight percent on the abscissae, whereas temperature is usually given in degree Celsius, and additionally, but less common in more recent publications, in degree Fahrenheit, on the ordinate. Some American publications persist in using degrees Fahrenheit, particularly in the iron and blacksmithing fraternity, which can be very confusing, as the temperature scale they are referring to is frequently not mentioned, or not defined, in the publication concerned.

Greek letters such as α, β, μ, δ, etc. are customarily used in order of their appearance – ordinarily upon cooling and increasing solute concentration but with arbitrary exceptions – to designate crystalline phases in metallic systems. Unfortunately phase designations are not used consistently, and there are several serious confusions in terminology, for example, with a particular Greek letter meaning one phase in one binary system and a different phase in another, or phases having the same crystal structure are labelled with different letters.

Complications caused by the labelling of the phase diagrams have been mitigated by employing stoichiometric formula instead, together with retaining established traditional phase names, which can be somewhat confusing, and with more complex alloy systems can become very annoying. Nevertheless, there are a few general conventions: solid solutions should be designated by the chemical symbol of the base element as subscript and a Greek letter additionally; disordered body-centred cubic structures are usually labelled with β (β’ for ordered) or γ for brass-type structures (e.g. Hansen and Anderko [35]; Chang et al. [17]; Massalski [63]). The region of the liquidus is labelled *L,* whereas the labelling of the solid phases with *S* will only be used in the following to discuss general reactions.

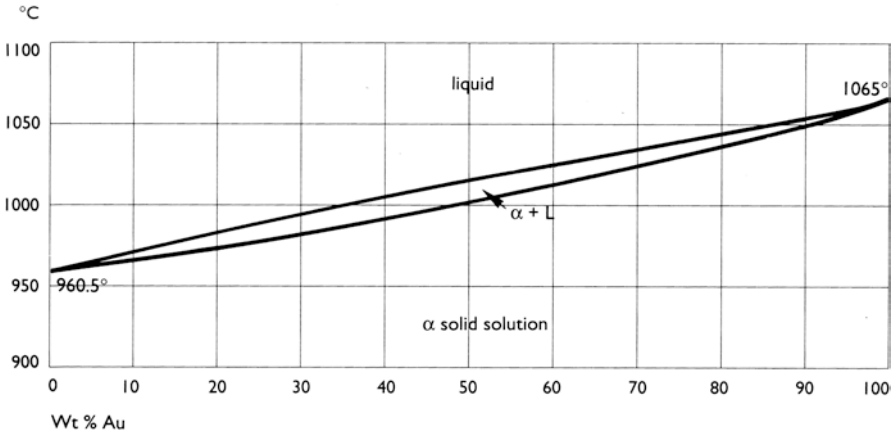

Fig. 4.2 The gold-silver equilibrium diagram

All metals show some solubility in the solid state but in very different proportions. Some metals are completely soluble in each other, and the easiest systems of this class are so-called isomorphous systems, because of the complete liquid and solid miscibility of two elements and a single-phase solid solution which forms for all alloy compositions in the solid state. The phase diagram for the gold-silver system which is a good example is shown in Fig. 4.2.

Gold and silver have the same cubic face-centred (fcc) crystal structure, with very small differences in their lattice constants and their atomic radii (Au = 0.1442 nm; Ag = 0.1444 nm). At any composition of the alloy as it cools down, it reaches the liquidus line and begins to solidify, until the solidus line is reached, at which point the entire alloy is a solid mass of crystals. This is a completely homogeneous solid solution shown on the diagram as the alpha phase, and the grains are usually close to their equilibrium predicted state. The gold-silver system in which complete solid solubility occurs between two components is actually uncommon: most metallic elements are not completely soluble in each other, and at different compositions, different phases form, and these can be seen in the polished and etched microstructures and are modelled by the equilibrium constraints affecting their composition and temperature stability.

Another simple system, but the least common form of binary phase diagram and totally different to the isomorphous systems, are systems with nearly no miscibility in the liquid nor in the solid state. Iron and lead is the best-known so-called monotectic system that has some relevance in ancient metallurgy (Fig. 4.3). In the melt, iron and lead separate due to their different specific gravity, so that the lighter iron solidifies on top of the liquid lead ($L \leftrightarrow S_{Fe} + L_{Pb}$) and finally two layers of solid iron and solid lead remain.

Much more important for many metallurgical processes, such as the so-called cupellation and liquation processes (Sect. 5.1.2), is a three-phase reaction; the monotectic reaction takes place when one liquid phase decomposes with decreasing

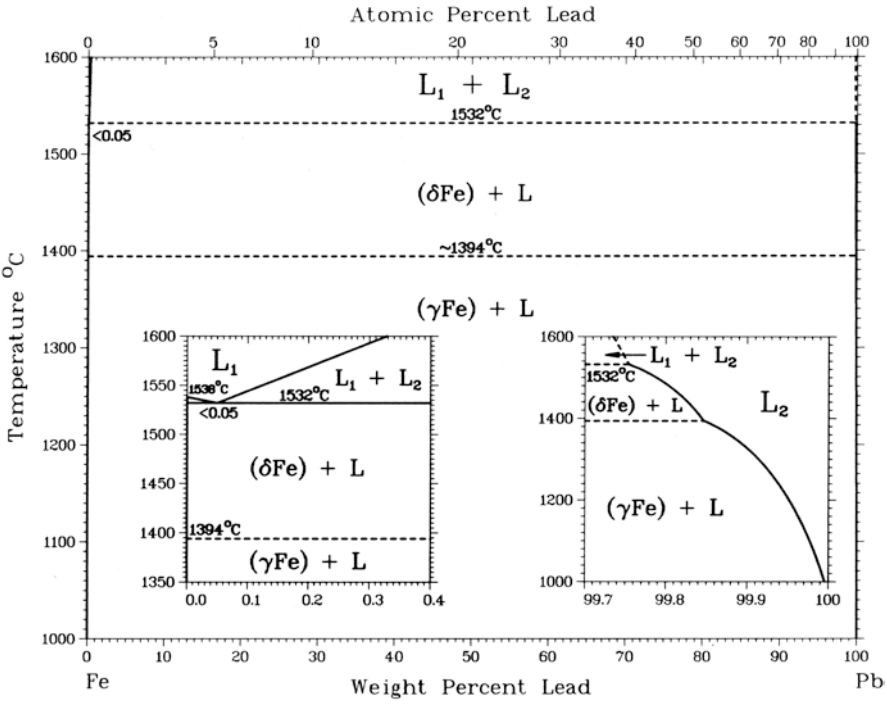

Fig. 4.3 Iron-lead monotectic-type equilibrium diagram. (From Massalski [63])

temperature into a solid phase and a new liquid phase of different composition is formed.

Some phase diagrams of monotectic alloys, such as copper and lead, shown in Fig. 4.4 contains a liquid miscibility gap, in which two liquid phases coexist over a certain composition range and finally constitute individual solid phases of copper and lead ($L_{Cu} + L_{Pb} \leftrightarrow S_{Cu} + S_{Pb}$).

Liquid copper and liquid lead are completely soluble in each other at high temperatures, but with higher lead percentages, between 36% and 87%, lead separates into two liquids on further cooling. Actually, the composition of a copper-lead alloy does not need to be within that range for the monotectic reaction to occur. During freezing of lead-rich copper-lead alloys, the copper-rich α_{Cu}-phase forms first, and the composition of the melt shifts towards the monotectic composition and decomposes. Both solids have only a very limited solubility for each other, and the microstructure of copper-lead alloys usually shows randomly distributed lead particles within a α_{Cu}-matrix. An example is shown in Fig. 4.5.

The fact that lead enters into these reactions with copper at higher temperatures helps to prevent the gross separation of lead from copper, and instead, the most common distribution is in the form of small globules or droplets of lead scattered throughout the object.

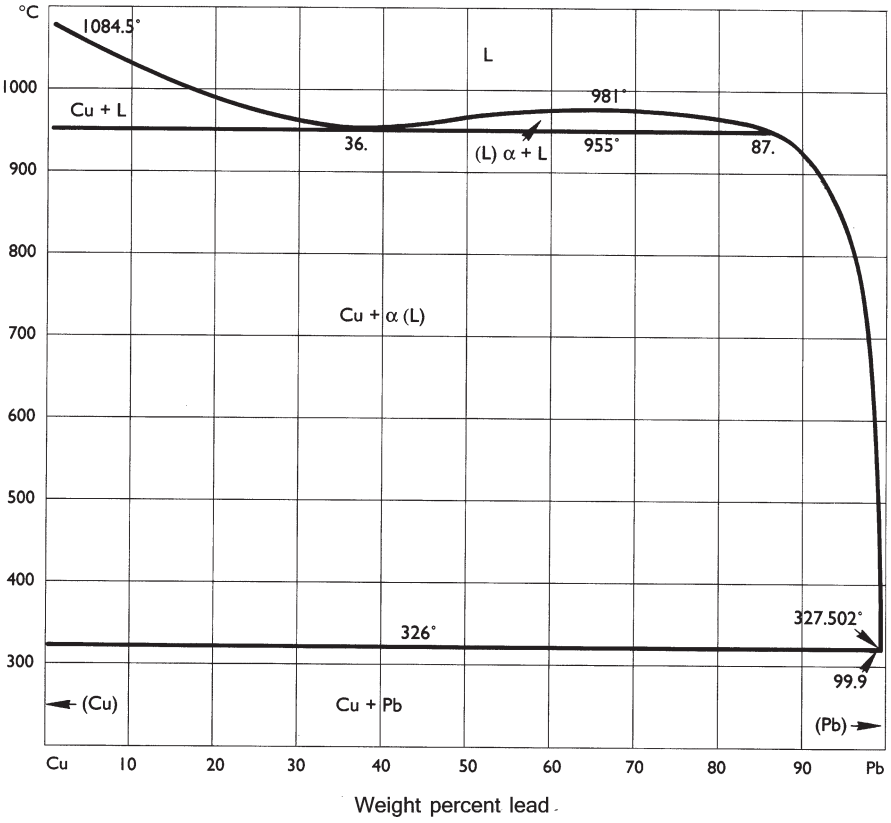

Fig. 4.4 The copper-lead phase diagram with miscibility gap

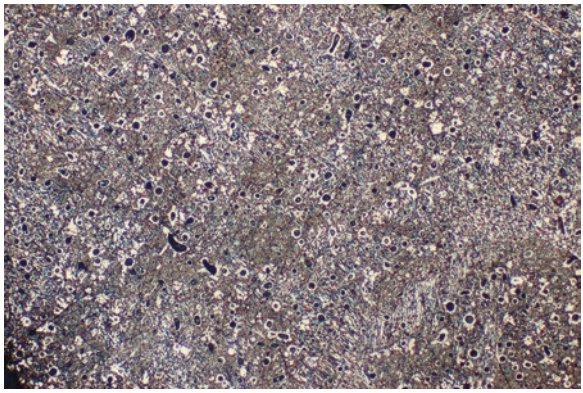

Fig. 4.5 Distribution of fine lead droplets in the ideal cast Chinese bronze mirror from the Han dynasty. The fine lead precipitation ensures that an even and highly reflective surface can be obtained from the mirror, of classic Chinese composition, 5% lead, 25% tin and 70% copper. Etched in ferric chloride, magnification ×200

The lack of solubility of lead in copper has been used in the past to de-silver copper-silver alloys. A cake of the silver-bearing copper is cast into a large disc with the addition of lead. On cooling the discs are held vertically in a furnace, and the lead is molten out by slow heating, leaving a porous copper cake behind, but as silver is attracted to the lead, the molten lead can be cupelled to remove the silver and can be smelted back to metallic lead again, allowing the whole process to be repeated with a new cake of copper, producing metallic silver as a useful by-product (see Chap. 5).

One of the most common types of equilibrium diagrams is that which includes a eutectic, a mixture of two phases in close spatial proximity, which microstructure is usually lamellar, shown in Fig. 4.6, or globular, as in Fig. 4.7.

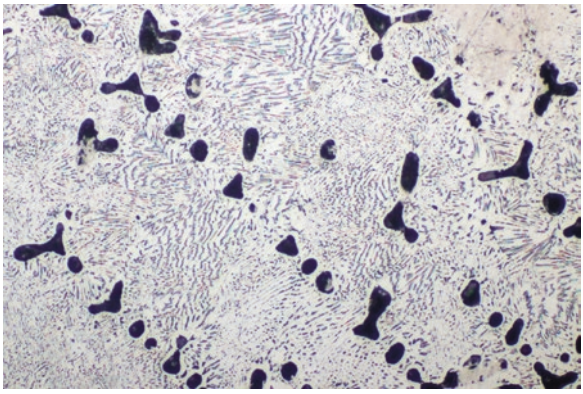

Fig. 4.6 60Ag40Cu alloy as cast. The alloy will precipitate copper-rich dendrites with an infill of the $\alpha_{Ag} + \alpha_{Cu}$ eutectic. As shown here, the eutectic is lamellar, with a fine spacing between the two phases which make up the eutectic. According to the phase diagram, the α_{Cu} dendrites should have about 8% silver content, as a heavily segregated alloy system, this value did not change on cooling, a fact confirmed by electron microprobe analysis. Etched in ferric chloride with nitric acid, magnification ×220

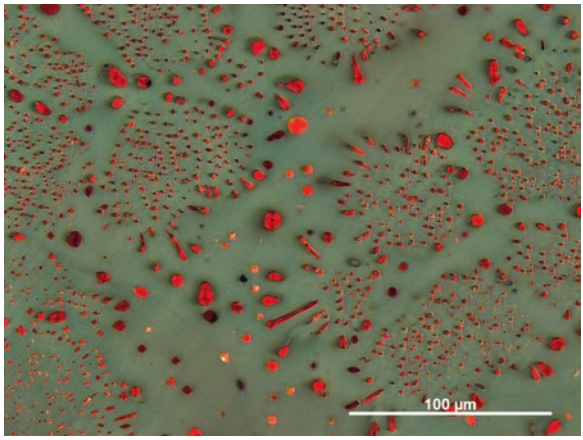

Fig. 4.7 Microstructure of a dealloyed and partly oxidized casting waste from the oppidum of Manching, showing globular microstructure of Cu-Cu_2O eutectic viewed with crossed polarized light

Simple binary eutectic systems are characterized by a solid-solid miscibility gap and have their minimum melting temperature at the eutectic point, when three phases are at equilibrium. The eutectic reaction converts one liquid phase directly into two distinct solid phases: $L \leftrightarrow S_\alpha + S_\beta$. The silver-copper system, which is shown in Fig. 4.8, is of timeless importance, as silver-copper alloys have a very long history (Chap. 5).

The area above the liquidus line shows the region where the mixture is liquid and the areas between liquidus and solidus line, where the alloy is a mixture of liquid and solid phases. The region below the eutectic isotherm is a mixture of two solid phases, a face-centred cubic silver-rich solid solution on the left side, here labelled α_{Ag}, or simple designated as (Ag), and a copper-rich solid solution of the right side. A typical range of microstructural types is shown in Fig. 4.9.

Due to traditional labelling, this phase is usually called β, whereas it is also face-centred cubic and is therefore sometimes labelled α_{Cu} or simply designated as (Cu). At the eutectic point, the molten alloy passes directly from liquid to solid, at 71.9% silver and 28.1% copper. Notice that the melting point of the eutectic is much lower than the melting point of either of the pure constituents, at 779 ° C. This is of great practical importance, since silver artefacts can then be soldered together with silver-rich alloys without the danger of the silver artefact itself becoming molten.

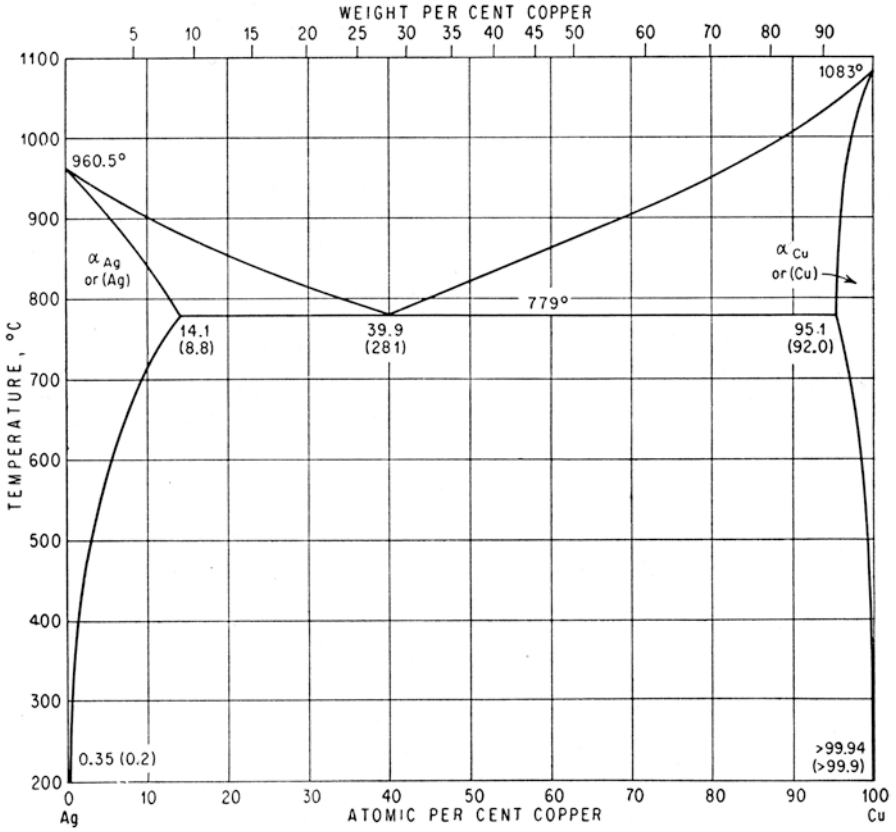

Fig. 4.8 The silver-copper phase diagram (after Hansen and Anderko [35])

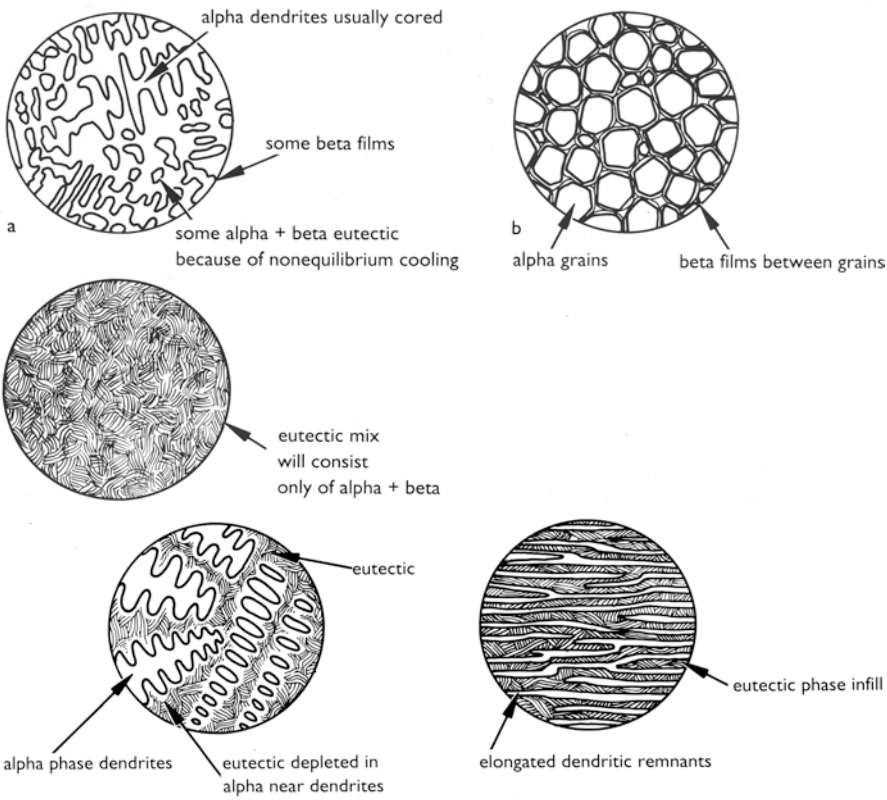

Fig. 4.9 Range of microstructural types of Ag-Cu alloys (after Scott [103])

Equilibrium is very sluggish in the silver-copper system, and in some alloys, very little change in composition of the cast phases takes place from the period of their solidification to their worked end product. Microstructures of alloys with compositions less than the eutectic are termed hypoeutectic and hypereutectic when greater than the eutectic composition. For alloys with a solid-to-solid transition, the phrases used are hypoeutectoid and hypereutectoid.

For soldering in precious metals, various proportions of copper and silver are used for this kind of operation, and a number of different recipes are recommended by classical recipes, such as those described by the Renaissance craftsman, Benvenuto Cellini [15, p. 93]: "…the solder I used was *ottavo*, that is a solder composed of one-eighth part of an ounce of copper to one of silver…….I bound the two legs to the body. Then I laid it on the wall over a good fire, and applied *quinto* to it, i.e., solder composed of one fifth of an ounce of copper to one of silver. As I worked with eleven-and-a-half silver to half copper I had nothing to fear as far as the latter was concerned and I would have everyone aware that if he wishes to make his job succeed he must not employ inferior silver…".

The statue that Cellini was working on was therefore cast in an alloy of 99.6% silver and 0.35% copper [15, 104]. This is practically pure silver with a melting

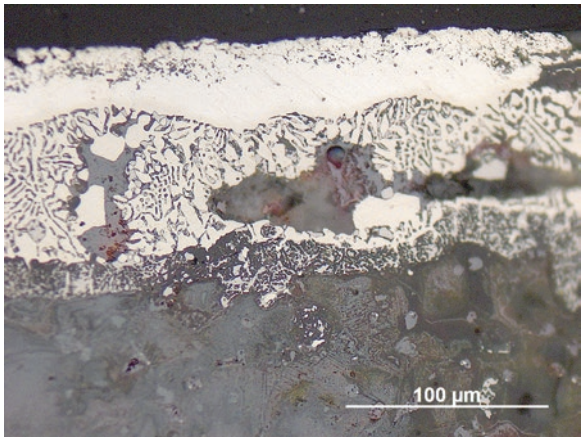

Fig. 4.10 Unetched microstructure of a soft-soldered silver sheet on a bronze surface viewed with bright-field illumination. The micrograph shows Ag_3Sn-Cu_3Sn eutectic between sheet and substrate, in which copper-rich phases are partly corroded

point of 961 °C. The ottavo solder has a composition of 91.1% silver and 9.9% copper, with a liquidus of 880 °C, while the quinto solder, used for heavier attachments, has a composition of 86.1% silver and 13.9% copper and has a liquidus at 845 °C. All of these alloys are hypereutectic and will precipitate silver-rich phases first during solidification. The phase diagram shows that the quinto alloy melts at a temperature over 100 °C less than that of the silver Cellini used for the statue itself.

Another important eutectic alloy in antiquity is that of the lead-tin system which produces a range of microstructures rather similar to that of the copper-silver system. The eutectic point of the lead-tin system, for example, is relevant to soft solders, which have been used from archaic Greece to modern times (Chap. 5). Eutectic points of several systems have usually no technological relevance to most customary pre-industrial alloys, but their phase diagrams are important in the interpretation of some unusual microstructures, which might have been produced accidentally, like that shown in Fig. 4.10 that shows a cross section of a fragment coming from a life-sized Roman statue found in Luxembourg [28].

This fragment has been plated by a silver sheet, which has been soldered to the bronze body by a tin solder. The eutectic point of the Ag-Sn system is at 221 °C and 96.2 atomic percentages of tin, where the liquid would decompose into the silver-rich intermetallic ε-compound (Ag_3Sn) and β_{Sn} [47], but the newly formed tin-silver solder has reacted with the bronze and decomposed eutectically to silver-rich ε-phase (Ag_3Sn) – labelled θ in the ternary system – and tin-rich ε-phase (Cu_3Sn) of the Cu-Sn system – labelled ε_1 in the ternary system [17].

Figure 4.11 shows a generalized eutectic equilibrium diagram and some of the typical types of microstructure associated with eutectic alloys of metals A and B. Alloy of composition I is a hypoeutectic alloy, having less of component B than the eutectic. If cooled under equilibrium conditions, at point c on the diagram, solid begins to precipitate. This solid is a primary solid solution of B in A. As cooling proceeds, the composition of the solid moves along the solidus line, and the liquid cools until it reaches the point E at which it breaks down into the two different phases of alpha plus beta as a fine eutectic mixture. This is shown in drawing (a). Similarly if an alloy of composition II cools down, then grains of beta phase will

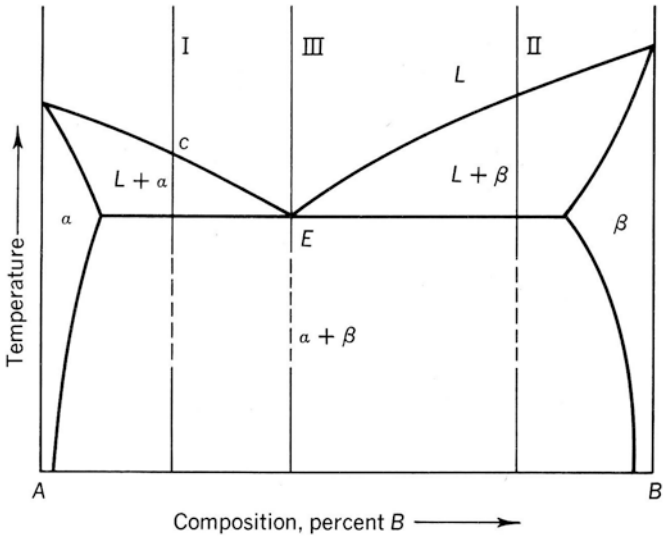

Phase diagram of the *A*-*B* system showing a typical simple eutectic diagram.

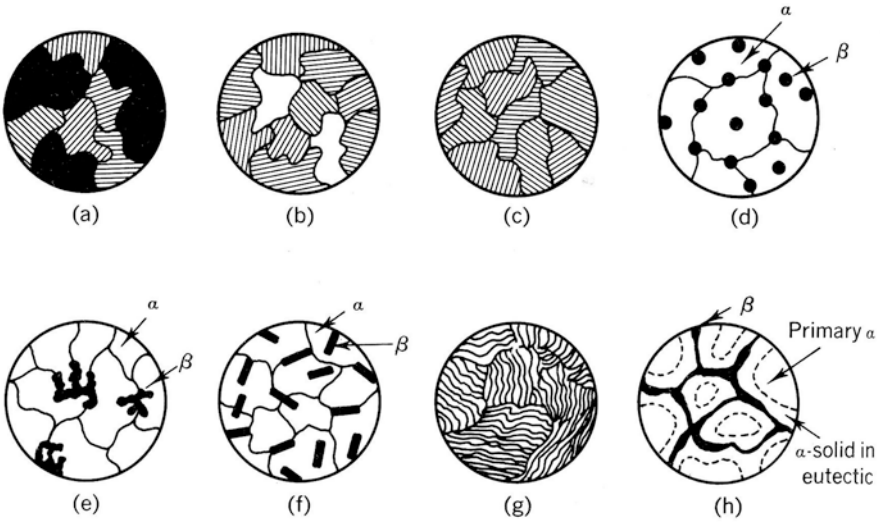

Fig. 4.11 Generalized eutectic equilibrium diagram and some of the typical types of microstructure associated with eutectic alloys of metals A and B

form, and the remaining infill will consist of the eutectic as shown in drawing (b). This alloy can be referred to as a hypereutectic, as it contains an excess of component B. Alloy III corresponds exactly to the eutectic point E and will pass directly from liquid to solid forming a fine intermixture of the eutectic as shown in drawing (c). If the eutectic composition is close to the composition of one of the phases mak-

ing up the eutectic, then a variety of different microstructures are possible. These structures are the nodular, often spheroidal, structures, shown in drawing (d), the irregular precipitates of drawing (e), acicular precipitates of drawing (f), coarse lamellae of drawing (g) and the divorced eutectic of drawing (h). There is a tendency for the two phases to separate into large regions so that there is considerable divergence from a normal eutectic structure. In the divorced eutectic, there is no distinctive boundary between the primary solid solution and the portion of the same solid solution in the eutectic.

A similar phase change to the eutectic decomposition is the so-called eutectoid reaction. The difference is the transformation of a solid phase into two other solid phases at a certain temperature: $S_\gamma \leftrightarrow S_\alpha + S_\beta$. Eutectoid transformations are best known from the copper-tin system and iron-carbon alloys (Sect. 4.6 and 5.2).

Some binary systems such as the copper-gold system, shown in Fig. 4.12, which have also the same type of lattice structure (fcc) do not show a distinct eutectic point but have a so-called congruent melting minimum, which is of great importance to ancient goldsmithing techniques, such as granulation. Congruently melting compounds melt or decompose like isomorphous systems to a single phase without compositional alteration as in the eutectic reaction but also at a definite temperature. The copper-gold system does have some complications, because ordered phases can form at certain compositions, which may create brittleness in gold alloys if they are not annealed correctly (Sect. 4.6).

The last of the basic schemes of binary phase diagrams is the peritectic equilibrium diagram. The peritectic reaction is characterized by a primary precipitation of a solid phase from the liquid, which is temporarily thermodynamically stable and in equilibrium with the melt. There are different mechanisms of peritectic reactions, but generally, the primary solid phase is metastable and persists only for a finite length of time, whereas below the peritectic temperature, a new solid phase is formed: $L + S_1 \leftrightarrow S_2$. "Pure" peritectic systems are less common and without significance to ancient alloys. Indeed some of the most important systems such as Cu-Sn or Cu-Zn show one or more peritectic reaction. Most binary systems of interest do not consist of only eutectic, monotectic or peritectic reactions but of combinations of the fundamental reactions described above (see Chap. 5).

4.2 Intermetallics

Isomorphous or eutectic systems result in the formation of one or two solid solutions of large variable composition, whereas in peritectic systems or more complex systems with peritectic reactions, intermediate phases occur, which have a finite stability. Intermediate phases often have structures which are different from the component elements, and some of them have only a narrow range of compositions, whereas others show an extended compositional stability range. Due to the restricted

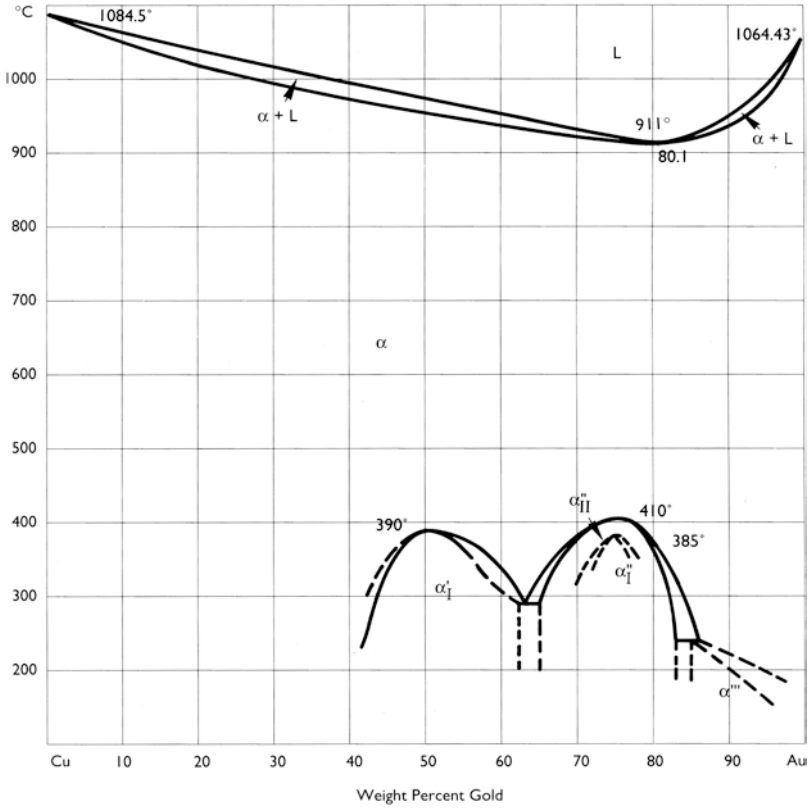

Fig. 4.12 Copper-gold equilibrium diagram

stoichiometric compositions of some intermediate phases, they are called intermetallic compounds. Modern physical metallurgical terminology differentiates between intermetallic compounds with sharply defined compositions and intermetallic phases with extended stability range and suggests using the term intermetallics for both (see Steurer [116]). Albeit their strict range of stoichiometry, intermetallic compounds do not obey normal valence rules, and their bonding is not only metallic (see Steurer [116]). The formation of intermetallics is relevant to many metallurgical processes and metalworking, since most intermetallics are much harder, have lower melting points and are more or sometimes less corrosion resistant than the solid solutions, and they usually have different colours. In consequence, the presence of intermetallics has significant influences on the mechanical, optical and casting properties of alloys. The formation of the δ-phase ($Cu_{41}Sn_{11}$) is not desirable in ancient bronzes, for example, on cold-working of alloys which contain the delta phase, because this phase tends to shatter when hammered, but the δ-phase is beneficial for reflectivity and polishing of special artefacts such as mirrors (Sect. 5.1). The presence of silver-coloured γ-phase (Cu_3As) on the surface of

objects made of arsenical copper has been discussed as being an intentional effect, which in some cases it may be, rather than due to inverse segregation. Silver-coloured copper alloys containing high amounts of tin, arsenic, antimony or nickel have been used in many cultures at different times to imitate silver (see Sect. 5.1). Beside nickel, the colour changes are all based on the presence of intermetallics.

4.3 Cast Structures

Inhomogeneity of metals is termed segregation. There are several forms of segregation. These are called normal, inverse and dendritic. Gravity segregation is usually not observed in ancient metals, although there are cases where lead has begun to pool to the bottom of some cast objects due to gravity, such as leaded bronze Roman mirrors. The most critical for copper alloys is dendritic segregation. An example is shown in Fig. 4.13.

As the liquid cools through the region where the first solid begins to form, small snowflake-like particles of solid begin to solidify. These are the dendrites. The dendritic structure is essentially affected by the cooling rate, which again depends on different factors such as elemental composition, size of the castings, mould material and temperature of the mould during casting as well as cooling rate. The spacing between adjacent arms in dendrites, so-called dendrite arm spacing (see Sect. 3.3.2.1), is made finer by increasing the cooling rate. Modern commercial copper alloys show minimum dendrite arm spacing of 10–100 µm [24], while small archaeological items have less than 10 µm.

Another common form of segregation produces columnar grains, long radiating crystals, which are usually seen in chill castings, copper ingots or copper electrotypes, and an example is illustrated in Fig. 4.14.

Chill castings are castings that have been made into an unheated mould. The columnar grains of chill castings are not very common in ancient cast materials,

Fig. 4.13 Casting dendritic segregation in a 20% tin 80% copper, tin bronze, air cooled from 1200 °C. Dendritic segregation results in the alpha + delta eutectoid structure being present between the alpha phase initial solidification. Etched in ferric chloride, polarized, magnification ×150

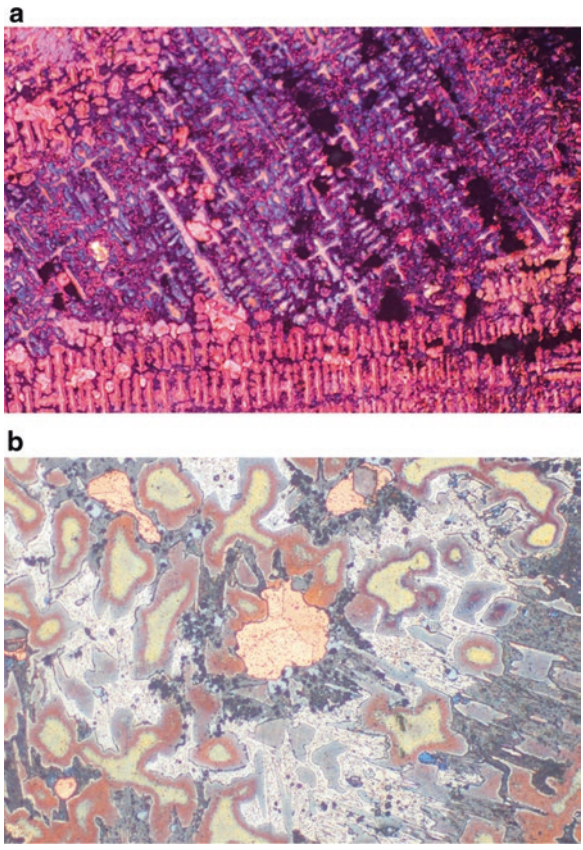

Fig. 4.14 (**a**) Luristan ceremonial dagger handle showing extensive coring and separation of the alpha + delta eutectoid, some of which has corroded, resulting in loss of tin and redeposition of metallic copper within the corroded matrix, clearly seen here. Colour etched in Klemm's reagent, magnificaton ×320. (**b**) Etched in ammonium persulphate followed by dilute ferric chloride. In the centre of the photomicrograph the redeposited copper can be seen, with some grain detail in the form of lines of growth, set in the tin-bronze matrix of the dagger handle, showing cored grains and some areas of alpha + delta eutectoid. The redeposited copper is often twinned. Magnification x200

because of cooling slowly in ceramic moulds or the presence of substantial alloying elements such as arsenic or tin, which result in the solidification of higher-temperature phases first of all, and tin-rich or arsenic-rich liquid remains which then fills in the spaces between the dendritic crystals.

The silver-copper alloys, for example, are often heavily segregated, and the dendrites that begin to precipitate out may remain fixed in that state and composition when the alloy cools down to a solid state. The consequence of this is that the structure may be out of equilibrium and contain a series of dendrites surrounded either by the alpha (α_{Ag}) or beta phase (β_{Cu}) or the eutectic mixture itself. These kinds of structures, with dendrites or distorted dendrites as a result of working to shape, are quite common in ancient or historic silver-copper alloys. If alloys with low amounts of these alloying elements are annealed, then equi-axed grains can be produced as the dendritic segregation can be removed. If solute segregation has not been sufficiently removed by annealing before cold-working, banding occurs, which is shown in Fig. 4.15 for a tin bronze and in Figs. 4.16 and 4.17 for cupronickel-alloys with high amounts of iron and cobalt. This banding can persist across the recrystallized

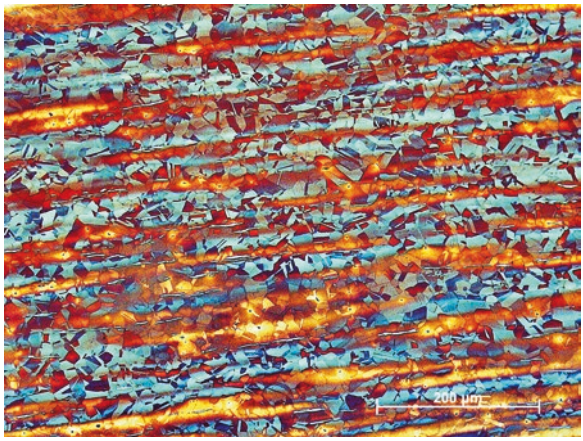

Fig. 4.15 Tin and antimony-rich banding in the microstructure, a late Bronze Age bronze ring with 3.6% of tin and 1.2% Sb from the Hünenburg, Germany. Etched with Klemm's reagent II

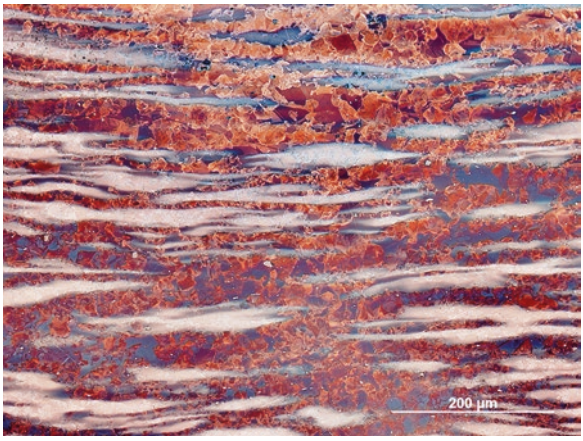

Fig. 4.16 Segregation of iron-nickel-cobalt-rich phases within the microstructure of a high-nickel copper alloy of a pin from Kesikkaya, Turkey. The recrystallized non-segregated grains of the copper-rich phases are revealed by Klemm's reagent III, whereas the segregations were not attacked by the etchant. The alloy contains 22% nickel, 5.8% iron and 2.7% cobalt and has a mean hardness of 180 HV 0.1 ± 10

grains and can be seen as shadows or lines on etching the sections of the objects under examination.

Banding of residual dendrites is very often observed in arsenical copper alloys, as shown in Fig. 4.18 [14, 55, 88], while banding in silver alloys can also be due to residual dendrites but is mostly influenced by the micro-segregation of solute elements due to cold-working [46, 54, 55, 124].

Highly leaded alloys were quite popular in the European Iron Age and Hellenistic and Roman period, as well as in Asia. Some examples of these types of alloys include Chinese bronze mirrors, whose classical composition calls for 25% tin, 5%

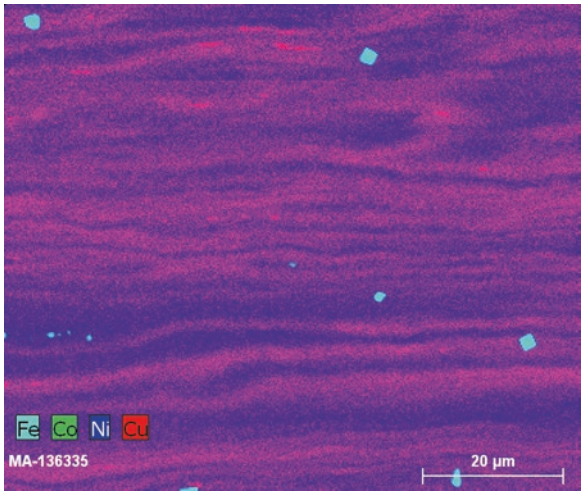

Fig. 4.17 Qualitative pseudo-coloured EDX-dot map of a wire ring from Boğazköy, Turkey. The alloy contains 20.7% nickel and 1.2% cobalt

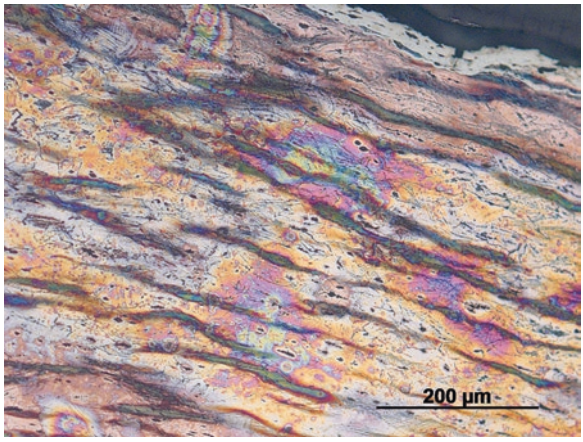

Fig. 4.18 Arsenic segregation of residual dendrites and silver-coloured cubic γ-phase ($Cu_{3-x}As$) on the surface of an eneolithic dagger from the cemetery of Singen, Germany. The alloy has a mean content of 5.2% arsenic; the γ-phase shows 27.5 to 29% arsenic

lead and 70% copper. Roman bronze mirrors, with less tin and more lead, up to about 8% lead were made in the Roman Iron Age.

An example of a heavily leaded bronze microstructure is shown in Fig. 4.19, a bronze Herm, in the collections of the J. Paul Getty Museum. The lead has pooled to some extent in certain areas of the heavily leaded casting. Segregation is quite common in these alloys. It is unusual for the lead to sink down through the alloy, in many cases it remains inside the alloy and in German is known as "Blocksaigerung" as the lead-rich phases follow the heat and agglomerate at the hottest spots, which is usually internal to the artefact concerned.

The casting condition is one of the most important factors involved in this phenomenon (see Hanson and Pell-Walpole [34]), but mould material, gating systems and the presence of elements such as tin, arsenic and antimony have a significant

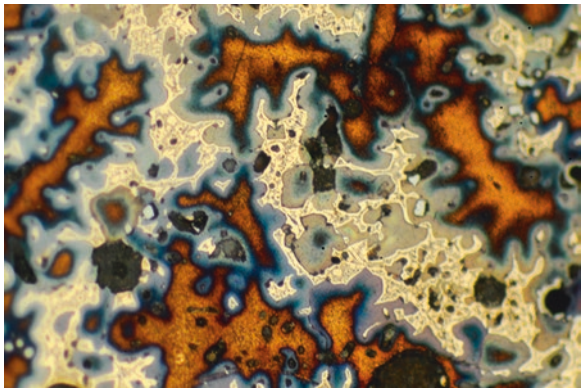

Fig. 4.19 Microstructure of a Greek bronze Herm in the collections of the J. Paul Getty Museum. The cast bronze Herm, a leaded bronze with about 8% tin content, 5% lead, is in the cast condition, with prominent coring present and areas where the alpha + delta phase of the bronze system can clearly be seen. Etched in ferric chloride, magnification ×120

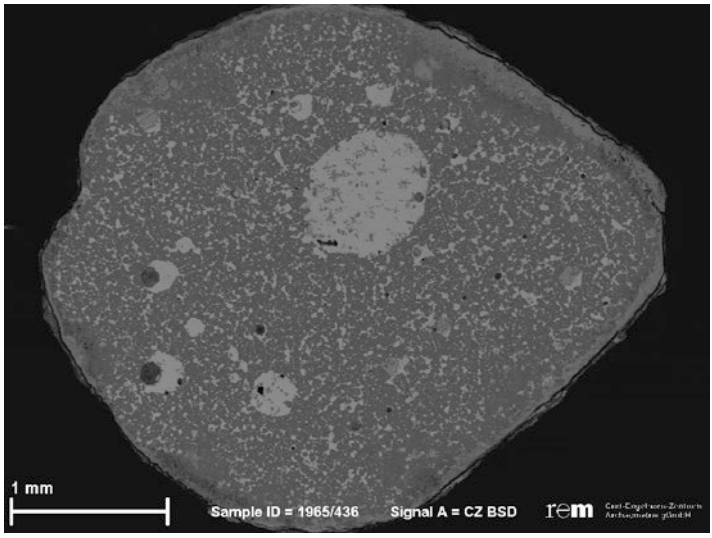

Fig. 4.20 SEM-backscattered electron image of a Late Iron Age ring from the oppidum of Manching, Germany with a mean lead content of 26% and 6.5% antimony shows heavy lead segregation in the centre and a mean hardness of 80 HV 1

negative effect on the segregation properties of copper-lead alloys. Figure 4.20 is a cross section of a typical Late Iron Age ring with a mean lead content of 26% and 6.5% antimony. The microstructure consists of randomly distributed lead particles and some macro-segregated drops of coalesced lead containing dendrites of α_{Cu}-solid solution, $\delta_{(Cu\text{-}Sb)}$-phase ($Cu_{4.5}Sb$) and globular sulphide (Cu_2S). The segregation of the lead has caused a monotectic reaction, when copper-rich α_{Cu}-phase, the $\delta_{(Cu\text{-}Sb)}$-phase and cooper sulphide decomposed from the liquid with decreasing temperature.

4.4 Pores and Non-metallic Inclusions

4.4.1 Pores

As mentioned above, the microstructure of an object consists not only of its metallic compounds but also of compounds of metals and non-metals, of non-metallic constituents and finally of pores. Porosity is commonly observed in ancient metals and often produces difficulties in castings. Casting defects and shrinkage cavities frequently occur within large castings, such as life-sized statues. Figure 4.21 shows a typical dendritic appearance of pores.

These occur when the casting system is not available to compensate for shrinkage during the transition from the liquid to the solid state. The so-called solidification contraction is due to the fact that solid metals have higher densities compared to the liquid and the molten metals decrease in volume as they solidify. When the alloy solidifies non-uniformly because of variations in temperature due to different wall thicknesses, inappropriate gating systems or other problems, local volume deficits can form cavities. Shrinkage cavities can contain gases or segregated metallic compounds such as lead or eutectic components. Gases such as oxygen or hydrogen are always present during the production of metals, and gas-metal reactions can form a variety of undesirable effects. Blowholes are casting defects that result in the evolution of gas bubbles entrapped in the solidifying metals (see Chap. 3, Fig. 3.20). Actually, most of the gas rises to the surface during solidification and escapes by spitting the hot liquid metal around. Pliny ([83], 34, 96) refers to this negative effect of hydrogen in the casting of large statues, which is due to the increased air moisture during summer time: *"Id quoque notasse ab re est, aes omne frigore magno melius fundi." (It is also not out of place to notice that all copper and bronze fuses better in very cold weather).*

Fig. 4.21 Heavy cored bronze casting waste from the oppidum of Manching, Germany with dendritic appearance of pores. Unetched specimen containing 9.5% tin and 7.2% lead

4.4.2 Non-metallic Inclusions

Blowholes and spitting are not the only effects of gas-metal reactions. These can form non-metallic constituents. There are usually extensive miscibility gaps in the liquid state and complete immiscibility in the solid state between metallic and non-metallic phases, such as oxides, silicates or sulphides. Therefore some non-metallic constituents exist already as separated liquid phases or as solid particles in the molten metal, or others are soluble in the melt and become distinct precipitations when solidification occurs. In any case, non-metallic phases are coarsely or finely dispersed in the solid metal as distinct inclusions. The inclusions in ancient metals are a valuable source of information as non-metallic inclusions cannot recrystallize during cycles of working and annealing and so act as additional messengers of change from the cast to the worked state. As working proceeds, inclusions tend to become flattened and elongated along the length of the section, and they retain this characteristic throughout their material existence, as illustrated in Fig. 4.22.

In heavily corroded alloys, where the bulk of the metal has been totally lost to corrosion, non-metallic inclusions can provide important clues as to whether the object has been deformed by working and annealing or is in a cast condition. This is because the inclusions are preserved in the corrosion products and, if elongated along the length of the section, are an indication that working and annealing, or hot-working to shape, has occurred.

There are different sources and reasons for non-metallic inclusions. Especially in pre-industrial metallurgy, there are a large variety of different non-metallic constituents. Modern metallurgy considers such inclusions to have deleterious effects on metals and should be eliminated if possible. Inclusion rating characterizes them by origin, and so they are classified to generally fall into two groups, those of indigenous and those of exogenous origin [122]. Indigenous inclusions can occur because of the reaction of the hot or molten metals with gas, when metals become compounds by oxidizing during manufacturing processes or due to their limited solubil-

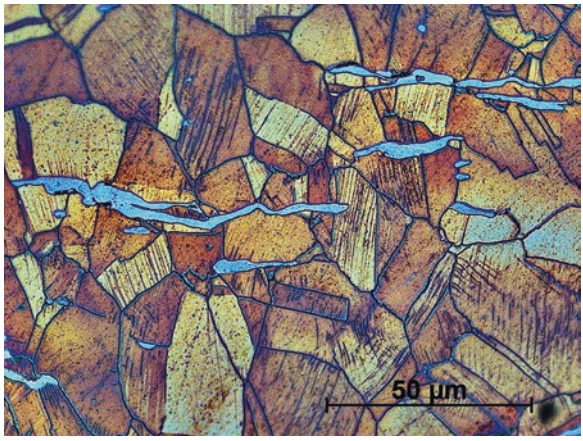

Fig. 4.22 Elongated copper sulphide ($Cu_{2-x}Fe_xS$) inclusions within the annealed and cold worked microstructure of Early Bronze Age miners pick from the Mitterberg mining district, Austria with a maximum hardness of 350 HV 0.1. Volume fractions of the inclusions have been determined to be 3.9–4.8%

ity in the solid metals. Exogenous inclusions form by interaction of molten metals with non-metallic material such as slag, furnace linings, moulds or crucibles. This classification is helpful, but cannot be transferred one-to-one to non-metallic inclusions of ancient metals. Most of the inclusions in ancient metals would be classified as those of indigenous origin, even when they are constituted with the involvement of exogenous sources. Similar to modern metallurgy, non-metallic inclusions are best known from ferrous alloys but especially as a result of the bloomery process (Chap. 5), where they derive from different origins than those in modern steelmaking processes. Due to the solid-state reduction of iron ore to solid metal, all wrought iron produced in the bloomery process usually contains large volume fractions of slag inclusions, which originate from the first step of production, the smelting process. Iron can already be reduced from its oxides at about 640 °C, which is considerably below the melting point of iron at 1535 °C [59]. However, the iron ores contain numerous impurities such as silica or alumina, often referred to as the "gangue" minerals, which must be removed if the smelting is to be successful. To achieve this, these minerals must be separated out as a liquid slag, for which the temperature in the furnace must be kept at about 1150–1350 °C, and it is this which can be difficult to achieve while also retaining enough carbon monoxide to effect reduction of iron [81, pp. 131–140]).

To separate metal from slag, the slag should be of low viscosity to create a liquid or pasty mass or retain enough fluidity to be tapped. The viscosity of slag depends on the basicity of the slag, as alkaline oxides lower the viscosity of slag significantly [1], for which reason fluxes such as limestone could be added. Actually, there is hardly any evidence for deliberate flux additions to European bloomery processes before medieval times, when the earliest blast furnaces in Europe were developed [11, 12, 81]. Therefore, metal-slag separation usually has not been very effective, and most bloomery iron contains large volume fractions of slag inclusions, which predominantly derive from the smelting and contain information about the process and the ore used. This information can be retrieved utilizing analytical methodologies with a high-spatial resolution. Electron microanalysis is capable of revealing the smelting conditions, but for information concerning provenance of the iron, more sensitive methods such as laser ablation-inductively coupled plasma-mass spectrometry (LA-ICP-MS) should be used (see Coustures et al. [19]; Dillmann et al. [27]).

In contrast to modern steel, the inclusions in early bloomery iron are exclusively oxides, with iron oxide, wüstite (FeO) and iron silicate and fayalite (Fe_2SiO_4) as the main phases, shown in Figs. 4.23 and 4.24, whereas higher iron oxides do not survive the reducing conditions necessary to produce metallic iron but are present within purifying slag of later periods [11, 12]. The iron oxide phases are usually embedded in a matrix of glassy components with decomposition of silicate or spinel group minerals such as leucite or hercynite [11]. There is a correlation between the metal structure and certain mineral phase assemblages within the inclusions, which has already been described by Buchwald and Wivel [13]. Depending on the ratio of carbon monoxide (CO) and carbon dioxide (CO_2), the microstructure of bloomery iron can be very varied.

Fig. 4.23 SEM-backscattered electron image of a slag inclusion with wüstite dendrites in fayalite matrix within the ferritic part of a bloom from a shipwreck discovered close to Kyrenia in Cyprus and dated to the fourth century BC. Mean volume fractions V_V of the inclusions have been determined to be 11% ± 5

Fig. 4.24 SEM-backscattered electron image of fayalite and glass components of a slag inclusion within the microstructure of a Mongolian belt buckle from a rock tomb of Nükhen Khad in the Zhargalant Khairkhan mountains, dated to the sixth to eighth centuries AD

Figures 4.23 and 4.24 show typical iron-rich slag from ferritic or ferritic-pearlitic microstructures, whereas Fig. 4.25 shows glassy slag within pearlite. The volume fractions of wüstite, fayalite and glassy components correlate with volume fractions of ferrite and pearlite, because of the decomposition of wüstite to iron and the carburization of the iron within a reducing atmosphere (see Buchwald [11]; Buchwald and Wivel [13]).

Wrought iron does not only contain inclusions which originate from the smelting process. Every forging must be done under red heat, and this leads to oxidation of

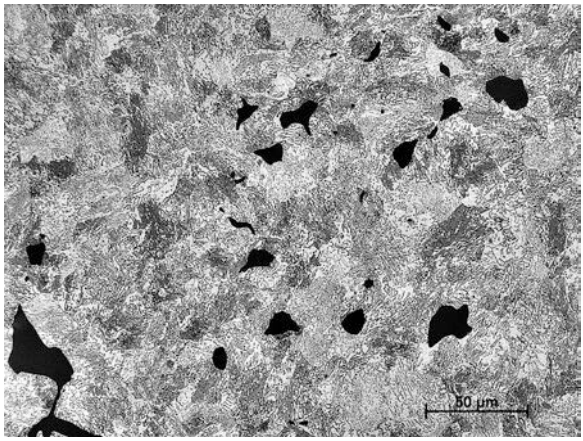

Fig. 4.25 Glassy slag inclusions within the pearlite-rich part of the iron rack of the bronze couch from the Hochdorf tomb, Germany, which is dated to the Early Iron Age (Ha D). Etched with nital

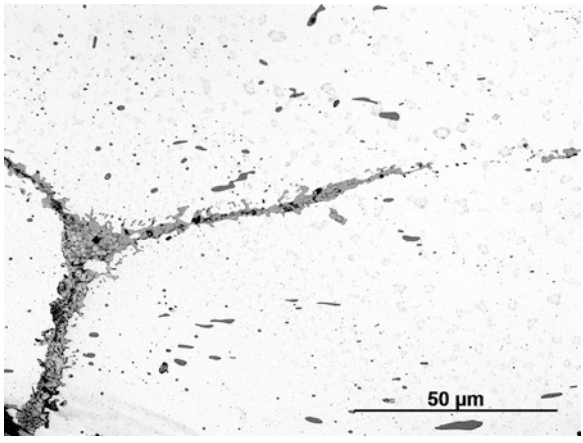

Fig. 4.26 Wüstite slag inclusions along the welding seams of a pattern welded early medieval sword

some of the iron. The fabrication of composites had to be carried out by forge welding (Chap. 5), and the need for fluxes for this process introduces new slag components. Figure 4.26 shows a massive formation of wüstite in the weld seam of an early medieval pattern welded sword from Mannheim, Germany.

With the rise of the indirect process following the development of the blast furnace during the Middle Ages, the characteristics of non-metallic inclusions in iron and steel change drastically. As with industrial steels, most inclusions derive from the fining of the cast iron, and most elements in the inclusions are oxidized minor constituents reacting with exogenous impurities [26, 50]. Iron sulphide inclusions (FeS_2) have been found in a pig iron from a high medieval smelting site near Reutlingen, Southern Germany, shown in Fig. 4.27. It is quite unlikely that the ironworkers were already using coal, but some ferruginous sandstone deposits are chatted with pyrite, which might have been used.

In copper alloys, sulphide inclusions tend to be more prominent constituents than oxides, but there are also a variety of compounds and minor accompanying ele-

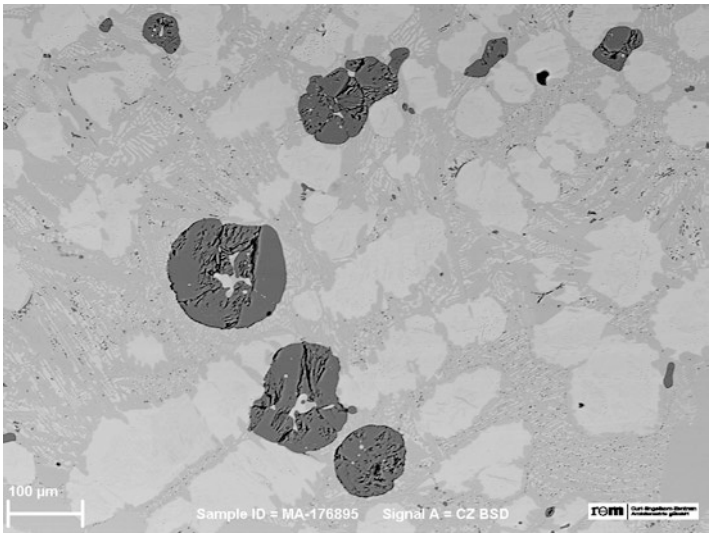

Fig. 4.27 SEM-backscattered electron image of iron sulphide (FeS_2) inclusions of a metal working debris from a smelting site near Reutlingen, Germany. The hypo-eutectic microstructure of the metallic matrix is already visible in the unetched state

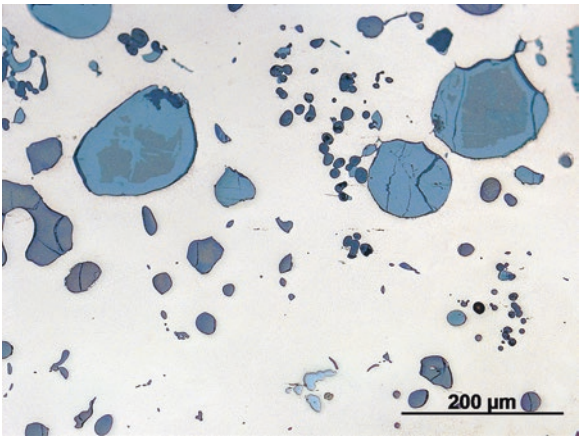

Fig. 4.28 Matte inclusion (dark-grey) and partly converted matte inclusion (blue-grey) in a planoconvex ingot of black copper from Urnfield period ingot storage. Metallic iron is light grey. Unetched and in bright-field illumination

ments within these inclusions. The determination of the bulk compositions of copper alloys is biased since some of the elements detected are present as components of the non-metallic inclusions, as well as metallic phases. Figure 4.28 shows a cross section of a late Bronze Age planoconvex raw copper ingot from Burladingen in Southern Germany. The mean volume fraction of the sulphide inclusions has been determined to be 8% (±2.2) by area analysis. Most of these inclusions contain iron in variable amounts. Contrary to the statements of Craddock [21], there is ample evidence for a matte smelting process in the Eastern Alpine region during the Bronze

Age (see contributions in Stöllner and Oeggl [117]), and according to this practice, most of the inclusions of that ingot are stoichiometrically related to the matte mineral bornite (Cu_5FeS_4). Indeed part of the iron is already removed by roasting, so that there are also iron-bearing copper sulphides ($Cu_{2-x}Fe_xS$) and some pure copper sulphide inclusions (Cu_2S) present, as seen in Fig. 4.22.

The total iron content of the sample has been determined by XRF to be 2.8%, which represents not only all the copper-iron-sulphides but also the metallic iron, which is precipitated from the molten copper (see Sect. 5.2). Matte inclusions rarely survive refining, alloying and casting of copper unchanged, but many sulphide inclusions of ancient copper alloys still contain iron ($Cu_{2-x}Fe_xS$), usually less than 1%. Sulphide inclusions of late Bronze Age cupronickel-alloys from Anatolia also contain nickel and cobalt [56], inclusions of paktong alloys (Chap. 5) contain nickel and zinc, while copper-arsenic-antimony alloys of the Nahal Mishmar hoard from the Judean Desert, dated to the fourth millennium BC, contain arsenic and antimony-bearing copper sulphide inclusions [119]. Sulphide inclusions may have traces of selenium and tellurium, which originate from sulphate-containing copper ores and which substitute part of the sulphur (see Rehren and Northover [91]; Zwicker [132]). The amount of selenium in copper sulphide inclusions is usually high enough to be established by EDX, whereas the concentration of tellurium is much less and its detection needs a more sensitive method of analysis such as WDS-EPMA.

In brasses, the iron content of copper sulphide inclusions is usually substituted by manganese (see, e.g. Barrena et al. [4]; Brüggler et al. [8]) and in paktong alloys as well. There are no investigations or experiments available to explain why this is the case at the moment, but the phenomenon is connected in all probability with the cementation process, when iron gets reduced and enters the solid solution (see Sect. 5.1). The compositions of non-metallic inclusions within brasses can vary within one object. Brasses usually contain copper-zinc or zinc-copper sulphides (CuZnS, $(Cu,Zn)_2S$, ZnCuS) or pure zinc sulphide (ZnS), rarely zinc-copper-disulphide inclusions ($ZnCuS_2$). They typically have traces of manganese and selenium. Zinc-bearing bronzes or gunmetal alloys do also show zinc-copper sulphides (see Willer et al. [129, Table 1]), but they still contain iron, because they derive from the bronze addition.

Copper oxide inclusions (Cu_2O) can derive from ores containing oxide or carbonate copper minerals or from the inner oxidation of copper. Native copper and raw coppers melted from sulphidic ores contain sulphide inclusions, but during melting it absorbs oxygen, and copper oxide inclusions can appear additionally to sulphides [125]. Eutectic and hypereutectic microstructures of copper and oxide are regularly found in casting waste (Fig. 4.7). Copper oxide inclusions in copper-arsenic alloys or copper-antimony alloys are often associated with other oxidized minor elements such as arsenic or antimony oxides [14, 73, 75], while more noble metals have no effects on the inclusions.

Other non-metallic inclusions in copper alloys, such as tin dioxide, cassiterite (SnO_2) shown in Fig. 4.29, are accidentally produced by the internal oxidation of bronze and rarely observed in artefacts (see Dungworth [29]), but they can be regularly observed in casting waste (Figs. 3.23 and 3.24). Scott [102], for example,

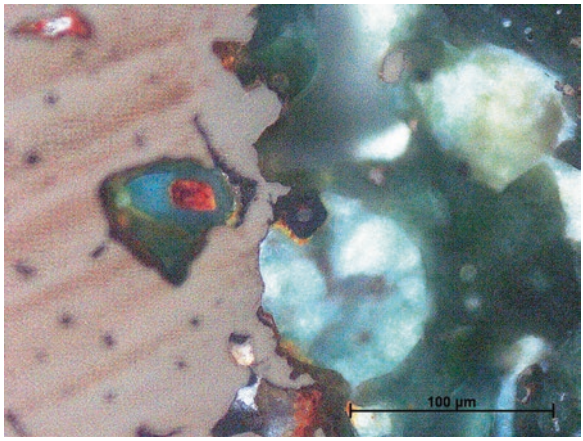

Fig. 4.29 Tin oxide inclusion (SnO_2) at the surface of fragment from a large Roman bronze relief from Mittelstrimmig, Germany, viewed under polarized light

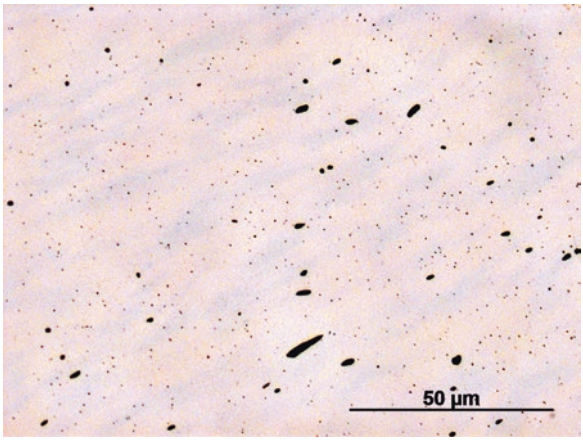

Fig. 4.30 Globular iron oxide inclusions (FeO) within the microstructure of a high-nickel (13.7% Ni) lunular pendant, from Boğazköy, Turkey. The mean value of iron determined by XRF is 2%, which is not only present in the oxide inclusions, but also in copper-nickel sulphide inclusions. The total volume fraction of the inclusions has been quantified to 0.4%. Imaged in bright-field reveal the segregations already in an unetched state

found small cubes or crystals of cassiterite in some Ecuadorian arsenical bronze alloys, which had been cast.

Iron and cobalt-bearing cupronickel-alloys from Anatolia show the presence of iron oxide inclusions (FeO), often containing variable amounts of nickel and copper shown in Fig. 4.30. They derive from the internal oxidation of the iron-bearing alloy [56]. Figure 4.31 shows iron oxide (FeO) inclusions within a Late Iron Age bronze scabbard from the Wederath cemetery in Germany. They are most probably of exogenous origin, although there is no reasonable explanation for their presence which can be stated categorically at present. Iron oxide inclusions in copper are rarely reported (e.g. Cope [18]), but some raw copper products, such as late Bronze Age

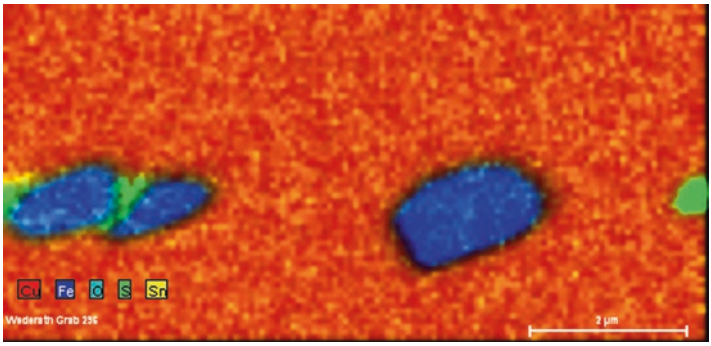

Fig. 4.31 Quantitative pseudo-coloured EDX-dot map of iron oxide inclusions within a Late Iron Age bronze scabbard from the necropolis of Wederath, Germany

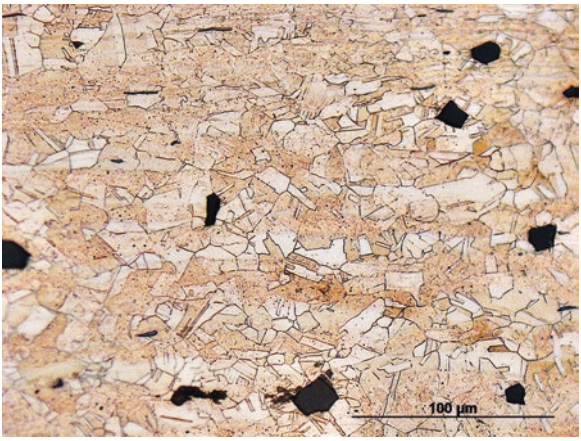

Fig. 4.32 Angular nickel-oxide inclusions (NiO) within a recrystallized matrix of a nickel-bearing α_{Cu}-solid solution of a needle from Boğazköy, Turkey. Etched with aqueous ammonium persulphate and viewed in bright-field illumination

oxide ingots or so-called *Aes rude* and *Ramo secco* bars from Italy, contain iron silicate slag and magnetite as relicts of the smelting process (e.g. Craddock and Meeks [22]; Ingo et al. [43]; Hauptmann et al. [37]; Matteoli and Storti [64]).

Nickel oxide inclusions, shown in Fig. 4.32, have been detected within a cupronickel-alloy from Anatolia [56].

The volume fractions of non-metallic inclusions in copper alloys can be several percent in raw copper and also in Early Bronze Age and chalcolithic items [49, 91, 118], but it is usually less than 1% in items of later periods (e.g. Willer et al. [129, Table 1]).

Silver alloys usually contain only copper oxide inclusions (Cu_2O), which derive from the inner oxidation of the silver alloy. An example is shown in Fig. 4.33.

Figure 4.34 shows a cross section of a silver disc fibula from the Early Medieval cemetery from Bedburg-Königshoven in the Rhineland, Germany. It contains a large volume fraction (11.5% ± 1) of tin dioxide inclusions (SnO_2), which are elongated along the length of the section. The mean tin content has been determined by

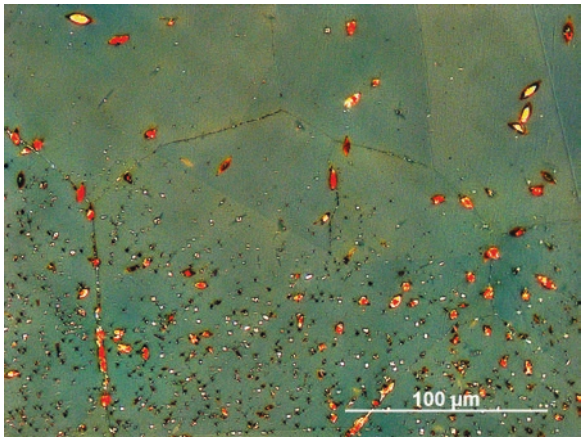

Fig. 4.33 Copper oxide inclusions (Cu_2O) near the surface of silver teeth of comb from Cumae, Italy, dated to the eighth century BC, viewed under polarized light after etching with potassium dichromate

Fig. 4.34 SEM/BSE image of SnO_2-rich inclusions in the microstructure of an early medieval silver disc fibula from the cemetery of Bedburg-Königshoven, Germany

XRF to be 8.9%. The maker of this fibula must have used scrap such as soft-soldered silver or bronze to produce the disc. By casting or annealing, the tin content of the alloy has been converted to oxides by internal oxidation, which caused fractures because of its hardness. Silver alloys are prone to this kind of oxidation as oxygen is quite soluble in hot silver. This can then oxidize the copper content to produce copper oxides.

Besides some copper oxide inclusions, which derive from internal oxidation, gold alloys are usually free of non-metallic inclusions. Indeed, X-ray diffraction studies have found both quartz and calcite inclusions in ancient Colombian gold

objects [45], both of which might be expected from the geological evidence. Gold objects from the ancient world can be flecked with platinoid inclusions, usually of the osmium-iridium group, as these are hard, cannot be molten and accompany the gold through its refining process [65]. Platinum-group metals are the common metallic inclusions in gold objects and, as these are not molten in the process of forming the gold object, behave very much like non-metallic inclusions. In some cases, the presence of these platinoid group inclusions is one line of evidence for the authenticity of the gold object concerned.

4.5 Plastic Deformation and Working and Annealing

Metals, when subjected to a force, can move to a certain, limited extent, by elastic deformation. This is termed as "recoverable" alteration, since when the force or load is taken away; the metal recovers to the same state that it was in before the force was applied. This kind of deformation is modelled by Hooke's law. In the elastic range, elastic modulus, so-called Young's modulus for the metal concerned can be determined. This can be plotted on a stress-strain curve, which is very important for the engineering properties of metals. Figures 4.35a and 4.35b shows the typical relationship between stress (force per unit area) and strain for a ductile metal such as copper. Young's modulus is given by stress/strain and has units of pressure. The yield strength is the region where deformation begins and strain hardening of the copper will then take place until the ultimate tensile strength is reached, when the copper starts to break apart until fracture occurs. Young's modulus for copper is 128 GPa, the yield strength about 322 GPa and ultimate tensile strength about 340 GPa.

Some metals, such as pure copper, may stretch elastically much more than hardened steel and will have a low value of Young's modulus as compared with the tough steel. In a stress-strain experiment, a cylindrical sample of the metal is pulled apart: it first stretches by elastic deformation and then by plastic deformation. The end of plastic deformation is characterized by a strain hardening region, and a necking of the test specimen occurs, which finally fractures and the metal then breaks, reaching the limit of its plastic deformation. In ductile fcc metals, such as copper, silver and gold, there is a large area of plastic deformation available. Steels can undergo plastic deformation too, but usually iron alloys have to be hot-worked in ancient usage, as they are too hard in the bcc state, as they can be worked in the high-temperature fcc region, making deformation much easier (Sect. 5.2). Metals can experience fatigue, which can occur in fcc metals, even in the elastic range of their treatment. This means that metallography is very important in assessing the formation of cracks in a variety of different alloying systems. In historic metalwork, for example, large outdoor sculptures made of zinc which were popular in many American and European cities, there is a severe danger of them fracturing, because the extent of plastic deformation of the metal is very limited. Therefore, elastic deformation occurs in these zinc sculptures, which either due to exceeding

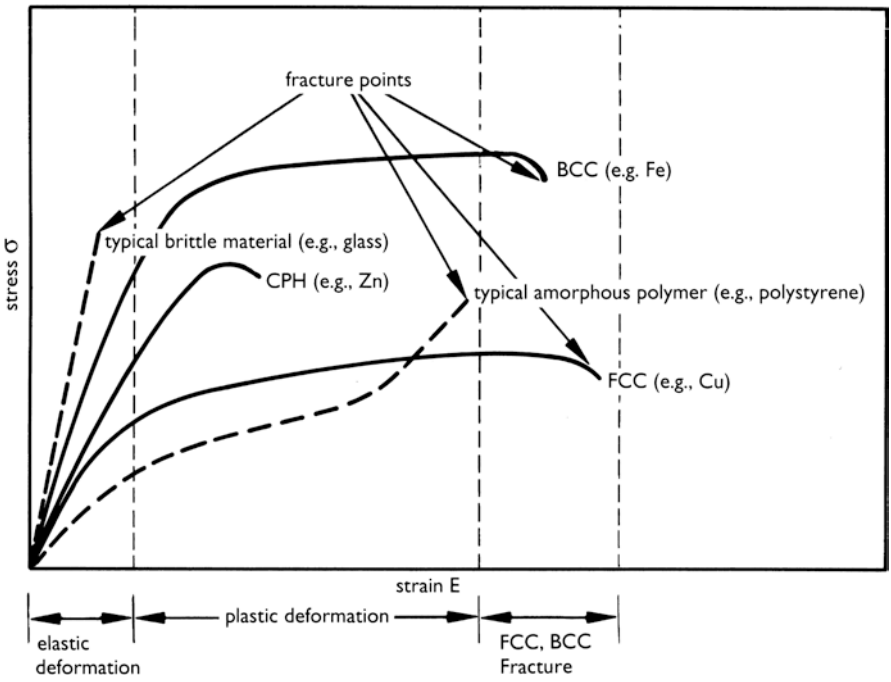

Fig. 4.35a Typical stress-strain curves for fcc, bcc and cph metals, compared with glass and a typical polymer. Fcc metals such as copper deform plastically for much longer than bcc metals such as iron. Cph metals such as zinc behave very differently than fcc metals like copper, because the cph lattice accommodates little movement by slip or dislocations compared with copper. In the elastic region, any elongation of the metal is recoverable if the applied stress is removed; the metal will return to its original shape. Once plastic deformation occurs, the shape is altered and cannot be returned to the original starting point

the elastic limit or metal fatigue over decades of exposure, they begin to break apart. Zinc is one of the metals of the cph system which tend to undergo mechanical twinning as they are deformed. This mechanism does not occur in fcc metals, such as copper, silver or gold.

Some ferrous alloys, in the bcc state, if heavily cold-worked can also show mechanical twinning. Metals, with very low plastic deformation, such as grey cast iron or white cast iron, are strong materials under compression but are very weak in tension. They are hard but brittle. This is why cast iron can be used as a support structure for historical buildings, where copper or bronze would be dangerous, as the latter are liable to too much plastic deformation. Cast iron is very hard but cannot undergo deformation by hammering. It cannot be used for making sword-blades but is good for absorbing the stress of compression.

The lattice of metallic systems is not perfect, and they have a number of dislocations of various types, particularly edge dislocations and screw dislocations. When a metal is plastically deformed, these dislocations pile up, until the metal becomes embrittled. These issues are discussed at much greater length in standard

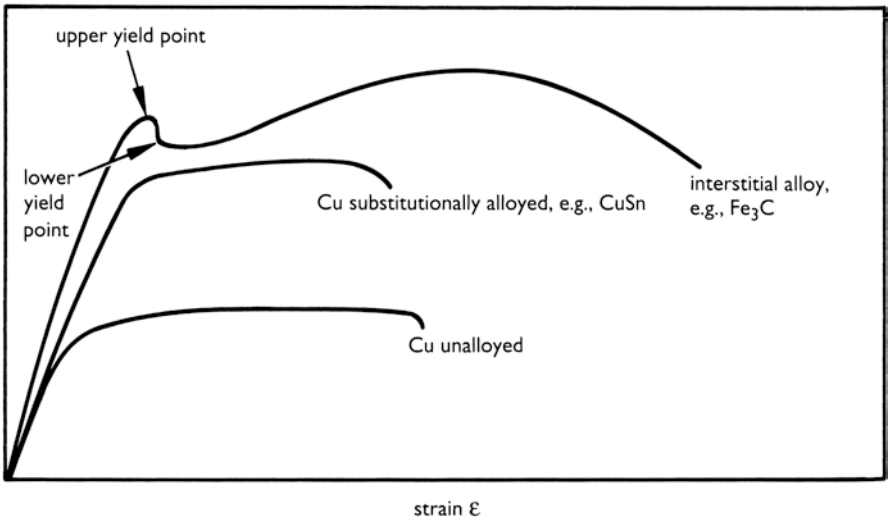

Fig. 4.35b Stress-strain curve for interstitial materials. Interstitial metals are small in size, such as carbon, and can be inserted into the lattice of some metals such as iron, to make steel. Interstitials tend to reside at the base of dislocations and anchor them. When slip occurs, carbon is left behind, and the dislocation is held until some higher stress is reached. When the stress factor is reached, an enormous number of dislocations occur that can now move at a lower stress than originally required; hence the two yield points for steels. Compare with the curve for unalloyed copper and for copper which is substitutionally alloyed with tin, as in the case of a bronze

metal textbooks (e.g. English et al. [30]; Hansen and Barlow [36]; Rodney and Bonneville [94]).

Annealing removes these congealed dislocations and returns the metal to a soft condition again. When fcc metals such as copper, silver and gold are worked and then annealed, they can recrystallize. The lowest energy system for this recrystallization is the formation of annealing twins. Annealing twins are mirror reflection planes of the atomic arrangement of the metal or alloy, and these can be revealed in a polished section by etching, when the rate of attack of the solid varies depending on the orientation of the metal crystals in three dimensions. When an fcc metal is cold-worked, the grains become distorted and elongated along the direction of working, and when annealed these grains will recrystallize to form twinned crystals with straight twin lines. An example from a Bronze Age bronze Palstave from Kent, England is shown in Fig. 4.36.

The other feature which may become apparent on deformation is that slip, or strain lines, may be evident in the crystal, because planes of atoms have slipped past each other due to heavy working. These strain lines are often unidirectional near the hammered surface of the object, or they cross over each other at certain orientations.

When the twinned and recrystallized grains are then further deformed, the crystals become distorted, and the twin lines become bent or curved. Further annealing

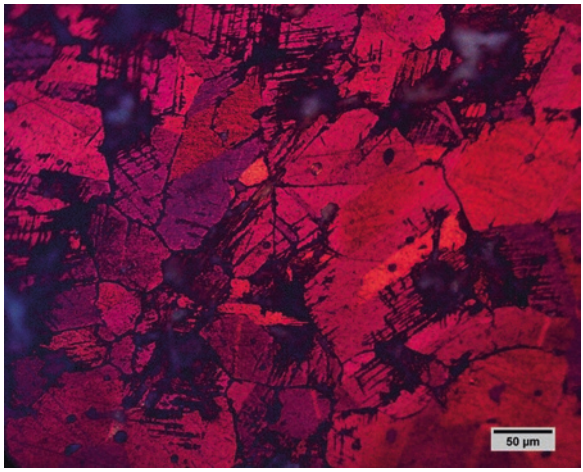

Fig. 4.36 Cold-worked cutting edge from a Late Bronze Age palstave from Kent with about 8.5% tin. Corrosion has outlined the strain lines through the grains seen here. Lightly etched in alcoholic ferric chloride

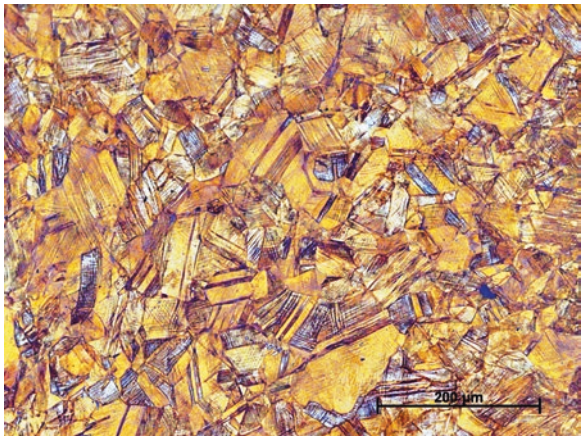

Fig. 4.37 Microstructure of a so-called Nauheim brooch from the Donnersberg oppidum, Germany shows heavy slipping and displaced twins. Etched with Klemm's reagent III

will reform the grains and create a new twinned grain structure, usually of a smaller size than those originally present. Some hot-worked alloys, such as struck coins, may retain a distorted grain structure.

Cycles of working and annealing are commonly used to shape copper and silver alloys. In order to avoid brittleness, the final working process is usually annealing. Chisels, knives, swords and palstaves may have their edges cold-worked in order to increase the hardness of the cutting edge, but also items like brooches were left worked to keep them semi-hard, as shown in Fig. 4.37.

Hot-working combines the effects of cold deformation and annealing in one stage and creates recrystallized grains. Not all alloys are suitable for being hot-worked, such as lead-bearing copper alloys, and some brasses are described as "hot-short". This phrase implies that the alloy concerned will tend to break apart on hot-working or become brittle.

Iron and steel alloys, which are bcc in their room temperature state, can only be slightly deformed by cold-working. The alloys must be heated to red heat by the blacksmith, in the austenite region of the phase diagram, in order to deform them successfully. As the iron alloy cools down, it reverts to the bcc state and must be reheated in the forge to successfully shape it. When body-centred cubic (bcc) metals such as iron are plastically deformed at normal temperatures, the type of motion that occurs depends on a number of factors, including the type and the rate of deformation. At low strain rates with moderate amounts of deformation, slip lines appear on the etched surfaces. Arrays of bands are known as Lüders lines or Lüders bands, which are caused by localized plastic deformation and usually occur in low-carbon steels after strain over the limit of elasticity. Lüders lines propagate at a front, which can move along the length of a tension with continued stressing. Slip lines in body-centred cubic metals are irregular and are usually described as "wavy" lines, which indicate that the dislocations are not confined to unique slip planes [71, p. 218].

Lüders bands are usually revealed by macro etching with Fry's Reagent [97, pp. 176–7]), which is not often suitable for small samples from archaeological objects. Figures 4.38 show the microstructure of a chain link from a Roman mail shirt. The chain links were die-cut from sheet metal, so that the grains around the hole are heavily deformed.

A different method has been applied to form Iron Age chain links from Bern-Tiefenau (Switzerland), which shows a textured microstructure in the longitudinal section in Fig. 4.39. The polycrystalline appearance of the grains and etching contrast is gone because they are axially aligned and elongated in the direction of principal strain. Such preferred orientated textures are best known from drawn wire, which is according to our present knowledge not yet known before the Viking Age (e.g. Odgen [77], 164), so that these chains would be the earliest examples, if their context would be secure.

Deformation twins, so-called Neumann bands, develop by extreme and rapid impact of stress. They were first described in iron meteorites but can occur in archaeological iron artefacts as a result of being heavily cold-worked. The twins

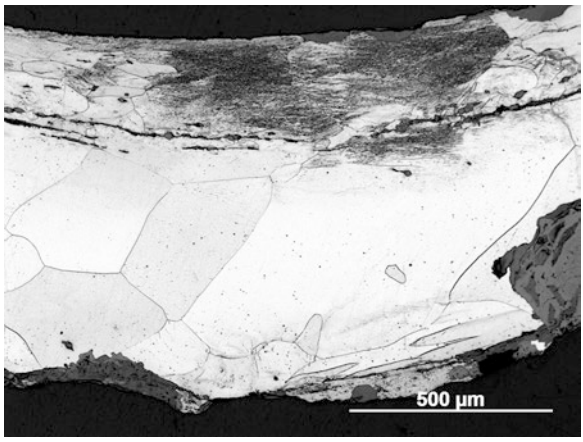

Fig. 4.38 Lüders lines at the inner side of a ferritic chain link from a Roman mail shirt from Lüttingen, Germany. Hardness values of such die-cut chain links varies from 150 to 250 HV 1. Etched with nital

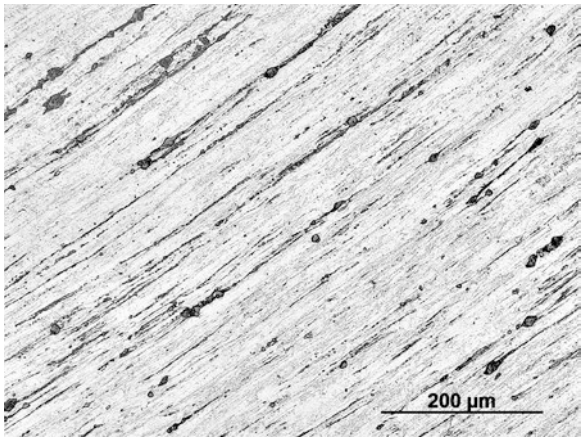

Fig. 4.39 Cracked slag stingers and unresolved microstructure of a ferritic chain link from an Iron Age mail shirt from Bern, Switzerland, having a mean hardness of 250 HV 1. Etched with nital

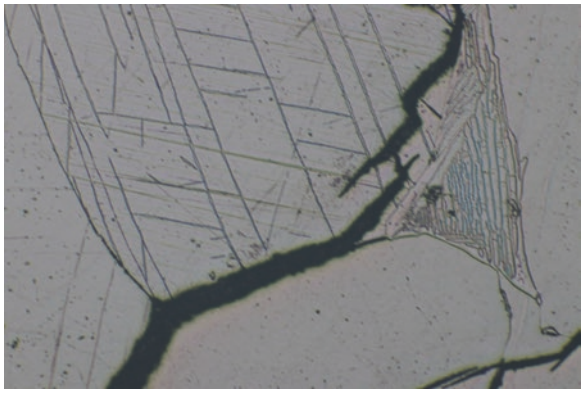

Fig. 4.40 Neumann bands in a heavily shocked meteorite from Chile. Magnification shown in scale bar, etched in nital.

usually initiate only in ferrite and never extend across a grain boundary. Neumann bands are regularly observed in the microstructure of ancient iron objects and are a clear indication for an impact shock (Fig. 4.40). Neumann bands often appear in ferritic hammers and European Iron Age swords [80, 100, p. 255]. The hammers clearly indicate the development of deformation twins during the use of the hammers as a striking tool, while the swords could have been occasionally cold worked [80, p. 152] or may have been destroyed during burial or devotional or religious ceremonies, as Uran [121, pp. 304–5] has pointed out. The Inuit, who used meteoritic iron quite a lot, practiced intentional cold-working to form and to sharpen their tools and weapons [10]. Knives of walrus ivory were made by inserting cold-hammered flakes of meteoric iron into a cut groove and holding them in place with bitumen or glue; small knives of caribou bone with meteoritic iron blades have been found from Inuarfigssuak, Greenland, originating from the Dorset or Thule culture [9, p. 411]). Examination of an ulo, or woman-knife, from Inuarfissuaq by Buchwald [9] showed a microstructure of distorted kamacite, with small sheared rhabdites and cloudy taenite lamellae, distorted from the cold-working which had been used to shape the iron.

Some brass and bronze alloys must also be hot-worked to deform them, such as high-tin bronzes with over 20% of tin. These alloys can be quenched, retaining the beta phase (Sect. 4.6.1.2), and this phase of the copper-tin system can be worked hot, around 700 °C, and then be shaped, before quenching, to retain the beta phase, followed by further working as required.

4.6 Solid-State Transformations

4.6.1 Non-diffusive Phase Transformations

4.6.1.1 Martensitic Transformations in Carbon Steels

Spontaneous diffusionless phase changes are generally termed martensitic transformations according to the best known and technically most significant transformations in the Fe-C system, but there are some nonferrous alloys where this kind of reaction is important as well. Martensitic transformations take place when cooling rates are fast enough to supress diffusion-controlled decomposition of high-temperature solid solutions and generally result in the formation of a distinct acicular microstructure called martensite, after the German scientist Adolf Martens.

The reaction ideally occurs by shear without changing the chemical composition, but in practice the cooling rates are not appropriate to transform all of the proportions of the solid solution into martensite (Sect. 4.6.1). The distinct acicular microstructure as a result of shearing is very characteristic for every martensitic structure and is readily recognized in the optical microscope after appropriate etching. This characteristic appearance of martensitic microstructures results from shape change of crystals due to their supersaturation of solvent atoms by those of the solutes. Ferrous martensite is principally a supersaturated solid solution of carbon in iron with a distorted form of α_{Fe} (bcc), which has become a body-centred tetragonal (bct) structure [51]. This transformation to martensite (bct) begins in the range from 400 to 200 °C depending on the carbon content. The interstitial solubility of carbon in unalloyed ferrite (α_{Fe}) is extremely low (0.02 wt %), whereas the high-temperature modification austenite (γ_{Fe}) is capable to solve between 0.8 and 2.11 wt % of carbon, independent of temperature, because of its larger interstices (see Sect. 5.3). Therefore the $\gamma_{Fe} \rightarrow \alpha_{Fe}$ transformation is accompanied by an atomic volume change and the decomposition of γ_{Fe}-solid solution into α_{Fe}-solid solution and carbon, which the latter is in fact not carbon but the interstitial solid solution cementite Fe_3C (see Chap. 5). Under equilibrium conditions, it would be a eutectoid reaction, where austenite decomposes into one of the most familiar eutectoid microstructures called pearlite: $\gamma_{Fe} \leftrightarrow \alpha_{Fe} + Fe_3C$. When iron-carbon alloys are heated above A_3 (see Sect. 5.2) and then plunged into water to quench austenite to room temperature, the carbon remains in solution, because there is not enough time to diffuse and to nucleate. But as mentioned before, the interstitial solubility of carbon in bcc α_{Fe} is extremely low, and additional interstitial solved carbon expands and

distorts the iron lattice, because regular positions are already occupied. Therefore, the transformation from γ_{Fe} (fcc) to α_{Fe} (bcc) is accompanied by shape deformation and volumetric expansion, which occurs according to the so-called Bain strain, uniformly expanded in two dimensions, but contracted in the third dimension and results in a tetragonal distorted crystal [3].

The initial surface of austenite is tilted and rotated by shear producing this very characteristic microstructure. Martensite can assume two types of morphologies. It crystallizes as acicular martensite needles if the carbon content is less than 0.6% called lath martensite, while above 0.6%, it assumes a plate-like morphology. These different morphologies are illustrated in Figs. 4.41 and 4.42.

Martensite plates grow very rapidly at speeds of the velocity of sound, which is why martensitic transformation is time-independent [3]. The change from austenite to martensite causes a considerable volume increase and different cooling rates between surface and core create additional stress, which can give rise to quench cracks. Iron Age files often show quenching cracks [100]. Compilations of the oldest quench-hardened iron objects of the Near East and Europe from the late Bronze Age to the Iron Age show that the possibilities of structural phase transformation of iron were recognized early on [53, pp. 200–201, 60, 82]) and some classic authors refer to the processing of iron in terms of heat treatments. Homer writes: *"…just as when a smith plunges into cold water a great axe-head or adze to treat it – for this is what gives strength to the iron – and it hisses fiercely, in the same way the Cyclops' eye sizzled around the olive stake…".*

TTT diagrams: The effects of the cooling rates on different iron and steel alloys can be followed using so-called time-temperature transformation diagrams (TTT diagrams), either isothermal or continuous cooling transformation diagrams (IT or CCT diagrams). The metallurgical literature often uses TTT as a synonym for isothermal transformation in general (see Krauss [51]). The isothermal TTT diagrams measure the rate of transformation at a constant temperature while time is varying. To derive an IT diagram, an iron alloy is heated to the austenitic region and then cooled rapidly to a lower temperature and held at that temperature, while the rate of

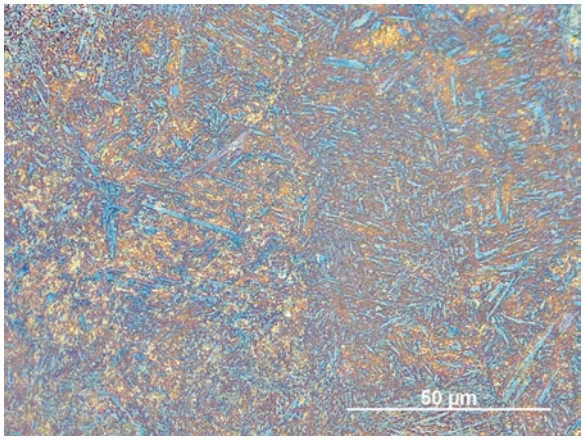

Fig. 4.41 Blue-coloured lath martensite in the microstructure of a Mongolian arrowhead from a rock tomb of Nükhen Khad in the Zhargalant Khairkhan mountains, dated to the sixth to eighth centuries AD. Maximum hardness of 660 HV 1 indicate a medium-carbon steel. Etched with sodium metabisulphite

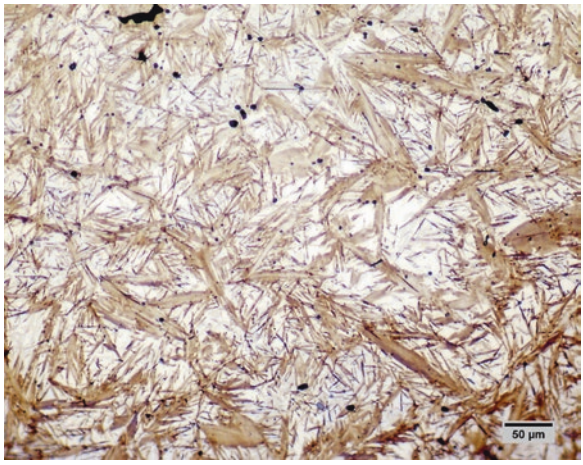

Fig. 4.42 Plate martensite in a cut French steel bead of the eighteenth century AD with a carbon content about 1.1% and a microhardness of 1000 HV. Made by cutting to shape followed by heating and quenching to create the martensite, followed by polishing like a gemstone to create the gem-like finish. Etched in picral

transformation is measured. IT diagrams are read along the time axes (Fig. 4.43). This kind of transformation never has been available to ancient blacksmiths, and the use of IT diagrams is very limited in its relevance to ancient ferrous alloys. More useful for ancient alloys are the CCT diagrams, as illustrated in Fig. 4.44, where the x-axis is the logarithm of time and y is temperature.

In the CCT diagrams, the extent of transformation as a function of time for a continuously decreasing temperature is measured. For example, an object heated to the austenitic region is cooled at a predetermined rate, and the degree of transformation is measured. CCT diagrams have to be read along the cooling curves.

4.6.1.2 Quenching of Copper Alloys

Microstructures analogous to the martensite of steel may be found in certain pre-industrial copper-tin and probably also in copper-antimony alloys. For low-tin bronzes, they may be quickly cooled which would affect the extent of dendritic growth, but the overall effects on the microstructure of the examples of bronze shown above would be slight. However, if the tin content is raised to more than 20%, then on quenching some of the higher temperature solid phases present in the phase diagram can be retained, producing an alloy with very different working properties than the cast equivalent. For alloys used as mirrors, the differences are not great in terms of working properties but become significant if the cast mirror is finished by turning on a lathe or if a cast bowl has to be cut and decorated after casting. Then the advantages of quenching these bronzes become apparent. Hot forged high-tin bronzes have been used in the Near East, in Central and especially Southeast Asia up from the mid first millennium BC to modern times for a variety of items (see Glover and Bennett [31]; Goodway and Conklin [32]; Northover [74]; Pryce et al. [84]; Ravich [87]; Srinivasan [111], Srinivasan and Glover [112].

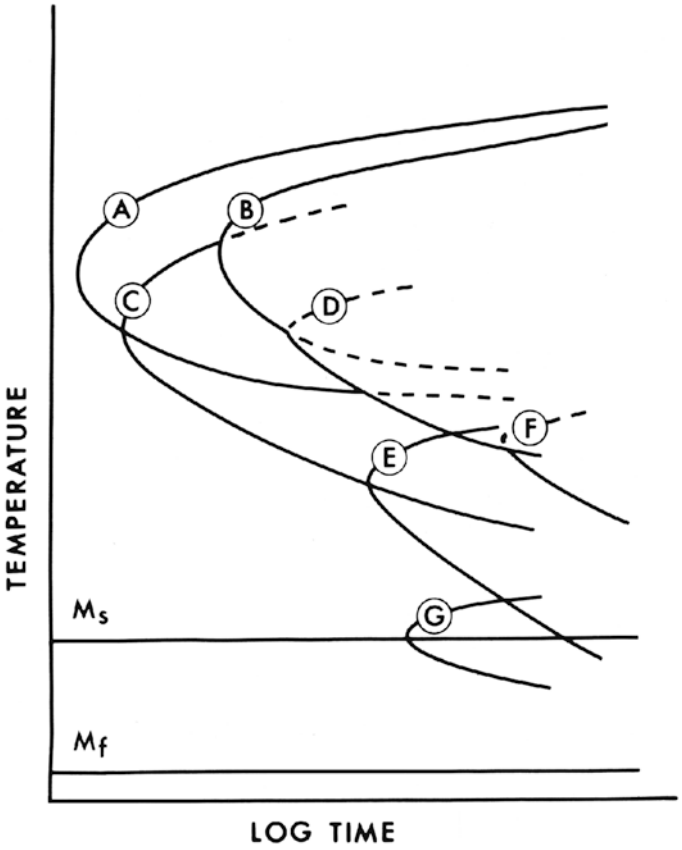

A: 0.01 vol fraction pearlite
B: 0.99 vol fraction pearlite
C: 0.01 vol fraction upper bainite
D: 0.99 vol fraction upper bainite
E: 0.01 vol fraction lower bainite
F: 0.99 vol fraction lower bainite
G: 0.01 vol fraction martensite

Fig. 4.43 Schematic IT diagram for plain carbon eutectoid steel (after Samuels [97]). For transformation according to IT diagrams, the specimens are cooled rapidly to IT temperature and hold there for a specific time and then quenched to room temperature

An example of the microscopic effects of quenching is shown in Fig. 4.45, part of a high-tin bronze bowl from the site of Ban Don Ta Phet, Southwest Thailand, dated to about 100 AD, of composition 22.7% tin and 76.2% copper.

Excavations on behalf of the Thai Fine Arts Department revealed a series of inhumation burials with 163 bronze vessels, 38 bronze bracelets, 7 bronze anklets, 16 bronze rings, 1 bronze ladle, 3 bird finials, 3 bells, and 579 iron artefacts and other material. The metalwork from this site has been published in summary form by Rajpitak and Seeley [85]. Etched beads suggest a date in third to second century BC. The bronze bowls ranging from 5 to 15 cm in diameter [85] are very thin, with

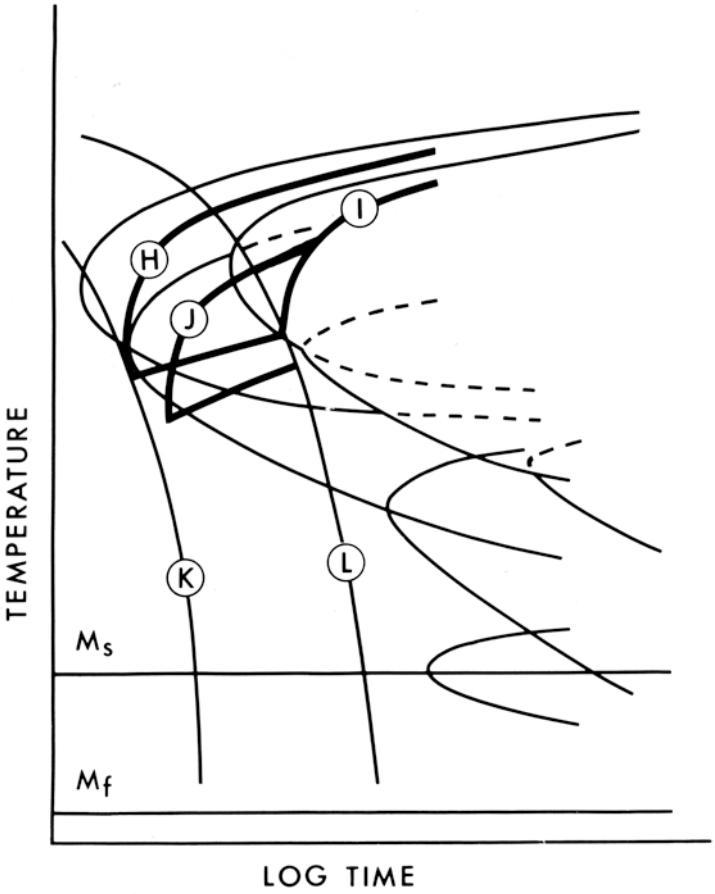

H: Start of transformation to pearlite
I: Finish of transformation to pearlite
J: Start of transformation to upper bainite
K: Critical cooling rate for suppression of diffusional transformation
L: Critical cooling rate for complete diffusional transformation

Fig. 4.44 Schematic CCT diagram for plain carbon steel (after Samuels [97]). Critical cooling rates K and L indicate complete non-diffusive and complete diffusive transformation of austenite. M_s marks the start of a martensitic transformation, while M_f is the temperature at which it is essentially complete. The curve H indicate the pearlite formation and curve J the bainite start. (After Samuels [97] Fig. C11 Courtesy American Society of Metals)

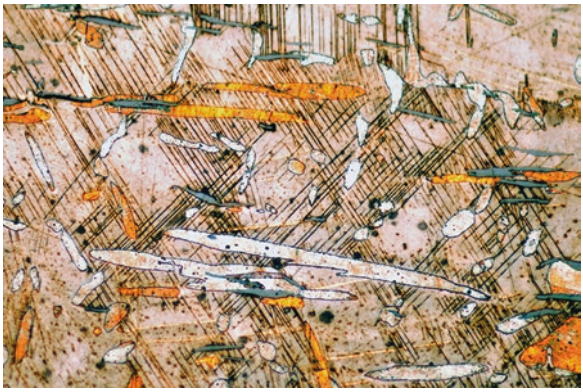

Fig. 4.45 Thai bronze bowl from the site of Ban Don Ta Phet, showing twinned alpha grains in a beta matrix. These twinned grains arise from the casting, heat treatment, quenching from about 650 °C, then reheating, hot-working, and subsequent quenching of the 22.7% tin bronze alloy, resulting in a beta or beta and gamma phase matrix with twinned alpha phase islands. Colour etched in Klemm's reagent II, magnification 280×

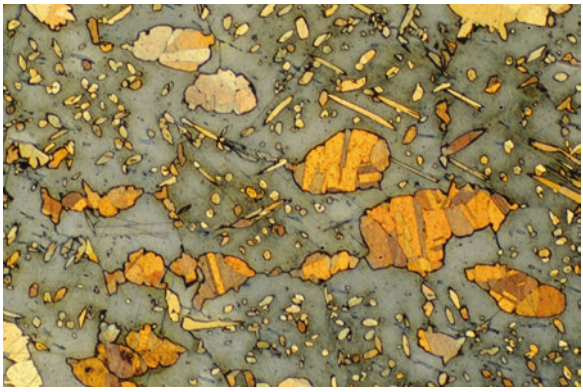

Fig. 4.46 High-tin bronze bowl, about 21.5% tin from Ban Don Ta Phet, quenched beta bronze, showing some alpha islands with the acicular beta-phase needles in the matrix of the cast, reheated and quenched bronze. Quenched from about 650° C. Colour etched, magnification ×280. Note that the twinned grains show straight twin lines as a result of hot-working to shape, where the hot-working combines deformation and recrystallization

wall thickness of 0.3–0.5 mm and with fine incised decoration. These bowls are made in a quenched high-tin bronze, such as that revealed by the section shown in Fig. 4.46. The 21–23% tin bronzes require heating to at least 300 °C before they can be worked [16], and the microstructure shows that it has been quenched from above 520 °C, which as we have already discussed is in the beta-phase field [89, 90]. Comparable fragments of high-tin bronzes have been reported by Marshall [62, 68] from Taxila, the ancient Gandharan capital on the North West Frontier of India, mostly from late phases, but Bhir Mound, the Mauryan city, from third to second

century BC contained a pair of bowls one with 21.55% tin, the ideal composition, as the microstructures shown in Fig. 4.46 are typical and show a preference for some alpha phase together with beta, rather than with slightly higher tin contents which are all beta phase.

This shows that the composition of these special alloys was very carefully controlled. Other important mentions of these alloys are those of Smith [109] from Pimai; Phase III at Ban Chiang [128], dating to 500–0 BC, a bronze bowl from Coimbatore, South India, and artefacts from Adichanallur in the Nilgiri Hills [7], two Koryu Dynasty bowls from Korea [123] and some Islamic bronze vessels from Iran [70, 74]. Rajpitak and Seeley [85] mention the account of Nearchus in his description of India written in the fourth century BC, fragments of which survive in Strabo's geography (Strabo 15.1.67) which states that Indians used vessels which were cast rather than beaten and which broke like pottery when dropped on the ground. This suggests that the brittle high-tin bronzes may well be described here. Recent work in South Indian by Srinivasan [111] and Srinivasan and Glover [112] confirms the evidence for use in this area, as the bronzes are still being made by traditional methods. Metallurgical investigations on bowls and vessels from Nilgiri megaliths and Adichanallur burials showed they consisted of 23–25% tin wrought to between 0.2 and 1 mm with a Vickers Hardness of 290–300 HV.

A bowl excavated from Taxila dated to 1000 BC showed it to be a beta bronze with 24% tin. Three samples excavated from Mohenjo-daro thought to be dated to 2500 BC were found to contain 22.1% tin, 22.2% tin with 14% lead and 26.8% tin. Srinivasan and Glover [113] found that yet another extant tradition of mirror making in South India utilizes cast alloys with 32% of tin, retaining a cellular delta microstructure such as that shown in Fig. 4.47, where Neville and Haycock show the same kind of structure, namely, delta phase in a matrix of alpha + delta, for their 31.2% tin bronze.

Srinivasan and Glover [113] provide an account of the casting of mirrors in the village of Aranmula, Kerala. These are very close to the composition of the delta phase, $Cu_{41}Sn_{11}$, whose ideal formula is 32.55% tin. The technique involves the use of a special closed crucible with attached mould, the account of which is of some

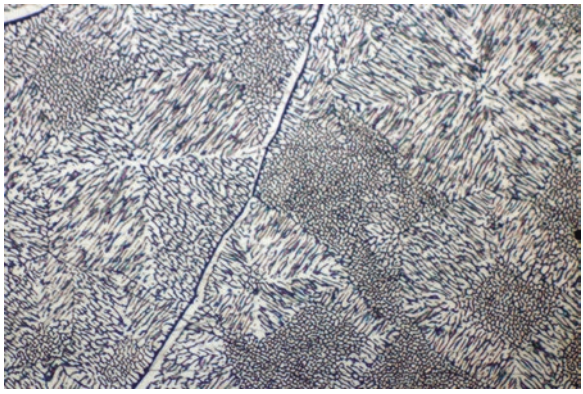

Fig. 4.47 Cellular delta microstructure from the cast condition of bronze with 28% tin

interest. The hardness of the delta phase when cast is extraordinary, reaching values of 500 HV, harder than that of a medium-carbon steel, which is around 400 HV.

There may be a number of reasons for this choice of alloy. Firstly, the high-tin alloys are not injurious to health for food-keeping as a brass bowl would be; secondly, the quenched alloy can be hot-worked to shape it and can be ground or cut to decorate the surface in a way in which the high-tin alloys cannot if slow-cooled because of the brittle delta; and thirdly for the colour. The 23% tin bronze is a good golden colour that could be visually attractive and simulate gold. The alloy, while not too brittle, is hard, with Vickers numbers between 180 HV to 260 HV.

As the alpha phase in these alloys is frequently twinned, we can reconstruct the fabrication methodology from the microstructure. Firstly the alloy is carefully made of exactly the right composition and cast into shape, roughly, probably in a mould. Then the alloy is reheated above 600 °C and hot-worked. The alloy is reheated above 600 °C and quenched. It undergoes a martensitic transformation to the beta phase.

The alloy can now be turned on a lathe to smooth the surface or to cut decoration into the surface of the bronze. It can be reshaped if necessary by reheating again, working and quenching, followed by polishing to finish.

We know that operations such as this must have been involved, for otherwise the alpha phase would not be twinned from the hot-working process as Fig. 4.46 reveals. Examination of the etched section shows the presence of some alpha phase copper-rich grains, sometimes acicular and which occur in areas with specific orientation as well as a random scatter. The overall cast structure of these types of high-tin alloys can be seen in Fig. 4.48.

In the background matrix of this bronze is a banded martensite, a variety of the β phase that proves that the bowl must have been quenched from the temperature region of 520–586 °C. This is slightly lower than the usual quenching temperature for these bronzes, which is generally in the 650–750 °C range. Some additional studies of the composition of these alloys confirm the general impression that the metalsmiths were deliberately striving for a composition which includes the alpha and beta phases, without knowledge, of course, of the phase relationships, but

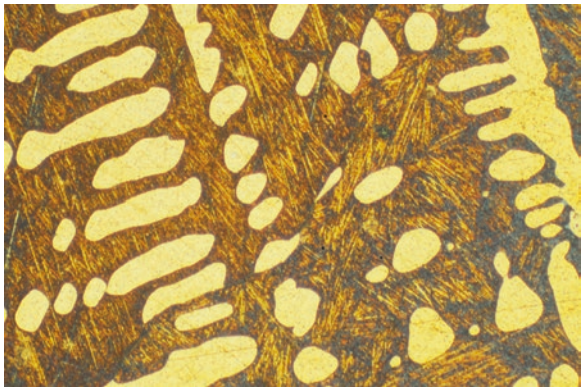

Fig. 4.48 High-tin bronze alloy in cast and quenched condition showing the suppression of the delta phase in the background, where beta-phase needles occur and with prominent alpha-phase dendritic cast structure. Etched in ferric chloride, magnification ×120. From the site of Ban Don Ta Phet, Thailand

purely from their sophisticated observations on the behaviour of metals. A study by Park and co-workers [78] showed that, on deformation, the small amounts of alpha present in the 22% tin bronzes, spanning the grain boundaries, act as micro-bridges interlocking the adjacent grains. The alpha phase apparently reinforces the boundary regions, an effect which is very sensitive to the alpha fraction and can be best obtained with tin contents close to 22%.

The hardness data obtained by Rockwell hardness testing is between 99.5 and 105.5 HRB for a 22% tin bronze [78]. Bowls from Korea, from the Unified Silla period (668–935 AD) made in this alloy, have wall thicknesses of 0.2 mm. Even a minor change in tin content, to 24% where the microstructure is entirely beta, would not have allowed this degree of hot-working. Here the phase diagram and its application is an essential component to understanding the microstructure of these quenched alloys. When quenched from high temperatures, the β phase is retained, and the alloy undergoes a martensitic transformation.

Time-temperature transformation or continuous cooling transformation diagrams are important in understanding the nature of the changes which may take place on cooling alloys at certain defined rates, as already mentioned above. The chart shown in Fig. 4.49 is the work of Goodway and Conklin [32] and shows that if very fast cooling takes place in the log time axis closest to the origin, then the whole structure will be martensitic. Less drastic cooling conditions will create a range of different options in which the start of the martensitic transformation will be delayed or result in variations in the type of martensite produced.

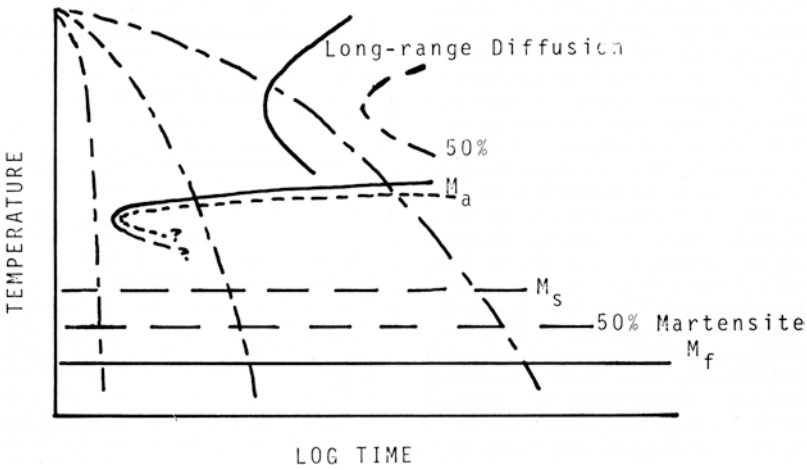

Fig. 4.49 Proposed onset and finish of martensitic transformations in the high-tin bronzes after Goodway and Conklin [32]. The chart shows that if very fast cooling takes place in the log time axis closest to the origin, then the whole structure will be martensitic. Less drastic cooling conditions will create a range of options in which the start of the martensitic transformation will be delayed or result in variations in the type of martensite produced

Probably another non-ferrous martensitic structure has been reported from copper-arsenic-antimony alloys of the Nahal Mishmar hoard [74, 106]. It has been suggested that the needle-like structure of the antimony-rich part could be of martensitic origin.

4.6.2 Diffusional Phase Transformations

4.6.2.1 Intermediate Structure: Bainite

Incomplete hardening results in the formation of one or more transformation products in addition to martensite. There are different reasons why critical cooling rates for a transformation to a principally martensitic state cannot be achieved, such as temperatures which cannot be realistically met, self-tempering, size and composition. The temperature of the red-hot steel, as well as the kind of the quenching media, the size of the object and the composition of the steel, which refers mostly to carbon, phosphorous and nickel for ancient steel, influences the hardening significantly.

The martensitic start temperatures (Ms), especially of hypoeutectoid steels, are strongly affected by their carbon contents. The transition temperatures increase with decreasing carbon content, and the incubation time for the onset of diffusion-controlled reactions is much shorter. So-called slack quenching results in the nucleation of carbide containing non-equilibrium phases such as bainite and fine lamellar pearlite, formerly known as troostite. For example, at a cooling rate of 140 °C/s, mixed structures may develop. In areas of the metal protected from the full effects of rapid quenching, the full martensitic transition cannot occur, and very dark etching nodular forms called troostite develop.

Troostite was named after the French metallurgist Louis Joseph Troost [108, p. 225] and is not resolved by the optical microscope. Therefore, troostite used to be regarded as a separate phase in its own right, although since the introduction of electron microscopy, we now know that it is a form of very fine pearlite and the term has become obsolete in metallographic nomenclature. Indeed troostite has a very distinct shape, and it is quite common in ancient iron implements where quenching has resulted in the edge or tip being hardened to martensite, but further back from this edge, troostite occurs because the rate of cooling has not been so high in this region. An example is shown in Fig. 4.50, which shows the troostite nodules in a region from a Japanese sword blade of the eighteenth century AD, further into the body of the blade, above the martensite of the cutting edge.

The high-temperature modifications of structure can get quite complex, and the region in which lath-shaped aggregates of ferrite and carbides are formed involves intermediate structures called bainite. The mechanism and characterization of bainite formation is a phenomenon which was discussed very controversially and

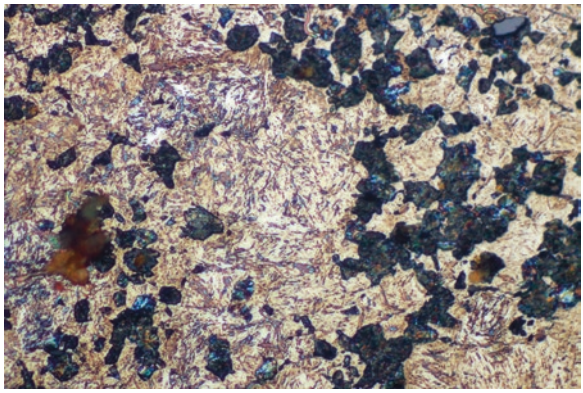

Fig. 4.50 Japanese sword blade showing the transition from martensite needles to black-blue-etching troostite as the quenching rate back from the cutting edge begins to become less. Troostite is very finely spaced pearlite nodules. Etched in nital, magnification ×430

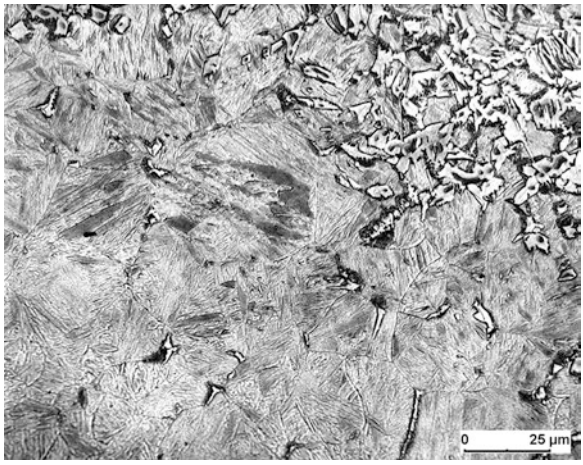

Fig. 4.51a Martensitic structure with colonies of proeutectoid ferrite of an Iron Age metalworking file from the Altburg near Bundenbach in Rhineland-Palatinate, Germany. Etched with picral

which is still in dispute [39, 97]. The microstructure was first defined by Davenport and Bain in 1930 [23] as an "intermediate appearance of dark-etching characteristics, but definitely acicular". They named it temporarily martensite-troostite, but in honour of Bain's pioneering efforts, these intermediate structures were named "bainite" by his colleagues [97]. There are large numbers of different terms and definitions for the variety of bainitic microstructures resulting from the transformation conditions and the alloying elements [39]. Two different morphologies which form in carbon steels are designated upper and lower bainite. Both can be essentially defined as a non-lamellar two-phase product of ferrite and carbides. Etching produces roughness around the carbides, and therefore bainite appears dark, compared to martensite, as seen in Figs. 4.51a and 4.51b.

The transformation to bainite is a diffusional decomposition of supersaturated austenite in which bainite is formed as aggregates of subunits of ferrite with a different nature to the carbide precipitation. Bainite formation involves lattice shear transformation, analogously to martensite as well as diffusion-controlled decomposition of austenite in its breakdown to pearlite (see Bhadeshia [2]).

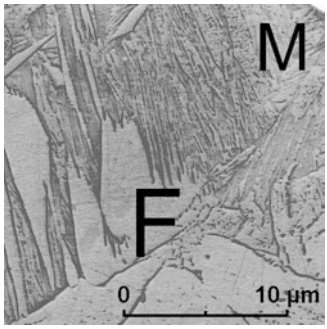

Fig. 4.51b Detail of fig. 4.51a. The inverted scanning electron micrograph shows dark etched bainite structure with carbide precipitations between ferrite (F) and martensite (M). Etched in nital

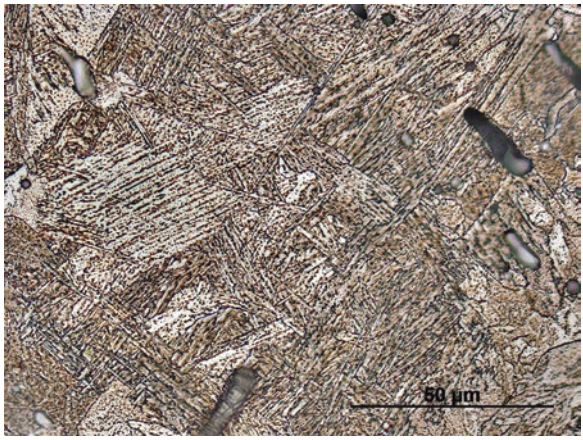

Fig. 4.52 Brown etched upper bainite in in the microstructure of another Mongolian arrowhead from a rock tomb of Nükhen Khad. Etched with Beraha's reagent I

The morphology of upper bainite, formed in the temperature range from 550 to 400 °C, is rather similar to Widmanstätten ferrite as it is composed of long ferrite laths free from internal precipitation (Fig. 4.52). Upper bainite consists of sheaves of ferrite with cementite (Fe_3C, orthorhombic) particles, which grow parallel between the ferrite plates, as shown in Fig. 4.53. In contrast to upper bainite, the carbides in lower bainite are significantly finer, and they precipitate within the plates. They are too fine and cannot be resolved in the light microscope.

The carbon has diffused to the grain boundaries, but does not form fine lamellae of ferrite and cementite, which is the case with troostite. As with Widmanstätten ferrite, the bainitic ferrite laths manifest the Kurdjumov-Sachs relationship $[(011)_\alpha \parallel (111)_\gamma]$ with the parent austenite [2]. Lower bainite that forms in the range from 400 to 250 °C appears more acicular than upper bainite, with more clearly defined individual plates assuming a lenticular habit. The most common carbide in

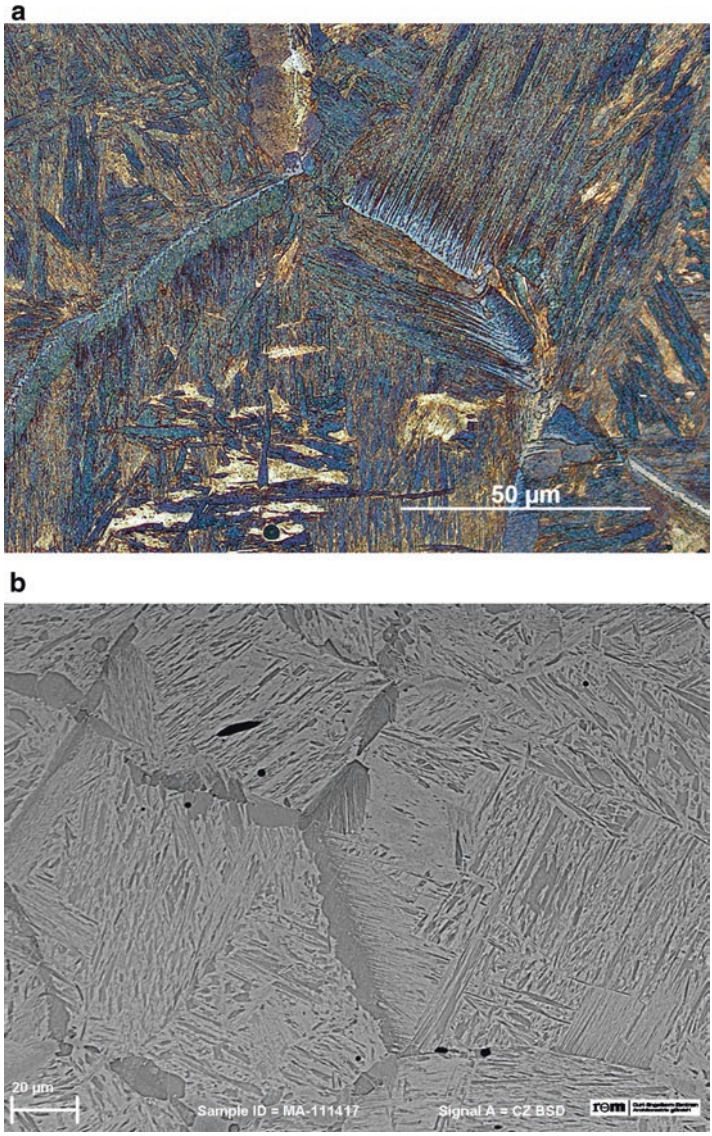

Fig. 4.53 Same arrowhead as in Fig. 4.52, but from another position and etched with sodium metabisulphite, shows lath martensite with aligned sheaves of bainite. The feathery appearance of the bainite lath is shown in the SEM image. The hardness of this arrowhead varies from 160 to 500 HV 1

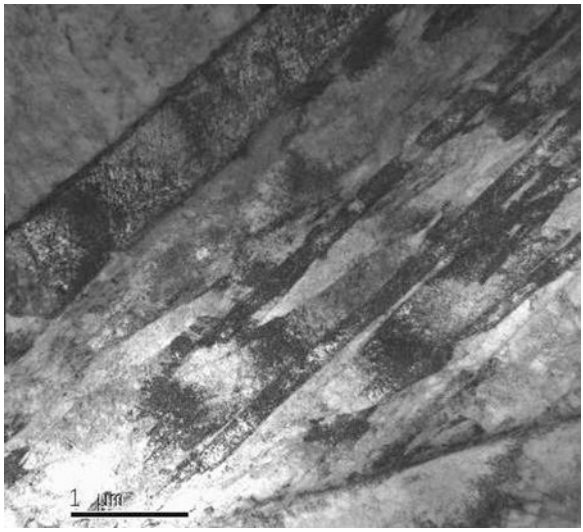

Fig. 4.54 Transmission electron bright-field micrograph from a cutting edge of a socketed axe from the Iron Age oppidum of Manching, Germany showing lower bainite plates with fine carbide precipitations

lower bainite is ε-carbide ($Fe_{3-x}C$) with a hexagonal crystal structure that forms prior to cementite [2]. The orientation relationship of ε-carbides and α_{Fe} has been determined to be:

$$011_{\alpha} \parallel 0001_{\varepsilon}$$

$$\{100\}_{\alpha} \parallel \{10\bar{1}2\}_{\varepsilon},$$

which implies a misfit $\{100\}_{\alpha}$ congruent 5° from $\{10\bar{1}2\}_{\varepsilon}$ [2].

Bainite is not frequently reported in early steels, because it is not easy to identify, as the microstructural details are so fine that their resolution is possible only using electron microscopy and only a certain volume fraction of the austenite would transform to bainite with the remainder decomposing to pearlite after an extended delay. As only small volume fractions are present in ancient iron implements, the problems associated with the identification of bainitic microstructures make the recognition in light microscopy difficult. The precipitations within quench-hardened structures can be misinterpreted as a result of the tempering of martensite, as Lang and Williams [53] have already pointed out, and confusion in nomenclature is not uncommon in the archaeometallurgical literature.

Liu et al. [57] obtained a so-called Bagaryatski orientation relationship – which is most frequently observed in bainite as well [2, 42] – between cementite precipitate and parent ferrite of the structure in prehistoric Jordanian iron objects. These results and also some needle-shaped precipitations in Roman shears are seen as effects of quench ageing [57, 76]. Quench ageing is caused by precipitation of carbides from supersaturated ferrite quenched by rapid cooling from high temperatures. Figure 4.54 shows an ion beam thinned sample of the cutting edge of a socketed axe from the Iron Age oppidum of Manching in Southern Germany.

Transmission electron micrograph reveals fine carbide precipitations within ferrite plates, and the orientation relationship between carbides and iron was determined by selected area electron diffraction to be

$$011_{\alpha} \parallel 0001_{\varepsilon}$$

$$\{100\}_{\alpha} \parallel \{10\bar{1}2\}_{\varepsilon},$$

which matches the orientation relationship of ε-carbides and α-iron in upper bainite.

4.6.2.2 Precipitation Reactions

4.6.2.2.1 Tempering of Quenched Steel

The precipitation of finely dispersed particles – very often intermetallic compounds – within the matrix strengthens and hardens some alloys, and this is purposefully used in modern non-ferrous metallurgical practice, called precipitation or age hardening. Other precipitations developed by heat treatment of metastable solid solutions do not increase but reduce hardness and increase toughness instead. This practice is best known from quench-hardened martensitic steel, which practice is called tempering.

Iron tools or weapons need to be hard but not too brittle. The high hardness and also the brittleness of martensite are based on its specific distorted structure, formed by shear, because of the supersaturation with carbon. To reduce internal stress by rearrangement of the lattice, it is necessary to reduce the carbon content by diffusion. To achieve the right degree of toughness without losing too much hardness, martensitic steels have, therefore, to be reheated after quenching, just to the right temperature. Tempering of steels occurs below the A_1 temperature, usually in the range of 200–400 °C and involves different steps of decomposition during which fine carbides precipitate (see Krauss [51]). The orientation relationship of carbides and α_{Fe} is similar to that in bainite (Sect. 4.6.2.1). There are different stages of structural change in dependence of degree of temperature to balance hardness and toughness. The blacksmith could control this by observing the colour change of the objects: because very thin iron oxide layers form, whose thickness depends on the temperature, interference colours occur. These colours which were also used as patination (e.g. “blueing”) allow a good control of the process. Rostoker and Bronson [96], using notes of Richardson from the 1880s, compiled a list of recommended temperatures/colours for a variety of tools (see Table 4.1). It shows how good tempering could be adjusted by experience to the usage of a tool, e.g. if hard or soft cast iron or wrought iron has to be cut.

Tempering of quenched iron objects has not been practiced in the European Iron Age [100] but became widespread with the Roman conquest, as it can be observed within Roman weapons [6, 25, 38]. Indeed it has not become a regular practice of Roman blacksmiths, as tools or cutlery are only sporadically tempered (see Kastowsky and Mehofer [48]; Maddin et al. [61]; Pleiner [79]; Senn Bischofberger [105]; Schaaber [99]).

Table 4.1 Compilation of recommended temperatures with corresponding colours for a variety of tools

Temperature	Colour	Tools
200 °C	Faint straw	Milling and gear tooth cutters, tools to cut hard cast iron
230 °C	Straw yellow	Dies, razors, drills for tempered saws
240 °C	"Yellow"	Pen knives, screw tops, dies, taps
250 °C	Deep straw	Taps, cutting edges of drills, chipping chisels, butchers' knives, tools to cut soft cast iron
275 °C	Bronze	Axes
290 °C	Peacock	Stone cutting chisels, springs, axes, tools to cut wrought iron
310 °C	Full blue	Drill stems, saws, tools to cut soft metals, axes
340 °C	Light blue	(needles, hacksaws, screwdrivers)
370 °C	Black	–

After Rostoker and Bronson [96: Table 1.5]

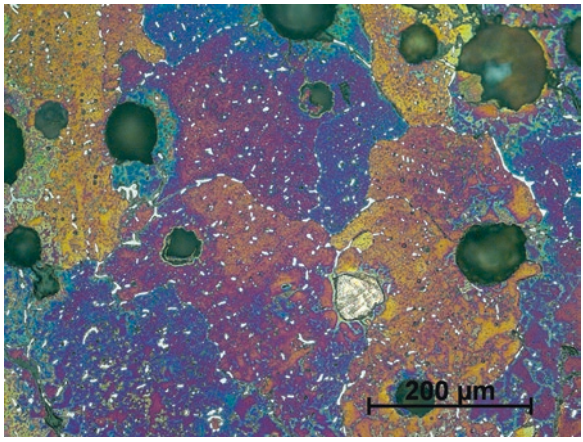

Fig. 4.55 Precipitation of intermetallic Cu_9NiSn_3 phase within a matrix of cast and annealed Drago-fibulae from the Fliess hoard, Austria. Etched with Klemm's III

4.6.2.2.2 Ageing of Copper Alloys

Quenching and tempering are practiced in several modern copper alloys, such as those containing aluminium, manganese or nickel, and also in some special brasses [24]. To our knowledge, ancient coppersmiths were not aware of ageing, but it obviously happened accidentally. It has been observed within the microstructure of a bronze brooch from the Early Iron Age (Ha C) Hoard from Fliess in Tyrol containing mean values of 14.8% tin and 2% of nickel [58]. The microstructure is still as-cast, and according to the high-tin content, the eutectoid $\alpha + \delta$ should be expected. In fact, a ternary intermetallic compound has been observed (Fig. 4.55), which is stoichiometrically related to Cu_9NiSn_3, which is labelled γ in the ternary system [17]. With reference to modern age-hardening practices of Cu-Ni-Sn alloys, it has been concluded that these precipitations result from uncontrolled ageing during solidification [58], but it could be also because of reheating the object for

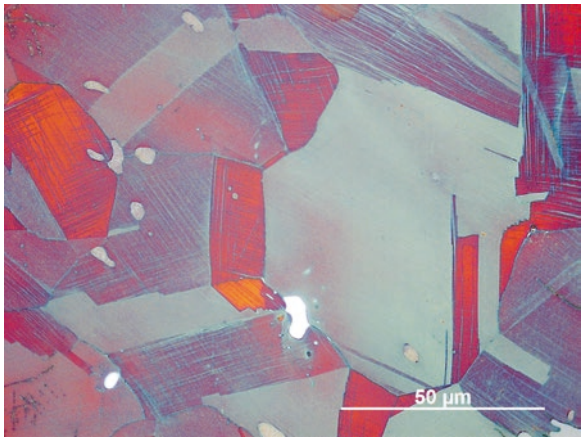

Fig. 4.56 Precipitation of intermetallic $(Cu_{1-x}Ni_x)_3Sn$ phase within a matrix of annealed and reworked α_{Cu} solid solution of a nickel-bearing bronze belt plate from Svenstrup, Denmark. Etched with Klemm's III

destruction. More recently several nickel-bearing bronzes from Denmark, dated to Nordic Bronze Age II, have been investigated and are illustrated in Fig. 4.56, which also show ternary intermetallic precipitations, which are not stoichiometrically related to Cu_9NiSn_3, but would refer to the γ'-phase $(Cu_{1-x}Ni_x)_3Sn$ (see [17]), with some amounts of arsenic and antimony, due to the fahlore origin of the copper. The microstructure of these objects are cold worked and annealed so that the ageing must have happened during annealing.

4.6.2.2.3 Ordering of Gold Alloys

Gold-copper Certain alloys will undergo an ordering reaction when annealed or even when slowly cooled. Such solid-state transformations may also cause trouble in some alloying systems, and often quenching of the alloy is used to prevent these transformations in the solid state from taking place. Gold-copper alloys, important both in ancient and historic periods, are one such system where, as can be seen from the phase diagram given above, a number of ordered phases can form. The gold-copper system is an important one, and a great deal of investigative work has been carried out. One of the first scientists who reported on this system was Roberts-Austen and Rose ([93], pp. 105–112). Pure gold melts at 1064.4 °C and copper at 1083.1 °C [126]; the equilibrium diagram, shown in Fig. 4.12, reveals that a melting minimum exists at 911 °C, corresponding to a composition of 80.1 wt.% gold and 19.9 wt.% copper.

A classic paper of 1916 by Kurnakow, Zemoznzny and Zasedatelev showed that solid-state transformations were taking place well below the eutectic temperature, and it was soon recognised that these transformations were due to ordering at certain compositions. A great deal of work has subsequently been carried out, and the nature of the ordering reactions reported in scores of papers (see Hansen and Anderko [35, p. 198]). Four reactions are well-defined; these are Cu_3Au(I), CuAu(I), CuAu(II) and $CuAu_3$.

$CuAu_3$: Between about 65 and 80 at.% gold (85–92 wt.% gold), a superlattice forms by a peritectoid transformation at about 240 °C [92].

CuAu: At about 25 at.% gold (50.8 wt.% gold), a change from the disordered face-centred cubic gold-copper solid solution occurs. There is evidence to suggest that $CuAu_3$ exists in two modifications. Scott [101] found a long period superlattice stable at about 34.0 °C, while most of the field is occupied by Cu_3Au(I), an ordered fcc structure formed from the disordered solid solution by annealing below 390 °C [20].

CuAu(I): At about 47–63 at.% gold (70–85 wt,% gold), a tetragonal superlattice forms in which alternate planes contain only copper or only gold atoms. Since the investigations of Johansson and Linde [44], the fine structure of AuCu has been extensively investigated; both long period superlattices and antiphase domains have been found of which CuAu is a classic example: CuAu(I) will form below 385 °C.

CuAu(II): Between about 385 and 410 °C, an orthorhombic superlattice will form [44], which may arise from either the disordered fcc alloy or from the tetragonal CuAu(I). It was found that, unlike normal order-disorder transformations, where the size of the ordered region is a function of the time of annealing and of the temperature at which it is carried out, the domains in CuAu(II) tend to remain the size at which they first formed. Isothermal studies of CuAu have shown [52, p. 871] that the long-period superlattice forms from the disordered alloy by slow nucleation and growth to give CuAu(I). However, CuAu(ll) grows in pyramidal plates, and in a polished section, the formation of these plates is accompanied by surface relief effects which appear to be martensitic transformations [110]. Each plate exhibits a system of fine parallel sub-bands which are twins in the orthorhombic lattice on the (101) plane. This is of interest, because some investigators have reported the existence of a martensitic transformation in ternary gold-copper-silver alloys which are probably, in fact, due to the appearance of CuAu(II).

Root ([95], p. 76) found that the hardness of copper-gold alloys, annealed above 420 °C, showed a maximum which was close to the eutectic composition. Figure 4.57 is from Rapson and Groenwald ([86], p. 38, Figure 10) and shows the variation in quenched and slow-cooled gold-copper alloy hardness values, given on the Brinell scale. For a series of conversion charts for this kind of data, see Scott [104] and Sect. 3.3.3.1.

Gold-Silver-Copper This system has also received a great deal of study, although not in as fine detail as the gold-copper system. Early work was carried out by Sterner-Rainer [114, 115] and later investigations by Hultgren and Tarnapol [40], McMullin and Norton [67] and Masing and Kloiber [69]. The ternary diagrams are shown in Figs. 4.58 and 4.59, the latter being from Rapson and Groenewald [86, p. 32], redrawn by Scott [103].

Figure 4.58 shows isothermal sections of the solidus revealing a large, two-phase field to the areas of high copper and silver content and low gold. The insolubility of copper and silver in each other and the solubility of both in gold account for the

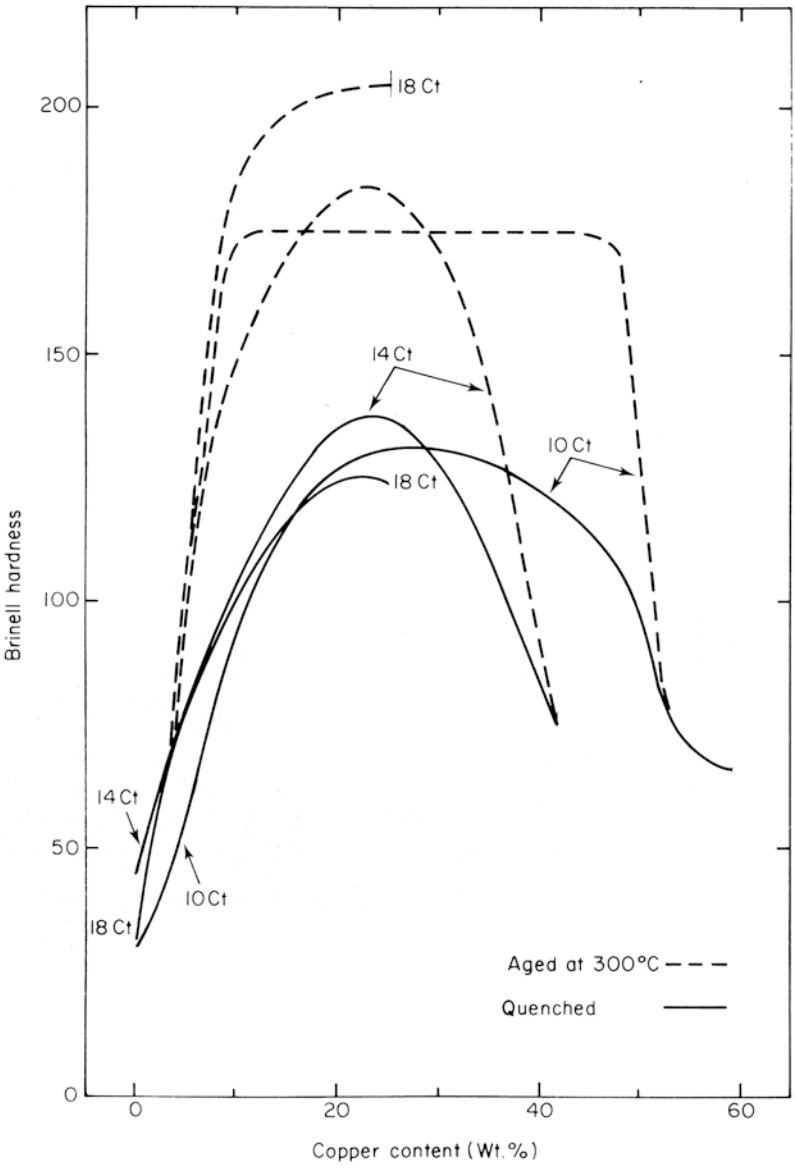

Fig. 4.57 Hardness variation on cooling or quenching of a range of gold-copper alloys

nature of the diagram in which the two-phase field becomes progressively smaller as the gold content increases. Pseudo-binary sections of the AuAgCu ternary system are shown in Fig. 4.59 and illustrate this effect of the temperature coordinates passing up the prism and composition in triangular sections.

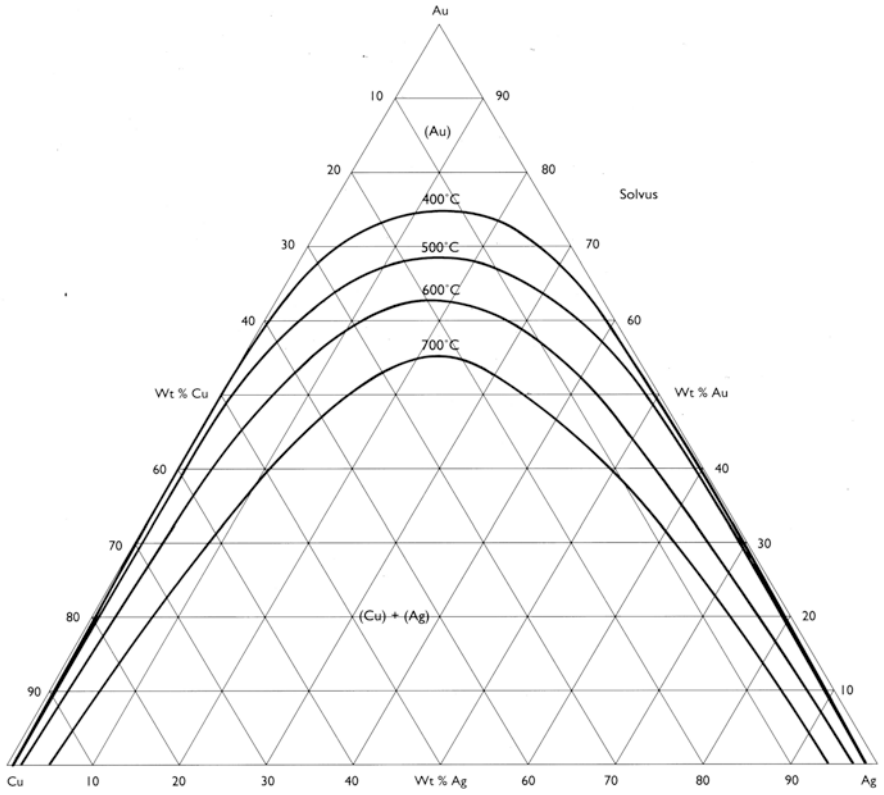

Fig. 4.58 The solidus diagram of the copper-silver-gold system, showing the miscibility gap in the solid state, which derives from the eutectic decomposition in the Ag-Cu system. (From Rapson and Groenwald [86])

The liquidus of Fig. 4.59 shows an eutectic valley half-way across the copper-silver binary extending into the gold alloys where liquidus temperatures can be as low as 850 °C. The discussion of the working properties of these alloys has been simplified by the publication of an important paper by McDonald and Sistare [66, pp. 66–73]). They define a factor f' where:

$$f' = \text{Ag wt.\%} \times 100 / \text{Ag wt.\%} + \text{Cu wt.\%}$$

By defining the gold content of the alloy to be examined and the factor f', it is possible to divide the ternary alloys into three regions based on the value of f'. For example, for 58% gold alloys (14 carat), the following regions can be defined:

Type I: f' 0–10% or from 90% to 100%. The microstructure will be that of a (AuCuAg) solid solution, and the alloys are soft in the annealed condition and cannot be age-hardened.

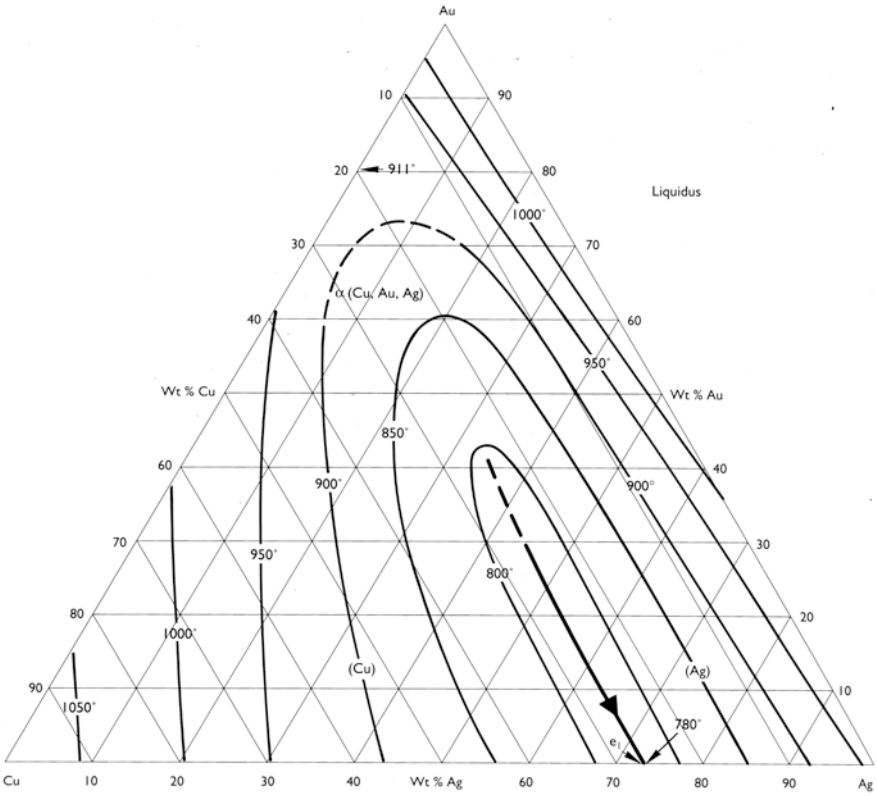

Fig. 4.59 Liquidus curves for the copper-silver-gold ternary system with the eutectic valley. (From Rapson and Groenwald [86])

Type II: *f′* 10–25% or from 75% to 90%. If cooled slowly to equilibrium at room temperature, (AgAu) will be precipitated in copper-rich alloys, while (CuAu) will be precipitated in silver-rich alloys. Type II alloys are moderately soft in the annealed state but can be age-hardened.

Type III: *f′* 25–75%. These can decompose into both (AgAu) and (CuAu). Hard in the annealed condition, difficult to quench, they can harden considerably during slow air-cooling. The colour that these alloys can show is given in the ternary colour diagram of Fig. 4.60; it can be seen that copper red occupies not only the copper corner but also most of the copper-rich and gold-rich side of the diagram. It is only at the gold-rich end of the diagram that any of the ordered phases seen in the copper-gold binary alloy appear.

McDonald and Sistare [66] only mention the existence of AuCu within the 18 carat (75 wt. % Au) gold alloys. There are then two hardening mechanisms which can occur under equilibrium conditions: ordering in high gold content alloys and precipitation hardening in a wide range of type II and type III alloys. Figure 4.57

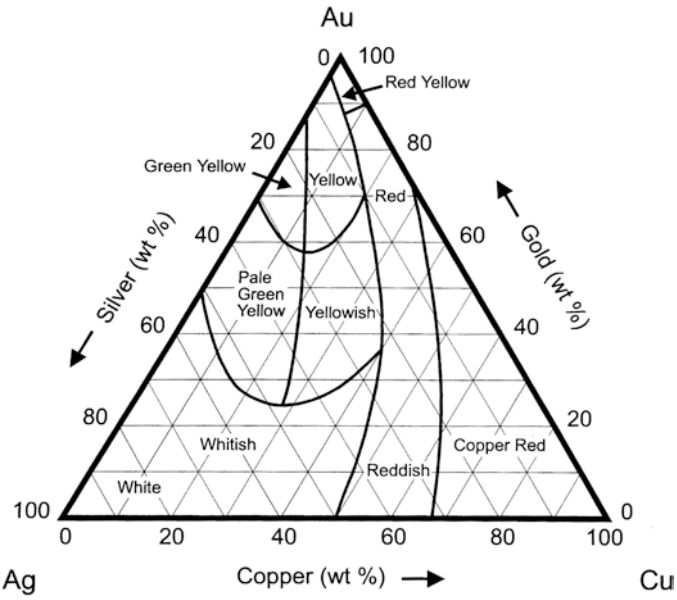

Fig. 4.60 Colour ranges for ternary gold-copper-silver alloys

shows the extent to which quenched gold-copper alloys are age-hardened and Wise [130, pp. 133–137] gives the effects of aging on various gold-silver-copper alloys. Like gold-copper alloys they also retain lower hardness values than alloys of the same composition which have been precipitation hardened by heat-treatment. The conditions under which these alloys harden are typically that of heating for 2–4 h at 205–315 °C, although some degree of hardening will also occur on cooling in air after annealing. McDonald and Sistare [66] found that annealing at 650 °C for 30 min was sufficient to recrystallize and homogenize all the alloy types. Although these alloys make very good castings, some experience is required to work them to shape by hammering and annealing operations. The ternary alloys tend to work-harden quite rapidly, and the extent to which they can be hammered without annealing is limited to 70% reduction at most.

However if annealing treatments are carried out too often, for example, if percentages reductions are less than 30%, then grain growth during annealing can be excessive and weak coarse-grained structures develop which are the cause of "orange-peel" effects on further working. These effects have been noted in the surfaces of some ancient Colombian tumbaga alloys [102].

McDonald and Sistare [66] found that quenched alloys of type I, II and III all showed homogeneous solid solution microstructures even where the slow-cooled alloys show a two-phase structure. It is interesting to note that a document of 1555 preserved in the Archive of the Indies refers to quenching as a part of Indian metal-working technology in Tamalameque, lowland Colombia [120]):

…and then the said chief and Indians burned a little charcoal on some baked clay with three cane blowpipes and placed a crucible on this with a piece of caricoli, which was brought with them, along with small quantities of low-grade gold after it had melted they took out the crucible and poured a little water over it and in this way, placing it (a bracelet) in the fire, taking it out and putting it in water and hammering it on an anvil with the stones described they worked until they had increased its size many times…

The advantages of water quenching after annealing would be to ensure that the alloy is kept in the most easily worked state before attempting to carry out further working. The preferred working method, which this document records, is definitely that of cold-working rather than hot-working. Metallurgical examination carried out in this thesis also shows that the Colombian Indians generally finished their hammering by a final process annealing. This would have been a sensible operation because many of the ternary alloys are very susceptible to stress corrosion. It is also of interest to note in this connection that Graf [33] found that the homogeneous Au-Ag-Cu alloys were more susceptible to stress corrosion cracking than that alloys of the same composition in the two-phased state.

References

1. Bachmann, H.-G.: The Identification of Slags from Archaeological Sites Institute of Archaeology Occasional Publication No. 6. Institute of Archaeology, London (1982)
2. Bhadeshia, H.K.D.H.: Bainite in Steels, 2nd edn. IOM Communications Ltd, London (2001)
3. Bhadeshia: Physical metallurgy of steels. In: Laughlin, D., Hono, K. (eds.) Physical Metallurgy III, 5th edn, pp. 2157–2214. Elsevier, Amsterdam et al. (2014)
4. Barrena, M.I., Gómez de Salazar, J.M., Soria, S.A.: Corrosion of brass archaeological blinker: characterisation of natural degradation process. Mater. Lett. **62**(24), 3944–3946 (2008)
5. Barrett, C.S., Massalski, T.B.: Structure of Metals: Crystallographic Methods, Principles and Data, International Series on Materials Science and Technology 35, 3rd rev edn. Pergamon, Oxford/New York/Seoul/Tokyo (1993)
6. Biborski, M., Kaczanowski, P., Kedzierski, Z., Stepinski, J.: Ergebnisse der metallographischen Untersuchungen römischen Schwertern aus dem Vindonissa-Museum Brugg und dem Römermuseum Augst, Jahresbericht 1985 der Gesellschaft Pro Vindonissa, pp. 45–80 (1985)
7. Breeks, J.W.: An Account of the Primitive Tribes and Monuments of the Nilagiris. Allen, London (1873)
8. Brüggler, M., Dirsch, C., Drechsler, M., Schwab, R., Willer, F.: Ein römischer Schienenarmschutz aus dem Auxiliarlager Till-Steincheshof und die Messingherstellung in der römischen Kaiserzeit. Bonner Jahrbücher. **212**, 121–152 (2012)
9. Buchwald, V.F.: Handbook of Iron Meteorites 1–3. University of California Press, Berkeley (1975)
10. Buchwald, V.F.: Ancient Iron and Slags in Greenland. Meddelelser om Grønland, Man & Society 26. Danish Polar Center, Copenhagen (2001)
11. Buchwald, V.F.: Iron and Steel in Ancient Times. Historisk-filosofiske Skrifter 29. Det Kongelige Danske Videnskabernes Selskab, Copenhagen (2005)
12. Buchwald, V.F.: Iron, Steel and Cast Iron before Bessemer. Historisk-filosofiske Skrifter 32. Det Kongelige Danske Videnskabernes Selskab, Copenhagen (2008)
13. Buchwald, V.F., Wivel, H.: Slag analysis as a method for characterization and provenancing of iron objects. Mater. Charact. **40**, 73–96 (1998)

14. Budd, P.: Alloying and metalworking in the Copper Age of Central Europe. Bull. Met. Mus. **17**, 3–14 (1992)
15. Cellini, B.: The Treatises of Benvenuto Cellini on Goldsmithing and Sculpture. Trans. C.R. Ashbee, Dover, New York (1967)
16. Chadwick, R.: The effect of composition and constitution on the working and some physical properties of the tin bronzes. J. Inst. Met. **64**, 331–346 (1939)
17. Chang, Y.A., Neumann, J.P., Mikula, A., Goldberg, D.: Phase Diagrams and Thermodynamic Properties of Ternary Copper-Metal Systems. International Copper Research Association Series on the Metallurgy of Copper 6. NSRD, Washington, DC (1979)
18. Cope, L.H.: The metallurgical analysis of Roman Imperial silver and aes coinage. In: Hall, E.T., Metcalf, D.M. (eds.) Methods of Chemical and Metallurgical Investigation of Ancient Coinage Royal Numismatic Society Special Publication 8, pp. 3–47. Royal Numismatic Society, London (1972)
19. Coustures, M.P., Béziat, D., Tollon, F., Domergue, C., Long, L., Rebiscoul, A.: The use of trace element analysis of entrapped slag inclusions to establish ore – bar iron links: examples from two Gallo-Roman iron-making sites in France (Les Martys, Montagne noire, and les Ferrys, Loiret). Archaeometry. **45**, 599–613 (2003)
20. Cowley, J.M.: X-ray measurement of order in single crystals of Cu_3Au. J. Appl. Phys. **21**(1), 24–30 (1950)
21. Craddock, P.T.: Early metal mining and production. Edinburgh University Press, Edinburgh (1995)
22. Craddock, P.T., Meeks, N.D.: Iron in ancient copper. Archaeometry. **29**(2), 187–204 (1987)
23. Davenport, E.S., Bain, E.C.: Transformation of austenite at constant subcritical temperatures. Trans. Am. Inst. Min. Metall. Eng. **90**, 117–144 (1930)
24. Davis, J.R. (ed.): ASM Specialty Handbook: Copper and Copper Alloys. ASM International, Materials Park (2008)
25. Dieudonné-Glad, N., Parisot, J.: Etude métallographique d'épées celtiques et romaines du musée Denon à Châlon-sur-Saône. In: Nicolini, G., Dieudonne-Glad, N. (eds.) Les métaux antiques: travail et restauration. Monographies Instrumentum 6, pp. 153–163. Monique Mergoil, Montagnac (1998)
26. Dillmann, P., L'Héritier, M.: Slag inclusion analyses for studying ferrous alloys employed in French medieval buildings: supply of materials and diffusion of smelting processes. J. Archaeol. Sci. **34**, 1810–1823 (2007)
27. Dillmann, P., Schwab, R., Bauvais, S., Brauns, M., Disser, A., Leroy, S., Gassmann, G., Fluzin, P.: Circulation of iron products in the North-Alpine area during the end of the First Iron Age (6th–5th c. BC): a combination of chemical and isotopic approaches. J. Archaeol. Sci. **87**, 108–124 (2017)
28. Dövener, F., Schwab, R., Willer, F.: Kleine Zeugnisse einstiger Größe – Vier Bronzestatuen-Fragmente aus Luxemburg. Archaeologia Luxemburgensis. **4**, 141–160 (2018)
29. Dungworth, D.: Serendipity in the foundry? Tin oxide inclusions in copper and copper alloys as an indicator of production process. Bull. Met. Mus. **32**, 1–5 (2000)
30. English, A.T., Chin, G.Y., Wonsiewicz, B.C.: Structures resulting from plastic deformation. In: Lyman, T. (ed.) Metallography, Structures and Phase Diagrams ASM Handbook 8, pp. 211–216. American Society for Metals, Metals Park (1973)
31. Glover, I., Bennett, A.: The high-tin bronzes of Thailand. In: Jett, P. (ed.) Scientific Research on Ancient Asian Metallurgy: Proceedings of the Fifth Forbes Symposium at the Freer Gallery of Art, pp. 101–114. Archetype, London (2012)
32. Goodway, M., Conklin, H.C.: Quenched high-tin bronzes from the Philippines. Archeomaterials. **2**, 1–27 (1987)
33. Graf, L.: The causes and mechanism of stress-corrosion cracking of homogeneous non-supersaturated alloys as derived from experimental work with alloys containing noble metal components. In: Scully, J.C. (ed.) The Theory of Stress-Corrosion Cracking in Alloys: Research Evaluation Conference Held at Ericeira, Portugal over the Period 29 March to 2 April 1971, pp. 399–341. NATO Scientific Affairs Division, Brussels (1971)

34. Hanson, D., Pell-Walpole, W.T.: Chill-Cast Tin Bronzes. Edward Arnold, London (1951)
35. Hansen, M., Anderko, K.: Constitution of Binary Alloys. McGraw-Hill, New York/Toronto/London (1958)
36. Hansen, N., Barlow, C.Y.: Plastic deformation of metals and alloys. In: Laughlin, D.E., Hono, K. (eds.) Physical Metallurgy II, 5th edn, pp. 1681–1764. Elsevier, Amsterdam et al. (2014)
37. Hauptmann, A., Maddin, R., Prange, M.: On the structure and composition of copper and tin ingots excavated from the shipwreck of Uluburun. Bull. Am. Sch. Orient. Res. **328**, 1–30 (2002)
38. Horstmann, D.: Metallkundliche Untersuchungen an Klingen von zwei römischen Dolchen Ausgrabungen und Funde in Westfalen-Lippe 9/B, pp. 111–135 (1995)
39. Hillert, M. (ed.): Viewpoint set No. 25 "bainite". Scr. Mater. **47**, 137–212 (2002)
40. Hultgren, R., Tarnapol, L.: The effect of silver on the gold-copper superlattice Au-Cu. Trans. Am. Inst. Min. Metall. Eng. **33**, 228–237 (1939)
41. Hume-Rothery, W., Raynor, G.V.: The Structure of Metals and Alloys. Institute of Metals Monograph and Report Series 1. The Institute of Metals, London (1956)
42. Illescas, F.J., Asensio, J., Guilemany, J.M.: TEM study of bainitic low-carbon HSLA steel: the orientation relationships of cementite. Pract. Metall. **44**(6), 334–346 (2007)
43. Ingo, G.M., de Caro, T., Bultrini, G.: Microchemical investigation of archaeological copper based artefacts disclosing an ancient witness of the transition from the value of the substance to the value of the appearance. Microchim. Acta. **144**(1), 87–95 (2004)
44. Johansson, C.H., Linde, J.O.: J.O.: Röntgenographische und elektrische Untersuchungen des CuAu-Systems. Ann. Phys. **417**(1), 1–48 (1936)
45. Juleff, J.: X-ray diffraction studies of gold. Unpublished BSc thesis, Institute of Archaeology, London (1981)
46. Kallfass, M., Paul, J., Jehn, H.: Investigations on the embrittlement of an antique Roman silver bowl. Practical Metallogr. **2**, 317–323 (1985)
47. Karakaya, I., Thompson, W.T.: The Ag-Sn (silver-tin) system. Bull. Alloy Phase Diagr. **8**(4), 340–347 (1987)
48. Kastowsky, K., Mehofer, M.: Metallographische Analysen an den kaiserzeitlichen Depots aus Mannersdorf am Leithagebirge. In: Pollak, M. (ed.) Stellmacherei und Landwirtschaft: zwei römische Materialhorte aus Mannersdorf am Leithagebirge, Niederösterreich. Fundberichte aus Österreich Materialhefte A 16, pp. 55–65. Berger, Wien (2006)
49. Kienlin, T.L.: Traditions and transformations: approaches to eneolithic (Copper Age) and Bronze Age metalworking and society in Eastern Central Europe and the Carpathian Basin. British Archaeological Reports International Series 2184. Archaeopress, Oxford (2010)
50. Kiessling, R.: Non-metallic Inclusions in Steel III: The Origin and Behaviour of Inclusions and their Influence on the Properties of Steels. Percy Lund, London (1968)
51. Krauss, G.: Steels: Heat Treatment and Processing Principles. ASM International, Materials Park (2000)
52. Kuczynski, G.C., Hochman, R.F., Doyama, M.: Isothermal transformations in CuAu. J. Appl. Phys. **26**, 871–874 (1955)
53. Lang, J., Williams, A.R.: The hardening of iron swords. J. Archaeol. Sci. **2**, 199–207 (1975)
54. La Niece, S.: Metallography in numismatics. In: Oddy, A., Cowell, M. (eds.) Metallurgy in Numismatics 4, Royal Numismatic Society Special Publication 30, pp. 114–133. Royal Numismatic Society, London (1998)
55. Lechtman, H.: Traditions and styles in central Andean metalwork. In: Maddin, R. (ed.) The Beginning of the Use of Metals and Alloys (BUMA I), pp. 344–378. MIT Press, Cambridge, MA (1988)
56. Lehner, J.W., Schwab, R., Pernicka, E., Schachner, A.: Cupronickel and the rise of the Hittite State: metallurgical investigations of Late Bronze Age copper alloys at Boğazköy-Hattuša (forthcoming)
57. Liu, K.H., Chan, H., Notis, M.R., Pigott, V.S.: Analytical electron microscopy of early steel from the Bacqah Valley, Jordan. In: Romig Jr., A.D., Goldstein, J.I. (eds.) Microbeam Analysis-1984, pp. 261–263. San Francisco Press, San Francisco (1984)

58. Lutz, J., Schwab, R.: The Early Iron Age hoard from Fliess in Tyrol and ore resources in the Eastern Alps. In: Pernicka, E., Schwab, R. (eds.) Under the Volcano. Forschungen zur Archäometrie und Altertumswissenschaft 5, pp. 25–34. M. Leidorf, Rahden/Westf (2014)
59. Lychatz, B.: Die Metallurgie des Rennverfahrens. Freiberger Forschungshefte D 245. Technische Universität Bergakademie Freiberg, Freiberg (2013)
60. Maddin, R.: A history of martensite: some thoughts on the early hardening of iron. In: Olson, G.B., Owen, W.S. (eds.) Martensite: A Tribute to Morris Cohen, pp. 11–19. ASM International, Materials Park (1992)
61. Maddin, R., Hauptmann, A., Baatz, D.: A metallographic examination of some iron tools from the Saalburgmuseum. Saalburg Jahrbuch. **46**, 5–23 (1991)
62. Marshall, J.: Taxila: An Illustrated Account of Archaeological Excavations Carried Out at Taxila Under the Orders of the Government of India Between the Years 1913 and 1934, vol. 1–3. Cambridge University Press, Cambridge (1951)
63. Massalski, T.B. (ed.): Binary alloy phase diagrams 1–2, Ohio. American Society of Metals, Materials Park (1986)
64. Matteoli, L., Storti, C.: Metallographic research on four pure copper axes and one related metallic block from Eneolithic Italian cave. J. Hist. Metall. Soc. **16**(2), 65–69 (1982)
65. Meeks, N.D., Tite, M.S.: The analysis of platinum-group element inclusions in gold antiquities. J. Archaeol. Sci. **7**(3), 267–275 (1980)
66. McDonald, A.S., Sistare, G.H.: The metallurgy of some carat gold jewellery alloys. Part I – coloured gold alloys. Gold Bull. **11**, 66–73 (1978)
67. McMullin, J.F., Norton, J.T.: On the structure of gold-silver-copper alloys. Trans. Am. Inst. Min. Metall. Eng. **33**, 228–237 (1949)
68. Marshall, J.: Taxila, 3 vols. Cambridge University Press, Cambridge (1951)
69. Masing, G., Kloiber, K.: Ausscheidungsvorgänge im System Kupfer-Silber-Gold. Z. Met. **32**, 125–132 (1940)
70. Melikian-Chirvani, A.S.: The white bronzes of early Islamic Iran. Metrop. Mus. J. **9**, 123–151 (1974)
71. Michalak, J.T.: Plastic deformation structures in iron and steel. In: Lyman, T. (ed.) Metallography, Structures and Phase Diagrams ASM Handbook 8, pp. 218–220. American Society for Metals, Metals Park (1973)
72. Mizutani, U., et al.: Electron theory of complex metallic alloys. In: Laughlin, D.E., Hono, K. (eds.) Physical Metallurgy I, 5th edn, pp. 103–202. Elsevier, Amsterdam et al (2014)
73. Northover, J.P.: The exploration of long-distance movement of bronze in Bronze and early Iron Age Europe. Bull. Inst. Archaeol. Univ. Lond. **19**, 45–72 (1982)
74. Northover, J.P.: Exotic alloys in antiquity. In: Rehren, T., Hauptmann, A., Muhly, J.D. (eds.) Metallurgica Antiqua. In Honour of Hans-Gert Bachmann and Robert Maddin. Der Anschnitt Beiheft 8, pp. 113–121. Deutsches Bergbau-Museum, Bochum (1998)
75. Northover, P.: Copper in the Industrial Age. In: Degrigny, C., van Langh, R., Joosten, I., Ankersmit, B. (eds.) METAL 07, vol. 1, pp. 83–90. Elsevier, Amsterdam (2007)
76. Notis, M.R., Shugar, A.N.: Roman shears: metallography, composition and historical approach to investigation. In: Archaeometallurgy in Europe 1, pp. 109–118. AIM, Milan (2003)
77. Odgen, J.: The technology of Medieval jewellery. In: Scott, D.A., Podany, J., Considine, B.B. (eds.) Ancient & Historic Metals – Conservation and Scientific Research, pp. 153–182. National Museum of Singapore, Singapore (1994)
78. Park, J.S., Park, C.W., Lee, K.J.: Implication of peritectic composition in historical high-tin bronze metallurgy. Mater. Charact. **60**(11), 1268–1275 (2009)
79. Pleiner, R.: Zur Schmiedetechnik im römerzeitlichen Bayern. Bayerische Vorgeschichtsblätter. **35**, 113–140 (1970)
80. Pleiner, R.: The Celtic Sword. Clarendon Press, Oxford (1993)
81. Pleiner, R.: Iron in Archaeology: The European Bloomery Smelters. Archeologicky Ústav Avcr, Praha (2000)

82. Pleiner, R.: Iron in Archaeology: Early European Blacksmiths. Archeologicky Ústav Avcr, Praha (2006)
83. Pliny the Elder: Natural History, 10 vols, trans. H. Rackham. Harvard University Press/ William Heinemann, Cambridge/Harvard/London (1979)
84. Pryce, O., Murillo-Barroso, M., Bellina, B., Martinón-Torres, M.: Khao Sam Kaeo – an archaeometallurgical crossroads for trans-Asiatic technological traditions. In: Srinivasan, S., Ranganathan, S., Giumlia-Mair, A. (eds.) Metals and Civilizations, Proceedings of the International Conference, Beginning of the Use of Metals and Alloys, BUMA VII, Bangalore September 2009, Bangalore, pp. 33–46 (2015)
85. Rajpitak, W., Seeley, N.: The bronze bowls from Ban Don Ta Phet: an enigma of prehistoric metallurgy. World Archaeol. **11**(1), 26–31 (1979)
86. Rapson, W.S., Groenewald, T.: Gold Usage. Academic, London (1978)
87. Ravich, I.G.: Study of the composition of Scythian and Sarmatian bronze mirrors and technologies of their manufacture. Bull. Met. Mus. **16**, 20–31 (1991)
88. Ravich, I.G., Ryndina, N.V.: Early copper-arsenic alloys and the problems of their use in the Bronze Age of the North Caucasus. Bull. Met. Mus. **23**, 1–18 (1995)
89. Reeve, M.R., Bowden, J.S., Cuthbertson, J.W.: A report on the microstructure of tin bronzes containing 15–28% tin. Part One. Met. Ind. **78**, 23–25 (1953)
90. Reeve, M.R., Bowden, J.S., Cuthbertson, J.W.: A report on the microstructure of tin bronzes containing 15-28% tin. Part Two. Met. Ind. **78**, 49–52 (1953)
91. Rehren, T., Northover, J.P.: Selenium and tellurium in ancient copper ingots. In: Pernicka, E., Wagner, G.A. (eds.) Archaeometry '90, pp. 221–228. Birkhäuser, Basel/Boston/Berlin (1991)
92. Rhines, F.N., Bond, W.E., Rummel, R.A.: Constitution of ordering alloys of the system gold-copper. Trans. Am. Soc. Met. **47**, 578–597 (1955)
93. Roberts-Austen, W.C., Rose, K.T.: On certain properties of the alloys of the gold-copper series. Proc. R. Soc. Lond. **67**(435–441), 105–112 (1901)
94. Rodney, D., Bonneville, J.: Dislocations. In: Laughlin, D.E., Hono, K. (eds.) Physical Metallurgy II, 5th edn, pp. 1591–1680. Elsevier, Amsterdam et al (2014)
95. Root, W.C.: Gold-copper alloys in ancient America. J. Chem. Educ. **28**(2), 76–78 (1951)
96. Rostoker, W., Bronson, B.: Pre-industrial Iron. Archeomaterials Monograph 1. Archeomaterials, Philadelphia (1990)
97. Samuels, L.E.: Optical Microscopy of Carbon Steels. American Society for Metals, Metals Park (1980)
98. Saunders, N., Miodownik, A.P.: The Cu-Sn (copper-tin) system. Bull. Alloy Phase Diagr. **11**(3), 278–287 (1990)
99. Schaaber, O.: Beiträge zur Frage des Norischen Eisens. Metallkundliche Grundlagen und Untersuchungen an Funden vom Magdalensberg. Carinthia I, **153**, pp. 129–279 (1963)
100. Schwab, R.: Untersuchungen zur Technologie und Herkunft eiserner Werkzeuge und Waffen. In: Sievers, S., Leicht, M., Ziegaus, B. (eds.) Ergebnisse der Ausgrabungen 1996–1999 in Manching-Altenfeld Die Ausgrabungen in Manching 18, pp. 251–293. Reichert Verlag, Wiesbaden (2013)
101. Scott, R.E.: New complex phase in the copper-gold system. J. Appl. Phys. **31**(12), 2112–2117 (1960)
102. Scott, D.A.: Pre-Hispanic Colombian metallurgy: studies of some gold and platinum alloys. PhD thesis, Institute of Archaeology, University of London (1982)
103. Scott, D.A.: Metallography and microstructure of ancient and historic metals, Getty conservation institute, J. Paul Getty Museum, Malibu (1991)
104. Scott, D.A.: Ancient Metals: Microstructure and Metallurgy 1. Conservation Science Press, Los Angeles (2011)
105. Senn Bischofberger, M.: Das Schmiedehandwerk im nordalpinen Raum von der Eisenzeit bis ins frühe Mittelalter. Internationale Archäologie – Naturwissenschaft und Technologie 5. Verlag Marie Leidorf, Rahden (2005)

106. Shalev, S., Northover, J.P.: The metallurgy of the Nahal Mishmar hoard reconsidered. Archaeometry. **35**(1), 35–47 (1993)
107. Shim, J.H., Oh, C.S., Lee, B.J., Lee, D.N.: Thermodynamic assessment of the Cu-Sn system. Z. Met. **87**, 205–212 (1996)
108. Smith, C.S.: A History of Metallography. The University of Chicago Press, Chicago (1960)
109. Smith, C.S.: Bronze technology in the east: a metallurgical study of early Thai bronzes. In: Teich, M., Young, R. (eds.) Changing Perspectives in the History of Science: Essays in Honour of Joseph Needham, pp. 21–32. Heinemann, London (1973)
110. Smith, R., Bowles, J.S.: The crystallography of the cubic to orthorhombic transformation in the alloy AuCu. Acta Metall. **8**(7), 405–415 (1960)
111. Srinivasan, S.: The use of tin and bronze in prehistoric southern Indian metallurgy. J. Met. **50**(7), 44–48 (1998)
112. Srinivasan, S., Glover, I.: Wrought and quenched, and cast high-tin bronzes in Kerala State, India. Hist. Metall. **29**(2), 69–88 (1995)
113. Srinivasan, S., Glover, I.: Skilled mirror craft of intermetallic delta high-tin bronze ($Cu_{31}Sn_8$, 32.6% tin) from Aranmula, Kerala. Curr. Sci. **93**(1), 35–40 (2007)
114. Sterner-Rainer, L.: Die Verbindung Au-Cu in Goldlegierungen. Z. Met. **17**, 162–165 (1925)
115. Sterner-Rainer, L.: Die Edelmetall-Legierungen in Industrie und Gewerbe. Verlag Wihelm Diebener, Leipzig (1930)
116. Steurer, W.: Crystal structures of metallic elements and compounds. In: Laughlin, D.E., Hono, K. (eds.) Physical Metallurgy I, 5th edn, pp. 1–101. Elsevier, Amsterdam et al (2014)
117. Stöllner, T., Oeggl, K. (eds.): Bergauf Bergab – 10.000 Jahre Bergbau in den Ostalpen. Veröffentlichung aus dem Deutschen Bergbau-Museum Bochum 207. Verlag Marie Leidorf, Bochum (2015)
118. Stöllner, T., Schwab, R.: Hart oder weich? Worauf es ankommt! Pickel aus dem prähistorischen Bergbau in den Ostalpen. Festschrift Fritz Eckart Barth, Mitteilungen der Anthropologischen Gesellschaft in Wien. **139**, 149–166 (2009)
119. Tadmor, M., Kedem, D., Begemann, F., Hauptmann, A., Pernicka, E., Schmitt-Strecker, S.: The Naḥal Mishmar hoard from the Judean Desert: technology, composition, and provenance. Atiqot. **27**, 95–148 (1995)
120. Tamalameque. Averiguaciones en Tamalameque sobre los manyllas que Mando Hazer Juan de Azpeleta a los Yndios de su Encomienda de Anpihuegas. Justicia, Legajo 610–612, folios 2520–25 (manuscript) Archivo General de Indias, Seville. Trans in Museo del Oro Archives, Bogota, Colombia (1555)
121. Uran, L.: Observations métallographiques sur les épées celtiques en fer. Revue Aquitania Supplément. **1**, 299–308 (1986)
122. Vander Voort, G.F.: Metallography, Principles and Practice. McGraw-Hill, New York (1984)
123. Voce, E.: Examination of specimens from the Pitt Rivers Museum. In: Coghlan, H.H. (ed.) Notes on the Prehistoric Metallurgy of Copper and Bronze in the Old World. Pitt Rivers Museum Occasional Papers on Technology 4, pp. 110–111. University Press, Oxford (1951)
124. Wanhill, R.J.H., Steijaart, J.P.H.M., Leenheer, R., Koens, J.F.W.: Damage assessment and preservation of an Egyptian silver vase (300–200 BC). Archaeometry. **40**(1), 123–137 (1998)
125. Wayman, M.L., Duke, M.J.M.: The effects of melting on native copper. In: Hauptmann, A., Pernicka, E., Rehren, T., Yalçın, Ü. (eds.) The Beginnings of Metallurgy. Der Anschnitt Beiheft 9, pp. 55–63. Deutsches Bergbau-Museum, Bochum (1999)
126. Weast, R.C. (ed.): The CRC Handbook of Chemistry and Physics, 59th edn. CRC Press, Boca Raton (1978)
127. Weins, W.N., Bleed, P.: Why is the Japanese sword curved? MRS Proc. **185**(p), 691–698 (1990)
128. Wheeler, T.S., Maddin, R.: The techniques of the early Thai metalsmith. Expedition. **18**(4), 38–47 (1976)
129. Willer, F., Schwab, R., Mirschenz, M.: Römische Bronzestatuen am Limes: Archäometrische Untersuchungen zur Herstellungstechnik. Bonner Jahrbücher. **216**, 57–207 (2017)

130. Wise, E.M.: Gold: Recovery, Properties, and Applications. Van Nostrand Company, Toronto/New York/London (1964)
131. Zhang, Y.M., Yang, S., Evans, J.R.G.: Revisiting Hume-Rothery's rules with artificial neural networks. Acta Mater. **56**(5), 1094–1105 (2008)
132. Zwicker, U.: Archaeometallurgical investigation on the copper – and copper-alloy-production in the area of the Mediterranean Sea (7000–1000 B.C.). Bull. Met. Mus. **15**, 3–32 (1990)

Chapter 5
The Metallurgy of Pre-industrial Metals and Alloys

5.1 Nonferrous Metals and Their Alloys

5.1.1 Copper and Copper Alloys

5.1.1.1 Unalloyed Copper

Unalloyed copper has a face-centred cubic (fcc) structure and a hardness of 40 HV in the annealed state. Native copper, which is not as pure as modern refined copper and which usually shows irregular grain sizes, has been found to be slightly harder with hardness from 45 to around 80 HV, and its hardness can be increased by cold-work to around 140 HV (135 HB), without any additional alloying elements, although it has only a very limited strength, even after significant reduction (see Böhme [12]; Coghlan [26]; Maréchal [93]; Tylecote [179]).

The use of native copper goes back in time at least 10,000 years and must have occurred in most geographic areas at a very early period in human prehistory. When Neolithic cultures first began using it, around the eighth millennium BC, they fashioned the metal into small ornaments and simple copper blades. The first undisputed evidence for human exploitation of native copper deposits comes from the aceramic Neolithic site of Çayönü Tepesi in southeastern Turkey, where beads of malachite and native copper were found that date back around 8750–9250 years before the present day [105]. In addition, worked copper dating from the eighth to the seventh millennium BC has been found in both Anatolia and Mesopotamia. Even at this early period, some of the copper objects had been heated to anneal them, so they could be hammered into shape, ready ductility being one of the chief assets of native copper.

Evidence for the smelting of copper, in the form of primitive slags, has been found at such Anatolian sites as Catalhöyük, dating to the sixth millennium BC, an unusually early date that has stimulated scholarly discussion about the real technological origin of the slag. Radivojević and co-workers [133] recently re-examined

D. A. Scott, R. Schwab, *Metallography in Archaeology and Art*, Cultural Heritage Science, https://doi.org/10.1007/978-3-030-11265-3_5

the materials excavated in the 1960s by the British archaeologist Dr. James Mellaart and confirmed the evidence of copper minerals, some "slagged" material and a solid-state formation of metallic copper. Furthermore they interpret this material as the result of accidental copper reduction, which unavoidably directs us to the assumption that extracted copper could first have been formed in a campfire.

Many early artefacts from different cultures and continents are made of nearly pure copper, and there is generally little doubt that native copper was the first metal used by man, although Moorey [102] used to claim that it was lead that came first (see Chap. 2). Native copper is a malleable and ductile material, which is easy to cold-work into small, useful objects such as pins or needles or into small ornaments such as necklace beads, dangles or rings. Indeed some more compact objects such as the macehead from Can Hassan in Anatolia dated around 6000 BC (51–53.5 mm in diameter and 433.2 g weight) or some small axe heads have been produced by rolling and forging copper sheet into shape [164, 198].

Native copper use is sporadic, and without sensitive analytical methods such as INAA, ICP-MS or ICP-OES, it is difficult to determine definitively, because of the very low concentrations of trace impurity patterns – with the exception of arsenic and silver, which are typically in the hundreds of mg/kg [12, 80, 188, 198]. There is a tendency for native copper to show metallographic features that are distinct from smelted copper, but much of these differences may be lost if the copper is extensively worked and annealed, or melted. Fig. 5.1 is a sample of native copper, which has been worked by natural forces in the earth over thousands of years, in which folding, characteristic of native copper, and often of native copper used in some artefacts, can still be seen.

Folding and elongated twinned grains are the characteristics of native copper. Growth features may also be seen in which impurities in the native copper are segregated to certain planes or discrete regions of the copper. Metallography combined with careful determination of trace elements may still afford clues to the origin of the copper to allow some conclusions to be reached. Fig. 5.2 shows the variation in mechanical properties of pure copper with percentage reduction in area by rolling.

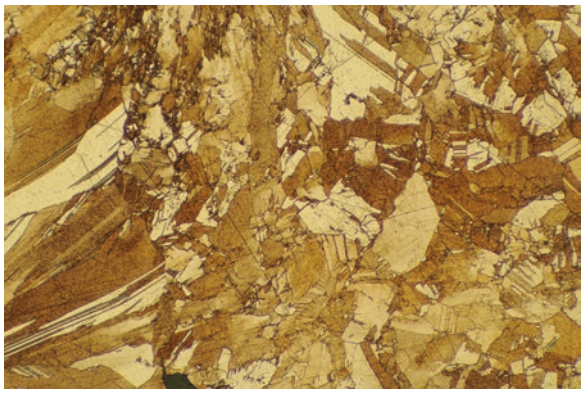

Fig. 5.1 Native copper from the Great lakes area of North America. Naturally worked here to create elongated and folded grain structure, typical of native copper. Etched in ferric chloride, magnification x300

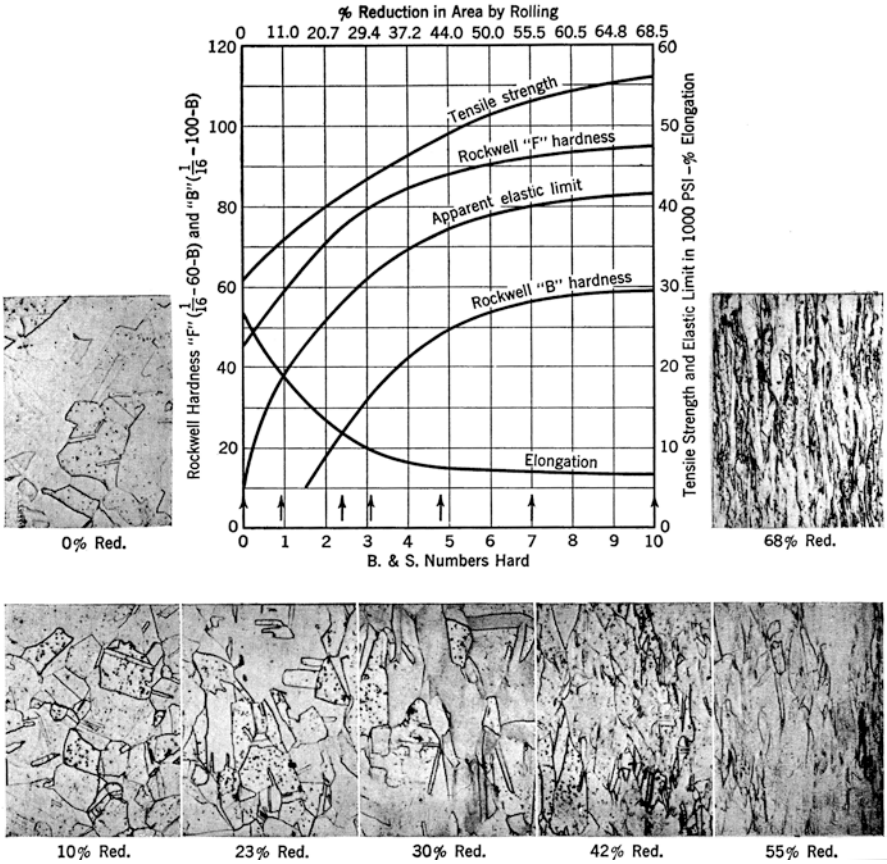

Fig. 5.2 Drawings of the typical microstructural appearance of copper, from no reduction in thickness to 68% reduction, when the copper grains begin to become squashed in the direction of working. The elongation goes down substantially, while the hardness continues to rise. (From Samans [147], 60 Fig. 2.16)

The grains present at 0% reduction have a Rockwell scale hardness of about 45 HRF, which is comparable with the Vickers number. The copper grains become deformed and squashed on rolling to 68% reduction as seen in the photomicrographs. The Rockwell hardness is now increased to 95 HRF, the tensile strength goes up but the elongation drops greatly after only 30% reduction in thickness, as the copper becomes increasingly brittle.

Another metallographic feature derives from the solid-solid miscibility gap between copper and silver, which can occur as particles of metallic silver, which may be a characteristic for some native coppers ([188], p. 55; [198], p. 286). They would disappear after annealing or melting, but Fig. 5.3 shows the microstructure of the copper disc from Hornstaad on the shore of Lake Constance in Southern Germany. The disc is one of the earliest finds in Central Europe and is dated to the

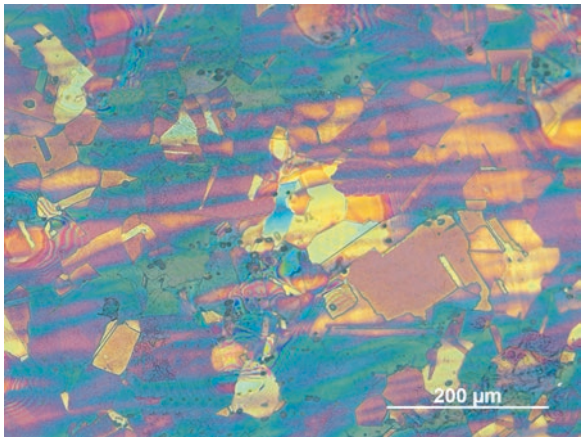

Fig. 5.3 Banding due to segregation in the microstructure of the Hornstaad copper disc is visualized by etching with Klemm's reagent II and viewed with bright-field illumination

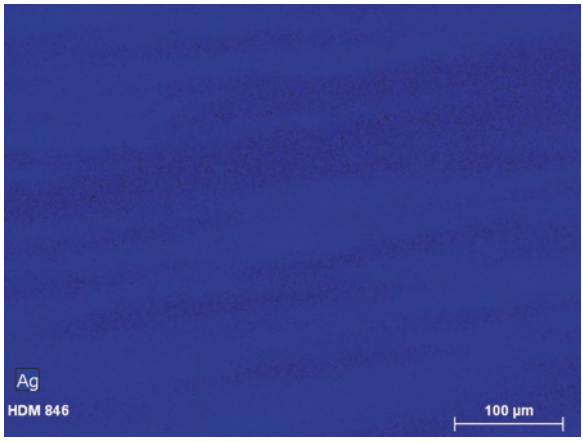

Fig. 5.4 EDX dot map of the silver distribution of a selected area in the microstructure of the Hornstaad disc establishes silver segregation

beginning of the fourth millennium BC. It contains several hundreds of mg/kg of arsenic and antimony, but 1.22% of silver [73]. In Chap. 3 the cuprite inclusions are illustrated (Fig. 3.16), while the segregation of silver becomes plain by colour etching and EDX element map (Figs. 5.3 and 5.4).

The use of native copper was common in the New World, especially in the period known as the Old Copper Culture of North America, which lasted from about 3000–1000 BC and produced ornaments and axes of native copper. Examination shows that New World metalworkers had discovered how to work and anneal copper, in much the same way as in the Old World. The Hopewell Culture of Mound City, Ohio, is one of the best-known examples of these traditions. Because native copper was especially plentiful in the New World, it was still being used during the Christian era by the indigenous peoples of North America and Alaska from the time of the Spanish conquest of the Americas in the fifteenth century onward (see Ehrhardt [53]). Iron and unalloyed copper were the only two metals used in southern Africa

before 1100 AD. Copper was used for much decorative metalwork, while iron was used for spears, axes, hoes and knives [77].

As explained above and in Chap. 2, man had discovered how to reduce copper ores to metal in the Neolithic Period, and the extractive metallurgy of copper was rapidly developed to smelt even complex ores. Pyrometallurgically produced copper contains several accidental impurities, which are primarily related to the mineralization of the ores. Other metals such as antimony, arsenic, nickel, silver and many others may replace the copper content in several minerals, and some of them can be absorbed by the copper during the smelting process. The amount of impurities is affected by several factors such as ore dressing, roasting, smelting and refining technology. The loss of volatile elements seems not to be such an impact, but temperature, oxidizing or reducing conditions in the furnace and most of all the distribution behaviour of the accompanying elements are important. All impurities have a significant influence on the microstructure and properties of copper, but their effects are quite different due to their distinctive solubility and constitution. These effects, of course, depend on the amount of an element, but the impact on the properties of an alloy is quite different, as an element is solved in the α_{Cu}-solid solution such as nickel or precipitated as a separated phase which occurs with lead or bismuth, forms intermediate compounds as in the case of arsenic or antimony or converted to a non-metallic compound which occurs as inclusions such as those formed by iron or selenium (see Chap. 4). Some minor elements of copper often exceed a specific value in ancient copper alloys, which involves drastic property alteration of copper such as colour, strength, hardness, castability, recrystallization temperatures and more. They were deliberately used in ancient times and will be discussed in the following chapters.

Apart from some exceptional cases, such as Iron Age copper ingots from Italy (Sect. 4.4), copper-iron alloys have not been of great value in ancient times, because the solubility of iron is very limited in copper alloys and iron gets easily oxidized. Small amounts of iron have little effect on the mechanical properties of copper but raise the annealing temperature. It is generally accepted that the iron content of ancient copper alloys indicates higher temperatures and stronger reducing conditions, so that the increases in iron content in copper may be linked to successive stages of technological innovation ([35], pp. 138–139; [71], p. 208). Indeed the maximum solid solubility of iron in pure copper is only 0.14 wt % ([47], p. 4), and when the amount of iron present exceeds this limit, metallic iron precipitates out as fine dendritic or rounded masses from the solution. The highly reducing conditions in the furnaces were capable of reducing iron-bearing minerals such as chalcopyrite ($CuFeS_2$) to metallic iron. Former copper-iron phase diagrams show that there would be a high solubility of iron in molten copper [39], but by the presence of carbon of up to 0.02%, a miscibility gap appears, forming two immiscible liquid phases [169]. Carbides should be regularly present in iron inclusions due to the reducing furnace conditions, and so the liquid phase separation should promote the oxidation of the iron-rich phase. Therefore iron precipitations in copper are often of cast iron [28, 39].

Figure 5.5 shows the microstructure of a Late Bronze Age oxhide ingot from Bulgaria, which consists of quite large grains (N_L = 170 µm) of α_{Cu}-solid solution

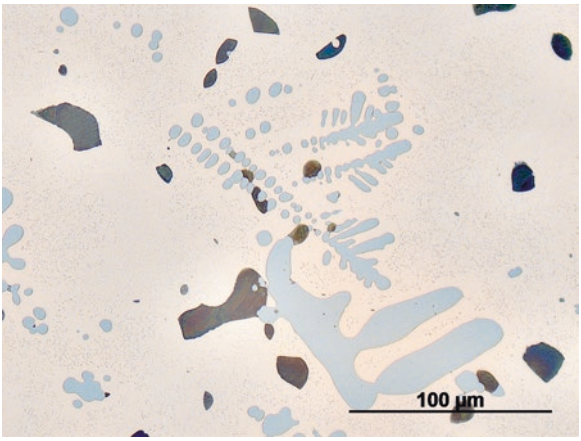

Fig. 5.5 Matte inclusions (mean $V_V = 3.2\%$), coarse dendritic and finely dispersed metallic iron in the microstructure of an oxhide ingot from Varna, Bulgaria

(88 HV 1 ± 5) with a very high volume fraction ($V_V = 9.5\%$) of coarse dendritic and finely dispersed metallic iron. The iron dendrites are locally segregated and partly converted to Fe_2O_3 at the surface. Precipitations of metallic iron are also present in the Bronze Age plano-convex raw copper ingot shown in Fig. 4.28 (Chap. 4) and many others.

The presence of metallic iron clearly indicates the strong reducing atmospheres during copper smelting, but the remelting of the copper under oxidizing conditions would have converted all iron to oxide. Several experiments have shown that the iron can easily be removed by remelting under highly oxidizing conditions, skimming off the oxidized dross, taking most of the iron with it [39]. Iron is indeed still present in black copper in the form of matte inclusions, which usually show volume fractions of several percentages (see Sect. 4.4). Refined copper can still have a substantial amount of iron content in the form of iron-bearing sulphide inclusions. Therefore the major content of iron of ancient copper alloys measured by bulk analysis usually represents the iron content of the non-metallic inclusions, so that the iron content is correlated to the volume fractions of the non-metallic inclusions [91]. Hauptmann [71] reports that the level of iron concentrations in Faynan copper, from the Bronze Age of Jordan, can be as low as 0.001% up to 76%.

Metallographic studies showed that some of the iron content was due to inclusions of copper-rich ferrite (α_{Fe}) as well as iron phosphides. Iron phosphides in copper are not common, but they occur in all periods in Faynan copper from Jordan and are characteristic of this region and can be explained by phosphorus-bearing ores, and by charcoal, which in the Arabah may include up to 10% phosphorus as the pentoxide in the ash [71]. The system copper-iron-phosphorus-oxygen is discussed further by Hauptmann [71]; one point of interest is the discovery of a eutectic intergrowth of iron with iron phosphide (Fe_3P). In the later Mameluk period, Hauptmann [71] found two-phased copper-iron alloys, one with more than 50% iron, where iron is precipitated in the copper and copper is precipitated in the iron. The intentional addition of iron to copper might have started during the Renaissance period, but not

earlier. For example, the foundry of the Vischer family in Nürnberg, which was active in the fifteenth and sixteenth centuries and created numerous large sculptures, regularly used brass alloys with several percentages of iron [142]. There are no microstructures available from these sculptures, but we can assume that the iron has been deliberately added, because the concentrations are consistent and that it is present as metallic precipitations. Because of the presence of alpha-phase iron as ferrite, the copper alloys containing iron are often ferromagnetic and can be picked up or attracted with a magnet, which has long been known for some ancient coinage alloys (see Zwicker et al. [200], pp. 408–11).

5.1.1.2 Arsenical and Antimonial Copper

Before the appearance of tin bronze, arsenical copper alloys have been used systematically in Europe, Asia and America for many centuries [23, 86, 111]. There is still debate over whether they were deliberately produced from the smelting of copper ores with added arsenic minerals or whether they began as accidental arsenical impurities in copper ores themselves (see Hauptmann [71] for references). Probably both explanations are correct in different times and places. The deliberate or accidental smelting of copper ores with arsenates resulted in the first primitive versions of copper-arsenic alloys with golden colour and good hardening properties; some of these early alloys were perhaps derived from the smelting of mixed copper-arsenic minerals such as olivenite ($Cu_2(AsO_4)(OH)$), or clinoclase ($Cu_3(AsO_4)(OH)_3$), or others (see Charles [23]; Rapp [136]). The gossan, the weathered cap of copper mineral deposits, may be leached by weathering and enriched in arsenic and sometimes antimony as well. The extraction of copper from these kinds of deposits and the smelting of them naturally result in the production of copper-arsenic alloys. Arsenic-bearing copper sulphide inclusions within objects from the Chalcolithic Nahal Mishmar hoard (Sect. 4.4) show that sulphidic minerals such as enargite (Cu_3AsS_4) or tennantite (Cu_3AsS_3) have also been used ab initio (see Charles [23]). The benefits of arsenic to the properties of copper have been described by Northover [111], Lechtman [86] as well as many other writers. The atomic diameter size of arsenic differs by 2% from copper and according to the phase diagram, shown in Fig. 5.6; the limit of solid solution of arsenic in copper is 7.9%.

Between 7.9% and 20.8% of arsenic, a second phase, gamma, forms which is an ordered phase of composition Cu_3As with 28.2% arsenic. The alloys tend to be heavily segregated as a result of the wide and steep incline in the liquidus and the distance of separation between the liquidus and solidus in the region of the α_{Cu}-phase. As solidification in this system is heavily segregated, the formation of the gamma phase will accompany the alpha phase as eutectic ($\alpha_{Cu} + \gamma$) infill in cast ingots with as low as 2% arsenic [96, 111]. Many alloy microstructures with lower arsenic contents are characterized by the presence of primary dendrites of the alpha phase, with an infill of the ($\alpha_{Cu} + \gamma$) eutectic (Fig. 5.7).

Since the alloys tend to be heavily cored from the cast state, the eutectic may be somewhat divorced and appear as principally gamma phase precipitates surrounded by

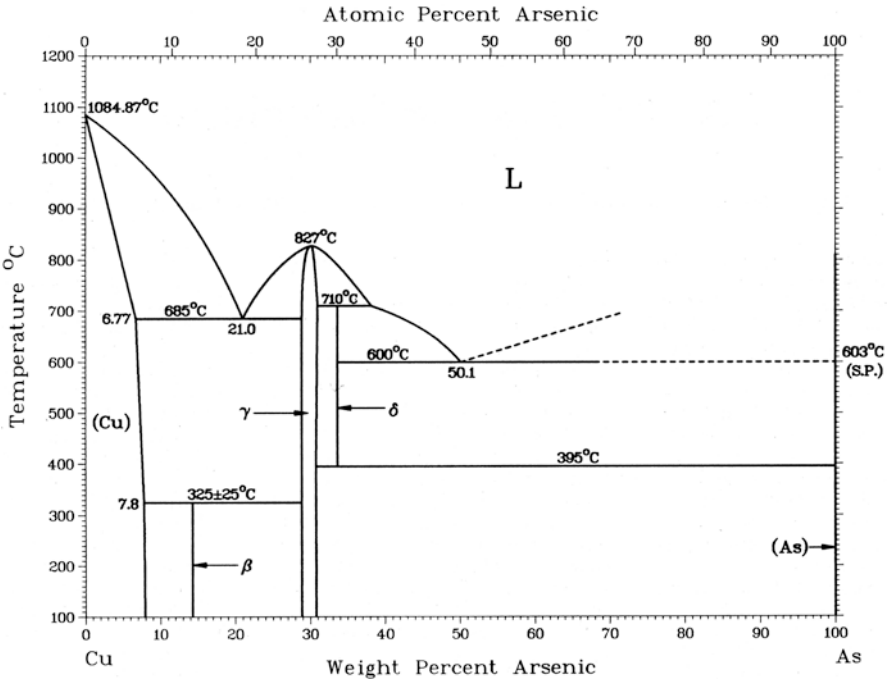

Fig. 5.6 Copper-arsenic phase diagram. Note the presence of an ordered, gamma phase at 30% arsenic; the presence of a beta phase, at about 15% arsenic; and the steep slope of the liquidus curve which results in heavily segregated castings. (After Massalski [94])

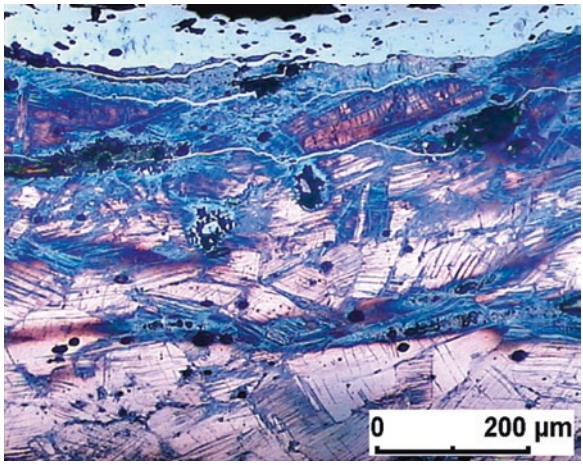

Fig. 5.7 Slip lines, arsenic segregation of residual dendrites, arsenic-bearing copper oxide inclusions and silver-coloured cubic γ-phase ($Cu_{3-x}As$) on the surface of an Eneolithic dagger from the cemetery of Singen, Germany. The inhomogeneity is also reflected by large variations in the microhardness between 120 and 200 HV 0.1. Etched with acid ferric chloride

cored alpha grains or dendrites. Fig. 5.8 shows a heavily worked copper-arsenic alloy sheet from the site of Mozan in Syria. The fingers of the dendritic segregation can be seen passing through the heavily worked sheet fragment, superimposed on the strain lines as a result of heavy working to shape with cold-working being the final stage.

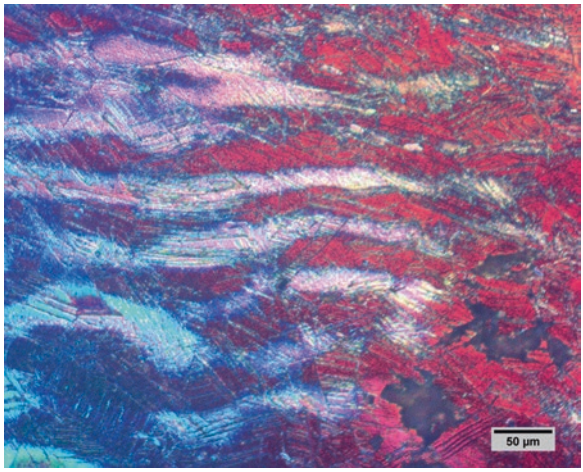

Fig. 5.8 Copper-arsenic alloy from the site of Mozan, Syria, with about 2–4% arsenic. Alloy shows interesting casting segregation in waves of areas with higher arsenic concentration, still present in the worked and annealed small fragment. Note the heavily deformed strain lines from cold-working of this artefact. Colour etched in Klemm's reagent and viewed under polarized light

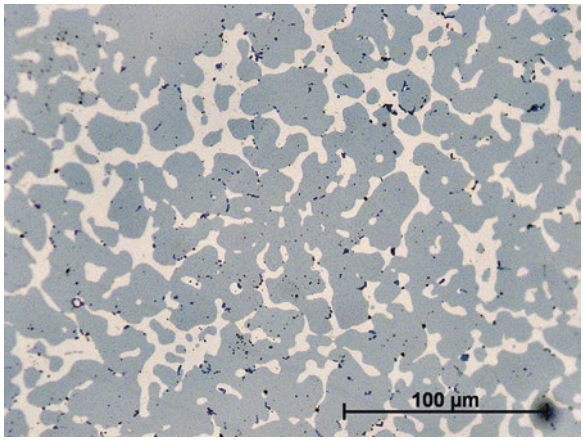

Fig. 5.9 Dendrites of tin-bearing α_{Cu}-solid solution (170 HV 0.1) and finely dispersed interdendritic α_{Cu}-Cu_3As eutectic (150 HV 0.1) in the microstructure of the silver-coloured arsenic-rich part of the Lori-Berd bracelet, Armenia, viewed under bright-field illumination. The same area is shown in Fig. 3.19 viewed under polarized light

Inverse segregation forms a silver-coloured layer of γ-compound (see Sect. 4.3). These ordered phases have essentially no ductility, so if the arsenic content of copper-arsenic alloys becomes too high (circa 13%), then they may crack badly on hammering. The majority of arsenical copper alloys in Europe and South America have less than five percentage arsenic and were used for tools and primarily for weapons due to their good mechanical properties. Some Carthaginian coins dating in the mid third century BC contain up to 12.2% arsenic, which formed silver coloured layers on the surface [81]. Indeed high-arsenical copper alloys with up to 23% of arsenic have been used to produce silver-coloured bells in Mexican metallurgy [74], and higher arsenic contents with up to 28% of arsenic have been deliberately used in the Caucasus region [98, 138].

Figure 5.9 shows the microstructure of the arsenic-rich part of a bracelet from the Royal tomb of Lori-Berd in Armenia, dated to the twelfth century BC (see also Fig. 3.19). This bracelet is one of several bimetallic objects within the tomb, which is

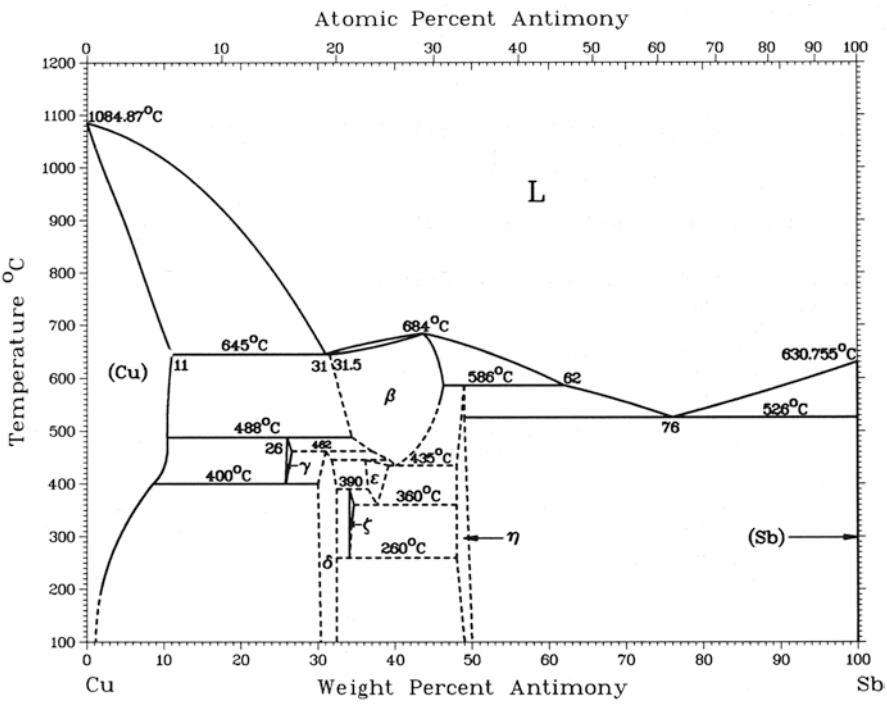

Fig. 5.10 The copper-antimony equilibrium diagram. (After Massalski [94])

deliberately made of a classical binary tin bronze with 9% tin (see Figs. 3.11 and 3.25) and a quaternary lead-bearing hypereutectic arsenical copper with 27.6% arsenic and 1% of tin. This small tin content is quite essential; as it primarily shows the deliberate alloying of tin with arsenical copper and as a synergistic effect, the solid solubility limits in the ternary Cu-As-Sn system are extended by tin to a composition approximately 2% richer in arsenic [14]. The Caucasian as well as Mexican metalworkers used these highly fluid high-arsenical alloys to produce gold- and silver-coloured bimetallic objects.

Some arsenical copper alloys also contain antimony as a minor, sometimes as the major, component (e.g. [71, 170]). The copper-antimony equilibrium diagram (Fig. 5.10) shows a sharp decrease in solubility of antimony in the alpha solid solution below 400 °C eutectoid temperature. The solid solution should lose some alpha to form an alpha + epsilon phase at full equilibrium, which is not obtained in ancient alloys, but some intermediate phases may occur.

Copper-antimony alloys were less common than arsenical copper, but antimony-bearing alloys were used in many different regions of the world during several periods. Their appearance is much more sporadic but also significant for specific periods and regions. The extent to which antimony was used in different cultures is still not fully accounted for. For example, Scott [158] reported on the presence of copper-tin-antimony alloys used for a La Aguada-style plaque from South America. Several

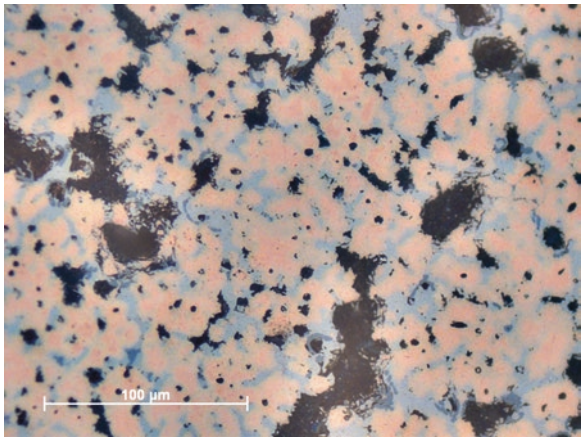

Fig. 5.11 Ring from the oppidum of Manching, Germany, containing 7.8% Sb, 2.0% Sn and 25% Pb showing shrinkage cavities fulfilled with lead. Mean hardness is only 79 HV 1, but intermetallic compounds (Cu_4Sb) and non-metallic inclusions (Cu_2S) bias microhardness (92 HV 0.1)

copper-antimony alloys are known from Hungary [46], Switzerland [113] and Germany, belonging to the Late Bronze Age culture of Europe [150]. Celtic tribes have practised a more deliberate and serial use of high antimony-bearing copper alloys during the La Tène period, the European Late Iron Age. During the first century BC, bronzes with up to 10% of antimony came into use, and lead isotope study shows that they were fabricated from mixed high-leaded Roman Republican bronze scrap with additions of local antimony-bearing fahlore copper to produce coins, rouelles, mirrors and different kinds of rings, parallel to or instead of silver-coloured high-tin cast alloys [150, 151]. According to their compositions, these antimony bronzes form a variety of intermetallic compounds, and their microstructure is characterized by segregation and shrinking, shown in Fig. 5.11.

When antimony is only a minor component, the intermetallic compounds are still stoichiometrically related to $Cu_{41}Sn_{11}$, in which a part of the tin is replaced by antimony, and to $Cu_{4.5}Sb$, where part of the antimony is replaced by tin when tin is a minor component. When tin and antimony are both major components, a ternary phase $Cu_{76}Sn_{12}Sb_{12}$ appears which is a requirement for the ternary system to be in the homogeneous range between $Cu_{76}Sn_{18}Sb_6$ and $Cu_{78}Sn_8Sb_{14}$ [20]. As Northover [112] has already pointed out, these compounds are much more complex than they appear as modelled by the ternary system, as they are also modified by arsenic, silver and especially nickel impurities. Some early Roman life-sized statues from the Germanic provinces show a significant percentage of antimony, and it has been suggested that scrap of Celtic origin could have been added in the early phase of occupation [194].

These alloys disappeared completely during the Roman Iron Age, but leaded antimonial bronze became popular again in Northern Europe for casting domestic vessels from the twelfth to the eighteenth century [51]. Antimony might have been an alternative to tin during times of deficiency. For example, a shortage of tin during the Second World War made antimonial bronzes attractive again ([18], p. 171).

5.1.1.3 Bronze

True alloys of copper with tin began to be made in the Old World from the fourth to the third millennium BC and were pervasive and universal during the Bronze Age, which gave it its name in prehistory. Bronze, in its traditional sense, is a binary alloy of copper and tin, whereas modern nomenclature includes all copper alloys, which do not have zinc or nickel as the major alloying element. Nevertheless, in a historical context, bronze is essentially an alloy of copper with tin. Bronze is one of the most employed alloys over the past 4000 years. Bronze rapidly replaced copper and copper-arsenic alloys in the Near East and the eastern Mediterranean during the late third millennium BC and probably in Southwest and Central Asia some centuries before [124]. Nevertheless arsenical copper was still favoured in some areas such as Egypt and Anatolia or in some cultures of the Central Andes [88, 104]. True bronze alloys with tin were made in the New World during the early centuries AD, much later than corresponding developments in the Old World. Tin bronze in the New World is especially associated with the Inca hegemony from the thirteenth to the fourteenth century AD, but some antecedents are found in regions where tin was plentiful, as in present-day Bolivia, Argentina and Chile. This alloy remained unknown in North America.

The advent of tin bronze still holds many mysteries as to its sources and the development of knowledge needed to mine and extract the tin and use it to alloy with different metals (Sect. 5.4). In many regions, tin ores were not readily available, and this suggests long-distance trade in tin, but nevertheless, bronze was produced in increasing regularity in most parts of the Old World (see Pigott [124]). Empirical knowledge soon led to the production of bronzes with about 5–10% of tin, as tin was the rarer commodity, and bronzes with over 14% of tin tend to be brittle because of the delta phase, so as a result alpha-phase bronzes or alpha phase with a small delta-phase component became common everywhere. In regions where tin was plentiful, such as ancient Thailand or southern India, specialized bronze production could be used to create high-tin bronzes, with about 21% tin, while in China, bronze mirrors were often made, in a variety of tin bronzes, usually leaded, with an ideal composition of about 25% tin, 5% lead and 70% copper, which has a good combination of silvery colour and high reflectivity. In the Islamic world bronzes are rare, as brass was the dominant alloy, but some high-tin alloys, described in Persian literature as safidruy, were nearly exclusively used for special items such as mirrors, vessels and dies [84, 97, 131].

The working and casting properties of bronze alloys led to the eponymously named Bronze Age, in which the alloy dominated both for cast ornaments and for worked and annealed sheet work, weapons and tools. The full-phase diagram is shown in Fig. 5.12 and under usual casting conditions in Fig. 5.13, where the epsilon phase does not really occur at all in normal tin bronzes. There is a large size difference of 15% between copper and tin, the melting point of tin is very much lower than copper, and tin is a body-centred tetragonal metal, unlike copper in terms of lattice size and shape, for which reason the solid solubility at room temperature should be very limited. In practice tin is a solute that has a reasonable high solubil-

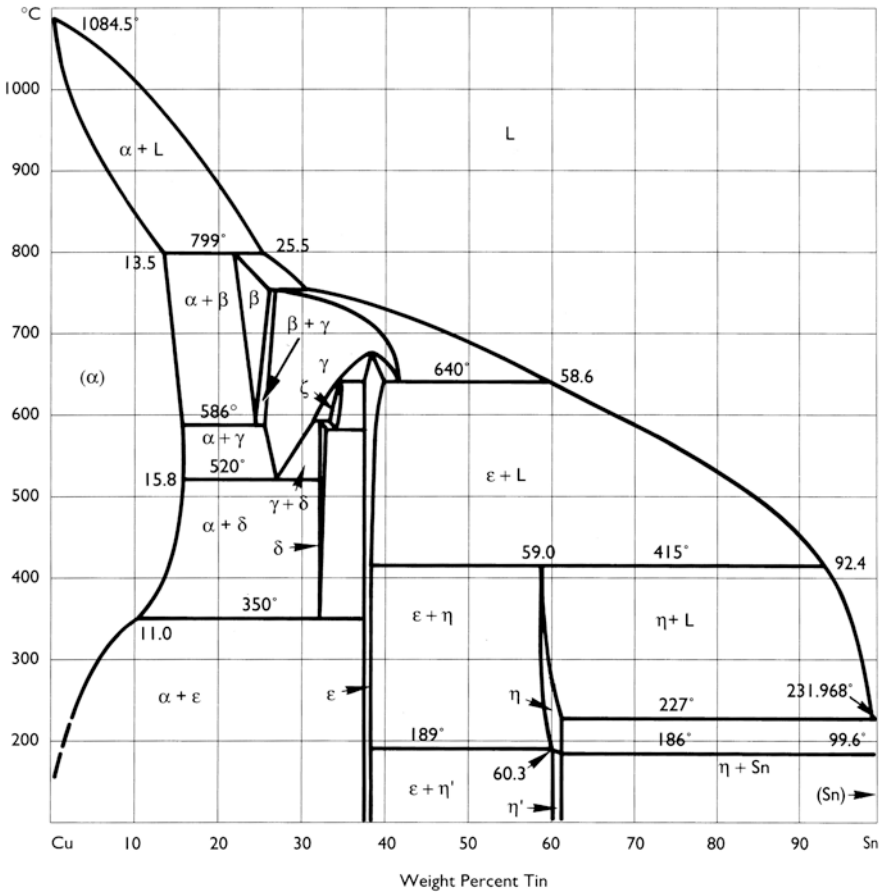

Fig. 5.12 The full copper-tin equilibrium diagram. The most important parts of the diagram for ancient metallurgy are those with less than 30% of tin and those with more than 90% of tin. The intermediate alloys, such as 50% tin and 50% copper, are rarely used. After Scott [154]

ity, and therefore the solid solution has a quite appropriate strength. The solid solution hardening of tin is more effective than that of the most other solutes.

Indeed the mismatch between copper and tin creates a variety of complexities in the phase diagram, and there are a series of intermediate phases (β, γ, δ, ε, ζ, η and η') causing problems for processing. In general, the bronze system can be divided into the low-tin bronzes, from 1 to 16% tin, and the high-tin bronzes from 16% to 30% tin. The α_{Cu}-solid solution (fcc) is stable up to 15.8% tin at temperatures between 520 and 586 °C and would decompose below that temperature into α + δ and then into α + ε under equilibrium conditions, except that full equilibrium in these bronzes is never reached and the alpha + delta phase survives instead.

Cold forged bronze mirrors, such as the so-called Etruscan mirrors, usually contain between 10% and 16% tin and are single-phased, because they were quenched

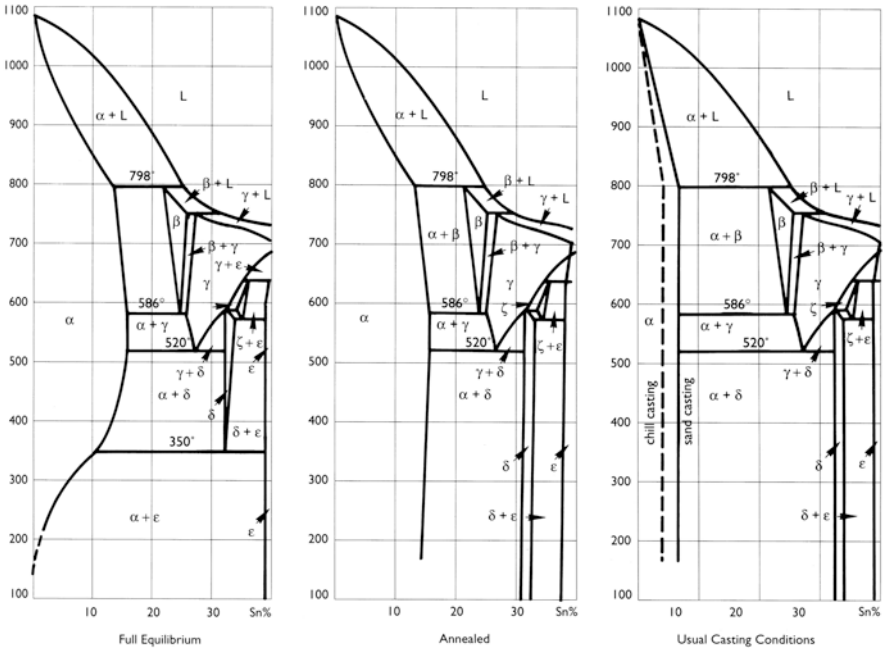

Fig. 5.13 Three versions of the copper-tin diagram up to 40% tin. After Hanson and Bell-Walpole [70] redrawn by Scott [154]. These diagrams are most useful in showing, firstly, full equilibrium, which is never practically attained, and then, in the centre, the fully annealed state of the alloys in which the epsilon phase does not appear and a wide alpha-phase region exists, and then on the right, under usual casting conditions, the field of alpha is restricted, being smaller in the chill castings, as opposed to the sand castings, and the field of the eutectoid alpha + delta is expanded as a result

to suppress eutectoid decomposition [62, 117, 168]. These mirrors show hardness values between 150 and 325 HK [117]. Cast high-tin bronze alloys with more than 20% of tin show hypo-, hyper- or eutectoid structure (Fig. 5.14) with regard to their tin contents and have been used in Europe and Asia to produce mirrors, coins and bells, whereas hot-working of high-tin bronze alloys was exclusively practised in the Near East and in Central and especially Southeast Asia, which has already been described in Sect. 4.6.1.2. Low tin bronze is difficult to hot work, as α_{Cu} is weak at elevated temperature and slightly hot plastic within a narrow temperature range.

The colour of these cast alloys turns to a pale silver-white or grey-white colour, and their hardness range is between 350 and 400 HV. They take a high polish, often survive in burial environments well and are brittle, so that if dropped they may shatter like glass.

In practice, equilibrium transformation to ε-phase is much too slow, taking thousands of hours of annealing, and α + δ eutectoid occurs in bronzes containing less than 10%, or even as little as 5%, depending on the size of the casting and the mould system. The mechanical properties of bronze alloys can be rationalized on the basis

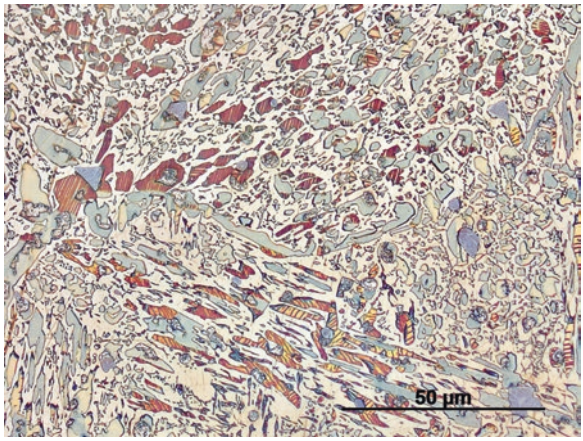

Fig. 5.14 High-tin bronze mirror with 27% tin and 5.5% Pb from Song Khoai, Vietnam. Etched with Klemm's reagent III

of the phases formed, and a useful comparison chart is shown in Fig. 5.15, which compares the bronzes with the hardness values obtained by steel in the quenched and air-cooled condition. The mechanical properties of binary tin bronzes are shown in Fig. 5.16.

Looking at the Brinell hardness (HB), which is roughly comparable with the more usual Vickers hardness (VH), the hardness rises rapidly from around 100 to reach 300 HB at 25% tin. A Brinell hardness of 300 is very hard and difficult to cut with a jeweller's saw in terms of sampling of such artefacts. On the other hand, the elongation falls away to nothing as soon as the delta phase begins to be an issue, between 5% and 10% tin in as-cast alloys. When the tin content increases above 5%, it becomes increasingly difficult to avoid the appearance of the delta phase, which has a high hardness and therefore undesirable properties. Many ancient cultures had arrived at the same conclusion empirically, and some palstaves or axes from Bronze Age Britain and elsewhere were annealed after casting to absorb most of the delta phase, even if 10% of tin is present (see Fig. 4.36).

Even small volume fractions of the delta phase can lead to the local embrittlement and consequently to crack formation during forging. Modern wrought bronze alloys contain between 5% and 8% of tin to keep them suitable for cold-working without homogenization and quenching. Indeed many prehistoric forged bronzes contain more than 10% of tin. The microstructure of bronzes with more than 16% of tin is already dominated by α + δ-eutectoid, and both the tensile strength and reduction in overall thickness are equally affected.

5.1.1.4 Brass

Brass is an alloy of copper with zinc, which has been used for thousands of years and which is one of the most common copper alloys until today. Nevertheless it has been a difficult story to unravel all of the occurrences of zinc and brass in different

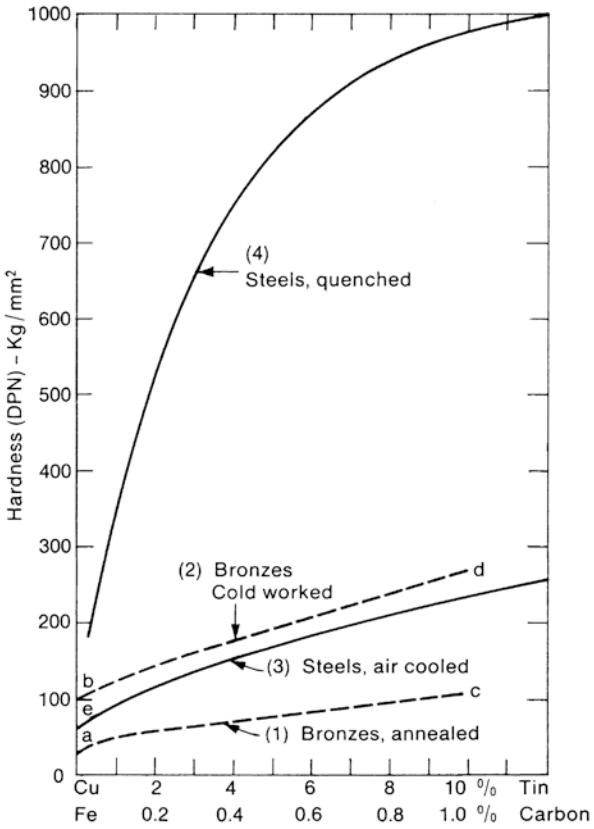

Fig. 5.15 Vickers hardness as a function of composition and treatment of tin bronze and steel. (From Smith [163])

cultures at different times. Craddock [35, 36, 43] has done much work on this topic, and the story is not yet finished. This difficulty is partially due to the fact that zinc production as a metallic element in its own right is hard to achieve by normal smelting activities, as zinc metal boils at a temperature (907 °C) below that needed for its extraction. Therefore ancient brass makers developed a direct reduction process in which zinc oxide or carbonate minerals, generalized under the name of calamine, together with metallic copper is heated in a closed container under strong reducing conditions, when the zinc vapour is absorbed by copper to form brass. It is generally assumed that it has been a solid-state process at lower temperatures, especially in the early phase of brass making, due to the small size and the poor refractory fabrics of the crucibles (e.g. Bayley and Rehren [8]). Several experimental replications and thermodynamic calculations of this procedure, which is called the cementation process or sometimes the calamine process, primarily dealt with the question if there is an upper limit of the amount of zinc that could be absorbed, and there has been a lot of debate about this. Actually some of these experiments and the conclusions drawn

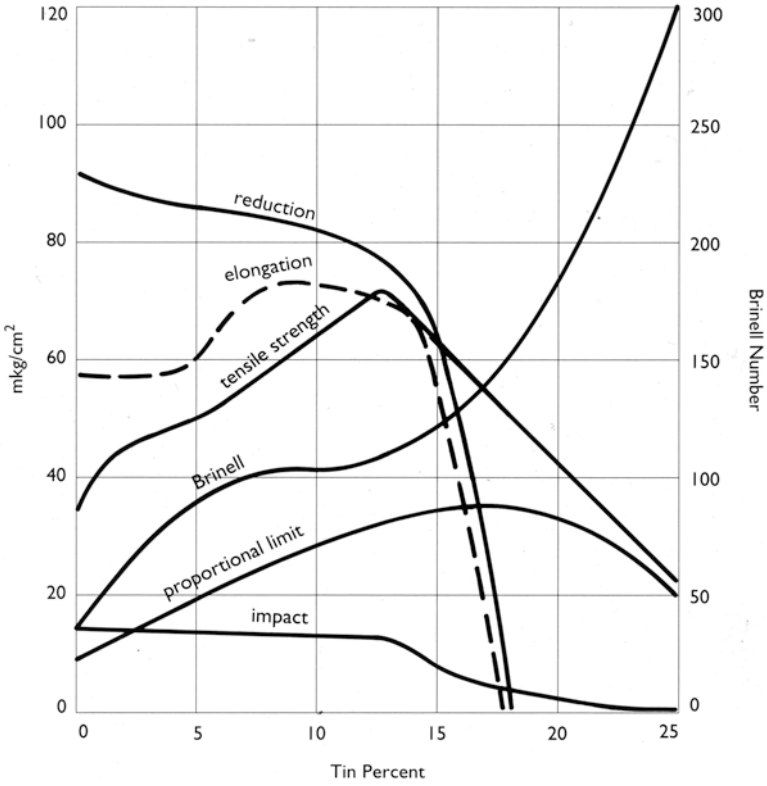

Fig. 5.16 Mechanical properties of copper-tin alloys. After Hanson and Bell-Walpole [70] redrawn by Scott [154]

are quite misleading and neglect the analytical evidence for the compositions and microstructures of ancient brass alloys, although the upper level of about 30% zinc is a commonly quoted limit.

The copper-zinc system is similar to the copper-tin system, but a more complicated one with some rather complex phase transformations with increasing zinc contents. Zinc is close-packed hexagonal (cph), but the atomic radius difference between zinc and copper is only 4%, which is why copper and zinc form a complete series of solid solutions with four intermetallic phases. The copper-zinc equilibrium diagram, shown in Fig. 5.17, possesses a large region in which the primary substitutional α_{Cu}-solid solution exists, where copper and zinc are mutually soluble in each other with a maximum of 39% by weight of zinc.

This is the region of the so-called single-phased alpha brasses, which accounts for most of the known occurrences in antiquity (Fig. 5.18). Single-phased alpha brasses are extremely ductile and malleable and exhibit good cold-working properties. Other than bronze, the tensile properties of α-brass increase with increasing zinc content, while it hardens less rapidly and is therefore suitable for complex hammering and casting work.

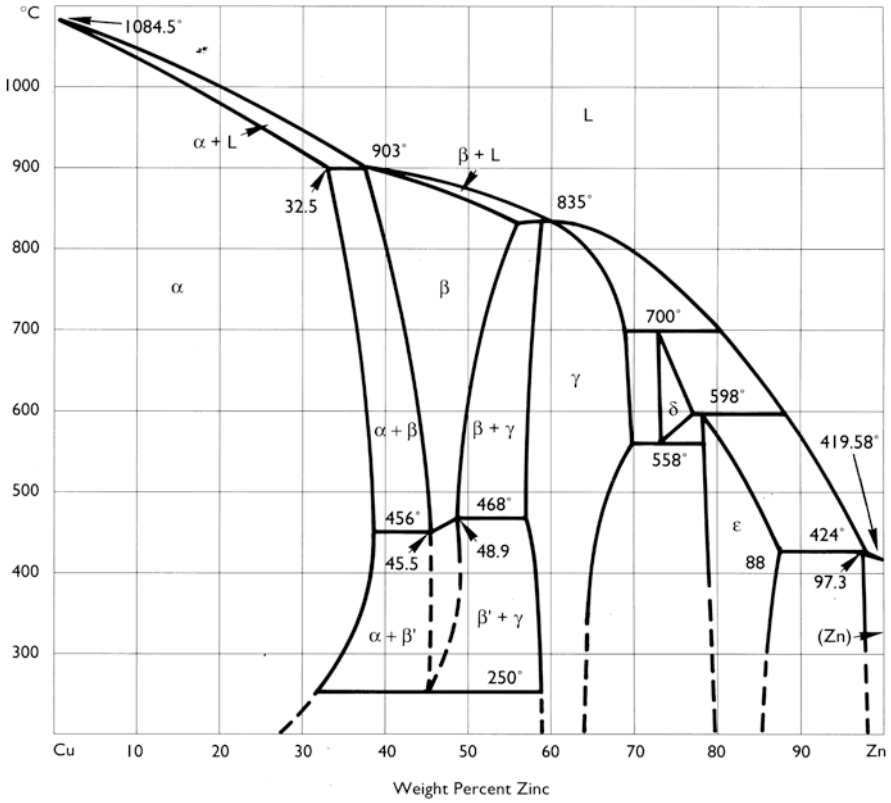

Fig. 5.17 The copper-zinc system. Most ancient alloys are single-phase alpha brasses, since the alpha phase can accommodate so much zinc. After Scott [154]

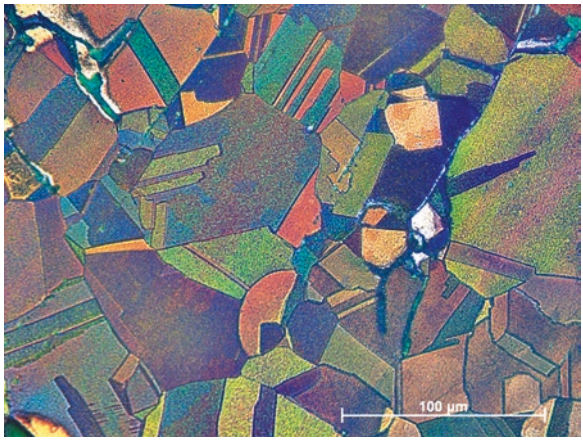

Fig. 5.18 Typical Roman brass alloy with 21% of zinc and a microhardness from 90 to 140 HV 0.1. The visor of a gladiator helmet from Herculaneum, Italy (first century AD), has been totally annealed at this position of the sample but reworked at others. Etched with ammonium persulfate and viewed with polarized light

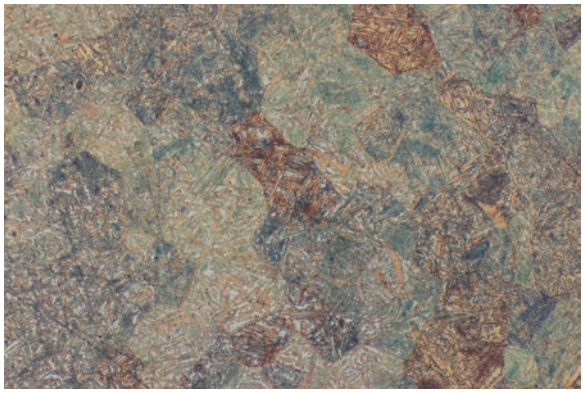

Fig. 5.19 A 60% copper and 40% zinc cast laboratory ingot showing the alpha + beta structure of these high-zinc cast alloys. The microstructure consisted of beta grains at high temperature, which then break down into grains of alpha + beta, outlined by the former beta grain boundaries. Colour etched, magnification x180

However, since zinc has a higher valence, as the zinc content rises, a second, more energetically stable phase forms after the saturation of the valence electrons in the face-centred cubic (fcc) α_{Cu}-solid solution. This takes the form of the body-centred cubic (bcc) β-phase. According to the phase diagram, the maximum solubility of zinc in the α_{Cu}-solid solution at 20 °C would be about 35% assuming equilibrium, but this is hard to obtain with traditional technologies. Therefore, brasses containing between 32% and 39% zinc often have a duplex structure of α- and β-phases (see Davis [47], p. 35), and nearly all additional elements shift the solid solubility of zinc in copper. It is very uncommon in ancient brasses to find alloys with more than 28% zinc content.

So-called yellow brass with more than 32% of zinc becomes increasingly difficult to cold-work, because of the relatively brittle β constituent, and is better hot-worked with increasing zinc content. The α/β-brasses are common in historic brass alloys as they have different colours and hardening properties than the α-brasses; typical compositions range from 30% to 45% of zinc (Fig. 5.19).

As zinc content increases, the β-phase is predominant, and beyond 50% of zinc, the complex body-centred cubic γ-phase appears which severely impacts the ductility and workability of the higher-zinc brasses. An alloy of 58% copper and 42% zinc is completely within the β field at high temperatures between 700 and 800 °C and becomes a mixture of α/β on cooling. This kind of alloy can also be worked hot as the beta phase is soft and malleable in this range of temperatures, and when cooled under different conditions and reheated to certain temperatures, a variety of microstructural textures are created.

The Mughal "Ayn-i-Akhbari" document of the sixteenth century distinguishes three qualities of brass, for which the first can be cold-worked, the second must be hot-worked and the third can only be cast ([1], p. 249–50). The cold-workable alloy must be α-brass, while the hot-worked must be two-phased α/β-yellow brass with more than 32% of zinc, which became frequently used in the Islamic world from the sixteenth century onwards and indicates the use of metallic zinc [108].

Haedecke [65] came to the conclusion on the basis of his calculations and his experiments that in the cementation process, a maximum content of only 31% (± 1) zinc at about 900 °C can be achieved, which actually corresponds quite well to the maximum solubility of zinc in the α_{Cu}-solid solution at 902 °C and most probably also at room temperature. Indeed numerous experiments have shown that up to 40% zinc and even more can be reached in this process (see Bourgarit and Thomas [13] for further references), but this general possibility is not reflected by the abundant analysis of ancient brass alloys, in which zinc levels rarely exceed 30%. Indeed, in the ancient world, any brass object purporting to be authentic comes under suspicion if the zinc content is greater than 30%.

Some incorrect analysis and the analysis of objects of uncertain origin or date have confused the situation considerably (see Craddock [35]). It is however a striking argument that with the advent of metallic zinc imports from Asia to Europe ([38], p. 63; [192], p. 34), brass objects with up to 36% of zinc emerge regularly in Europe from the end of the sixteenth century onwards, but not in earlier periods [130, 192]. Up to our present knowledge, metallic zinc has first been used for coins in India from the thirteenth century AD [42], and the first zinc production sites in China date to the fourteenth century [199]. Even when the industrial production of metallic zinc became possible in Europe in the middle of the eighteenth century, the cementation process remained the standard method for brass production until the beginning of the nineteenth century. As a two-step process, it even survived until the end of the nineteenth century. In this so-called "Arcoschmelzen" process, a brass alloy containing about 20% of zinc was produced by cementation that was further alloyed by the addition of metallic zinc [182].

Before the advent of metallic zinc, brass has been exclusively produced in the cementation process, which obviously limits the zinc content, but due to its highly reducing conditions, several impurities such as lead or arsenic and especially iron enter the alloy – from which only lead is usually visible in the microstructure – but with higher iron contents, small pools of iron can be seen. Craddock and his coworkers ([41], p. 78) have already pointed out that Islamic copper alloys contain less iron than contemporary European brasses, which could be due to sulphidic ore smelting, which were roasted to convert the sulphides to oxides before using them to produce brass by the cementation process. In contrast to tin, zinc increases the solubility of iron in copper, and as mentioned in Sect. 4.4, non-metallic inclusions within brass usually do not contain iron anymore but can contain manganese, and in modern forgeries, there may be manganese sulphides present.

Finds of a few very early brass pieces, like those recovered in Shaanxi and Shandong, Shaaxi province, dating to the fifth to the third millennia BC [55, 68] are an issue and might be questioned due to the reliability of their archaeological contexts.

The first zinc-bearing copper alloys appear in the Aegean, the Middle East and the Caucasus already from the third millennium BC [171], while in Western Europe, the first zinc-bearing copper alloys arrived only in the first millennium BC ([7], p. 9; [91]). In India also there are several examples of brasses from the first millennium BC contexts, but not as a regularly used alloy ([43], pp. 211–12). The first evidence

for a deliberate and regular brass production in Europe comes from the Hellenistic world at the beginning of the first century BC (see Craddock [35]). Following Roman times, brass has become the most widely used copper-base alloy in certain regions. In the medieval Islamic world, nearly all copper alloys contain zinc as a significant alloying element (Craddock et al. [41]), whereas in Southeast Asia, bronze has been preferred, and brasses do not carry authority before the fifteenth century [132, 181].

There might have been quite different reasons why brass has become the dominant alloy in some cultures, while bronzes were employed only for special objects as the highest in cost, but there are also some obvious technological advantages of brass such as excellent castability, good workability, strength and corrosion resistance, which make brass one of the most commonly used copper alloys until today. Those alloys are usually not binary copper-zinc alloys but also contain tin and lead due to their specific purposes or as a result of the re-use of scrap of diverse origin.

The addition of tin to brass modifies the phases known from the Cu-Zn equilibrium phase diagram and produces a microstructure with two or three phases at rather low tin concentrations [6]. The eutectoidally transformed γ-phase of the ternary system corresponds to the intermetallic δ-phase of bronzes. Wrought brass alloys, which are not produced by the addition of metallic zinc, known as speltering, typically have higher-zinc contents than casting alloys and do not contain significant lead or tin – usually much less than 1%. Therefore, all wrought alloys are single-phased, as such percentages of zinc and tin can dissolve in solid copper to form a solid solution. Typical quaternary cast alloys (Cu-Zn-Sn-Pb), which are traditionally called gunmetals or in a more modern nomenclature leaded red brasses, show eutectoid presence and lead particles besides in the α_{Cu}-solid solution. Such alloys were frequently used for cast items until today. A typical microstructure of this type is shown for an Islamic inkwell in Fig. 5.20.

5.1.1.5 Leaded Copper Alloys

Cast copper alloys are frequently leaded with lead contents of 5% or even much more. Lead additives improve the casting properties of copper alloys, since the viscosity of the melt is reduced and thus the mould filling capacity is increased. Due to its low melting point and its insolubility in copper, lead remains liquid until it freezes at 327 °C and thus is useful in the localized filing or smoothing the surface of cast artefacts. Lead linearly lowers the liquidus temperature, improves the fluidity of the alloy in the melt and increases the freezing range, which has the effect of making the alloys of copper easier to cast. The fluidity of the cast ternary alloy of copper, tin and lead is very good, and as it cools, the alloy takes a good replica of the surface of the mould with the high-tin varieties. Although lead does not alloy with copper (<0.02% Pb) as the alloy cools down, and the lead simply occurs as a series of globules or interdendritic solid particles, the alloys at high temperatures have very good casting characteristics which allow them to be molten between 800 and 900 °C.

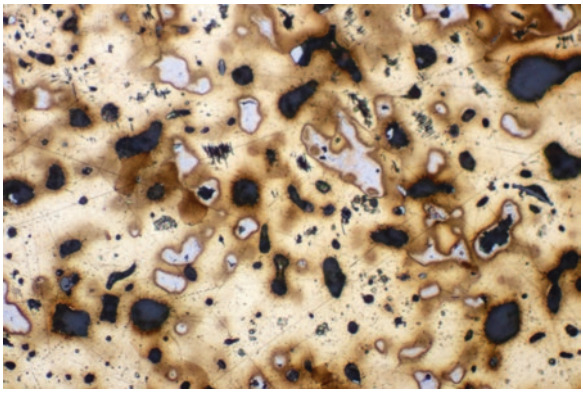

Fig. 5.20 Islamic inlaid inkwell from the eastern Iranian province of Khorasan. Probably made in Herat from the period of the late twelfth to the early thirteenth century AD. Composition 65% copper, 5% tin, 20% zinc and 10% lead. The alloy, although consisting of four major constituents, can be considered a ternary mix of copper, zinc and tin because the lead forms immiscible droplets visible in the section. The inner areas of each grain are richer in copper and the outer richer in zinc and tin. The prominent coring shows that the inkwell was not extensively worked or annealed following fabrication; however, some strain lines can be seen in the section suggesting some final working probably due to chasing of the surface to receive the inlaid metal strips. Note the light copper-tin-zinc phase occurs here, different in appearance from the copper-tin eutectoid. Etched in ferric chloride, magnification x180

European Late Bronze Age metallurgy is characterized by the advent of leaded bronze, but other regions such as China and Egypt also utilized the alloy from the middle of the second millennium BC [34]. Lead minerals do not usually occur with copper ores, so we would expect the lead content to usually represent a deliberate addition of lead. Indeed alloying practice with lead was regionally dependent, with some cultures using heavily leaded bronzes while low and random lead contents are common in others regions [34, 110]. Heavily leaded copper alloys with around 10% of lead or more appear only occasionally in many regions during the Late Bronze and Early Iron Age. In Southeastern Europe, heavily leaded axes and ingots with lead contents between 20% and 60% and lead ingots are known which clearly indicate the deliberate use of lead [146, 174, 175]. Lutz and Schwab [91] on the other hand have shown that the lead contents of the objects from the Early Iron Age hoard from Fliess (Austria), which are usually only between 0.1% and 2% lead, are correlated with other impurities coming from the copper ore. Therefore their lead contents might have been the result of smelting galena or other lead mineral-bearing copper ores under highly reducing conditions than alloying practice as such, and this may often be the case in copper alloys with only a trace amount of lead content.

Since the middle of the first millennium BC, cast copper alloys are frequently highly leaded, and lead became abundant due to the rise of silver extraction. During Roman times, heavily leaded bronzes became the rule, and life-sized statues with 20–30% or more are not unusual [194]. The equilibrium diagram and the monotec-

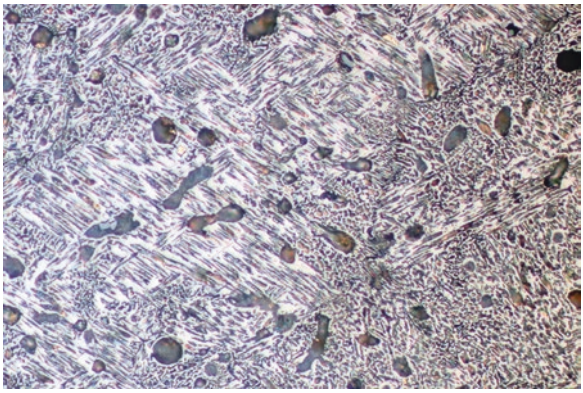

Fig. 5.21 Roman bronze mirror from Canterbury, showing an acicular, Widmanstätten patterning of the high-tin bronze, which is also leaded. Lead is present in the small globular particles, and the structure is of alpha + delta eutectoid phase with lead globules well-scattered. This helps with the polishing of such alloys and they make good mirrors. Composition 25% tin, 4% lead and 71% copper. Etched in ferric chloride, magnification x230

tic reaction have been described in Chap. 4, which show that the microstructure will consist of two distinct phases and that the copper matrix will contain globules of lead. Practically all of the copper will freeze before the lead-copper eutectic forms. This lead-copper eutectic is, for all practical purposes, pure lead, as it consists of 99.9% lead and 0.1% copper. This means that the lead is segregated while the solidification process is taking place. Ordinarily, the separation of lead globules would be expected to result in massive segregation, and an unusable material would result. However, in practice the gross segregation is limited by the formation of a dendritic structure upon casting in the copper-rich alloys, and, with a high cooling rate, the lead is finely dispersed among the copper grains or dendrites. With very high lead content alloys, the two liquids that separate out form an emulsion when they are cooled from about 1000 °C [92]. This emulsion results in a division into very fine droplets so that gross separation cannot occur. With leaded copper, brass or bronze alloys, the lead usually occurs as small, finely dispersed spherical globules scattered at the grain boundaries and within the grains themselves. If the cast alloy is kept in a heated mould, some of the lead may begin to undergo segregation, as the microstructure of the Roman mirror shown in Fig. 5.21 or discussed in Chap. 4 illustrates.

5.1.1.6 Cupronickel and Nickel Silvers

Cupronickel and nickel silvers are quite modern copper alloys, because nickel itself has not been known as a separate element before the eighteenth century, although some regions did produce copper-nickel alloys at an early date. Today the copper-nickel alloys are called cupronickels or nickel silvers, which usually are

copper-nickel-zinc alloys. They became popular during the nineteenth century for making cutlery, tableware, musical instruments, coins, etc., because of their pleasing silver colour, good corrosion resistance and moderate strength. Copper and nickel are soluble in each other over the entire compositional range. This means that, unlike copper-antimony or copper-iron alloys, the alloys are easily worked and very ductile. As copper and nickel are mutually soluble, there is no second phase present in this system, and therefore the alloy is more resistant to corrosion as there is no galvanic difference between phases in this system. If the grain size can be refined to produce small grains, then the alloy is ideal for the items mentioned before. At higher concentrations of nickel (ca. >10 wt. %), the metal is silver in colour, and the influence on the colour of alloys is one of the most evident effects of nickel. In addition to its colour, the metal has varying performance characteristics, including corrosion resistance, increased ductility, hardness and a higher tensile strength relative to unalloyed copper. The probably accidental impact of nickel to bronze during annealing has already been exemplified in Sect. 4.6. Some historical names such as "German silver" or "Argentan", or the German term "Neusilber", refer to their silver-imitating colour (see Ledebur [89]). Some languages use trade names such as Maillechort (after the producers Maillet and Chorier) and Alfénide (after the producer Alphen) in French or Alpaca (after an Austrian product called "Alpakka") in Spanish (see Ledebur [89]).

Nickel is usually a minor component in ancient copper alloys, but indeed, there are several nickel-bearing copper alloys known from the Near East, from Asia, from America and also from Europe. Hauptmann [71] illustrates a distribution map from the Near East with Early Bronze Age objects containing more than 1% of nickel and also more than 1% of arsenic, whereas nickel-bearing fahlore copper, so-called Singen copper, containing up to 7% of nickel is widely distributed in Europe during the Early Bronze Age (see Krause [79]).

Cupronickel with nickel contents up to 20% is known from Bactrian coinage dating to the second century BC in Central Asia [30, 193]. The Bactrian kings Agathocles and Pantaleon, along with their contemporary Euthydemus II, are unique in the ancient world, in that they were the first in the world to issue copper-nickel coins [193]. A much earlier but also regular use of cupronickel during the second millennium BC at the site of Boğazköy– the Late Bronze Age capital of the Hittite Empire known then as Hattuša – has recently been evidenced by Lehner and co-workers (forthcoming). Nickel-copper alloys with nickel contents up to 22% have been observed, showing intensive banding segregation which are chiefly due to the inhomogeneous distribution of nickel, cobalt and iron, which are also present in small but significant percentages (see Sect. 4.3). These nickel-rich alloys are obviously based on the smelting of chalcopyrite ores, which are interspersed with pentlandite ((Fe, Ni) $_9S_8$) and occasionally with some arsenopyrite. Scott [153] found that a Hittite seal was made in a copper-nickel alloy with cobalt and iron content, and a Hittite bronze bullhead was found to be made, in fact, in a copper-nickel alloy with about 21% nickel content.

Lechtman [87] describes bronze alloys of the Middle Horizon (MH, 600–1000 AD) of both Wari and Tiwanaku (Tiahuanacu) cultural sites in the Andean

cultural area, with particular attention to their elemental composition and site distribution. Alloys of copper-arsenic and copper-tin were in use until the Spanish entrada, but a ternary alloy of copper-arsenic-nickel was confined to the Middle Horizon period. Wari areas manufactured only arsenic bronze alloys in the Middle Horizon. In the area dominated by Tiwanaku, two alloys were used simultaneously, the ternary alloy of copper-arsenic-nickel and copper-tin bronze. There is no evidence of the use of the ternary alloy following the collapse of Tiwanaku. It is interesting that the same type of copper-arsenic-nickel alloys should also have been reported by (Chen and co-workers [24]) from the remote frontiers of the Shang Kingdom (c. 1600 BC–c. 1046 BC): these are the Hanzhong bronzes from southwest Shaanxi, China. More than 200 bronze objects found in Hanzhong, during the Shang Dynasty, were analysed for their composition and microstructure. Forty-three typologically distinct, and probably culturally indigenous, items were found to be compositionally distinctive as well. Three special alloys, arsenic bronze, antimonial bronze and copper-nickel-arsenic ternary alloys, were found to have been utilized.

A deliberate nickel-alloyed copper was first used in China, called paktong for white copper. The name can alter between packfong and baitong, depending on the pronunciation in different Chinese dialects [76, 89]. It has been produced by a two- or three-stage process, in which copper ores such as chalcopyrite have been co-smelted with pentlandite obtaining a copper-nickel matte, and after removal of the sulphur, the cupronickel crude metal has been alloyed with other metals such as zinc [76]. Typical paktong alloys contain between 5% and 20% of nickel and 20% and 50% of zinc and were known in East Asia since the fourth century AD but became very popular in Europe during the eighteenth century (see Gilmour and Worrall [60]; Jianjun [76]; Ledebur [89]). Fig. 5.22 shows the microstructure of a hammered

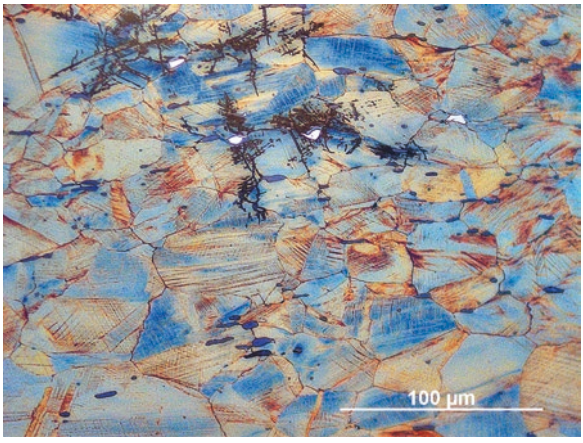

Fig. 5.22 Microstructure of a Chinese paktong alloy from the collection of the Reiss Engelhorn Museum in Mannheim, Germany, without secure date. Cold-work and annealing are obvious by elongated sulphide inclusions ($V_V = 0.8\%$) and lead particles, slip lines passing through annealing twins and precipitations of Cu_2NiZn (mean microhardness 162 HV 0.1 ± 20). Etched with Klemm's reagent III and viewed in bright-field illumination

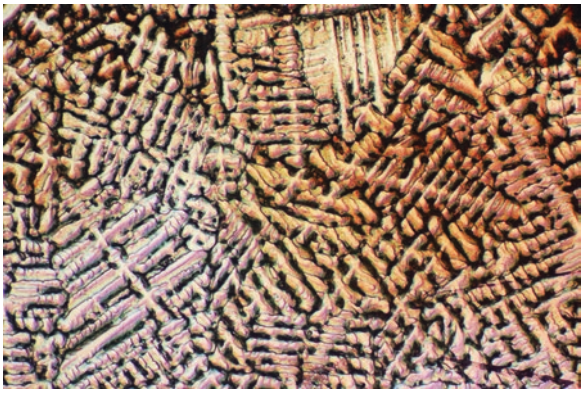

Fig. 5.23 Historic paktong alloy, showing probable delta phase between the dendrites, while the dendrites themselves appear as two different phases, probably a copper-nickel-tin-rich phase as the whiter component and a yellow phase which is probably copper-zinc-tin with a higher-zinc content. Etched in ferric chloride, magnification x 120

Chinese vase made of a paktong alloy with 11% nickel and 29% zinc. Here again the precipitations of intermetallics due to ageing during cold-working and annealing become obvious. Fig. 5.23 is a cast paktong alloy with 45% zinc and 7% nickel.

5.1.2 Lead, Silver and Their Alloys

In modern metallography and physical metallurgy handbooks, lead and silver are not discussed together anymore, because their properties, use and metallographic preparation procedures are different. Both metals are nowadays available in high purity, independent from each other, and they are not used for mutual alloys. In historical metallurgy silver is automatically strongly connected with lead, because they nearly always occur together and lead has been essential for the extraction of silver. Percy [120] has written in his preface to *Metallurgy of Lead* that the book was originally intended to contain the metallurgy of lead, silver and gold but had to be restricted it to the metallurgy of lead. However, he does describe the refining of silver by cupellation in detail. In the mid-nineteenth century, various wet leach processes were already developed, but the extraction of silver by cupellation remained common in Europe for economic reasons, whereas in the New World, silver extraction by amalgamation (patio process) had become more popular. The development of the cyanide process in the late nineteenth century has displaced all previously used processes for industrial application. Today low-grade and complex silver-bearing ores can be exploited by flotation and smelting.

The earliest silver artefacts were made during the fourth millennium BC and are found in the areas of Persia, Anatolia, Mesopotamia and Egypt [99]. Silver and gold both became trade commodities by the middle of the third millennium. In prehis-

toric Central Europe, silver is generally rare in archaeological contexts before the arrival of the Romans, whereas in the Aegean, for example, it is well represented from the third millennium BC onwards, and on the Iberian Peninsula, the use of silver began in the early second millennium BC. Lead isotope studies have shown that some lead-silver mines, which have been historically or archaeologically dated to younger periods, may have been known and exploited much earlier. An example is Nakhlak in Iran, which is dated by excavation to the Sassanid period and could already have been used as early as the fourth millennium BC [109]. The Athenian mines of Laurion and the mines on the Greek island of Sifnos, whose information has been passed down to us by Herodotus, have been worked from the first half of the third millennium [99] and finally the mines in the Montevecchio basin on the island of Sardinia. It was generally assumed that they were not mined before the Imperial Roman era, but recent research has shown that they were used during the fourth and third century BC [48].

Silver occurs as a native metal in small quantities, and the distribution of its minerals as minor component in the ore deposits of other metals is limited. The main sources of silver were, and still are, argentiferous lead or lead-zinc ores, respectively. Indeed Craddock [35] and Meyers [99] have already pointed out that the present-day situation might be quite misleading, as native silver and silver-rich layers such as the cementation zones of deposits, important to incipient silver metallurgy, were in relatively shallow depths and have long since been exhausted. The smelting of ores from gossan deposits and weathered polymetallic sulphides, in generalized form called argentiferous jarosites, is best documented for the Huelva province in southwestern Spain. The so-called El Argar culture is connected with an extensive use of silver in southeastern Iberia during the Bronze Age, and compositional analyses of objects reveal that most probably native silver or silver chlorides (mainly cerargyrite) were used as resources [5].

It is generally believed that silver metallurgy derived from lead smelting technology, being extracted from cerussite ($PbCO_3$) and mostly galena (PbS), using the so-called cupellation process. The extraction of silver from its ores by cupellation is generally a two-step process, which is based on a monotectic reaction (see Chap. 4) and the easy and quick oxidation of lead, compared to silver. The first step can be a simple subsidiary process of ordinary lead smelting, or a deliberate process when the ores do not contain sufficient lead, and lead or lead ores must be added. The Ag-Pb-system is basically an eutectic type, but one in which the eutectic composition occurs very close to the lead and with a very restricted solubility for each other in the solid state, shown in Fig. 5.24.

Liquid silver and liquid lead are completely soluble in each other, but in an analogous manner to the copper-lead system (Chap. 4), practically all of the silver will solidify before the lead-silver eutectic forms and primary dendrites of silver will be embedded in the lead. Due to the high solubility in the liquid state, lead is an excellent collector of silver, and also of other precious metals, and most of the silver in the ore passes into the lead reduced. To extract the silver from the lead, the lead-silver metal has to be fed to a special furnace, the cupellation hearth, where it is melted again at a high temperature of between 960 and 1000 °C, and air is blown

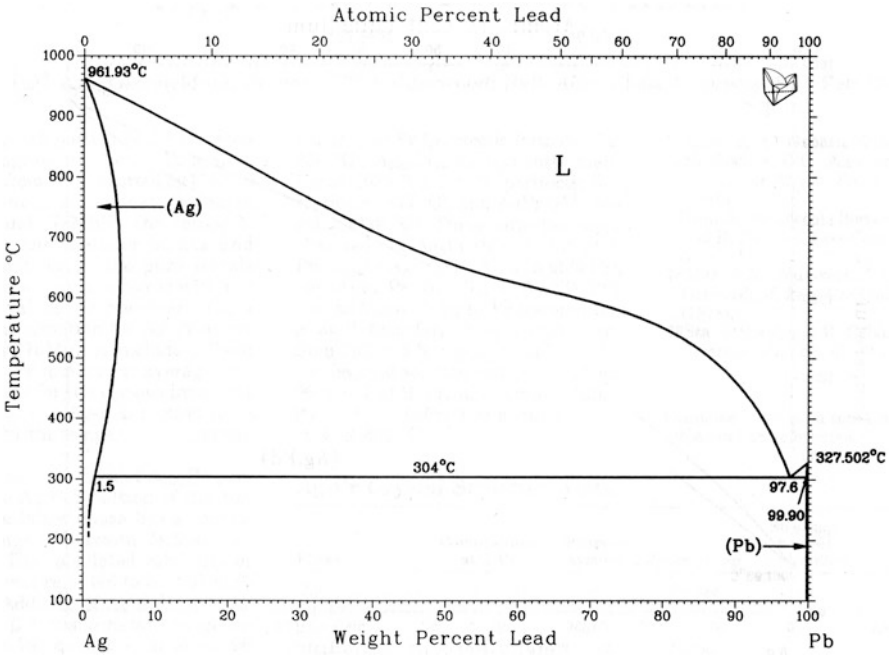

Fig. 5.24 Ag-Pb constitutional diagram. (From Massalski [94])

over the surface of the melt to form litharge (PbO), which must be continuously skimmed. The high temperature is required to keep the litharge molten to discharge it and finally to melt the remaining silver. Silver is not oxidized by air and it is insoluble in litharge. Litharge is a highly oxidizing agent which is capable of converting various metals into oxides and will dissolve them. Liquid litharge is also a corrosive substance which reacts rapidly with silicates, for which reason linings of hearths were made of a mixture of lime, clay and bone ash, while assaying vessels, the so-called cupels, which give the process its name, were often made of pure bone ash [9]. Litharge does not occur in nature, and pieces of discarded litharge from Syria and Eastern Anatolia provide evidence for silver production by cupellation in the fourth millennium BC [99, 109].

Litharge cakes could have been reduced to metallic lead or directly salvaged for further silver extraction. Silver ores, like the ores from the famous Rio Tinto mines in southwest Spain, which do not contain enough lead themselves had to be leaded additionally to extract the silver. Indigenous Iberian people, the Phoenicians, Carthaginians and Romans worked the so-called argentiferous jarosite deposits there whose silver content could be as high as 1000 ppm, but most would be lost on smelting unless lead or lead ore was added, which soaks up the silver. The lead had to be brought some distance to Rio Tinto and imported especially for silver extraction, and lead isotope studies of silver smelting debris such as slag, litharge and lead

from Huelva have been shown to have variable lead isotope ratios matching different Spanish ores ([40], p. 211; [75], pp. 391–395; [2], p. 275; [106], p. 88).

A version of the smelting of argentiferous lead is given by Pliny (Natural History, Volume IX, Book XXXIV, 159): "…there are two different sources of black lead, as it is called, either found in a vein of its own and produces no other substance mixed with it, or it forms together with silver, and is smelted with the two veins mixed together (this mixture is galena). Of this substance the liquid that melts first in the furnace is called stagnum (or stannum, an alloy of silver and lead), the second liquid is argentiferous lead, and the residue left in the furnaces is impure lead which forms a third part of the vein originally put in; when this is again fused it gives black lead, having lost two-ninths in bulk".

In prehistoric up to pre-industrial times, metallic lead itself has nearly always been a by-product of silver smelting or was predominantly smelted for the extraction of silver. Pure lead has an extraordinary low hardness of 4 HV and recrystallizes rapidly at atmospheric temperature. Therefore it cannot be hardened by plastic deformation nor polished, which the latter would also be useless, as lead instantly oxidizes and tarnishes when exposed to the atmosphere. These are the reasons why metallic lead was quite unsuitable for ornaments, in contrast to galena, which is polishable because of its much higher hardness between 50 and 60 HB (Sperl [166], 801). The false labelling of lead minerals as "metals" and the relative easy extraction from its ores have given rise to the assumption that lead could have been one of the first metals to be smelted, as mentioned already in Chap. 2. The practical applications of lead and lead alloys in ancient times have been relatively minor compared to other metals. Ancient lead has widely been used for marine purposes due to its high resistance to corrosion in sea water, for solders, seals and badges due to its low melting point and softness, and often simply as weights and as a filling material, because of its gravity, cheapness and high abundance. Lead sling bullets, which have been used from the Aegean Bronze Age, might be a symbol for the disposition to waste this metal. In Roman times, the demand for lead increased considerably, and several thousands of lead ingots, mostly coming from ancient shipwrecks, with tonnes of lead on a single cargo, have been found (see Parker [119]; Rothenhöfer and Hanel [145]).

Figure 5.25 shows the microstructure of a Roman lead water pipe from Petra in Jordan, which has a wall thickness of nearly two centimetres. The complete length of some of these pipes used all over the Roman world would conform to the Roman standard of 10 pedes (296 cm) and have a total weight of nearly 200 kg [58]. With post-medieval letterpress technology, antimony and tin-alloyed printing types came into use (see Berger [11]). Antimony significantly hardens lead and makes it more resistant to compression; however, these alloys tend to become brittle above the eutectic composition of 11% antimony (see Ashtakala et al. [3]), but the addition of tin makes it tougher. The specimen preparation of lead and lead alloys by mechanical methods is quite troublesome, and lubricated abrasive papers and final etch-polishing are recommended. Scott [157] has published a suitable method for the etch-polish of lead samples.

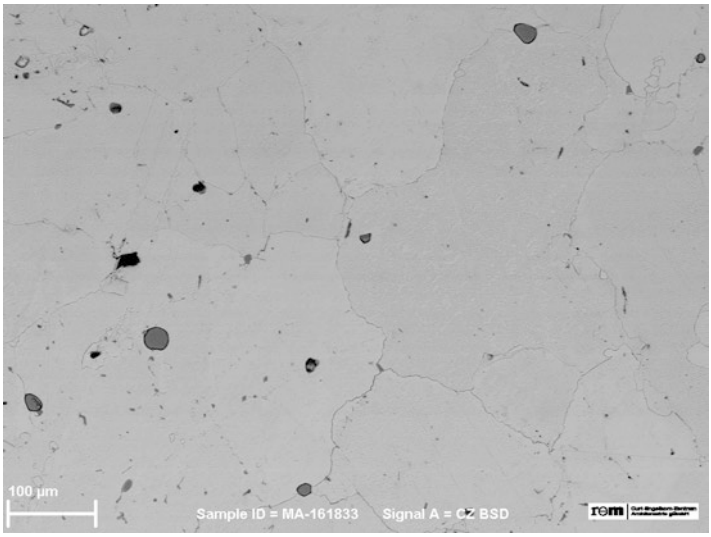

Fig. 5.25 SEM-BSE image of the microstructure of a Roman lead water pipe from Petra in Jordan. Large grains are revealed by etching with aqueous solution of nitric acid. The fine grains are false structure due to abrasion damages. The grey inclusions are β_{Sn} solid solution

In most ancient societies, silver has not played such a dominant role as gold, and the increase of silver production is usually coincident with the introduction of silver coinage or other monetary issues (see, e.g. Craddock et al. [43]; Wells [191]). Pure silver is very ductile and soft with a hardness of 25 HV to 27 HV when annealed ([28], p. 671), which is actually too soft to be practicable for many purposes. Native silver is relatively pure but contains some trace elements (see Craddock [35]), but which do not affect the microstructure, which should be single-phased. Silver from the cupellation process, in contrast, rarely contains less than 0.1% lead ranging up to several percent and a considerable concentration of gold, which is also not affected by oxidation during the cupellation process, which itself tends to enrich bismuth so that this element cannot be removed completely [95, 122]. The copper content can effectively be reduced, but some copper may survive the highly oxidizing cupellation and may be present up to 2% of copper or even more [122]. According to the phase diagram of Ag-Bi, which is very similar to the Ag-Pb diagram, the microstructures of such silver alloys should contain lead and bismuth precipitations. Wanhill [186, 187] who has published numerous papers about the embrittlement of ancient silver, supposes that precipitation of lead, and less commonly bismuth, is involved in the intergranular corrosion of silver. An example of corroded ancient silver is given in Fig. 5.26 which has the mechanical strength of a biscuit!

The grain embrittlement in the silver-copper alloys is gradually lost as the copper content rises. Instead, these alloys when cast and heavily worked and annealed tend to preserve a dendritic microstructure. An alloy not far removed from the eutectic of composition 60% silver and 40% copper is shown in the cast condition in Fig. 5.27. It contains 50% copper and 50% silver.

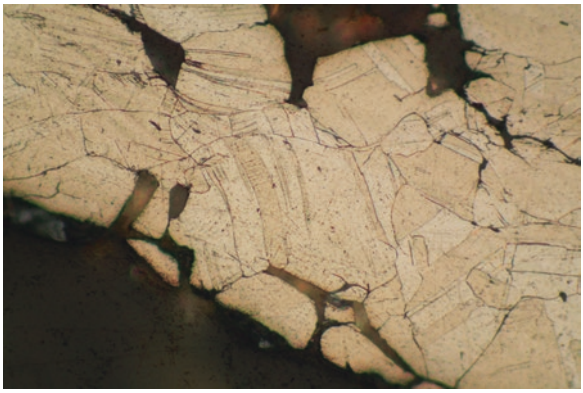

Fig. 5.26 Sasanian silver bowl in the collections of the J. Paul Getty Museum, showing typical features of embrittled silver. The surface has undergone extensive oxidation which is often seen. Below that, the silver grains have begun to separate along grain boundaries. Note that the grain boundaries are also meandering due to copper precipitation. This is called discontinuous precipitation. Unetched, magnification x230

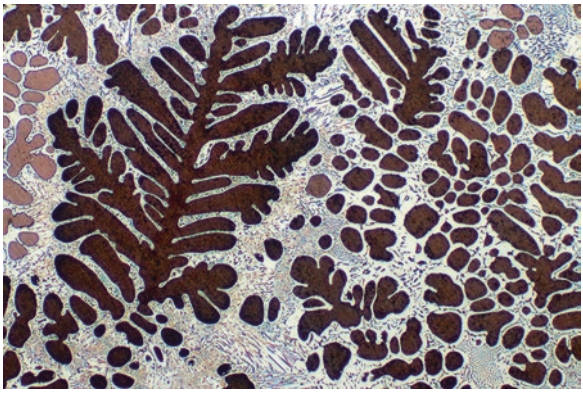

Fig. 5.27 50Ag50Cu cast alloy. The microstructure shows well-developed copper-rich dendrites with an infill of the silver-copper eutectic phase, whose delineation into the lamellar eutectic structure can be clearly seen here. EPMA analysis shows the copper-rich dendrites to be 93% copper and 7% silver, showing no movement in composition on cooling from the initial deposition of the copper-rich dendrites. Etched in acidified potassium dichromate, magnification x120

Much use was made of silver-copper alloys, not only for silver solders but also for copper-silver alloys which could then be enriched in silver to make their surfaces appear as if made in solid silver; an example is shown in Fig. 5.28.

Very relevant to corrosion and to all other properties of these silver-copper alloys is the behaviour of copper as an alloying element. From an early stage, metalsmiths learnt to alloy some copper with their extracted silver to produce a harder product, as copper is the most effective hardener to silver. The silver-copper alloys are strengthened by the silver-copper eutectic or α_{Cu}-phase precipitation, but silver-

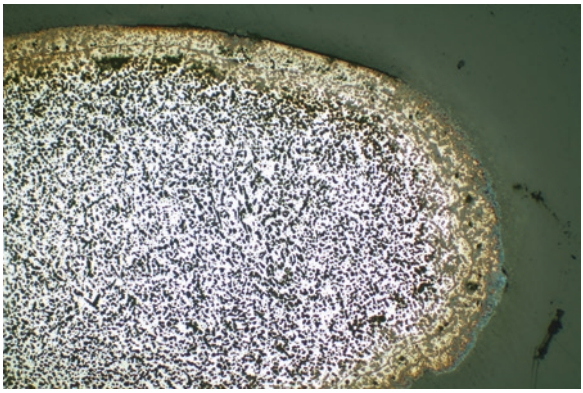

Fig. 5.28 Cast silver-copper alloy from the Strozzi silver basin in the collection of the J. Paul Getty Museum. The section shows a cast silver-copper solder of composition about 82% silver and 18% copper. Here the composition is close to the eutectic composition, and silver-rich dendrites will form with an infill of the copper-rich phase either as segregated cast copper-rich phase or as an infill of the eutectic. Etched in potassium dichromate, magnification x80

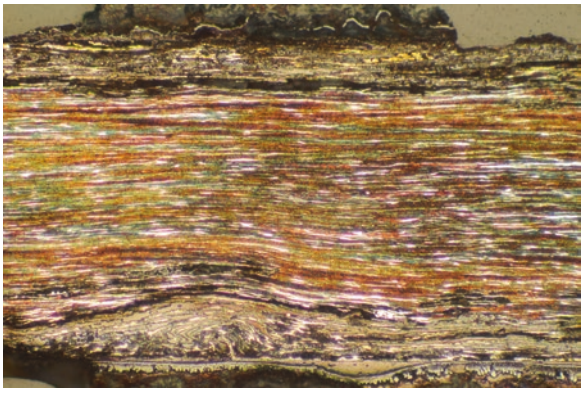

Fig. 5.29 Heavily worked silver-copper alloy from the site of La Compania, Los Rios Province, Ecuador, from a secondary chimney urn burial of the tenth century AD. The heavily worked silver-copper alloy was originally about 30% silver and 70% copper. The silver-rich beta phase survives, while the copper-rich phase has corroded away. Note that dendritic segregation essentially remains. Unetched, magnification x220

copper alloys achieve a significant increase in hardness values if cold-worked. Silver alloyed with copper and subsequently cold-worked and annealed, followed by further hammering, exhibits much greater hardness, and values of 200 HV and more can be achieved ([32], p. 676). Silver-copper alloys have been used over the full range of compositions of the binary system, already illustrated in Fig. 4.9, and the different annealing and other properties of some of the alloys are shown in Fig. 5.29. Figure 5.30 shows data for a number of binary alloys, which have been reduced to 49.7% thickness by cold-working. There is a different response to

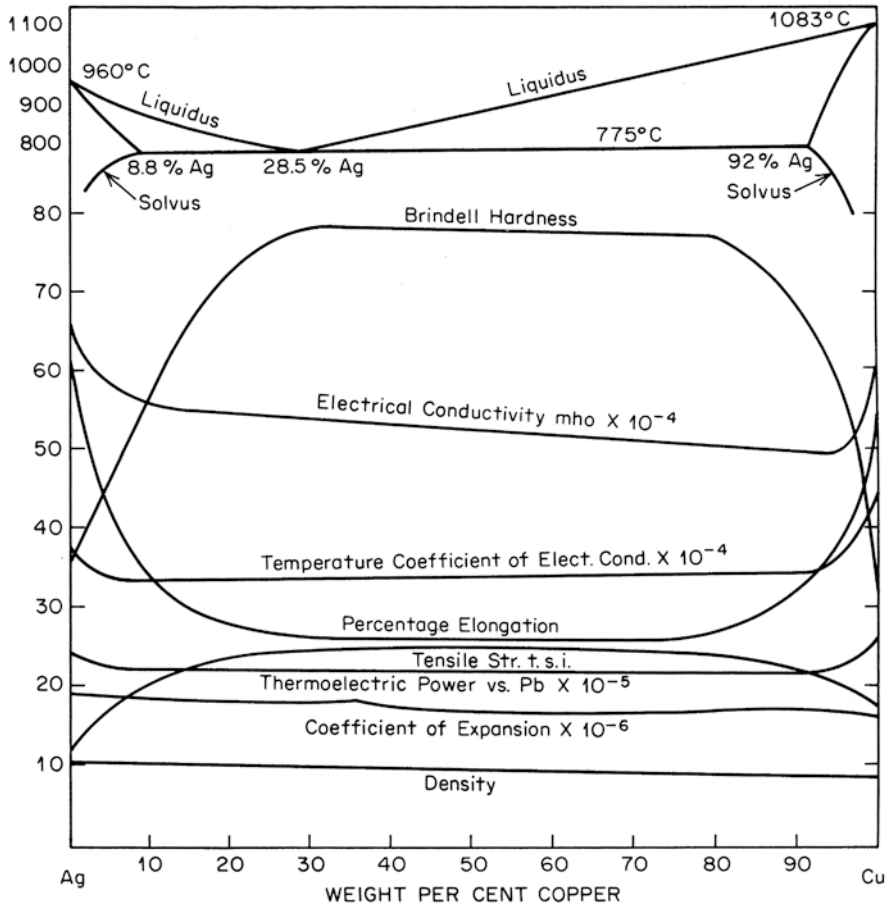

Fig. 5.30 Diagram showing tensile strength, Brinell hardness and percentage elongation for the silver-copper alloys. After Butts and Coxe, adopted by Scott [159]

annealing depending on the composition. Alloys with 95% silver and 5% copper only reach a tensile strength of 50×10^3 psi (pounds per square inch), while those of 72% silver and 28% copper reach 74×10^3 psi (Fig. 5.31).

The increase in tensile strength of some of the alloys when the annealing temperature exceeds 593 °C (1100 °F) is of interest. This is due to age-hardening which occurs when these alloys are air-cooled from above 593 °C. Wires of the silver-copper eutectic alloy when drawn to a 99.5% reduction in area can reach a tensile strength of 130×10^3 psi ([19], pp. 252–4).

The maximum solubility at the eutectic temperature of 779 °C of copper in α_{Ag} solid solution is 8.8 wt. % and 8 wt. % of silver in α_{Cu}-solid solution but drops nearly to zero (0.1%) at room temperature (see Chap. 4). Therefore, the microstructure of silver-copper alloys would be duplex in all compositions, but single-phased alloys can be produced in all mixing ratios by rapid quenching. About 3–4% of copper is

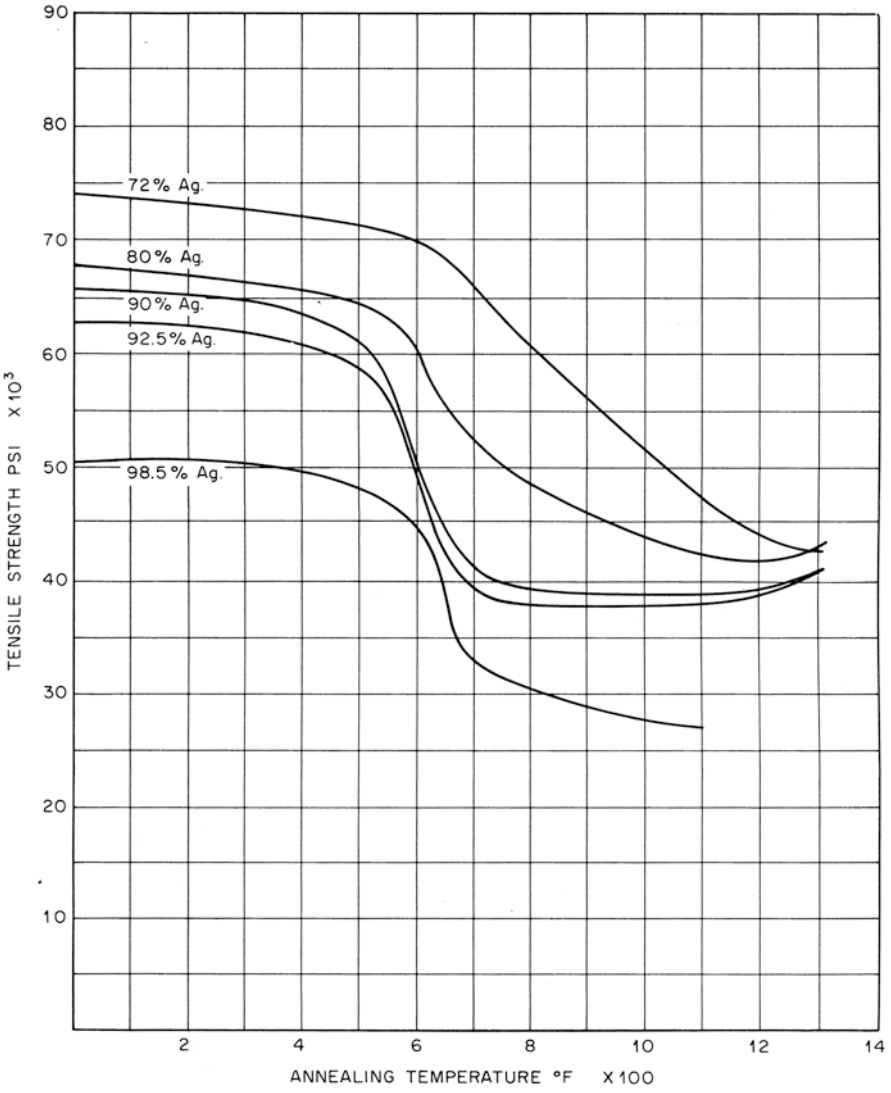

Fig. 5.31 Chart of tensile strength against annealing temperature for silver-copper alloys. After Butts and Coxe, adopted by Scott [159]

a common addition in the Old World, and this continued in the production of "Sterling" silver which usually has around 8% copper content. In pre-Hispanic South America, a whole range of silver-copper alloys were produced and were used for a variety of artefact types. By adding more copper, silver alloys could be debased, which could later be surface-enriched in silver by pickling in plant juices or mineral salts, or used as solders with lower melting points than the two constituent components, often for joining silver or gold components together.

Gordon and Knopf [63] carried out some investigations of the mechanical properties of silver-copper alloys in the cast condition to replicate studies of ancient alloys from the site of Machu Picchu, excavated in 1912 by Hiram Bingham, in which several tupu pins were found to be made of silver-copper alloys with about 68.6% copper and 29.4% silver, while a head band was made in 74.7% copper and 24.5% silver. Pickling of the surface in acidic plant juices will easily dissolve some of the copper from the surface, resulting in silver-enriched surface layers, effectively a form of depletion silvering (Chap. 6). Auriferous silver with 6–7% gold and almost equal amounts of copper are reported from Bronze Age objects in the Aegean and the Near East ([140], p. 4; [99], p. 279), while auriferous silver with high gold content and electrum from Cambodia have been depleted to counterfeit gold (Chap. 6).

Occasionally, artefacts made of solid, cast silver are found, such as the silver statuette of a naked female dating to the 26th Dynasty in the collections of the Metropolitan Museum [10]. Scott [155] also examined a small section from this statuette because of potential art historical doubts as to its authenticity, and it was deemed materially authentic. The silver statue Cellini was working on was cast in practically pure silver (Chap. 4). Pure silver for such a use is rare in solid castings, as it is very expensive. One way to economize is to use silver-copper alloys or coat the underlying metal with silver (Chap. 6).

The recycling of silver is technologically equal to the medieval liquation processes to extract silver from polymetallic ores (see Craddock [35], pp. 232–233). To extract silver from copper-silver alloys, lead and debased silver are molten together. Due to the liquid miscibility gap between copper and lead and the good miscibility between liquid silver and liquid lead, silver passes into the lead.

Figure 5.32 shows the microstructure of a lead-copper-silver alloy found together with a silver- and copper-bearing litharge slag in the oppidum of Manching in Southern Germany, which has probably been used to desilver silver-plated Roman Republican denarii [150]. The copper-rich α_{Cu}-solid solution is incompletely desilvered, but most of the silver is precipitated in the lead matrix. This is the first example for this process, which has been widely practised from Roman times [8, 35,

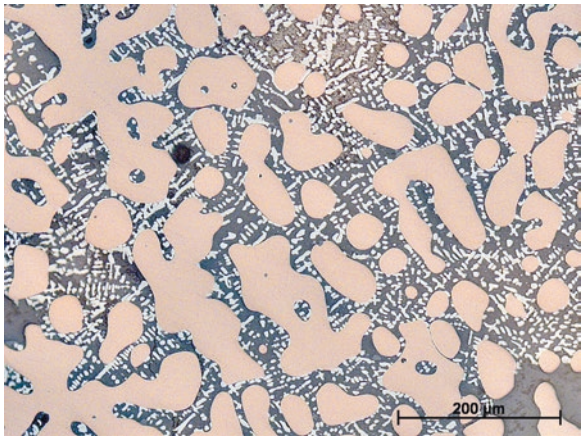

Fig. 5.32 Copper-lead-silver alloy from the oppidum of Manching, Germany, with 49% Cu, 37% Pb and 13% Ag. The dendrites of copper-silver solid solution are surrounded by interdendritic lead, which has absorbed most of the silver, visible as fine dendrites

139]. The origin and the application of the liquation processes to ores are still unknown, but some copper-bearing litharge slag from the Near East and Spain from the first millennium BC might be a relict of it (Middleton et al. [100], pp. 167–168; [141], p. 2594).

5.1.3 Gold and Gold Alloys

Gold is a ubiquitous native metal, which is usually found naturally alloyed with silver and sometimes with traces of iron in a wide variety of geographical locales. There are many ways in which the nature of gold deposits can be classified (see, e.g. Emmons [54], p. 4); one possible classification is as follows:

Deposits in veins and lodes.
Produced by hydrothermal solution and present in fissures, stratified planes, etc.
Recent placer deposits: formed in sands and gravels, consolidated and semi-consolidated along with a few other minerals.
Ancient placer deposits corresponding to placers formed in geological time, often occurring in conglomerates.
Deposits of marine placers which accumulate in the ocean.
Deposits which form through metasomatic contact: the original hydrothermal deposits are altered and the gold is irregular.
Deposits of other metals with gold as a subproduct.

Some of these deposits were utilized in antiquity. There are extensive placer gold deposits in many parts of the world, which were worked by hand panning, by opencast mining, or from Roman times on by large-scale so-called hydraulic systems. Hydraulic mining was already an excessive form of exploitation and used the erosive force of water to break up large amounts of the overburden and flush out the gold-bearing soils (see Craddock [35], pp. 87–92; [195], pp. 17–21). The ruins of this technology are still obvious in Northern Spain (see Domergue [50]). An attractive woodcut illustrated by Plazas and Falchetti ([126], p. 23), taken from Gonzalo Fernández de Oviedo (1535–48), shows Colombian Indians panning gravels in a stream, typical for much ancient gold-working. Deposits of gold quartz veins like in ancient Egypt were also worked by deep mining or opencast mining, and the gold was extracted from quartz by crushing and grinding [78]. Many areas of the world have gold deposits suitable for either panning or for mining.

High-purity gold is like silver, very ductile and soft with a hardness of 25 HB when annealed to 33 HB as cast ([4], p. 680), but ancient gold objects usually are not made of pure gold, as native gold is almost always a natural alloy. Gold can contain up to about 50% silver, when it is called electrum, while gold with higher silver contents is usually surface treated to retain a golden colour (Chap. 6). The electrum alloys, silvery in colour, were used in early Lydian coinage and are regarded as being artificially produced alloys rather than naturally occurring (Cowell et al. [31, 32]). Alloying with silver seemed to be common in Southeast Asia, with

evidence from Prohear (Cambodia), a site dating to the Iron Age [148]. Usually the silver content of native gold does not exceed 40% and is rarely lesser than 1%. Gold-silver alloys are single-phased (see Fig. 4.2), as the two fcc metals are mutually soluble in each other, producing a fcc α_{Au}-solid solution (see Chap. 4). Copper may be present in native gold in small amounts, up to about 2%, but rarely exceeds 0.5% in concentration, which is also a solid solution component in the $\alpha_{Au(Ag, Cu)}$ phase region. Indeed, detailed analyses of individual gold grains by electron microprobe analysis have shown that copper concentrations of up to 30% by weight can occur within individual grains (Stumpfl and Clark [167], pp. 938–939). This work was carried out on alluvial material from southeast Borneo, a complex geological metallogenic area, and there is no reason to suppose that gold from most other regions bears any similarities to the grains analysed. Nevertheless, the variation found, and the fact that most grains could be plotted in the ternary gold-silver-copper system, should be borne in mind.

There are many varieties of native gold. Natural gold can be flecked with inclusions such as tellurites, quartz or pyrite and with platinum-group metals (PGE). Most impurities are slagged by oxidizing melting of the gold, but inclusions of the platinum-group metals can occur. Palladium and platinum can form a continuous series of solid solutions, but the osmium-iridium-ruthenium group remain unalloyed and fleck the gold with tiny silvery inclusions, often taken as an indication of the authenticity of the gold object in question, since refined gold will not have such inclusions. Both the geological evidence and recent analyses point to a fairly simple gold mineralization being the most often used, in which low levels of impurities, apart from silver and copper, are found.

Gold artefacts may utilize gold from the following four different scenarios (after [116]):

(a) The gold nuggets can be used as found.
(b) The gold can have silver or copper alloyed with it.
(c) The gold can be refined to remove impurities such as silver.
(d) The gold can be refined and then alloyed with careful additions of silver, copper or other metals.

Some cultures, such as those of ancient Egypt, Rome, Colombia, Sumatra and Japan, made use of coloured gold alloys deliberately alloyed with other metals to produce a range of colours. Reddish gold, green gold, rose gold, silvery gold can all be produced by alloying techniques or surface treatment methods [14, 82, 83, 114, 115, 156, 160]. The treatment of gold-silver alloys for making burgundy-red surface films of complex sulphides was examined by Frantz and Schorsch [56], used for rosettes and sequins for the tomb of Tutankhamen.

Gold can be refined using a variety of techniques. Early methods of cementation employed salt and straw or salt and brick dust or other earths to oxidize the silver content to increase gold purity [135]. The production of gold leaf or foil is easier if the gold is of high purity, but Frantz and Schorsch [56] found some gold leaf from Egyptian Middle Kingdom wooden coffins ranged in gold purity from 85% down to about 30%. Moorey [103] mentions that in ancient Mari texts from the Old

Babylonian period, the term lurpianu (possibly a salt) associated with gold preparation occurs. Gold purification by cupellation was by no means a universally applied process, and many ancient gold objects were not made from cupelled gold.

The microstructure of gold and gold-silver alloys often reveals porosity from the dendritic segregation of the cast alloy, although these porosities are easily closed on hammering and annealing to shape. The resulting microstructure shows features common to all fcc metals, namely, annealing twins, strain lines and recrystallized homogeneous single-phase grains. An example of a gold alloy pin from ancient Ecuador is shown in Fig. 5.33.

5.1.3.1 Platinum-Iron Alloys

Platinum and platinum-gold alloys were extensively used in ancient Ecuador and Colombia, especially in the La Tolita region of Ecuador, where gold-platinum and platinum sintered surfaces over gold were produced [158, 159].

The diagram shown in Fig. 5.34 is of interest here since all of the native platinum used by the Indians of ancient South America (the only users in the ancient world) is, in fact, a native platinum-iron alloy [158, 160]. The native platinum of the region is a platinum-iron alloy, and the same is true for other areas of the world where a simple mineralization of platinum occurs. The platinum-iron diagram shows that three ordering reactions occur in the regions of composition corresponding to $PtFe_3$, PtFe and Pt_3Fe.

The new nomenclature proposed by Cabri and Feather [21] replaces some old terms, such as "polyxene" and "ferroplatinum", which are to be found in the metallurgical and geological literature prior to 1975. Their proposals are:

Native platinum is defined as a face-centred cubic alloy with Pt > 80 at.%.
Ferroan platinum is defined as a variety of native platinum (PtFe), with a face-centred cubic structure and with Fe between 20% and 50 at.%.
Isoferroplatinum is defined as a new species with a primitive cubic structure and a composition usually near Pt_3Fe.

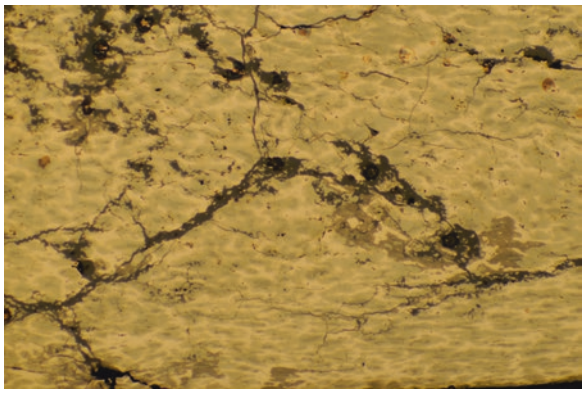

Fig. 5.33 Gold-copper-silver alloy from ancient Ecuador, from the Esmeraldas area, dated to the early centuries AD. As a lightly worked casting, the dendritic segregation of the alloy is still apparent in this microstructure. Approximate overall composition 55% gold, 8% silver and 37% copper

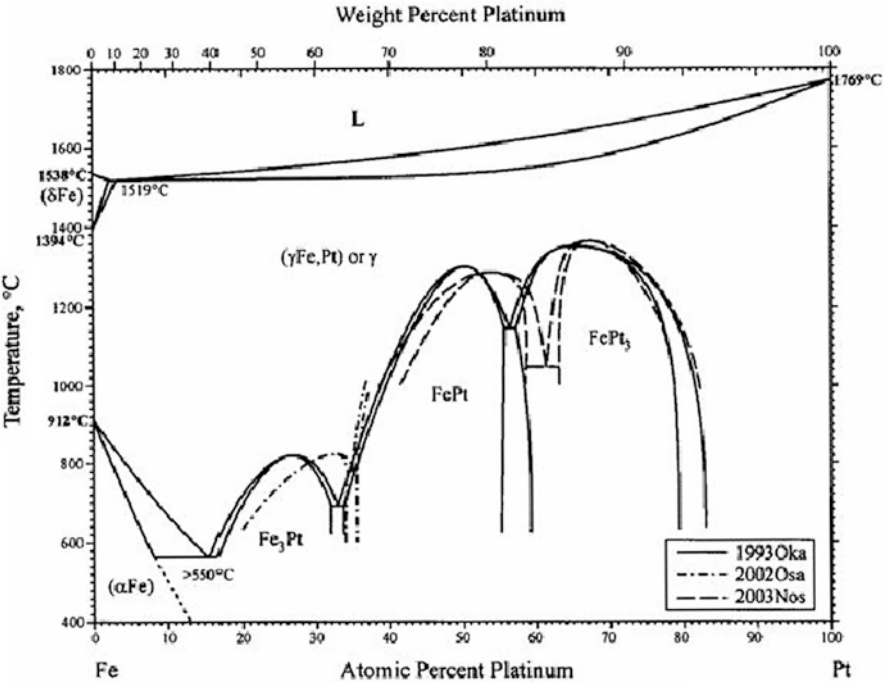

Fig. 5.34 Platinum-iron system. At levels of platinum content of 90–95% by weight, some of the platinum is present in the native state as a platinum-iron alloy, Ferroan platinum

Tetraferroplatinum is redefined as a distinct species with tetragonal symmetry and a composition near PtFe.

Synthetic ordered Pt_3Fe is not ferromagnetic, but cold-working can distort the structure, producing strong ferromagnetism [44].

In the native state, there are several elements which can substitute for either platinum or iron. Platinum can be partially replaced by Ir, Pd, Rh, Os and Ru, while iron can be replaced by Cu, Ni and Sb. Partial replacement of some of the platinum by, for example, iridium, will produce substantially higher microhardness values. It has also been pointed out by Cabri and co-workers [22] that platinum from placer deposits is significantly harder than commercially available platinum of identical composition that he ascribes to cold-working during fluvial transport.

5.1.3.1.1 Platinum-Gold Alloys

These alloys were used extensively by the Indians of the Esmeraldas-La Tolita region from the early centuries BC until around 800 AD [159]. The alloys represent the first example of powder metallurgy, since the platinum cannot be molten using primitive heating techniques, which can never reach 1800 °C. However, extensive

sintering is possible, and some interdiffusion on heating the composite means that the gold-platinum phase diagram becomes relevant.

Figure 5.35 is from Hansen and Anderko [69], redrawn by Scott [154], and is generally accepted as the correct equilibrium diagram. Previous to this the system had often been assumed to be a peritectic; a problem created by the very wide separation between the liquidus and solidus curves in the diagram. The type of precipitation which can take place in these alloys is, in many ways, the opposite of the discontinuous precipitation which takes place in the silver-copper system considered earlier.

The precipitation can be related to the second derivative of the Gibbs free energy where:

$$\left[d_2G\right]/\left[dc_2\right]T,P \geq 0 \tag{5.1}$$

$$\left[d_2G\right]/\left[dc_2\right]T,P \leq 0 \tag{5.2}$$

In the case of Eq. (5.1), the expected reaction is that of discontinuous precipitation, and in (5.2), the reaction is that of spinoidal decomposition. The features of spinoidal decomposition involve the breakdown of the solid solution, alpha, into a modulated structure which is made up of alternating layers of the separating phases.

Rapson and Groenewald [137] note that spinoidal decomposition could be expected to occur under certain ageing conditions in gold-silver-copper alloys. Tiedema and co-workers [173] were the first to report on this type of transformation. Using electron diffraction, they found periodic variations in composition; both coherent and incoherent precipitates were found. A wide range of properties can therefore be found in gold-platinum alloys, by changing the quenching temperature within the two-phase region and by age-hardening subsequent to quenching. Darling [45] provides a diagram which shows the great variation in observed hardness values, depending on the quenching temperature.

The diffusion of gold and platinum shown in Fig. 5.36 is of some interest for the ancient alloys, and it is worth noting in this respect the statement made by Darling [45] concerning this:

"...the phase boundary formed by diffusion between pure gold and platinum results from the shape of the diagram. Once the equilibrium phases are formed diffusion occurs across the interface between the gold and platinum solid solutions, each of which is constantly replenished from the reservoirs of pure gold and platinum. Because the partial diffusion coefficient of gold. in the gold-rich solid solution is approximately 75 times that of platinum, a pronounced Kirkendaal shift Kirkendall shift is observed and the marker interface moves considerable distances towards the gold-rich side of the couple…."

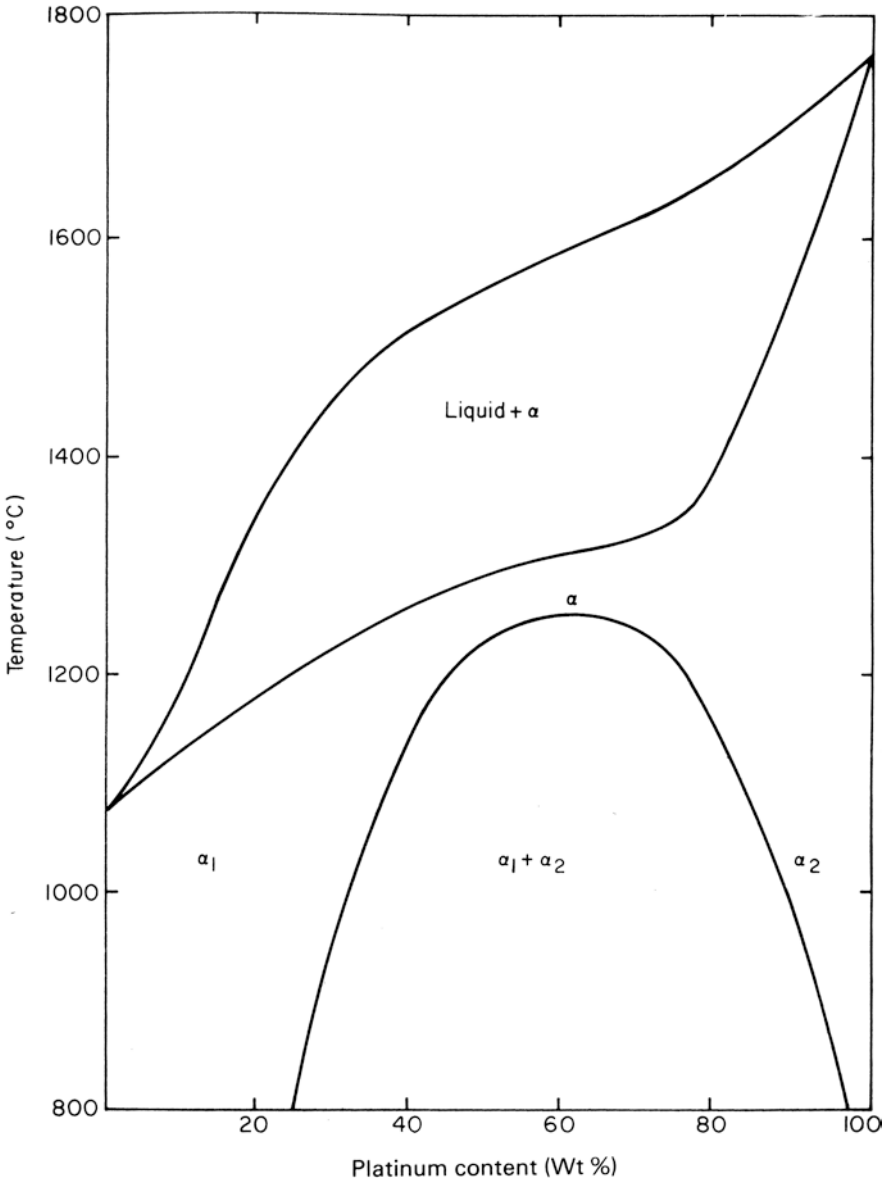

Fig. 5.35 The gold-platinum phase diagram (after Hansen & Anderko [69], redrawn by Scott [154]). At levels of platinum content of 90–95% by weight, some of the platinum is present in the native state as a platinum-iron alloy, Ferroan platinum

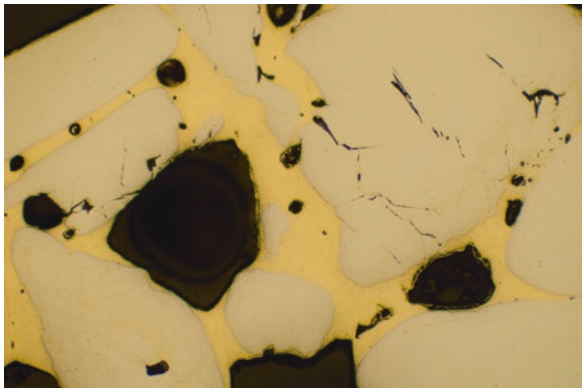

Fig. 5.36 Gold-platinum sintered alloy at the starting point. From the site of La Tolita. Collections of the National Museum of Denmark, Copenhagen. Etched in aqua regia, showing native platinum-iron laths and the initial gold matrix holding them together before they are broken up on heating and hammering. Magnification x 100

5.1.3.1.2 Platinum-Gold-Copper-Silver Alloys

Wise and Eash [197] studied the phases present in some Pt-Au-Cu-Ag alloys. In the alloys chosen, Pt and Au content remained at 50 atomic percent. It appears to be a peritectic system in which an alpha solid solution of the four constituents gives rise to a second phase, theta, which was suggested to have the formula $AuPt_2Cu_3$ by analogy to AuCu. A typical composition examined was Pt, 7.0 wt.%; Au, 63.8 wt.%; Ag, 15.5 wt.%; and Cu, 13.2 wt.%.

Looking at the factor f', defined in Eq. (5.2), this alloy gives a value of 54%, placing the equilibrium composition in the type III region. This alloy is already two-phased, and besides alpha (AuAgPtAu), the additional phases may be $alpha^{I}$ (AgAu) + $alpha^{II}$ (CuAu) + θ ($AuPt_2Cu_3$), a complexity which is not discussed by Wise and Eash. Further metallographic work is probably required to confirm the identity of the theta phase.

5.1.3.1.3 Platinum-Gold-Iron Alloys

Goedecke [61] reported the hardening of gold-platinum alloys by the addition of small percentages of iron. Subsequent work by Smith and co-workers [165], and by Leinfelder and co-workers [89], has confirmed these findings. The degree of hardness change is well-illustrated by this example from the work of Leinfelder et al. who water-quenched their alloys, annealing being carried out at 982 °C and ageing at 538 °C for 30 min. The grain boundaries in these alloys appear thickened as a result of some precipitation which has taken place. This is thought to be due to the appearance of Pt_3Fe at the grain boundaries. Leinfelder, O'Brien, Ryge and Fairhurst (ibid.) also found some evidence for a poorly developed intragranular structure.

5.1.4 Tin and Zinc

Pure tin is a white silvery metal, which melts at 232 °C and with a low hardness of 6 HV, which is only slightly higher than lead. When bent at room temperature, a sound known as "tin-cry" is audible due to the spontaneous twinning that emits a sound wave. Like lead, and other low-melting point metals, it recrystallizes at room temperature, and distortions during embedding or preparation can form false structure by subsequent recrystallization. Therefore metallographic sections of tin metal can be difficult to prepare in the same way that lead presents challenges due to softness and smearing during polishing. During the preparation, alternating between polishing and etching may be necessary to remove surface-altered microstructure, and standard literature should be consulted (e.g. [172]).

Tin is like iron an allotropic metal and occurs in three polymorphic forms. The metallic β_{Sn} or white tin has a body-centred tetragonal (bct) lattice structure, which is stable at and above room temperature. In contrast, α_{Sn}, or grey tin, which is stable below 13.2 °C (55.8 °F), is brittle and a dull-grey-brown powdery material. There are accounts of tin church organ pipes decomposing due to the allotropic change to α_{Sn} after prolonged exposure to sub-zero temperatures, a metallurgical change known as "tin-pest" (Tylecote [177], p. 51). The latter has a diamond cubic crystal structure and is therefore essentially non-metallic, because the atoms form a covalent structure in which electrons cannot move freely. The third allotrope, γ_{Sn}, crystallizes in the hexagonal structure and exists at temperatures between 161 °C and the melting point.

Prehistoric objects made of pure tin are quite scarce, and the most surviving examples of ancient tin are present as alloys or coatings. Because tin is bct, it tends to form a number of intermetallic phases with many other elements, including the bronze system, especially on tinned surfaces (Sect. 6.2.4). These intermetallic phases may be hard and brittle, which usually has disadvantages, although in ancient usage, this may be secondary to colour, as high-tin bronze mirrors were made brittle, but with highly reflective silvery-coloured surfaces. Tin does not form solid solution ranges of any great extent in other metals in general, and few elements have appreciable solid solubility in tin. There is a eutectic system with lead and eutectic reactions with gold or silver (Chap. 4), but only the lead-tin alloys, known and utilized in the ancient world as a soft solder or up from Roman times as an alloy called pewter, are relevant to ancient metals (Fig. 5.37).

Most ancient soft solders do not show eutectic composition (61.9% Sn) with the lowest melting point at 183 °C but usually are lead-rich with a wider freezing range between 180 and 260 °C, which are pasty long enough to facilitate the joint [152]. Indeed, these data must be treated with caution, as most ancient solders are badly corroded and the corrosion products of lead and tin have different solubility, and therefore their abundance in corrosion products and base metal is diverse (see Turgoose [176], p. 24). There is also a eutectic system with zinc, but this has only a few ancient parallels.

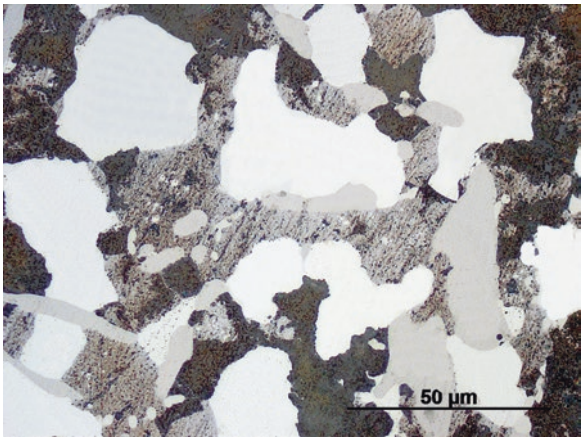

Fig. 5.37 Lead-tin solder with 62% Pb and 33% Sn from a silver handle or furniture fitting from the late Roman Traprain treasure, Scotland. The tin (β_{Sn}) has precipitated in a lead-rich matrix (α_{Pb} + eutectic) and has formed columnar intermetallic ε-phase (Cu_3Sn) with copper, which is present only at 0.3%. Most of the lead is corroded, so that it must have been anodic to tin, while the metallic lead-rich matrix is scratched and smooth. The whole sample has taken up 3.7% silver from the silver substrate, which has not reacted with the solder and is present as precipitates of α_{Ag} solid solution

Metallic tin ingots from Bronze Age shipwrecks such as the Uluburun shipwreck off the Turkish coast or at Salcombe off the coast of Southwest England, as well as Roman tin ingots found in the Mediterranean, which probably came directly from the smelting sites from the Iberian Peninsula, show a remarkably high purity for ancient metals [27, 72, 185]. The Bronze Age tin ingots have the same form as contemporary plano-convex or oxhide copper ingots, but the Roman tin ingots have a quite unusual form that Tylecote ([177], p. 47) has described as purse-shaped, consisting of two parts cast together with a handle.

The source of tin is probably mostly from cassiterite (SnO_2), which occurs in alluvial stream deposits. These could be used to produce tin bronze alloys by co-smelting with copper ores or by adding tin oxide to molten copper under reducing conditions, but it is more likely that metallic tin was produced first and then added to liquid copper (see Pernicka [121]). The scarcity of tin deposits and the primary occurrence of tin bronze in those regions that are devoid of tin ores is still a puzzle for archaeometallurgists, and it is remarkable that the earliest tin bronzes of the Bronze Age appear in northern Mesopotamia and Anatolia, the former of which has no tin [123, 189].

Tin and tin alloys may be extensively converted during corrosion into a number of different tin oxides and other compounds (see Dunkle et al. [52]), which, unlike copper, seems to afford little protection to corrosion in depth under some circumstances, for example, large tin ingots found in the sea off the coast of Cornwall were found to be completely mineralized.

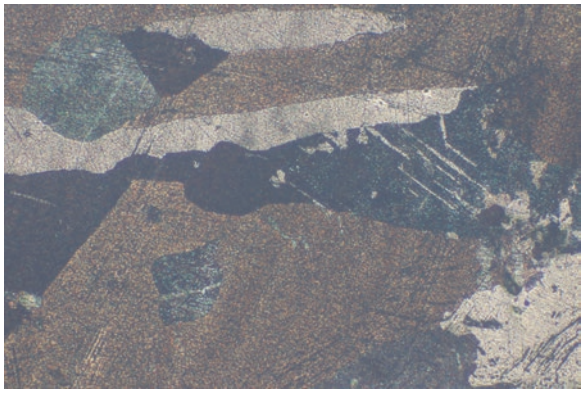

Fig. 5.38 Section across a tin ingot, showing columnar grain growth. Chill cast, 99.9% tin

A large ingot of copper under the same circumstances would be expected to have a substantial corrosion crust but not to be totally mineralized. The grain structure of pure tin can be quite large, and an example from a cast tin ingot, which has a flowing columnar microstructure, is shown in Fig. 5.38.

5.1.4.1 Zinc

Metallic zinc is also a white metal, which belongs to be close-packed hexagonal (cph) lattice group and is the only historic metal that forms crystals of this type. The close-packed hexagonal group has few active slip systems and undergoes mechanical twinning as a result of deformation, differentiating the process from annealing twins as a result of working and annealing, as in fcc metals (Fig. 5.39).

Zinc and zinc alloys can only be worked between the temperatures of 100 °C and 250 °C, because of the activation of an additional slip system when dynamic recrystallization occurs, so deliberate shaping may imply working between these temperature parameters. Above and below these temperature limits, the metal is too brittle to be worked to shape. The failure of zinc sculptures is due to insufficient means of stress absorption in metallic zinc, which can result in cracking and deformation under circumstances where a copper or bronze sculpture would be able to undergo plastic deformation, or at least absorb the stresses created by slight movement ([63], pp. 290–3). Zinc is insignificantly harder than lead or tin (30–35 HB) but also very difficult to prepare, and the metallographic examination of zinc has to be done with care, since the slightest deformation will induce mechanical twinning to considerable depth during sample preparation. Heating must be avoided because of the ability of zinc to recrystallize at room temperature (10 °C). The classic etching reagent for zinc alloys is Palmerton's reagent and alternatively the Klemm's I reagent can be tried, both given in the appendix, but zinc and zinc alloys are optically anisotropic, and the microstructure can be examined in polarized light without etching.

Metallic zinc was a rarity in the ancient world, as attempts to smelt zinc ores directly lead to zinc vapour disappearing up the furnace chimney. Reduction around

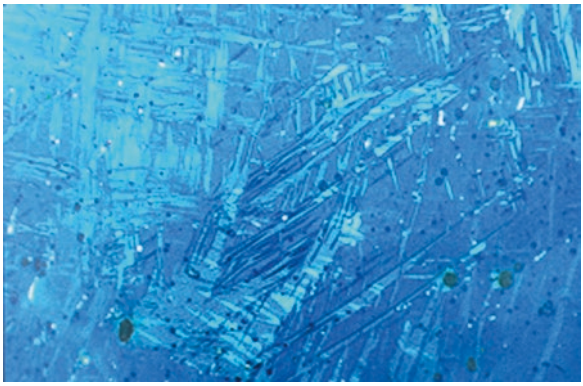

Fig. 5.39 Polished and etched section of late medieval Indian zinc coin. This etched in Palmerton's reagent and under polarized reflected light. Twinning in the zinc grains revealed here at a magnification of x60. From the microstructure it appears that the zinc coin was roughly cast into a blank and then struck. Probably hot striking would be necessary here

1000 °C is crucially important as below 950 °C no zinc is produced, but zinc metal already boils at 907 ° C, which is below the temperature needed for its extraction. Because of such properties, pure zinc smelting was not practised early on, and the only way in ancient times to create zinc metal was by downward displacement, into cool retorts below, as discovered by the Indians around the twelfth-thirteenth centuries AD, and regular zinc production in China began only in the fourteenth century AD (Sect. 5.1.1.4). Though few brass objects may have been found in earlier contexts in China, it does not seem that brass or zinc were common before the sixteenth century. Zinc, like lead, has not been of much practical value itself before recent times, and most of it was used in the production of brass. Before electrolytic refining, zinc was quite impure. The chief impurities of ancient zinc are lead and iron, which both have a very limited solubility, and iron forms hard and brittle intermetallics (see Grissom [64], Fig. 6). Arsenic and antimony, but especially cadmium, are frequently present, and brass made by speltering usually contains minor portions of cadmium (e.g. [190]). Unalloyed zinc has been used for Indian late medieval coins [42], and high-zinc alloys containing a small amount of copper were used in ancient India from the seventeenth century, probably earlier, to manufacture skilful metal ware, known as Bidri ware (Sect. 6.1.1).

It seems that there has been some confusion about early occurrences of metallic zinc, especially in Europe, and various isolated examples of zinc objects, usually lacking any real archaeological evidence, have entered the literature (see Craddock [37]). The discovery of a roll of sheet zinc at Agora in Athens datable to second to third century BC is an interesting example of nearly pure zinc, which has been discussed, generating a certain amount of controversy, but finally has come to be regarded as almost certainly authentic ([37], pp. 2–3). The Greeks were not producing zinc at that time and the origin is unclear, but it is the only piece from a controlled excavation.

5.2 Iron, Steel and Cast Iron

5.2.1 The Coming of Iron

The metallurgy and microstructures of pre-industrial iron and steel differ from modern ferrous alloys, because of the different processes applied to produce them. Different types of iron and steel are very revealing when examined metallographically. This is because the microstructure of ancient iron is very sensitive to changes in composition and notably to heat treatment. Most ancient ferrous materials are very heterogeneous, having been made from bloomery iron, which was never molten into a homogeneous mass of iron – even when it can be partly liquid.

In order to sketch the background, an account of the archaeological development of iron and steel metallurgy in the ancient world must also form part of the text for this chapter. Iron smelting was never discovered in the New World and did not reach it until the Spanish Invasion, so all of the occurrences of iron discussed here pertain to Africa, Asia and Europe.

There are sporadic finds of iron from the third and second millennium BC in the areas of Mesopotamia, Egypt, Syria, Lebanon, Palestine and surrounding regions [35, 128, 184]. This is the period when iron really starts to be noticed, probably as just another exotic material. Some of these finds have been shown to be made of meteoric iron, and others have been made by smelting, probably as a by-product of copper smelting operations, and would have been rare and precious products at this time. The possible use of meteoric iron in the ancient Near East has long been assumed, but evidence is hard to substantiate. Moorey [103] states that on the present evidence for iron terminology in ancient Egyptian and Hittite texts, terms for "iron of (or from) the sky" do not appear until the second half of the second millennium BC, during the Late Bronze Age, by which time smelted wrought iron was already known.

According to Craddock [35], some of the well-known small pieces of predynastic and early dynastic corroded iron from Egypt are totally devoid of nickel, but are almost certainly meteoritic in origin. Telluric iron, which was always very rare, might have under 5% of nickel, while meteoric iron has between 5% and 20% of nickel and often a Widmanstätten morphology (Fig. 5.40) throughout, although this is an oversimplification.

Research by Desch in 1928 suggested, on the basis of the high nickel content, that early examples of iron from Mesopotamia were of extra-terrestrial origin, a conclusion that perhaps needs re-examination. There are, however, some objects which possess the Widmanstätten structure of meteoric nickel-iron hexahedrite alloys, such as the iron ball or pellet from level II at Tepe Sialk in Iran, dating from the fifth millennium BC [59, 125, 144]. The presence of the Widmanstätten precipitation is a significant metallographic evidence, but it may not be a necessary condition if the meteoric iron became very hot during its fall to earth, which can produce a range of microstructures, such as some of those seen in parts of the Canyon Diablo meteorites: the iron is meteoritic but does not possess a Widmanstätten structure because that was partially destroyed as the meteorite fell to earth.

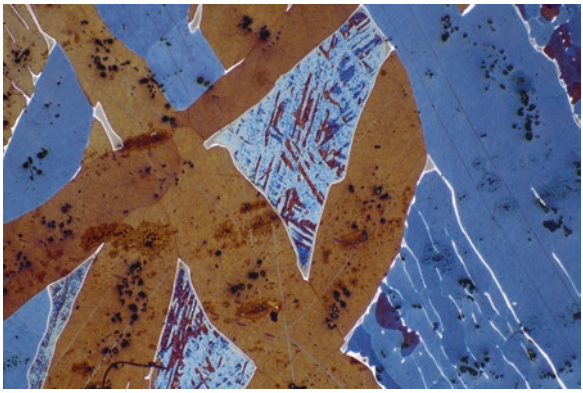

Fig. 5.40 Typical Widmanstätten microstructure of an iron-nickel alloy from Gibeon meteorite, Great Namaqualand, Namibia, Africa. The indigenous African population used many small fragments for jewellery. Kamacite is blue and taenite yellow, with a plessite field in the crosshatched pattern. Colour etched in Klemm's reagent I, magnification x230

Many meteorites in situ show signs of human activity in trying to hammer or dislodge parts of the iron from the main block for use. One in Mexico, the Descubridora meteorite, still has a broken copper chisel imbedded in a crack. The Inuit are also prominent users of meteoric iron, naming three meteorites as Woman (3 t), the Tent (30 t) and the Dog (0.4 t). From the Cape York meteorite of northwest Greenland, the Eskimos collected small fragments; one covered with vivianite was excavated by Danish archaeologists at Dundas, 100 km northwest of Savissivik. The presence of the ferrous phosphate, vivianite, on these artefacts probably originated from the reaction between the corroding meteorite and the decomposing bone from the midden where they were found [16, 161]. Iron can also be found in the native state on the Earth as telluric iron. Telluric iron is very rare and occurs in a limited number of deposits around the world, being found at Kassel in Germany, the Kola Peninsula and Russia and on Disko Island (Qeqertarsuaq), which lies to the west of Greenland. Only the Disko Island deposits appear to have been used by man [17].

The origins of the Iron Age in many parts of the Old World begin to become more apparent around 1200 BC; before that time the use of iron is very sporadic, but after 1200 BC, iron artefacts become much more numerous for reasons which are still part of a complex set of proximate causes, and there are many theories to account for the dominance it was to attain. The occasional adventitious production of iron in the process of smelting copper ores in which iron oxides have accidentally been reduced to metallic iron raises the possibility for the sporadic production of iron during the Bronze Age, as a rare material (Sect. 5.1.1).

A great deal remains to be learnt concerning mankind's march through the world of ferrous materials, but the picture that we have built up is more detailed than it was in the past, and old assumptions, such as the view that it was impossible to produce steel with a draft furnace or that the bloomery process only produced wrought iron, have been shown to be erroneous.

5.2.2 *Constituents of Ferrous Alloys*

The main importance of iron for technical purposes is that iron is one of the elements that crystallize in different structures depending on the external conditions of temperature and pressure. Such metals are called allotropic. Allotropic metals can transform from one crystalline structure to another during heating and cooling. At temperatures up to 910 °C, iron has a body-centred cubic (bcc) lattice structure, which is called alpha-iron (α_{Fe}) or ferrite, from the Latin word *ferrum* for iron. The metal is ferromagnetic up to its Curie temperature of 769 °C when it becomes paramagnetic but retains its body-centred cubic structure. This form of iron has once been called beta-iron (β_{Fe}), which has been dropped, because there is no crystalline change. Above 912 °C the bcc lattice of ferrite changes to a face-centred cubic (fcc) form, known as gamma-iron (γ_{Fe}) or austenite, in honour of the English metallurgist Robert Austin, which is stable up to 1410 °C. This face-centred cubic form is more easily hammered to shape than the body-centred cubic ferrite, because of a larger number of possible slip systems, but above all because there is a dynamic recovery and recrystallization of austenite during hot-work, which is why iron is worked red-hot by the blacksmith.

Above 1390 °C, it again becomes body-centred cubic (δ_{Fe}) by a spontaneous rearrangement of atoms and stays stable until 1534 °C, when pure iron melts. Pure iron could not be molten in ancient times, but cast iron could be, and was poured into moulds, notably in ancient China.

The allotropic transformation of iron is affected by alloying elements, which progressively lower or raise the transformation temperatures. The most significant alloying element is carbon. Carbon can dissolve in iron to a certain extent as an interstitial solid solution of carbon in the iron lattice. The solubility of carbon in iron at 727 °C is only 0.02%. Carbon is more soluble in austenite than ferrite, since the fcc lattice has larger interstices for the carbon atoms to fit into, allowing 2.11% of carbon to dissolve at 1148 °C. At room temperature, any excess carbon over 0.02% is precipitated as a second phase, the iron carbide cementite (Fe_3C), which nucleates at the ferrite grain boundaries, or as the two-phase eutectoid called pearlite.

Cementite, from the Latin word *caementum* for quarry stone, is an intermetallic compound of fixed composition with 6.67% of carbon and an orthorhombic crystal structure, which is very hard and brittle, with low tensile strength. Pearlite consists of a finely interspersed mixture of ferrite and cementite with its distinctive fine lamellar morphology. Sorby has described it as a constituent that "give rise to all the splendid colours of mother-of pearl" after being properly etched and observed at high magnification [162].

The light diffraction from the lamellar spacing can produce this optical effect, but in practice, pearlite appears dark after etching with attack etchants (see Chap. 3), because of the relief and shadowing between the attacked ferrite and the unscathed plate-like cementite, which can be resolved at higher magnifications (Fig. 5.41). Cementite is metastable and should decompose into iron and graphite under equilibrium conditions, but cementite shows long-life stability and equilibrium is not to be

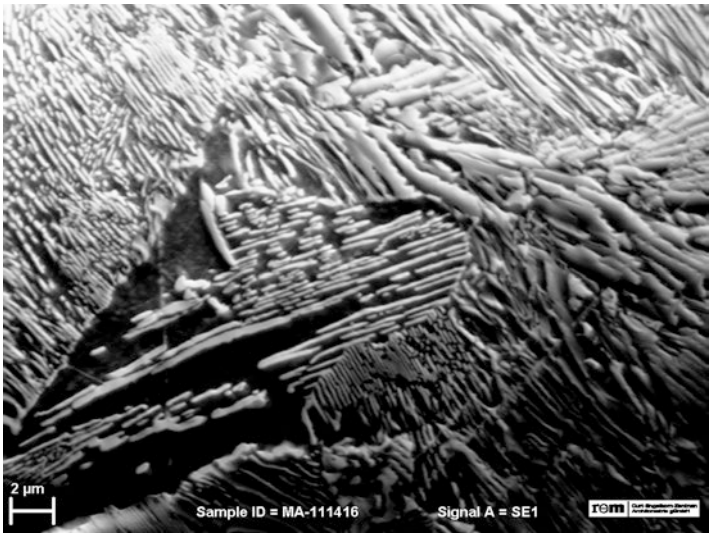

Fig. 5.41 Plates of cementite within a colony of pearlite in the microstructure of an Mongolian arrowhead. SEM secondary electron image after nital etch

achieved under normal conditions. Therefore the metastable Fe-Fe_3C system is relevant to the behaviour of most steels, as shown in the phase diagram of Fig. 5.42.

This phase diagram has been subject of many investigations with a long research history, for which reason the nomenclature and labelling can be confusing without additional information. In contrast to other constitutional diagrams, because of the great importance of iron and steel, all change points of phase transformations are labelled with letters, especially those that are important for the heat treatment of steels. The letter *A*, from the French word "arrêt" is additionally used with numerical subscripts. ABCD is the liquidus line and AHJEF is the solidus line. The change points of allotropic transformation are labelled A_2 for the Curie point, A_3 is the temperature of $\gamma_{Fe} \leftrightarrow \alpha_{Fe}$ and A_4 is the temperature of $\gamma_{Fe} \leftrightarrow \delta_{Fe}$.

As the carbon content increases, the proportion of pearlite in the alloy increases, reaching a maximum at 0.8%, which is called the eutectoid point, and the entire structure is made up of pearlite. The eutectoidal decomposition of austenite $\gamma_{Fe} \leftrightarrow \alpha_{Fe} + Fe_3C$ is the PSK line or A_1. Low-carbon steels, with less than 0.8% of carbon, are called hypoeutectoid steels, predominate in ancient ferrous metallurgy and consist of grains of ferrite with variable fractions of pearlite at the grain boundaries, shown in Fig. 5.43.

Ferrite can appear in different morphologies, and ancient iron objects often show proeutectoid acicular ferrite nucleated at the prior-austenite grain boundaries, as seen in Fig. 5.44, and which is called Widmanstätten ferrite. As the carbon content rises, the amount of pearlite in the steel increases. At 0.8% carbon, the alloy is almost entirely composed of pearlite as shown in Fig. 5.45.

At carbon contents above 0.8%, the microstructure is composed of pearlite and cementite, instead of ferrite and pearlite, and some examples will be given later in this section. These high-carbon steels are called hypereutectoid steels, which are

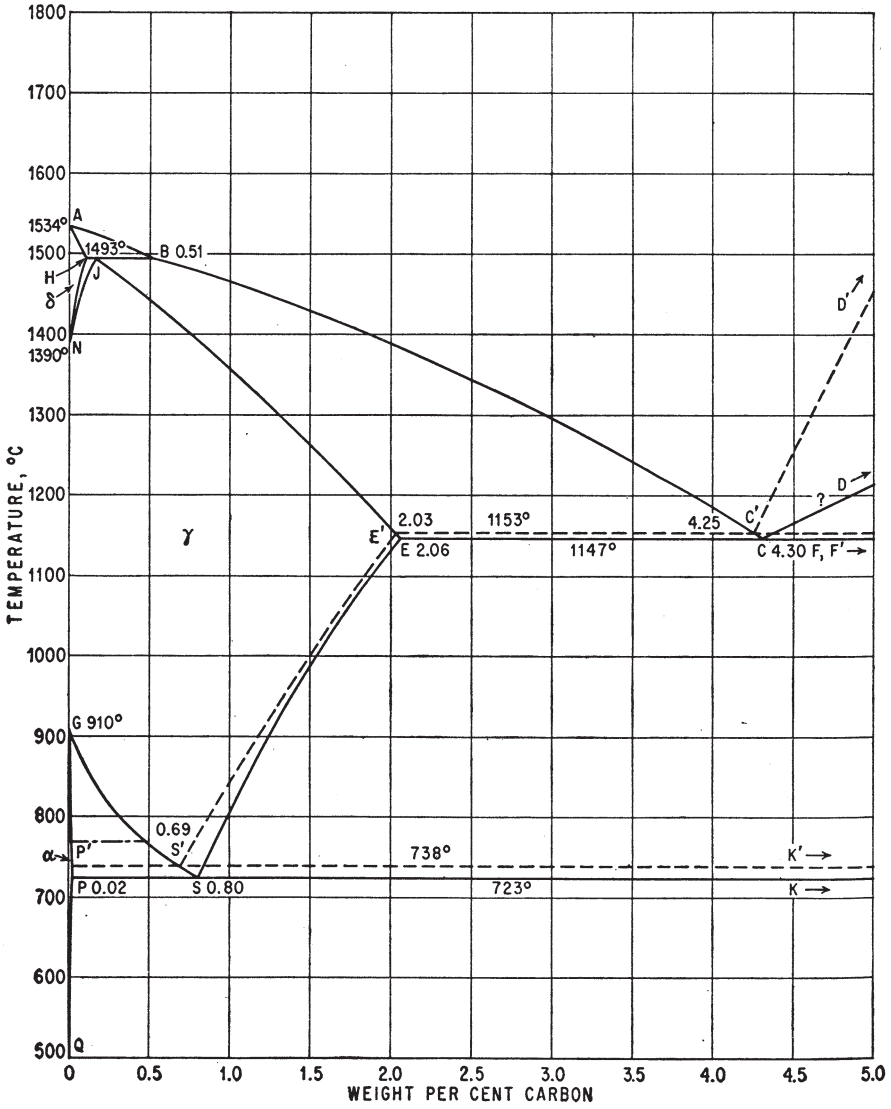

Fig. 5.42 The plain carbon-iron phase diagram, from Hansen and Anderko [69]

very difficult to work and tend to be rather brittle. In ancient metallurgy there were a number of different processes used to produce high-carbon steels, such as the well-known Wootz steels of ancient India, made in specially constructed ceramic crucibles, the steel being molten and solidified in the form of a small cake, which could then be forged into damascened blades or other decorative metalwork. An excellent account of the making and distribution of Wootz is given by Bronson [15]. An example of a small Wootz cake from the Deccan region of India is shown in Fig. 5.46.

The maximum solubility of carbon in γ_{Fe} is 2.11%, and this is the limiting composition separating steel and cast iron. The essential difference between steel and

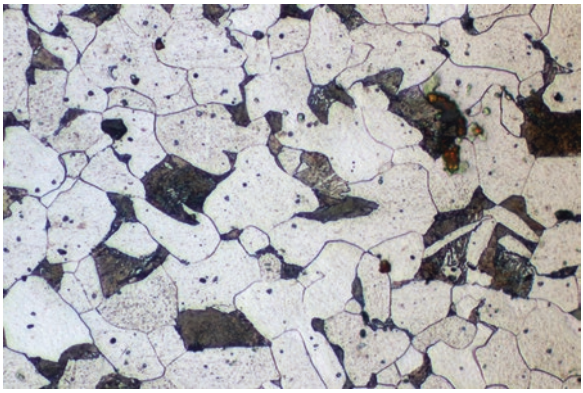

Fig. 5.43 Low-carbon steel with about 0.1% carbon showing white area of ferrite grains with small islands of pearlite. At low magnification, the spacing of the ferrite + pearlite lamellae which constitute the pearlite eutectoid cannot be resolved. Examination at x800 would enable the two phases in the eutectoid to be discerned. Etched in nital, magnification x200. The sample is from a historic collection made by Annotated Metallographic Samples Ltd in 1967 and is their sample N51

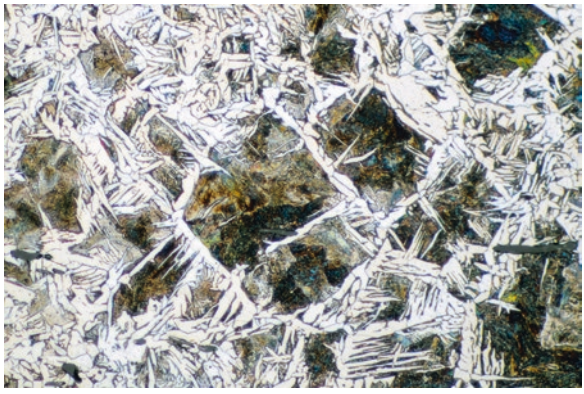

Fig. 5.44 A low-carbon steel with ferrite precipitated on prior-austenite grain boundaries with an infill of fine pearlite

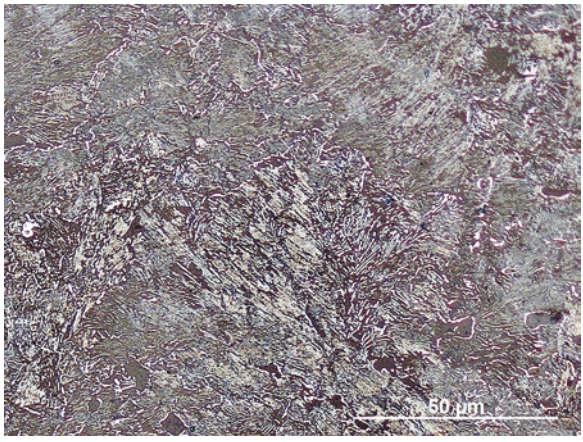

Fig. 5.45 Fine pearlite at the edge of an Early Iron Age (Ha C1) iron sword from the necropolis of Kaptol-Gradci near Požega, Croatia, with a maximum microhardness of 310 HV 0.1. Cementite remains white after etching with Klemm's reagent I

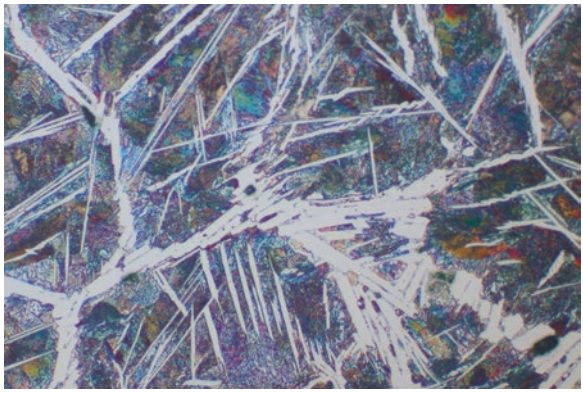

Fig. 5.46 Wootz steel cake from the Deccan region of India, site of Cunasamudram. The fine needles here are of cementite and the coloured infill is of pearlite. Carbon content about 1.1%. Etched in nital, magnification x140

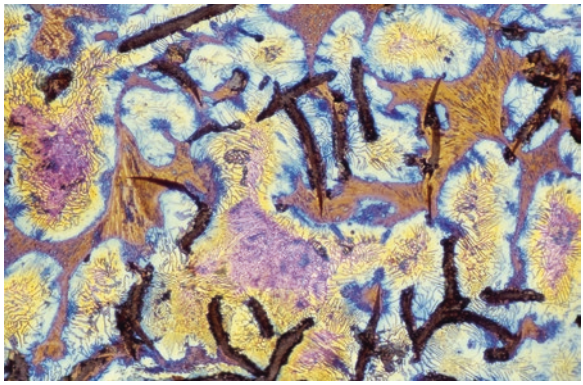

Fig. 5.47 Grey cast iron from the siege of Sandal Castle. The graphite flakes appear black, and the matrix is of pearlite with varying pearlite spacing. Etched in nital, polarized light, magnification x120

cast iron is the eutectic decomposition $L_{Fe} \leftrightarrow \gamma_{Fe} + Fe_3C$ at 1147 °C with hard and brittle cementite or weak graphite, instead of malleable γ_{Fe}. The eutectic structure of austenite and cementite is known as ledeburite I, named after the German metallurgist Adolf Ledebur, who was the first professor of metallurgy of iron at the Bergakademie Freiberg in Germany, where he first identified the eutectic in 1882. After the final eutectoidal decomposition of austenite, the microstructure of cast iron may consist of pearlite and cementite, which is called ledeburite II, but solidification rate and composition affect the formation of phases, and a variety of microstructures are possible (see Radzikowska [134]).

There are three principal types of cast iron: grey cast iron, white cast iron and mottled cast iron (mixed areas of white and grey). In the grey cast irons, there is free graphite in the structure, as some of the carbon is rejected from solution and solidifies as flakes of graphite, as the example in Fig. 5.47 shows. Grey cast irons are more commonly encountered in western metallurgy than the white variety. The free flakes of graphite can assume various morphologies, and the extent of the patterning of the graphite can be used to categorize the grey cast irons. The flakes of graphite can either be set in a matrix of pearlite or of pearlite and ferrite.

In white cast irons, all of the carbon is combined in the form of cementite and in dependence of their carbon contents; microstructures are hypoeutectic, eutectic or

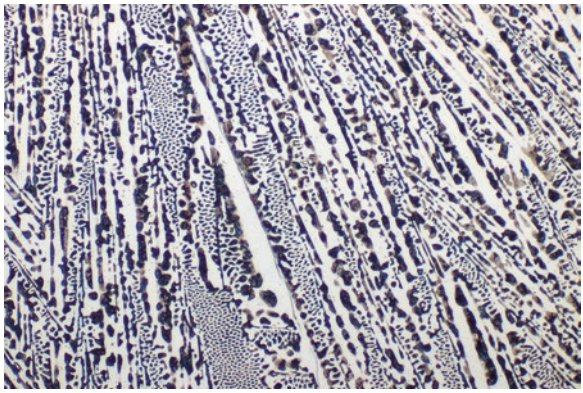

Fig. 5.48 Chinese Song Dynasty white cast iron with high carbon content, which must be in the region of 4% as there is a substantial amount of ledeburite present. Etched with nital, magnification x120

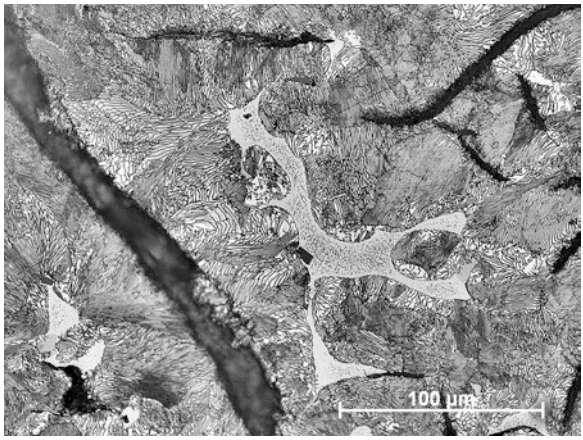

Fig. 5.49 Pressure tube of the fountain in the landscape park Wilhelmshöhe in Kassel, Germany, from the eighteenth century. Grey cast iron with steadite and graphite in a matrix of pearlite. Etched with nital

hypereutectic. Fig. 5.48 shows a typical microstructure of Chinese white cast iron. In the mottled group, both graphite flakes and cementite can be found in different regions of the sample artefact, sometimes deliberately made by chilling part of the mould and increasing the cooling rate, which favours the formation of cementite. Cast iron usually contains a large amount of impurities in addition to carbon, such as silicon, sulphur, phosphorus and manganese, and each of these elements produces changes in microstructure and properties (see Rostoker and Bronson [144]). Phosphorus forms a low-melting eutectic called steadite (Fig. 5.49). Steadite is generally a ternary eutectic of iron, iron phosphide (Fe_3P) and cementite, but for the same reasons mentioned below, graphite and a binary eutectic may occur [134]. Steadite is also a very brittle phase but is usually only present in small amounts scattered as isolated islands.

There are two important factors which influence the formation of graphite and cementite: solidification rate and composition. The iron-carbon phase diagram shows pearlite and cementite in the lower temperature field, from 695 °C to room temperature, although these are the phases that tend to form on rapid cooling; slow cooling, which is actually closer to the equilibrium conditions, supposed to be shown on these diagrams, favours graphite formation, so in this case the two phases

would be pearlite and graphite, not cementite and pearlite. To make a cast iron, the iron has to be smelted at temperatures higher than those used in the solid-state or bloomery process and under more reducing conditions. When these conditions are achieved, some of the carbon from the charcoal dissolves in the iron as it forms, lowering the melting point by several hundred degrees, so that the liquid iron can be tapped from the furnace and cast into moulds. The liquid iron contains between 3% and 5% of carbon in solution, and as the temperature drops, the solubility of the carbon in the iron is much less and can then appear in the iron either as cementite or as graphite. If the iron is relatively pure, then the type of iron which forms depends on the cooling rate: if quickly cooled, a white cast iron forms and, if slow, then grey. When such strong graphitizing constituents as silicon are present, the cementite may break down to graphite aggregate nodules in a matrix of ferrite and pearlite.

5.2.3 The Metallurgy of Pre-industrial Iron, Steel and Cast Iron

There is an essential difference between modern and early smelting of iron. The iron that was produced from so-called bloomery furnaces was not generally molten but made as an iron "bloom", a pasty mass of heterogeneous iron, slag, charcoal and sometimes unreacted ore, shown in Fig. 5.50.

The extraction of iron from its ores is much more difficult to achieve than the extraction of copper from the smelting of malachite or cuprite, because the conditions have to be more strongly reducing. It is essential to produce carbon monoxide at an adequate temperature in the smelting furnace, which is usually charged with iron ores, charcoal and maybe a flux to help to form a slag. Blooms are the products of a solid-state reaction, which is also called the direct process, because only one step is involved in producing malleable iron. Indeed blooms had to be reheated at

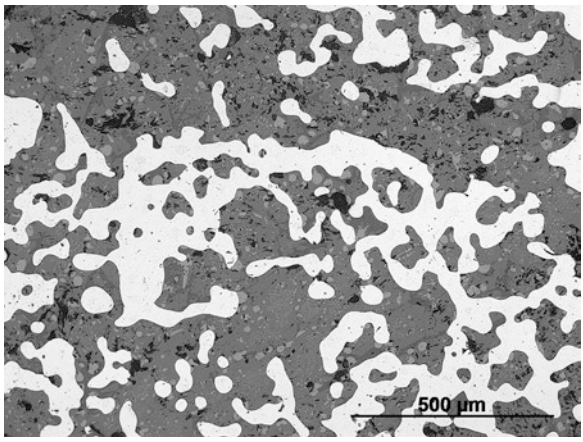

Fig. 5.50 Unconsolidated bloom from an Iron Age smelting site from Liel-Karlshof in the Upper Rhine Valley, Germany. The iron is entirely of coarse-grained ferrite (100 HV 1 ± 10) in a wüstite-fayalite matrix

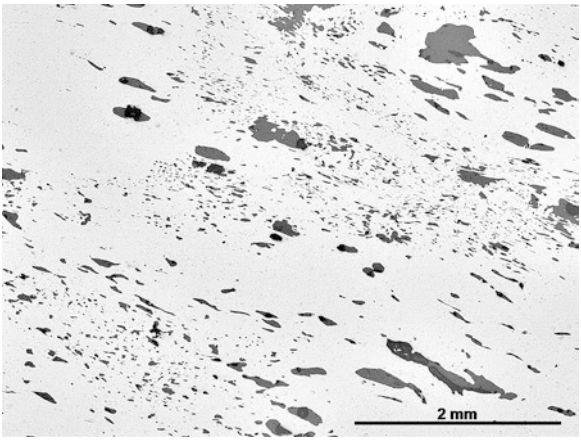

Fig. 5.51 Large volume fraction ($V_V = 9.2\% \pm 2.7$) of slag inclusions within a bi-pyramidal iron ingot from Waiblingen, Germany, dated to the Iron Age, containing wüstite dendrites within a fayalite matrix. The metal is mainly ferritic with some pearlite and a mean hardness of 185 HV 1 ± 20

smithing temperature (700–1100 °C) and forged to consolidate the cavities and to squeeze out the slag. As mentioned in Chap. 4, metal-slag separation usually has not been very effective, and bloomery iron consists of large volume fractions of slag inclusions distributed in the iron matrix, shown in Fig. 5.51.

Smaller blooms had to be welded together to produce useful artefacts or semi-finished products such as ingots for trade. It is the forging and consolidation of the bloom that convert the raw bloom into useable wrought iron, which still retains slag and may have variable carbon or phosphorus or other elemental constituents present, as a consequence of the inherent inhomogeneity of the pasty initial product (Fig. 5.52). The various alloying elements, such as carbon, phosphorus, nickel or sometimes arsenic and copper, coming from ore and charcoal, entered into solid solution by diffusion at high temperatures. Typical bulk concentrations of substitutional solutes in bloomery iron artefacts range between several hundred to several thousand mg kg^{-1}, whereas analytical methods with high lateral resolutions, such as EPMA, reveal local enrichments of several orders of magnitude, often concentrated at weld lines [118, 178]. An example is shown in Fig. 5.53 where the indistinct lines passing along the grains are due to copper and nickel distribution in the Anglo-Saxon sword.

The diffusivity of these elements is too small to achieve equilibrium during forging, and ferrite-stabilizing impurities such as phosphorus or arsenic raise the eutectoid temperature, whereas austenite stabilizers such as carbon or nickel reduce it. Therefore, it is somewhat like the hare and hedgehog, as ferrite has a higher solubility for phosphorus and carbon is more soluble in austenite. As a consequence, coarse-grained phosphorus segregated ferrite bands alternate with much finer pearlite-rich bands, parallel to the forging plane, as shown in Fig. 5.54. The regions of phosphorus segregations can be enhanced with selective etchants like Oberhoffer's or Klemm's reagent I (Fig. 5.55).

The repeated forging and hammering of iron results in a continual loss in weight as some metallic iron is oxidized and some slag expelled. The metal produced in the bloomery furnace is traditionally thought to be of low-carbon or carbon-free iron,

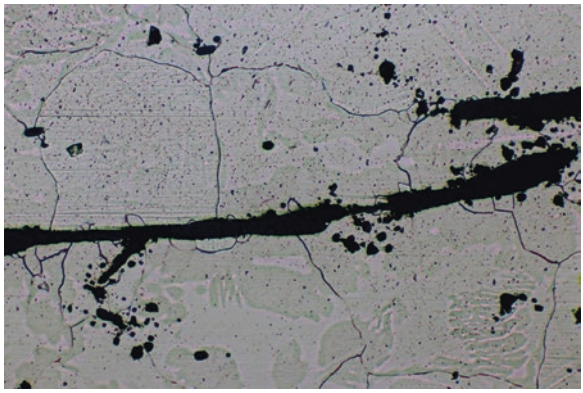

Fig. 5.52 Phosphoric iron from the Anglo-Saxon period. By focussing the microscope just below the plane of usual focus, the ghostlike phosphoric structure in the grains can be seen. Etched in nital, magnification x220

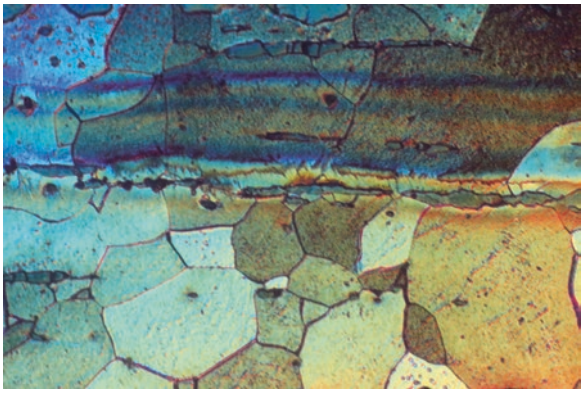

Fig. 5.53 Anglo-Saxon sword blade from Kent, showing principally ferrite grains with a number of bands passing along the length of the blade, some with a little carbon content or alloying impurities such as copper or nickel. Phosphorus may also be important here, as phosphoric iron had good working properties. Etched in nital, polarized with DIC, magnification x 180

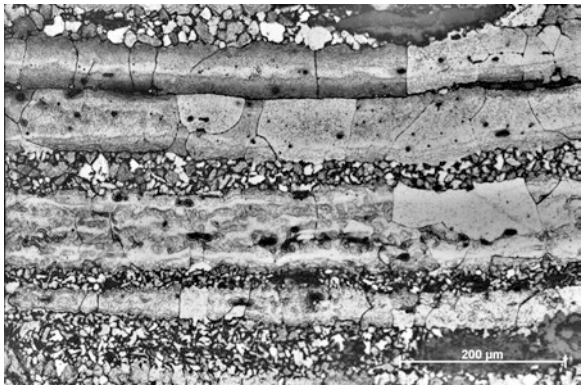

Fig. 5.54 Microstructure of a drawing knife from Iron Age oppidum of Manching, Germany, with coarse-grained ferrite (ASTM 1–7) and fine ferrite-pearlite bands (ASTM 9–14, max. 0.2% C). The ghost structure of phosphorus-rich parts is clearly visible. Microhardness HM varies from 1310 to 1650 N/mm^2. Etched with nital

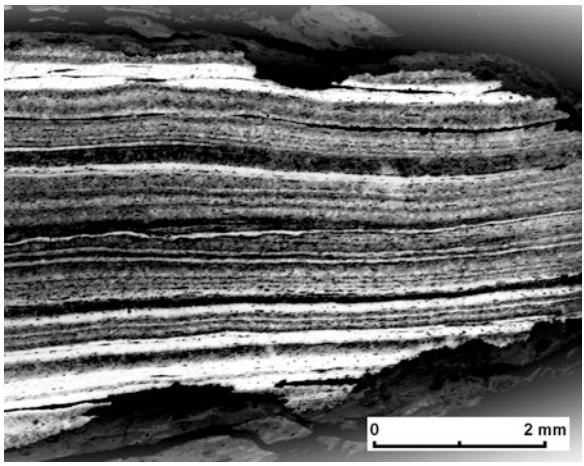

Fig. 5.55 Socketed axe from Iron Age oppidum of Manching, showing intensive banding after etching with Oberhoffer's reagent. The microstructure consists of irregular grains of ferrite (ASTM 4–9) with microhardness HM 1420–2250 N/mm^2

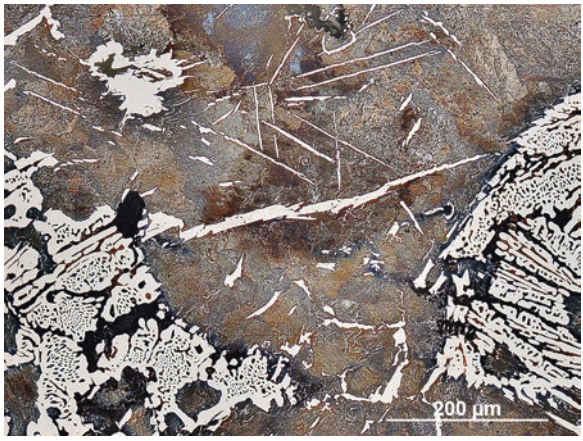

Fig. 5.56 Microstructure of an "ingot" from the Kyrenia shipwreck at the Cypriote coast shows relicts of hypoeutectic white cast iron with eutectic ledeburite (560 HV 1 ± 5) and proeutectoid cementite needles, indicating non-equilibrium conditions during the cooling of the billet, which is in fact a bloom. Etched with Klemm's reagent I

which has to be carburized in a second step. The belief that early iron could not represent the primary production of steel has been shown to be incorrect by a number of careful investigations. The great variations in the carbon content of the blooms are partially responsible for the heterogeneous pattern of use of steel and wrought iron. Indeed blooms are usually heterogeneously carburized, and many blooms show relicts of cast iron, shown in Fig. 5.56.

Cast iron has been inadvertently but very regularly produced in the bloomery process during all periods, but it has not been a deliberate final product in these cases. For a review, see Pleiner ([128], pp. 131–136 and pp. 230–250).

In China and the East, wrought iron was produced too, but the pre-eminent technological achievement was the early production of cast iron, rather than wrought iron. The earliest cast iron in China comes from the Henan and Shanxi provinces and dates to the ninth to early eighth century BC, whereas from the fifth century onwards, cast iron seemed to become more regularly available [66, 67]. Cast iron

can be molten at lower temperatures than wrought iron, allowing the Chinese to produce all manner of useful cast iron ornaments and implements, such as hoes, shovels, picks and ploughshares, which had a major impact on the agrarian economy of China (see Wagner [183]). In the west, the general date for the introduction of cast iron must have been between the eleventh and the thirteenth century AD, much later than China. The extent to which small amounts of cast iron may have been produced in the west before this time now seems to have been underestimated, and there are instances of the material being used much before this date, but in limited amounts.

Cast iron is not malleable and must be converted to wrought iron by fining to reduce the carbon content and all other impurities by oxidizing. In China a co-fusion process was also used in which bundles of cast and wrought iron bars were strongly heated so that the cast iron melted and some carbon diffusion took place. The process was repeated until relatively homogeneous steel was produced (Needham [107], pp. 26–30).

The joining together of smaller iron fragments or joining iron and steel together was carried out in the forge by reheating them to white heat and hammering them to effect an interfacial bond, called forge welding. High temperatures are required to liquefy the surface oxides, while fluxes may have to be added to avoid overheating the steels. One of the remarkable properties of the iron oxide coating that develops on heating is that it will not impede the welding of individual pieces of iron, whereas copper oxide prevents welding completely. This is just as well, since otherwise the utility of bloomery iron would have been terribly limited, especially since the temperatures required to actually melt pure iron are impossibly high. Forge welding is the basis for ancient blacksmithing technology to make deliberate composites of iron and steel and to form complex decorative composite artefacts such as pattern-welded weapons. When bloomery iron is used to create complex artefacts, such as a sword, the iron may be laminated or folded to create a microstructure consisting of many layers, as Fig. 5.57 illustrates.

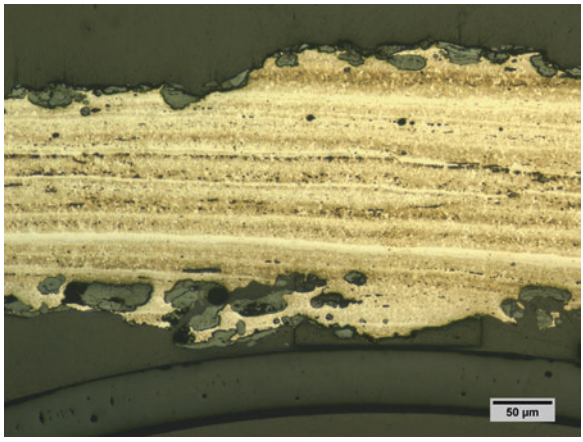

Fig. 5.57 Iron blade prepared from bloomery iron. Chinese Han Dynasty from Gansu Province. Here the iron blade has been made from a low-carbon steel bloom with many folds and prominent banding in copper and nickel segregation along the blade. Carbon content is about 0.3%

Deliberate longitudinally arranged alternating bands of different ferrous alloys have been used by the Celts for their swords from the third century BC onwards shown in Fig. 5.58, while the first "real" pattern-welded swords made of twisted ribbons of alternating ferrous alloys appear from the first century AD [127].

The ribbons were usually made of alternate mild steel strips and low-carbon but high phosphoric iron, to increase the optical contrast (see Lang [85]). Phosphoric iron was the most common variety of iron used in prehistoric blacksmithing technology and was intentionally selected for use in pattern-welded swords and blades, as shown in Fig. 5.59.

Complex pattern-welded weapons were made by using ribbons of steel twisted in opposite directions on both sides, with or without a central core and often with steel cutting edges (Fig. 5.60).

These were produced in Europe by Romans and Germans from the Roman Iron Age to the Viking Age when this technology almost died out due to the time, labour and materials required (see Pleiner [129]). Medieval cutlers produced pattern-welded knives up to the fourteenth century (Pleiner [129]). Southeast Asian blacksmiths composed high-nickeliferous iron, most probably meteoric iron, to produce

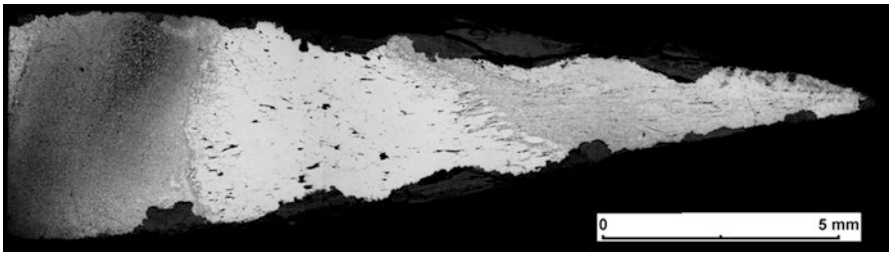

Fig. 5.58 Butt-welded sword blade from the Iron Age oppidum of Manching with carbon-rich and phosphorus-rich bands. The rod with the highest carbon content was used for the core and phosphoric iron for the edges. Etched with nital

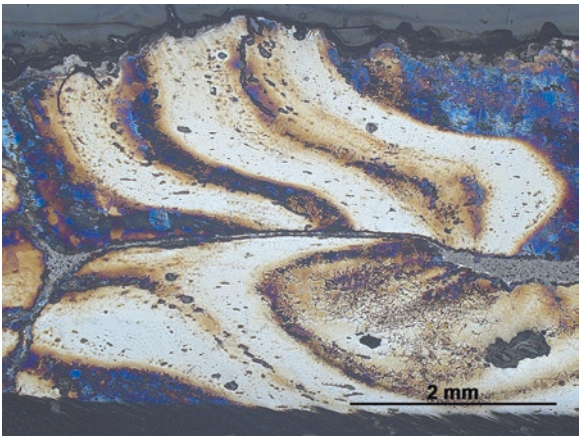

Fig. 5.59 Phosphorus-rich bands of a massive pattern-welded early medieval sword from Mannheim, Germany (see also Fig. 4.26), revealed by etching with Klemm's reagent I

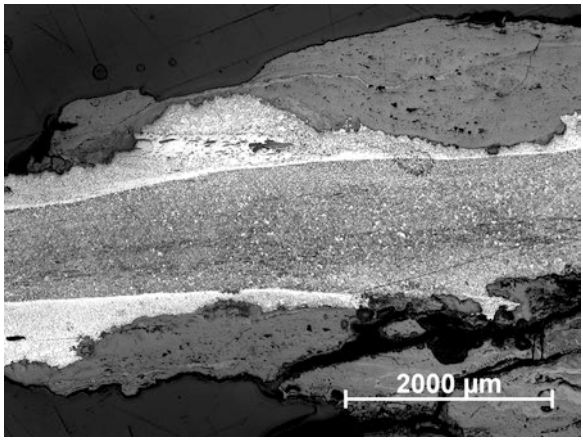

Fig. 5.60 Sword blade with a central steel core and pattern-welded side panels from the early medieval cemetery of Adelschlag in Bavaria. Nital etched

decorative laminated weapons, while Japanese swords can show a complex arrangement of multiple layers (see Rostoker and Bronson [144]).

5.2.4 Heat Treatment of Iron and Steel

The direct association between the upsurge of ferrous metallurgy and the demise of bronze as a material for basic commodities is a more complex one and has been discussed by various scholars over the past 30 years. Bronze and other copper alloys, in fact, continued to be used extensively up to modern times, but with further development of iron metallurgy, the use of iron gradually became predominant for a variety of reasons. Culturally determined factors were significant in iron production as well as locally available materials, as suitable iron ores are widespread. The latter has been considered to be the main reason why iron replaced copper alloys. Being much influenced by the Marxist view of history, Childe [25] put forward the theory that the rise of iron was responsible for the revolutions which took place at this time in the Old World, with power passing to larger groups of peoples of all backgrounds as a result of the invasions and loss of the old cities. In German Iron Age archaeology, the contrary model of the rise of new elites based on the control of iron ore deposits is still an extant theory, whereas in most cases, the potential for iron production based on the local availability of ore supplies still requires further research (see Dillmann et al. [49]).

Iron began to be used for ornamental or ritual purposes, and even in the Early Iron Age, iron became a marker of prestige and was not a product produced in vast quantities, but the transition was inevitable due to the increasing ability to produce iron relatively cheaply in sizable quantities and with specific properties.

A modern pure ferritic iron is relatively weak with a Brinell hardness of 60–100 HB, dependent of its grain size. The hardness of most ancient low-carbon wrought iron is from 80 to 200 HV, due to the local inhomogeneities in grain sizes and vary-

ing contribution of carbon and phosphorus. It is really the advent of steel which produces tools and weapons significantly harder than a good tin bronze and which can be configured to very precise specifications. The presence of alloying elements such as phosphorus hardens the ferrite but decreases its ductility and severely inhibits the carburization. The presence of phosphorus in iron has a very pronounced solid solution hardening effect, and 1% of phosphorus produces a Vickers hardness of about 200 HV, while 1.09% phosphorus gives already a value of about 250 HV (Tylecote and Gilmour [180], Fig. 4).

Phosphoric iron has been deliberately used in ancient times, but the major advantage of ferrous alloys is due to the allotropic transformation of iron. The distinctive structural phase transformations of steel by different quenching and annealing methods have generally been described in Chap. 4, but its application has been quite different in different epochs. It is well established that quench-hardening of iron implements had been practised during the European Iron Age, and tools such as files, hammers, axes or chisels were quite often quenched, independent of the carbon content, whereas weapons were not [149]. This practice of quench-hardening did not depend on the hardenability of the material but on the habit of the blacksmiths to undertake the operation for specific items. As mentioned in Chap. 4, tempering has not been practised at that period, but from the Roman Iron Age onwards, more sophisticated quenching and tempering of weapons can be observed. According to Wagner [183], Chinese blacksmiths produced quench-hardened swords from the third century BC, but it seems that these were not tempered deliberately.

It is not always true that martensite must be tempered, and in fact the martensite from the Japanese sword blade that has been shown in Fig. 4.50 is not tempered but kept as quenched [196]. The reason for the success of this technique is that the relative expansion of the martensite on quenching keeps this part of the blade under compression, as the slight curve of the blade is used to control the amount of compressive stress that the blade is effectively subjected to. This helps to prevent cracks from opening in the blade when the martensite cuts through hard materials, such as bone or wood, and is one of the key reasons for the superior toughness and cutting ability of the sword.

5.2.5 Microstructural Constituents of Iron Meteorites

Iron meteorites have been used by several early cultures and have recently been shown to have been used to make the famous iron dagger which was buried with King Tutankhamen in his tomb in the Valley of the Kings, long a subject of speculation as to whether it was made from smelted, man-made iron or from iron from outer space. Cornelli and co-workers [29] found 10.8% nickel with 0.58% cobalt, which supports the inference that the blade is indeed made from meteoritic iron.

We know that in Africa many small pieces of iron meteorites were collected. In some cultures, such as Greenland and Iceland, these were mounted in bone to be used as cutting tools. In Africa the large and dispersed Gibeon fall resulted in many

pieces being used in African jewellery; an example of a Gibeon meteorite microstructure has been shown in Fig. 5.40. The full story of this interesting conjunction of iron billions of years old and modern man has yet to be written.

Figure 5.61 shows the microstructure of a fragment of the Canyon Diablo meteorite which contains sufficient carbon to show the same structure of ferrite and pearlite as an ordinary steel. Other regions illustrate the development of plate martensite, typically found in steels containing over 0.6% of carbon which have been quenched rapidly.

The study of the microstructures of iron meteorites was greatly advanced by the three volumes published by Buchwald [16], which assembled the metallographic studies of iron meteorites going back nearly 100 years.

Those iron meteorites that contain less than 6% of nickel are often made of a single phase called kamacite, an alpha-phase (bcc) iron-nickel solid solution ($\alpha_{Fe,\,Ni}$). As the nickel content increases, the phase called taenite forms. Taenite is the gamma form of the fcc ($\gamma_{Fe,\,Ni}$) solid solution and contains between 25% and 50% nickel (Gaines et al. [57], p. 10). Taenite and interlocking plates of kamacite are responsible for the formation of the microstructure illustrated in one of the Great Namaqualand specimens above. This is the archetypal Widmanstätten structure, which was, in fact, first described by William Thomson in 1808 in the "Atti dell'Accademia della Scienze di Siena", although the common descriptive term is taken from the observations of Alois von Widmanstätten in the same year ([136], p. 150). The name for the variable mixture of kamacite and taenite is called plessite, and this phase is a very common component of iron meteorites, assuming a variety of textures and morphologies, as the illustrations in this section show.

Another major component of iron meteorites is cohenite, $(Fe,Ni,Co)_3C$, an orthorhombic mineral closely related to cementite, both of which were named around the

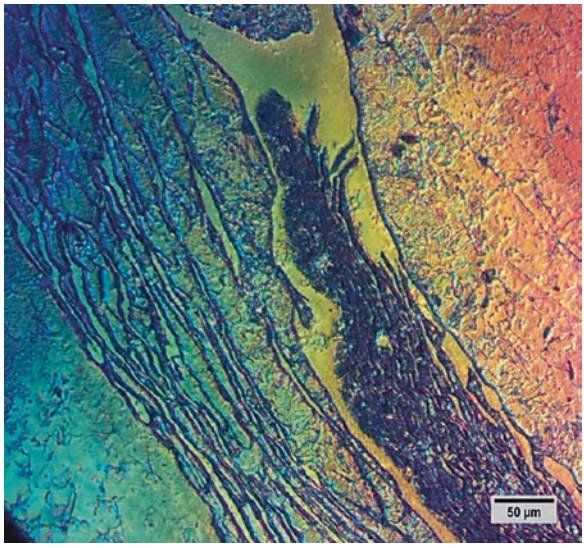

Fig. 5.61 Canyon Diablo meteorite under partial DIC illumination. Etched for 15 s in 2% nital. Due to the complexity of the phases here and the different polishing hardness, the DIC is particularly successful in revealing the phase differences. The long, stringy phases are called plessite, in a background of kamacite. Nearby, the darker-appearing phase is cloudy taenite. The fine lines in some regions may be Neumann bands

same time, as a result of metallurgical studies ([14], pp. 102–6). Unaltered prismatic crystals of schreibersite, $(Fe,Ni)_3P$, also called rhabdite, occur in many meteorites, accounting for some of the phosphorus content. Iron sulphide inclusions were observed in meteorites in 1766 by the Jesuit father, Domenico Troili, and named troilite, FeS, in his honour ([14], p. 106). Chemical analysis, about 100 years after this discovery, was able to show that this form of iron sulphide was different from pyrite or pyrrhotite.

As the meteorites plunge to earth through the atmosphere, many are subjected to considerable thermal shock and heating, resulting in Neumann bands and alteration of the microstructure of the surface zones of the meteorite. Neumann bands, which can also form in wrought iron artefacts, are parallel markings in ferrite which occur as a result of a large applied stress at temperatures below 500 °C (see Chap. 4). These bands will disappear when the iron is heated above about 600 °C. Neumann bands of the iron meteorite from Campo del Cielo, Argentina, have already been shown in Fig. 4.40.

Buchwald ([16], p. 457, Fig. 2) states that no class of iron meteorites can contain less than 5% of nickel, and Bühler ([18], p. 140) gives 5.3–5.7% for Class IIA which are the hexahedrites, which are less common. The conglomerate iron-silicate meteorites may have formed from the mixing of liquid metal and silicates at various depths within their celestial bodies. The pallasites consist of iron-nickel and olivine, while the mesosiderites represent mixtures of metal and achondritic stony material. The achondritic meteorites resemble terrestrial igneous rocks in composition with lumps of iron interspersed. Particular examples of the iron meteorites may actually display complex microstructures, which deviate substantially from the overall classification of them outlined above.

Vivianite formation could also be due to the weathering of phosphides or one of the phosphate minerals from the meteorites themselves such as farringtonite or graftonite, which are listed as possible components by Buchwald [16].

Metallographic examination in such cases should help to provide an answer, since there may be tiny remnants of meteoric minerals within the iron oxides, traces of nickel oxide within the corrosion layers, tiny rhabdites or pseudomorphic preservation of the Widmanstätten structure within the oxide layers, even after 50,000 years of burial.

The mineral that is most resistant to corrosion is schreibersite, $(Fe,Ni)_3P$. Even when everything else has been converted to oxide, tiny fragments of the phosphides may still be seen in metallographic section and can be analysed by electron microprobe. Buchwald [16] notes that chromite ($FeCr_2O_4$) and daubreelite ($FeCr_2S_4$) are also quite resistant but are rarely found in any event. Less resistant to corrosion are the high-nickel taenite rims of iron-nickel alloy, monocrystalline troilite, FeS and cohenite, $(Fe,Ni)_3C$. The martensitic component of plessite, although corroding relatively early, leaves a characteristic pseudomorphic pattern in the iron oxides. The iron sulphide (troilite) nodules which have been exposed to shock-reheating are very susceptible to corrosion since the finely disseminated iron and sulphide particles create local galvanic cells when penetrated by groundwaters. Because of simultaneous corrosion of iron and nickel, some meteorites can develop pentlandite, $(Fe,Ni)_9S_8$, crusts 5–20 microns thick. The extent of use of iron meteorites in prehistory remains to be researched in detail.

References

1. Al-Hassan, A.Y., Hill, D.R.: D.R.: Islamic Technology. An Illustrated History. Cambridge Univ. Press, Cambridge (1992)
2. Anguilano, L., Rehren, T., Müller, W., Rothenberg, B.: The importance of lead in the silver production at Riotinto (Spain). Revue d'archéometrie. **34**, 269–276 (2010)
3. Ashtakala, S., Pelton, A.D., Bale, C.W.: The Pb− Sb (Lead-Antimony) system. Bull. Alloy Phase Diagr. **2**(1), 86–89 (1981)
4. Bard, J.A., Sistare, G.H., McDonald, A.S.: Properties of gold and gold alloys. In: Metals Handbook, vol. 2, 9th edn, pp. 679–683. ASM International, Metals Park (1979)
5. Bartelheim, M., Contreras Cortés, F., Moreno Onorato, A., Murillo-Barroso, M., Pernicka, E.: The silver of the South Iberian El Argar Culture: a first look at production and distribution. Trab. Prehist. **69**(2), 293–309 (2012)
6. Bauer, O., Hansen, M.: Der Einfluß von dritten Metallen auf die Konstitution der Messinglegierungen III. Der Einfluß von Zinn. Z. Met. **22**(11), 387–391 (1930)
7. Bayley, J.: The production of brass in antiquity with particular reference to Roman Britain. In: Craddock, P.T. (ed.) 2000 Years of Zinc and Brass British Museum Occasional Papers 50, 2nd edn, pp. 7–26. British Museum, London (1998)
8. Bayley, J., Eckstein, K.: Silver refining – production, recycling, assaying. In: Sinclair, A., Slater, E., Gowlett, J. (eds.) Archaeological Sciences 1995. Oxbow Monograph 64, pp. 107–111. Oxbow Books, Oxford (1997)
9. Bayley, J., Rehren, T.: Towards a functional and typological classification of crucibles. In: La Niece, S., Hook, D., Craddock, P. (eds.) Metals and Mines: Studies in Archaeometallurgy, pp. 46–55. Archetype Publications in Association with the British Museum, London (2007)
10. Becker, L., Pilosi, L., Schorsch, D.: An Egyptian silver statuette of the Saite period: a technical study. Metrop. Mus. J. **29**, 37–56 (1994)
11. Berger, D.: Post-medieval printing type from Mainz and Oberursel, Germany, and the composition of early German type metal. Hist. Metall. **49**(2), 110–125 (2015)
12. Böhme, C.: Zur Frage der Härtung von Kupferwaffen und Geräten. Technische Beiträge zur Archäologie 2, pp. 126–130. Mainz (1965)
13. Bourgarit, D., Thomas, N.: From laboratory to field experiments: shared experience in brass cementation. Hist. Metall. **45**(1), 8–16 (2011)
14. Bray, W.: Techniques of gilding and surface enrichment in pre-Hispanic American metallurgy. In: La Niece, S., Craddock, P.T. (eds.) Metal Plating and Patination, pp. 182–192. Butterworth-Heinemann, Oxford (1993)
15. Bronson, B.: The Making and Selling of Wootz. A crucible Steel of India. Archeomaterials. **1**, 13–51 (1986)
16. Buchwald, V.F.: Handbook of Iron Meteorites. University of California Press, Los Angeles (1975)
17. Buchwald, V.F., Mosdal, G.: Meddelelser om Gronland. Man & Society, Copenhagen (1985)
18. Bühler, R.W.: Meteorite: Urmaterie aus dem interplanetaren Raum. Weltbild-Verlag, Augsburg (1992)
19. Butts, A., Coxe, C.D. (eds.): Silver. Economics, Metallurgy and Use. D Van Nostrand, Princeton (1967)
20. Chang, Y.A., Neumann, J.P., Mikula, A., Goldberg, D.: Phase Diagrams and Thermodynamic Properties of Ternary Copper-Metal Systems. International Copper Research Association Series on the Metallurgy of Copper, vol. 6, Washington (1979)
21. Cabri, L.J., Feather, C.E.: Platinum-iron alloys: a nomenclature based on a study of natural and synthetic alloys. Canad. Mineral. **13**(2), 117–126 (1975)
22. Cabri, L.J., Harris, D.C., Weiser, T.W.: Mineralogy and distribution of platinum-group mineral (PGM) placer deposits of the world. Explor. Min. Geol. **2**(5), 73–167 (1996)

23. Charles, J.A.: The coming of copper and copper-base alloys and iron. In: Wertime Th, A., Muhly, J.D. (eds.) The Coming of the Age of Iron, pp. 151–181. London, New Haven (1980)
24. Chen, K., Rehren, T., Mei, J., Zhao, C.: Special alloys from remote frontiers of the Shang Kingdom: scientific study of the Hanzhong bronzes from southwest Shaanxi, China. J. Archaeol. Sci. **36**, 2108–2118 (2009)
25. Childe, V.G.: The Bronze Age. Biblio and Tannen, New York (1930)
26. Coghlan, H.H.: Notes on the prehistoric metallurgy of copper and bronze in the Old World. In: Pitt Rivers Occasional Papers on Technology, vol. 4. Oxford University Press, Oxford (1975)
27. Colls, D., Domergue, C., Laubenheimer, F., Liou, B.: Les lingots d'étain de l'épave Port-Vendres II. Gallia. **33**, 61–93 (1975)
28. Cooke, S.R.B., Aschenbrenner, S.: The occurrence of metallic iron in ancient copper. J. Field Archaeol. **2**(3), 251–266 (1975)
29. Cornelli, D., Dorazio, M., Folco, L., El-Halwagy, M., Frizzi, T., Alberti, R., Capogrosso, V., Elnaggar, A., Hassan, H., Nevin, A., Porcelli, F., Rashed, M., Valentini, G.: The meteoritic origin of Tutankhamun's iron dagger blade. Meteorit. Planet. Sci. **51**(7), 1301–1309 (2016)
30. Cowell, M.R.: Analysis of cupro-nickel alloy used by Greek Bactrian coins. In: Maniatis Y (ed.) Proceedings of the 25th Archaeometry Conference, p 335–345. Athens (1989)
31. Cowell, M.R., Hyne, K.: Scientific examination of the Lydian precious metal coinages. In: Ramage, A., Craddock, P. (eds.) King Croesus' gold. Excavation at Sardis and the History of Gold Refining, pp. 169–174. British Museum Press, London (2000)
32. Cowell, M.R., Hyne, K., Meeks, N.D., Craddock, P.T.: Analyses of the Lydian electrum, gold and silver coinages. In: Oddy, A., Cowell, M. (eds.) Metallurgy in Numismatics 4. Royal Numismatic Society Special Publication 30, pp. 526–538. Royal Numismatic Society, London (1998)
33. Coxe, C.D., McDonals, A.S., Sistare, G.H.: Properties of silver and silver alloys. In: Metals Handbook, vol. 2, 9th edn, pp. 671–678. ASM International, Metals Park (1979)
34. Craddock, P.T.: Three thousand years of copper alloys: from bronze age to the industrial revolution. In: England, P.A., van Zelst, L. (eds.) Application of Science in the Examination of Works of Art, pp. 59–67. Museum of Fine Arts, Boston (1985)
35. Craddock, P.: Early Metal Mining and Production. Edinburgh University Press, Edinburgh (1995)
36. Craddock, P.T. (ed.): 2000 Years of Zinc and Brass British Museum Occasional Paper 50, 2nd edn. British Museum, London (1998a)
37. Craddock, P.T.: Zinc in classical antiquity. In: Craddock, P.T. (ed.) 2000 Years of Zinc and Brass British Museum Occasional Paper 50, 2nd edn, pp. 1–6. British Museum, London (1998b)
38. Craddock, P., Hook, D.: An economic history of the post-Medieval world in 50 ingots: the British Museum collection of ingots from dated wrecks. Br. Mus. Tech. Res. Bull. **6**, 55–68 (2012)
39. Craddock, P.T., Meeks, N.D.: Iron in ancient copper. Archaeometry. **29**(2), 187–204 (1987)
40. Craddock, P.T., Freestone, I.C., Gale, N.H., Meeks, N.D., Rothenberg, B., Tite, M.S.: The investigation of a small heap of silver smelting debris from Rio Tinto, Huelva, Spain. In: Craddock, P.T., Hughes, M.J. (eds.) Furnaces and Smelting Technology in Antiquity. British Museum Occasional Paper 48, pp. 199–217. British Museum, London (1985)
41. Craddock, P.T., La Niece, S.S., Hook, D.: Brass in the medieval Islamic world. In: Craddock, P.T. (ed.) 2000 Years of Zinc and Brass, pp. 73–114, British Museum Occasional Paper 50, revised edition. British Museum, London (1998)
42. Craddock, P., Cribb, J., Gale, N., Gurjar, I.: Sources of zinc in early India: the evidence of numismatics, trade and lead isotope analysis. In: Srinivasan, S., Ranganathan, S., Giumlia-Mair, A. (eds.) Metals and Civilizations. Proceedings of the International Conference Beginning of the Use of Metals and Alloys, BUMA VII, pp. 174–184. National Institute of Advanced Studies, Bangalore (2015)

43. Craddock, P.T., Hegde, K.T.M., Gurjar, L.K.: Early Indian Metallurgy: The Production of Lead, Silver and Zinc Through 3 Millennia in North West India. Archetype Publications, London (2017)
44. Crangle, J.: Some magnetic properties of platinum-rich Pt-Fe alloys. Journal de Physique et le Radium. **20**(2–3), 435–437 (1959)
45. Darling, A.S.: Gold-platinum alloys: a critical review. Platin. Met. Rev. **6**, 62–67, 106-111, (1962)
46. Davies, O.: Antimony bronze in Central Europe. Man. **35**, 86–89 (1935)
47. Davis, J.R. (ed.): ASM Specialty Handbook: Copper and Copper Alloys. ASM International, Materials Park (2008)
48. De Caro, T., Riccucci, C., Parisi, E.I., Faraldi, F., Caschera, D.: Ancient silver extraction in the Montevecchio mine basin (Sardinia, Italy): micro-chemical study of pyrometallurgical materials. Appl. Phys. A. **113**(4), 945–957 (2013)
49. Dillmann, P., Schwab, R., Bauvais, S., Brauns, M., Disser, A., Leroy, S., Gassmann, G., Fluzin, P.: Circulation of iron products in the north-alpine area during the end of the first Iron age (6th-5th c. BC): a combination of chemical and isotopic approaches. J. Archaeol. Sci. **87**, 108–124 (2017)
50. Domergue, C.: Les mines antiques. La production des métaux aux époques grecque et romaine. Antiqua et Picard, Paris (2008)
51. Dungworth, D., Nicholas, M.: Caldarium? An antimony bronze used for medieval and post-medieval cast domestic vessels. Hist. Metall. **38**(1), 24–34 (2004)
52. Dunkle, S.E., Craig, J.R., Lusardi, W.R.: Romarchite and associated phases as common corrosion products on pewter artifacts from marine archaeological sites. Geoarchaeol. Int. J. **19**(6), 531–552 (2004)
53. Ehrhardt, K.L.: Copper working technologies, contexts of use, and social complexity in the eastern woodlands of native North America. In: Roberts, B.W., Thornton, C. (eds.) Archaeometallurgy in Global Perspective. Methods and Syntheses, pp. 303–328. Springer, New York (2014)
54. Emmons, G.: Gold Deposits of the World. McGraw-Hill, New York (1937)
55. Fan, X., Harbottle, G., Gao, Q., Zhou, W., Gong, Q., Wang, H., Wang, C.: Brass before bronze? Early copper-alloy metallurgy in China. J. Anal. At. Spectrom. **27**(5), 821–826 (2012)
56. Frantz, J.H., Schorsch, D.: Egyptian red gold. Archaeomaterials. **4**, 133–152 (1990)
57. Gaines, R.V., Dana, J.D., Dana, E.S.: Dana's New Mineralogy: the System of Mineralogy of James Dwight Dana and Edward Salisbury, 8th edn. J. Wiley & Sons, New York (1997)
58. Gaspari, A., Lovenjak, M., Schwab, R.: The development of the water supply system in the roman Emona: state of research and results of the initial isotope analysis of the lead conduit. Antichita Altoadriatiche. **88**, 105–119 (2018)
59. Ghirshmann, R.: Fouilles de Sialk prés de Kashan 1933, 1934, 1937. P. Geuthner, Paris (1939)
60. Gilmour, B., Worrall, E.: Paktong: the trade in Chinese nickel brass to Europe. In: Hook, D.R. (ed.) Trade and Discovery: The Scientific Study of Artefacts from Post-Medieval Europe and Beyond. British Museum Occasional paper 109, pp. 259–282. British Museum, London (1995)
61. Goedecke, W.: Studien über die Vergütung der Legierungen des Systems Gold-Platin durch geringe Zusätze dritter Komponenten. In: Houben, H. (ed.) Festschrift zum Fünfzigjährigen Bestehen der Platinschmelze G. Siebert GmbH Hanau, pp. 72–100. Alberti, Hanau (1931)
62. Goodway, M.: Etruscan mirrors: a reinterpretation. In: Fleming, S.J., Schenck, H.R. (eds.) History of Technology: The Role of Metals MASCA Research Papers in Science and Archaeology 6, pp. 25–30. Museum Applied Science Center for Archaeology (MASCA), University of Pennsylvania, Philadelphia (1989)
63. Gordon, R., Knopf, R.: Late horizon silver, copper, and tin from Machu Picchu, Peru. J. Archaeol. Sci. **34**(1), 38–47 (2007)

64. Grissom, C.A.: The conservation of outdoor Zinc sculpture. In: Scott, D.A., Podany, J., Considine, B.B. (eds.) , pp. 279–304. Ancient & historic metals – conservation and scientific research, Singapore (1994)
65. Haedecke, K.: Gleichgewichtsverhältnisse bei der Messingherstellung nach dem Galmeiverfahren. Erzmetall. **26**(5), 229–233 (1973)
66. Han, R., Chen, J.: Casting iron in China. In: Humphris, J., Rehren, T. (eds.) The World of Iron, pp. 168–177. Archetype, London (2013)
67. Han, R., Duan, H.: An early iron-using centre in the ancient jin state region (8th – 3rd century BC). In: Mei, J., Rehren, T. (eds.) Metallurgy and Civilisation: Eurasia and Beyond, pp. 99–106. Archetype, London (2009)
68. Han, R., Ko, T.: Tests on brass items found at Jiangzhai, phase I. In: Linduff, K., Han, R., Sun, S. (eds.) The Beginnings of Metallurgy in China. Chinese studies 11, pp. 195–199. The Edwin Mellen Press, New York (2000)
69. Hansen, M., Anderko, K.: Constitution of Binary Alloys. McGraw-Hill Book Co., New York/Toronto/London (1958)
70. Hanson, D., Pell-Walpole, W.T.: Chill-Cast Tin Bronzes. Arnold, London (1951)
71. Hauptmann, A.: The Archaeometallurgy of Copper. Evidence from Faynan, Jordan. Natural Science in Archaeology. Springer, Berlin (2007)
72. Hauptmann, A., Maddin, R., Prange, M.: On the structure and composition of copper and tin ingots excavated from the shipwreck of Uluburun. Bull. Am. Sch. Orient. Res. **328**, 1–30 (2002)
73. Höppner, B., Bartelheim, M., Huijsmans, M., Krause, R., Martinek, K.-P., Pernicka, E., Schwab, R.: Prehistoric copper production in the Inn Valley, Austria, and the earliest copper in Central Europe. Archaeometry. **47**(2), 293–315 (2005)
74. Hosler, D.: Mesoamerican metallurgy: the perspective from the west. In: Roberts, B.W., Thornton, C. (eds.) Archaeometallurgy in Global Perspective. Methods and Syntheses, pp. 329–359. Springer, New York (2014)
75. Hunt Ortiz, M.A.: Prehistoric Mining and Metallurgy in South West Iberian Peninsula. British Archaeological Reports international series 1188. Archaeopress, Oxford (2003)
76. Jianjun, M.: The history, metallurgy and spread of paktong. Bulletin of the Metals Museum. **24**, 43–55 (1995)
77. Killick, D.: Cairo to cape: the spread of metallurgy through eastern and southern Africa. J. World Prehist. **22**(4), 399–406 (2009)
78. Klemm, R., Klemm, D.: Gold and Gold Mining in Ancient Egypt and Nubia: Geoarchaeology of the Ancient Gold Mining Sites in the Egyptian and Sudanese Eastern Deserts. Springer, Berlin (2013)
79. Krause, R.: Studien zur kupfer- und frühbronzezeitlichen Metallurgie zwischen Karpatenbecken und Ostsee. Vorgeschichtliche Forschungen 24. Verlag Marie Leidorf GmbH, Rahden (2003)
80. Kuleff, I., Pernicka, E.: Instrumental neutron activation analysis of native copper: some methodological considerations. J. Radioanal. Nucl. Chem. **191**(1), 145–161 (1995)
81. La Niece, S., Carradice, I.: White copper: the arsenical coinage of the Libyan revolt 241-238 BC. J. Hist. Metall. **23**(1), 9–15 (1989)
82. La Niece, S., Craddock, P.T.: Metal Plating and Patination. Butterworth-Heinemann, Oxford (1993)
83. La Niece, S., Meeks, N.: Diversity of goldsmithing traditions in the Americas and the old world. In: McEwan, C. (ed.) PreColumbian Gold. Technology, Style and Iconography, pp. 202–219. British Museum Press, London (2000)
84. La Niece, S., Ward, R., Hook, D., Craddock, P.: Medieval islamic copper Alloys. In: Jett, P., McCarthy, B., Douglas, J.G. (eds.) Scientific Research on Ancient Asian Metallurgy. Proceedings of the Fifth Forbes Symposium at the Freer Gallery of Art, pp. 248–254. Archetype, London (2012)
85. Lang, J.: The Anglo-Saxon cemetery at Dover Buckland, Kent, UK and the technology of some of the iron artefacts. In: Hauptmann, A., Modarressi-Tehrani, D. (eds.) Archaeometallurgy in

Europe III, Der Anschnitt Beiheft 26, pp. 185–192. Deutsches bergbaumuseum, Bochum (2015)
86. Lechtman, H.: Arsenic bronze: dirty copper or chosen alloy? A view from the Americas. J. Field Archaeol. **23**, 477–513 (1996)
87. Lechtman, H.: Middle Horizon bronze: centers and outliers. In: van Zelst, L. (ed.) Patterns and Process: A Festschrift in honor of Dr. Edward V. Sayre, pp. 246–268, Washington, DC (2003)
88. Lechtman, H.: Andean Metallurgy in Prehistory. In: Roberts, B.W., Thornton, C. (eds.) Archaeometallurgy in Global Perspective. Methods and Syntheses, pp. 361–422. Springer, New York (2014)
89. Ledebur, A.: Die Legierungen in ihrer Anwendung für gewerbliche Zwecke. Krayn, Berlin (1898)
90. Leinfelder, K.F., O'Brien, W.J., Ryge, G., Fairhurst, C.W.: Hardening of high fusing gold alloys. J. Dent. Res. **45**, 392–396 (1966)
91. Lutz, J., Schwab, R.: The early Iron age hoard from Fliess in Tyrol and ore resources in the eastern Alps. In: E. Pernicka, R. Schwab (eds.) Under the volcano. Forschungen zur Archäometrie und Altertumswissenschaft 5. pp 25–34, Verlag Marie Leidorf, Rahden/Westf. (2014)
92. Lord, J.O.: Alloy Systems; an Introductory Text. Pitman, New York (1949)
93. Maréchal, J.R.: Prähistorische Metallurgie: Zur Frühgeschichte der Metallurgie/ Considerations sur la metallurgie prehistorique. Aachen (1962)
94. Massalski, T.B. (ed.): Binary alloy phase diagrams 1–2, Ohio. American Society of Metals, Materials Park (1986)
95. McKerrell, H., Stevenson, R.B.K.: Some analyses of Anglo-Saxon and associated oriental silver coinage. In: Hall, E.T., Metcalf, D.M. (eds.) Methods of Chemical and Metallurgical Investigation of Ancient Coinage. Royal Numismatic Society Special Publication 8, pp. 195–209. Royal Numismatic Society, London (1972)
96. Meeks, N.: Surface characterization of tinned bronze, high-tin bronze, tinned iron and arsenical bronze. In: La Niece, S., Craddock, P.T. (eds.) Metal Plating and Patination, pp. 247–275. Butterworths, Oxford (1993)
97. Melikian-Chirvani, A.S.: The white bronzes of early Islamic Iran. Metrop. Mus. J. **9**, 123–151 (1974)
98. Meliksetian, K., Pernicka, E.: Geochemical characterisation of Armenian Early Bronze Age metal artefacts and their relation to copper ores. In: Hansen, S., Hauptmann, A., Motzenbäcker, I., Pernicka, E. (eds.) Von Maikop bis Trialeti. Gewinnung und Verbreitung von Metallen und Obsidian in Kaukasien im 4.-2. Jt. v. Chr. Beiträge des Internationalen Symposiums in Berlin vom 1.-3. Juni 2006. Kolloquien zur Vor- und Frühgeschichte 13, Bonn, pp. 41–58 (2010)
99. Meyers, P.: Production of silver in antiquity: ore types identified based upon elemental compositions of ancient silver artifacts. In: Van Zelst, L. (ed.) Patterns and Process: A Festschrift in honor of Dr. Edward V. Sayre, pp. 270–288, Washington DC (2003)
100. Middelton, A.P., Hook, D.R., Humphrey, M.: Scientific examination of some ceramic materials and samples of litharge. In: Ramage, A., Craddock, P. (eds.) King Croesus' gold. Excavation at Sardis and the History of Gold Refining, pp. 157–168. British Museum Press, London (2000)
101. Montero-Ruiz, I., Perea, A.: Brasses in the early metallurgy of the Iberian Peninsula. In: La Niece, S., Hook, D., Craddock, P. (eds.) Metals and Mines: Studies in Archaeometallurgy, pp. 136–139. Archetype Publications in association with the British Museum, London (2007)
102. Moorey, P.R.S.: The archaeological evidence for metallurgy and related technologies in Mesopotamia, c 5500-2100 BC. Iraq. **44**, 13–38 (1982)
103. Moorey, P.R.S.: Ancient Mesopotamian Materials and Industries: the Archaeological Evidence, Eisenbrauns, Winona Lake, Ind (1999)
104. Muhly, J.D.: The bronze age setting. In: Wertime Th, A., Muhly, J.D. (eds.) The Coming of the Age of Iron, pp. 25–67. Yale University Press, New Haven/London (1980)

105. Muhly, J.D.: Çayönü Tepesi and the beginnings of metallurgy in the ancient world. In: Hauptmann, A., Pernicka, E., Wagner, G.A. (eds.) Archäometallurgie der Alten Welt/Old world archaeometallurgy. Der Anschnitt Beiheft 7, pp. 1–11. Deutsches Bergbau-Museum, Bochum (1989)
106. Murillo-Barroso, M., Montero-Ruiz, I., Rafel, N., Hunt Ortiz, M.A., Armada, X.-L.: The macro-regional scale of silver production in Iberia during the first millennium BC in the context of Mediterranean contacts. Oxf. J. Archaeol. **35**(1), 75–100 (2016)
107. Needham, J.: The Development of Iron and Steel Technology in China. Newcomen Society, London (1958)
108. Newbury, B.D., Notis, M.R., Stephenson, B., Cargill III, G.S., Stephenson, G.B.: The astrolabe craftsmen of Lahore and early brass metallurgy. Ann. Sci. **63**(2), 201–213 (2006)
109. Nezafati, N., Pernicka, E.: Early silver production in Iran. Iranian Archaeol. **3**, 38–45 (2012)
110. Northover, J.P.: The Exploration of Long-Distance Movement of Bronze in Bronze and Early Iron Age Europe, vol. 19, pp. 45–72. Bulletin of the Institute of Archaeology / University of London (1982)
111. Northover, P.: Properties and use of arsenic-copper alloys. In: Hauptmann, A., Pernicka, E., Wagner, G.A. (eds.) Archäometallurgie der Alten Welt/Old world archaeometallurgy. Der Anschnitt Beiheft 7, pp. 111–118. Deutsches Bergbau-Museum, Bochum (1989)
112. Northover, J.P.: Analysis of copper alloy metalwork from Arbedo TI. In: Schindler, M.P. (ed.) Der Depotfund von Arbedo TI und die Bronzedepotfunde des Alpenraums vom 6. bis zum Beginn des 4. Jh. v. Chr.. Antiqua 30, pp. 289–315. Schweizerische Ges. für Ur-und Frügeschichte, Basel (1998)
113. Northover, J.P.: Interdisziplinäre Untersuchungen zu den Metallfunden. In: Bauer, I., Ruckstuhl, B., Speck, J. (eds.) Die spätbronzezeitlichen Ufersiedlungen von Zug-Sumpf 3/1, Die Funde der Grabungen 1923–37, pp. 102–143. Kantonales Museum für Urgeschichte Zug, Zug (2004)
114. Oddy, A.: Gilding of metals in the Old World. In: La Niece, S., Craddock, P.T. (eds.) Metal Plating and Patination, pp. 171–181. Butterworth-Heinemann, Oxford (1993)
115. Ogden, J.: Aesthetic and technical considerations regarding the colour and texture of ancient goldwork. In: La Niece, S., Craddock, P.T. (eds.) Metal Plating and Patination, pp. 39–49. Butterworth-Heinemann, Oxford (1993)
116. Ogden, J.: Metals. In: Nicholson, P.T., Shaw, I. (eds.) Ancient Egyptian Materials and Technology, pp. 148–176. Cambridge University Press, Cambridge (2000)
117. Panseri, C., Leoni, M.: The Manufactering Technique of Etrusan Mirrors. Stud. Conserv. **3**, 49–63 (1957)
118. Panseri, C., Leoni, M.: Research on an iron spearhead from the Etruscan Sanctury of Fanum Voltumnae, fourth to third centuries B.C. In: Levey, M. (ed.) Archaeological Chemistry. A Symposium, pp. 205–229. University of Pennsylvania Press, Philadelphia (1967)
119. Parker, A.J.: Ancient Shipwrecks of the Mediterranean and the Roman Provinces. British Archaeological Reports International Series 580. Tempus Reparatum, Oxford (1992)
120. Percy, J.: The Metallurgy of Lead, Including Desilverization and Cupellation. Murray, London (1870)
121. Pernicka, E.: Die Ausbreitung der Zinnbronze im 3. Jahrtausend. In: Hänsel, B. (ed.) Mensch und Umwelt in der Bronzezeit Europas, pp. 135–147. Oetker-Voges, Kiel (1998)
122. Pernicka, E., Bachmann, H.-G.: Archäometallurgische Untersuchungen zur antiken Silbergewinnung in Laurion III. Das Verhalten einiger Spurenelemente beim Abtreiben des Bleis. Erzmetall. **36**(12), 592–597 (1983)
123. Pernicka, E., Eibner, C., Öztunalı, Ö., Wagner, G.A.: Early bronze age metallurgy in the Northeast Aegean. In: Wagner, G.A., Pernicka, E., Uerpmann, H.-P. (eds.) Troia and the Troad: Scientific Approaches, pp. 143–172. Springer, Berlin/Heidelberg/New York (2003)
124. Pigott, V.C.: Looking east: the coming of tin bronze in the context of bronze age trans-eurasian exchange – an overview. In: Jett, P. (ed.) Scientific Research on Ancient Asian Metallurgy: Proceedings of the Fifth Forbes Symposium at the Freer Gallery of Art, pp. 85–100. Archetype, London (2012)

125. Photos, E.: The question of meteoritic versus smelted nickel-rich iron: archaeological evidence and experimental results. World Archaeol. **20**(3), 403–421 (1989)
126. Plazas de Nieto, C., Falchetti de Saenz, A.M.: El Dorado: Colombian Gold. Australian Art Exhibition Corp. Ltd, Sydney (1978)
127. Pleiner, R.: The Celtic Sword. Clarendon Press, Oxford (1993)
128. Pleiner, R.: Iron in archaeology: the European Bloomery smelters. Archeologický Ústav AV ČR, Praha (2000)
129. Pleiner, R.: Iron in Archaeology: Early European Blacksmiths. Archeologický Ústav AV ČR, Praha (2006)
130. Pollard, A.M., Heron, C.: The chemical study of metals – the European medieval and later brass industry. In: Pollard, A.M., Heron, C. (eds.) Archaeological Chemistry, pp. 196–238. The Royal Society of Chemistry, Cambridge (1996)
131. Ponting, M.J.: From Damascus to Denia: scientific analysis of three groups of Fatimid period metalwork. Hist. Metall. **37**(2), 85–105 (2003)
132. Pryce, T.O., Baron, S., Bellina, B.H.M., Bellwood, P.S., Chang, N., Chattopadhyay, P., Dizon, E., Glover, I.C., Hamilton, E., Charles, F.W., Higham, C.F.W., Kyaw, A.A., Laychour, V., Natapintuk, S., Nguyen, V., Pautreau, J.-P., Pernicka, E., Pigott, V.C., Pollard, M., Pottier, C., Reinecke, A., Sayavongkhamdy, T., Souksavatdy, V., White, J.: More questions than answers: the Southeast Asian Lead Isotope Project 2009–2012. J. Archaeol. Sci. **42**, 273–294 (2014)
133. Radivojević, M., Rehren, T., ShahinaFarid, S., Pernicka, E., Camurcuoğlu, D.: Repealing the Çatalhöyük extractive metallurgy: The green, the fire and the 'slag. J. Archaeol. Sci. **86**, 101–122 (2017)
134. Radzikowska, J.M.: Metallography and microstructures of cast iron. In: Vander Voort, G.F. (ed.) Metallography and Microstructure ASM Handbook 9, pp. 565–587. ASM International, Materials Park (2004)
135. Ramage, A., Craddock, P.: King Croesus' Gold: Excavations at Sardis and the History of Gold Refining. British Museum, London (2000)
136. Rapp Jr., G.: On the origins of copper and bronze alloying. In: Maddin, R. (ed.) The Beginning of the Use of Metals and Alloys, pp. 21–27. MIT Press, Cambridge (1988)
137. Rapson, W.S., Groenwald, Y.: Gold Usage. Academic, London (1978)
138. Ravich, I.G., Ryndina, N.V.: Early copper-arsenic alloys and the problems of their use in the Bronze Age of the North Caucasus. Bulletin of the Metals Museum. **23**, 1–18 (1995)
139. Rehren, T., Kraus, K.: Cupel and crucible: the refining of debased silver in the Colonia Ulpia Traiana, Xanten. J. Rom. Archaeol. **12**, 263–272 (1999)
140. Rehren, T., Hess, K., Philip, G.: Auriferous silver in Western Asia: ore or alloy? Hist. Metall. **30**(1), 1–10 (1996)
141. Renzi, M., Montero-Ruiz, I., Bode, M.: Non-ferrous metallurgy from the Phoenician site of La Fonteta (Alicante, Spain): a study of provenance. J. Archaeol. Sci. **36**(11), 2584–2596 (2009)
142. Riederer, J.: Metallanalysen Nürnberger Messingerzeugnisse der Vischer-Werkstatt. Berliner Beiträge zur Archäometrie. **8**, 89–99 (1983)
143. Roeder, J.F., Notis, M.R.: Phase equilibria in the Cu-rich corner of the Cu-As-Sn system. Z. Met. **78**(11), 802–809 (1987)
144. Rostoker, W., Bronson, B.: Pre- industrial Iron. Archeomaterials Monograph 1. Archeomaterials, Philadelphia (1990)
145. Rothenhöfer, P., Hanel, N.: The romans and their lead – tracing innovations in the production, distribution, and secondary processing of ancient metal. In: Burmeister, S., Hansen, S., Kunst, M., Müller-Scheeßel, N. (eds.) Metal Matters: Innovative Technologies and Social Change in Prehistory and Antiquity. Menschen – Kulturen – Traditionen 12, ForschungsCluster 2, pp. 273–282. M. Leidorf, Rahden/Westf (2013)
146. Rusu, M.: Bemerkungen zu den großen Werkstätten- und Giessereifunden aus Siebenbürgen. In: Lorenz, H. (ed.) Studien zur Bronzezeit. Festschrift für Wilhelm Albert v. Brunn, pp. 375–402. Von Zabern, Mainz (1981)
147. Samans, C.H.: Metallic Materials in Engineering. The Macmillian Company, New York (1963)

148. Schlosser, S., Reinecke, A., Schwab, R., Pernicka, E., Sonetra, S., Laychour, V.: Early Cambodian gold and silver from Prohear: composition, trace elements and gilding. J. Archaeol. Sci. **39**(9), 2877–2887 (2012)
149. Schwab, R.: Untersuchungen zur Technologie und Herkunft eiserner Werkzeuge und Waffen. In: Sievers, S., Leicht, M., Ziegaus, B. (eds.) Ergebnisse der Ausgrabungen 1996–1999 in Manching-Altenfeld. Die Ausgrabungen in Manching 18, pp. 251–293. Reichert, Wiesbaden (2013)
150. Schwab, R.: Resources and recycling: copper alloys and non-ferrous metalworking in the oppidum of manching (Germany). In: Pernicka, E., Schwab, R. (eds.) Under the Volcano. Forschungen zur Archäometrie und Altertumswissenschaft 5, pp. 175–188. M. Leidorf, Rahden/Westf (2014)
151. Schwab, R.: Supply and demand: metal recycling in Southern Germany at the end of the late Iron Age. In: Montero, I., Perea, A. (eds.) Archaeometallurgy in Europe IV. Bibliotheca Prahestorica Hispana 33, pp. 227–236. Consejo Superior de Investigaciones Científicas, Instituto de Historia, Madrid (2017a)
152. Schwab, R.: Archäometallurgische Untersuchung von Weichlot an der Trierer Silberkanne. In: Kaufmann-Heinimann, A., Martin, M. (eds.) Die Apostelkanne und das Tafelsilber im Hortfund von 1628. Trierer Silberschätze des 5. Jahrhunderts Trierer Zeitschrift Beiheft 35, pp. 171–173. Rheinisches Landesmuseum Trier, Trier (2017b)
153. Scott, D.A.: Analysis of two Hittite art objects: a cupronickel bull and a cupronickel cylinder seal. Unpublished report to the UCL Conservation Deparmment, UCL London (1982)
154. Scott, D.A.: Metallography and microstructure of ancient and historic metals, Getty Conservation Inst., J. Paul Getty Museum Malibu (1991)
155. Scott, D.A.: Technical Report to the Metropolitan Museum on the examination of a sample from an Egyptian silver statuette. (unpublished internal document). Personal communication to RE Stone (1994)
156. Scott, D.A.: Goldwork of pre-Columbian Costa Rica and Panama: a technical study. In: Vandiver, P.B., Druzik, J.R., Madrid, J.L.G., Freestone, I.C., Wheeler, G.H. (eds.) Materials Issues in Art and Archaeology IV, pp. 265–275. Materials Research Society, Pittsburgh (1995)
157. Scott, D.A.: A note on the metallographic preparation of ancient lead. Stud. Conserv. **41**(1), 60–62 (1996)
158. Scott, D.A.: Technical examination of ancient South American metals: some examples from Colombia, Peru and Ecuador. Boletín Museo del Oro. **44-45**, 79–105 (1998)
159. Scott, D.A.: Ancient Metals: Microstructure and Metallurgy Vol 1. CSP Press, Los Angeles (2011)
160. Scott, D.A.: Gold and Platinum Metallurgy of Ancient Colombia and Ecuador. CSP Press, Los Angeles (2012)
161. Scott, D.A., Eggert, G.: The vicissitudes of vivianite as pigment and corrosion product. Stud. Conserv. **52**(sup1), 3–13 (2007)
162. Smith, C.S.: A History of Metallography. The University of Chicago Press, Chicago (1960)
163. Smith, C.S.: The interpretation of microstructures of metallic artefacts. In: Application of Science in the Examination of Works of Art, pp. 20–52. Museum of Fine Arts, Boston (1965)
164. Smith, C.S.: Metallographic study of early artifacts made from native copper. In: Suchodolski, B. (ed.) Actes du XIe Congre's International d'Histoire Des Sciences Proceedings, International Congress on the History of Science, pp. 237–243. Zakład Historii Nauki i Techniki, Warsaw (1968)
165. Smith, D.L., Burnett, A.P., Brooks, S., Anthony, D.H.: Iron-platinum hardening in casting gold for use with platinum. J. Dent. Res. **49**, 283–288 (1970)
166. Sperl, G.: Zur Urgeschichte des Bleis. Z. Met. **81**(11), 799–801 (1990)
167. Stumpfl, E.F., Clark, A.M.: Electron-probe microanalysis of gold-platinoid concentrates from southeast Borneo. Trans. Inst. Min. Metall. **74**, 933–946 (1965)

168. Swaddling, J., Craddock, P., La Niece, S., Hockey, M.: Breaking the mould. The overwrought mirrors of Etruria. In: Ridgway, D., Serra Ridgway, F.R., Pearce, M., Herring, E., Whitehouse, R.D., Wilkins, J.B. (eds.) Ancient Italy in its Mediterranean Setting. Accordia Specialist Studies on the Mediterranean 4, pp. 117–140. Accordia Research Institute, London (2000)
169. Swartzendruber, L.J.: Cu-Fe (Copper-Iron). In: Subramanian, P.R., Chakrabarti, D.J., Laughlin, D.E. (eds.) Phase Diagrams of Binary Copper Alloys, pp. 167–172. ASM International, Materials Park (1994)
170. Tadmor, M., Kedem, D., Begemann, F., Hauptmann, A., Pernicka, E., Schmitt-Strecker, S.: The Naḥal Mishmar hoard from the Judean Desert: technology, composition, and provenance. Atiqot. **27**, 95–148 (1995)
171. Thornton, C.P.: Of brass and bronze in prehistoric Southwest Asia. In: La Niece, S., Hook, D., Craddock, P. (eds.) Metals and Mines: Studies in Archaeometallurgy, pp. 123–135. Archetype Publications in association with the British Museum, London (2007)
172. Thwaites, C.J., Warwick, M.E., Scott, B.: Tin and tin alloys. In: Mills, K. (ed.) ASM Handbook 9th edition Volume 9: Metallography and Microstructure, pp. 449–457. ASM International, Materials Park (1985)
173. Tiedema, T.J., Bouman, J., Burgers, W.G.: Precipitation in gold-platinum alloys. Acta Metall. **5**(6), 310–321 (1957)
174. Trampuž Orel, N., Heath, D.J.: Analysis of heavy leaded shaft-hole axes. In: Hänsel, B. (ed.) Mensch und Umwelt in der Bronzezeit Europas, pp. 237–247. Oetker-Voges, Kiel (1998)
175. Trampuž Orel, N., Heath, D.J., Hudnik, V.: Chemical analysis of Slovenian bronzes from the Late Bronze Age. In: Mordant, C., Pernot, M., Rychner, V. (eds.) L'atelier du bronzier en Europe du XXe au VIIIe siècle avant notre ère I, pp. 223–237. Comité des travaux historiques et scientifiques, Paris (1998)
176. Turgoose, S.: The corrosion and lead and tin: before and after excavation. In: Miles, G., Pollard, S. (eds.) Lead and Tin: Studies in Conservation and Technology, UKIC Occasional papers 3, pp. 15–26. UKIC, London (1985)
177. Tylecote, R.F.: The Prehistory of Metallurgy in the British Isles. Institute of Metals, London (1986)
178. Tylecote, R.F.: Oxidation enrichment bands in wrought iron. J. Hist. Metall. Soc. **24**(1), 33–38 (1990)
179. Tylecote, R.F.: Early copper base alloys; natural or man-made? In: Mohen, J.-P., Eluère, C. (eds.) Découverte du Métal, Amis du Musée des Antiquités nationales Millénaires 2, pp. 213–221. Picard, Paris (1991)
180. Tylecote, R.F., Gilmour, B.J.J.: The metallography of early ferrous edge tools and edged weapons, British archaeological report British series 155. Oxford (1986)
181. Vincent, B., Bourgarit, D., Jett, P.: Khmer Bronze Metallurgy during the Angkorian period (Twelfth to Thirteeth Centuries): technical investigation of artifacts from the National Museum of Cambodia, Phnom Penh. In: Jett, P. (ed.) Scientific Research on Ancient Asian Metallurgy, pp. 124–153. Archetype, London (2012)
182. Wagner, J.R.: Die Metalle und ihre Verarbeitung. Wigand, Leipzig (1866)
183. Wagner, D.B.: Iron and Steel in Ancient China Handbook of Oriental Studies 9. E.J. Brill, Leiden/NewYork/Köln (1993)
184. Waldbaum, J.C.: The first archaeological appearance af iron and the transition to the Iron age. In: Wertime, T.A., Muhly, J.D. (eds.) The Coming of the Age of Iron, pp. 69–98. Yale University Press, New Haven/London (1980)
185. Wang, Q., Strekopytov, S., Roberts, B.W., Wilkin, N.: Tin ingots from a probable Bronze Age shipwreck off the coast of Salcombe, Devon: composition and microstructure. J. Archaeol. Sci. **67**, 80–92 (2016)
186. Wanhill, R.J.H.: Embrittlement of ancient silver. J. Fail. Anal. Prev. **5**(1), 41–54 (2005)
187. Wanhill, R.J.H.: Case histories of ancient silver embrittlement. J. Fail. Anal. Prev. **11**(3), 178–185 (2011)

188. Wayman, M.L., Duke, M.J.M.: The effects of melting on native copper. In: Hauptmann, A., Pernicka, E., Rehren, T., Yalçın, Ü. (eds.) The Beginnings of Metallurgy. Der Anschnitt Beiheft 9, pp. 55–63. Deutsches Bergbau-Museum, Bochum (1999)
189. Weeks, L.: Early Metallurgy of the Persian Gulf: Technology, Trade, and the Bronze Age World. Brill, Boston (2004)
190. Weirong, Z., Xiagxi, F.: Application of zinc and cadmium for dating and authenticating of metal relicts in ancient China. Bull. Metals. Mus. **22**, 16–21 (1994)
191. Wells, P.S.: Resources and industry. In: Green, M.J. (ed.) The Celtic World, pp. 215–229. Routledge, London/New York (1995)
192. Welter, J.-M.: The zinc content of brass: a chronological indicator? Techne. **18**, 27–36 (2003)
193. Widemann, F.: Documentary and archaeological evidence for an antique copper-nickel alloy (baitong) production in southern China and its exports to India. In: Mei, J., Rehren, T. (eds.) Metallurgy and Civilisation: Eurasia and Beyond, pp. 26–34. Archetype Publications, London (2009)
194. Willer, F., Schwab, R., Mirschenz, M.: Römische Bronzestatuen am Limes: Archäometrische Untersuchungen zur Herstellungstechnik. Bonner Jahrbücher. **216**, 57–207 (2017)
195. Wilson, A.: Machines, power and the ancient economy. J. Rom. Stud. **92**, 1–32 (2002)
196. Weins, W.N., Bleed, P.: Why is the Japanese sword curved? In: Vandiver, P., Druzik, J., Wheeler, G.S. (eds.) Material Issues in Art and Archaeology II, Material Research Society Symposium Proceedings 185, pp. 691–701. Materials Research Society, Pittsburgh (1991)
197. Wise, E.M., Eash, J.T.: The role of platinum metals in dental alloys III. The influence of platinum and palladium and heat treatment upon the microstructure an constitution of basic alloys. Transactions of the American Institute of Mining and Metallurgical Engineers. **33**, 228–237 (1933)
198. Yalçin, Ü.: Der Keulenkopf von Can Hasan (TR). Naturwissenschaftliche Untersuchung und neue Interpretation. In: Rehren, T., Hauptmann, A., Muhly, J.D. (eds.) Metallurgica Antiqua. In Honour of Hans-Gert Bachmann and Robert Maddin. Der Anschnitt Beiheft 8, pp. 279–289. Deutsches Bergbau-Museum, Bochum (1998)
199. Zhou, W., Martinón-Torres, M., Chen, J., Liu, H., Li, Y.: Distilling zinc for the Ming Dynasty: the technology of large scale zinc production in Fengdu, southwest China. J. Archaeol. Sci. **39**, 908–921 (2012)
200. Zwicker, U., Nigge, K., Urbon, B.: Verteilung metallischer Elemente in Patina-Schichten. Microchimica Acta Supplement. **8**, 393–419 (1979)

Chapter 6
Metal Plating, Patination and Corrosion

6.1 Patinas and Corrosion

Surface treatment and patination have been used extensively in ancient and historic metallurgy [68], and practically all metallic substrates are capable of being altered in one way or another. Microstructural studies are often the only way to adequately investigate these surface coatings and patinations. Natural corrosion may, under suitable circumstances, be considered a form of patination, or metals may be deliberately patinated in order to alter surface characteristics. Hughes [26] and Hughes and Rowe [27] make an interesting distinction between four types of surface alteration systems: Firstly, those that rely on a complex metallurgy, but a simple colouring technique in order produce different surface colours. Simple organic coatings are an example used on a wide range of alloys. The second category is the use of a simple metallurgy and complex colouring, the approach taken in the nineteenth century, where fairly standard bronzes or brasses were given a wide variety of colours. Eclecticism, which Hughes [26] says hovers on the edge of kitsch, was used in the late nineteenth century and finally a simple metallurgy and simple colouring such as the oxidized finished on silver and small-scale architectural fittings.

Ancient authors have interesting sides concerning surface appearance, for example, Pliny [44] writes of the artist Aristonidas who sought to capture in a sculpture the madness of Athamas, after he had hurled his son Learchus from a rock: "... he made a blend of copper and iron, in order that the blush of shame should be represented by rust of the iron shining through the brilliant surface of the copper; this statue is still standing at Rhodes" (Natural History 34.40), while Plutarch [45] conducts a philosophical dialogue concerning the attractive blue-green colouration where the bronzes at Delphi possessed a turquoise blue surface patina. For further detailed discussion, see Scott [58]. The deliberate colouration of ancient statues, to make attractive patinated surfaces, has been reviewed by Born [9]. Dark brown or black surfaces were much admired as an alteration to bronze or brass, since additional skill or sophistication was shown by the ability to make golden bronze a dark

D. A. Scott, R. Schwab, *Metallography in Archaeology and Art*, Cultural Heritage Science, https://doi.org/10.1007/978-3-030-11265-3_6

shiny colour and the rarity of it, as in the case of Corinthian bronze, made people carry small statues of it to show off to their friends, as mentioned by Cicero.

Ancient and historic metals may now exist as composite material consisting of metallic remnants and corrosion products. The study of corrosion and patinas is an important part of the description of ancient metals, which has been the subject of numerous papers and books to which the interested reader is referred to here for a great deal of further information which cannot be dealt with in detail in this book, and a basic synopsis is given here (viz. Baas Becking et al. [4]; Berthelot [7]; Bertholon et al. [8]; Born [9]; Brown et al. [12]; Chase [13]; Gettens [20]; Meeks [37]; Scott [58]; Scott and Eggert [67]).

A few general observations will be made here in the context of metallography, but for further reading, see Scott [63–65]. Metallic samples together with their corrosion products must be retained for metallographic examination because they are an important part of the object itself. Corrosion involves the ingress of external environmental factors as well as the outgress of metallic ions to the environment, often resulting in complex layers of corrosion being built up over time, which must be preserved by the metallographer. These diagenetic events are the subject of the works referred to above.

The term patina is generally used for films or crusts of corrosion which are protective, attractive or deliberately produced on the surface of the metal to create a desired finish, colour or texture to the object in question. The production of specific patinas on metallic surfaces has been the subject of many seminal works such as that of Hughes and Rowe [27] to which the interested reader is referred to for more information. A patinated metal may retain the outer morphology of the object in question and may alter the colour to specific requirements, while general corrosion may obliterate or totally obscure the metallic surface.

We can categorize patina and corrosion studies of ancient metals and metallography into several types:

1. The object itself is completely corroded. In such cases a decision has to be made as to whether a sample of the object is worth the effort to mount for examination or not. Some of these totally corroded fragments are interesting or revealing of aspects of fabrication of the original object. They may or may not retain a pseudomorphic morphology of the metallic grains, such as twins, strain lines, non-metallic inclusions, core material from lost-wax or piece-mould casting, organic material pseudomorphs or traces of organic substances that once touched the object, or which it contained, such as wine or meat. Iron objects may be corroded beyond recognition of the original shape, while gold alloys, silver, copper, lead, bronze and tin are more likely to retain vestiges of the fundamental structural morphology of the artefact. However, corroded cast iron artefacts may still contain components such as ledeburite which are more corrosion resistant and which may be partially preserved as pseudomorphs.
2. The object appears to be visually totally corroded but may have vestigial remnants of original metallic constituents present. These will become evident on polishing and may allow electron microprobe study of the original chemical

composition in cases which outwardly appear hopeless. Pseudomorphs are equally likely as in type I.

3. The object appears to be partially corroded with a possible original surface present. Samples from objects showing this kind of preservation are frequently very informative. Not only is there a substantial amount of remaining metal present, but the interface between metal and corrosion may reveal traces of patination or a distinct junction between corrosion events which have built up over the original surface of the object and corrosion events which have occurred within the metallic matrix itself.
4. The object is visually uncorroded but may be patinated to alter the surface colour or texture. Metallographic examination here may be important, not only for the metallic interior but also for characterization of the patina or coating. Gilding, tinning, silvering or other surface coatings or patinas can be revealed by metallography. For example, chocolate-coloured coatings on a Renaissance bronze were shown to be of platinum, deposited by electrochemical replacement plating on bronze; gold coatings less than one micron thick were found on Moche metalwork, showing that gold had been deposited by electrochemical replacement gilding without the aid of a battery by the Moche; black-surfaced bronzes from ancient Egypt were produced by treating the surface of particular bronze alloys to create brown to black surface patinas; historic iron surfaces were treated by bower-barffing to deliberately oxidize the surface as a protective finish.

Broadly speaking, metallic corrosion is governed by three types of interactions: epitaxial, topotaxial or fractal, the latter often leading to chaos theory and random events dominating the corrosion, especially in the case of iron corrosion where there may be little remaining structural detail left. In copper alloys, the initial corrosion products are epitaxially deposited with the consequence that there is a good chance that retention of structural detail can be observed in a metallographic section. The initial corrosion product of copper alloys is usually cuprite or rarely tenorite, details of which are given in Table 6.1, and cuprite predominates as an initial corrosion product. Further detailed studies are given in Scott [58].

Depending on the environment in which the corrosive events concerning the metallic object took place, this cuprite may appear quite crystalline and deep red in colour, viewed under polarized light or in darkfield illumination (Chap. 3). Deep red cuprite crystals or intergrowths within the corroded metal itself are a good indication of the material authenticity of the object in question, and these features can

Table 6.1 Corrosion product of copper alloys

Mineral name	Formula	Crystal system	Colour	Mohs hardness
Cuprite	Cu_2O	Cubic	Submetallic red	3.5–4
Tenorite	CuO	Monoclinic	Metallic grey black	3.5
Spertiniite	$Cu(OH)_2$	Orthorhombic	Blue to blue green	1–2?
Malachite	$Cu_2(CO_3)(OH)_2$	Monoclinic	Pale green	3.5–4
Azurite	$Cu_3(CO_3)_2(OH)_2$	Monoclinic	Vitreous blue	3.5–4
Georgeite	$Cu_5^{2+}(CO_3)_3(OH)_4{\cdot}6H_2O$	Monoclinic	Pale blue	?

readily be seen in the polished and unetched section of the object and are relied upon as an important indicator of authentic long-term burial. Etching tends to dissolve out these copper oxides or copper sulphides, which will either entail the regrinding of the sample followed by repolishing to retrieve the as-polished condition or very careful repolishing alone.

In some alloys or environments, yellow or yellow-red pleochroism manifests fine-grained or poorly crystalline cuprite, which either contains a fair amount of tin or zinc (Chap. 3), or has grown quickly, as in artificial patination systems often used to create inauthentic patinas on archaeological fakes. Different environments may also affect the extent to which the deep red colour of cuprite in cross section can occur.

As corrosion penetrates into an alloy, it may itself act as a natural etchant by attacking those regions more heavily stressed or corroding one phase preferentially. Figure 6.1 shows the section through a Bronze Age blade from Hungary, where the strain lines close to the surface are obvious, as corrosion has outlined them for us here (see also Fig. 3.9). Note that some of these grains of α_{Cu}-bronze have been eaten away entirely along the edge of this section.

Corrosion may create obscuring crusts with complex interlayers contiguous with the metallic surface, as shown in Fig. 6.2. Here the junction between the remaining metal of this Chinese bronze mirror of the Warring States period and the external corrosion can be seen.

There are essentially four zones of corrosion seen in this photomicrograph: the internal corrosion of the bronze alloy, a surface zone which is a discontinuity between the internal and external environment, and a thick external corrosion crust, whose outer later is composed of green corrosion products with occasional soil minerals. Note here the clear delineation between internal and external corrosion events. The view of the same section, under plane-polarized light at higher magnification, reveals something of the corrosive events at the original surface of the mirror (Fig. 6.3).

The Widmanstätten structure of the alpha + delta phases of the bronze continues to create an inhomogeneity in the corrosion crust close to the metal surface, and

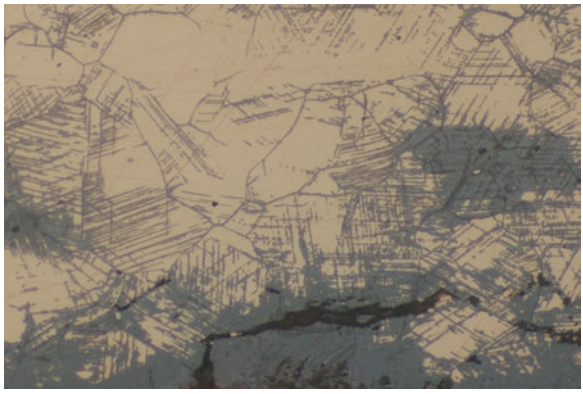

Fig. 6.1 Hungarian Bronze Age dagger blade section. The low-tin bronze has undergone extensive corrosion, with penetration along slip panes, some of which show perfect pseudomorphic preservation of microstructural detail. Unetched, magnification, x180

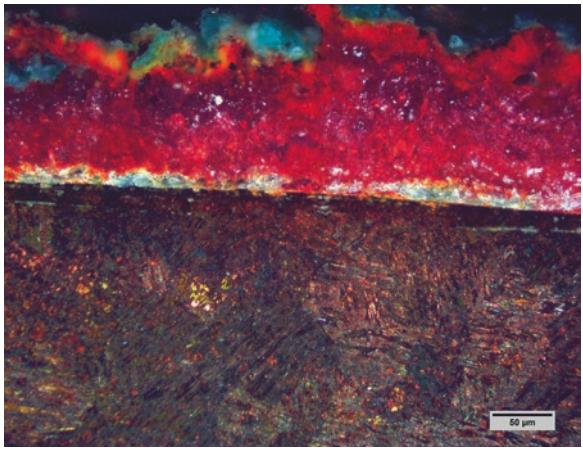

Fig. 6.2 Chinese bronze mirror from the Warring States with four different layers. The sound metal is on the left hand side, followed by a heavily corroded matrix, then a layer of redeposited copper, followed by the external corrosion crust. Unetched, polarized light, magnification x90

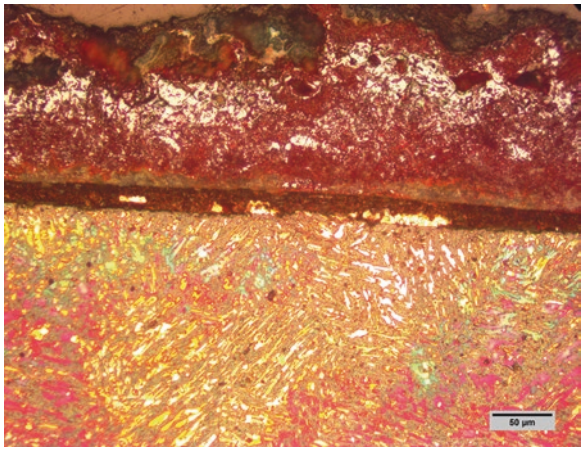

Fig. 6.3 Same bronze mirror as Fig. 6.2 viewed under polarized light with DIC. The Widmanstatten structure of the corroded interior is covered with a layer of redeposited copper along the surface of the original mirror external plane, and then to the left hand side, the corrosion crust covers the redeposited copper. Unetched, magnification x180

within the double boundary layer, copper has been deposited from solution during burial, resulting in the bright yellow phase seen in the photomicrograph of Fig. 6.2. The redeposition of copper from solution is a common event in the burial corrosion of Chinese bronzes and many others as well (see Bosi et al. [10]), and redeposited copper may be precipitated at surface boundaries or the original surface as Figs. 6.2 and 6.3 illustrate. The metallographer must be aware of these issues when interpreting the microstructure of ancient metals.

Dezincification is another type of de-alloying, which causes the selective removal of zinc from the alloy by the corrosion of the solid solution and the redeposition of copper as a porous layer. Stress corrosion cracking and dezincification are the most familiar forms of brass corrosion, and two types of dezincification are common: the plug and the layer type. The layer type is a uniform attack over the surfaces and is hardly documented for ancient single-phased brasses. The plug type can regularly be observed, but it is different to the intensive dezincification of modern yellow

brasses, as single-phased α-brasses are less prone to dezincification than high zinc brasses. Brasses containing less than 15% of zinc have the same oxidation resistance as copper; therefore they are relatively immune to dezincification and impurities such as tin or arsenic increase the de-alloying resistance. Selective corrosion and de-alloying in ancient and historic brasses usually are metallurgically influenced and take place in localized areas after cold-work without sufficient annealing, as can be seen in Fig. 6.4, whereas drastic forms of dezincification can be perfectly studied in "antique" objects coming from the art market (see Schwab et al. [52]).

Pseudomorphic characteristics of particular phases may be preserved within the corrosion crust, and these can reveal structural detail near the surface. In ideal cases mineralized wood, textiles or other organic components are replaced with corrosion products and the micromorphology of these organic materials preserved within the corrosion crust, which can then be seen in cross section. The common forms of green-coloured alteration products of copper are shown in Table 6.2; for further

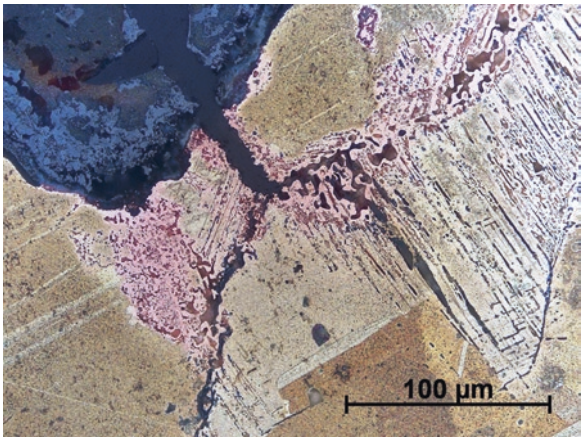

Fig. 6.4 Redeposited copper along corroded slip lines and stress corrosion cracks within a fulfilled groove on the surface of a Benin memorial head from the eighteenth century, which is made of leaded brass with 24% zinc. The head has never been buried, but the ornament has been enchased, and localized accelerated corrosion has been taken place by residual stress. Etched with acidified ferric chloride and viewed under bright-field illumination

Table 6.2 A tabulation of the important green-coloured copper and bronze corrosion products which are often encountered in corroded metallic sections. (After Scott [58])

Mineral name	Formula	Crystal system	Colour	Mohs hardness
Malachite	$CuCO_3{\cdot}Cu(OH)_2$	Monoclinic	Pale green	3.5–4
Azurite	$2CuCO_3{\cdot}Cu(OH)_2$	Monoclinic	Vitreous blue	3.5–4
Georgeite	$CuCO_3{\cdot}Cu(OH)_2$	Monoclinic	Pale blue	?
Chalconatronite	$Na_2Cu(CO_3)_2{\cdot}3H_2O$	Monoclinic	Greenish blue	3–4
Rosasite	$(Cu,Zn)_2CO_3(OH)_2$	Monoclinic	Bluish green	4.5
Aurichalcite	$(Cu,Zn)_5(CO_3)_2(OH)_6$	Orthorhombic	Pearly pale green	1–2
Claraite	$(Cu,Zn)_3(CO_3)(OH)_4{\cdot}4H_2O$	Hexagonal	Translucent blue	2

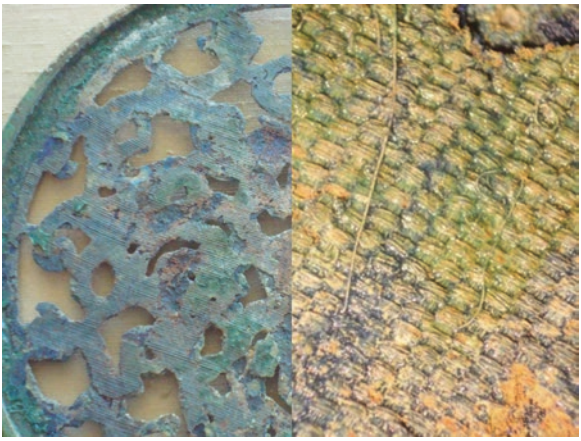

Fig. 6.5 Macroscopic view of the reverse side of the back of a Warring States mirror casing, showing the corrosion in cuprite and malachite which has preserved the traces of the textile interlayer. On the right hand side, at a magnification of x35, the silk textile pseudomorph can be seen in detail, entirely preserved in copper corrosion products

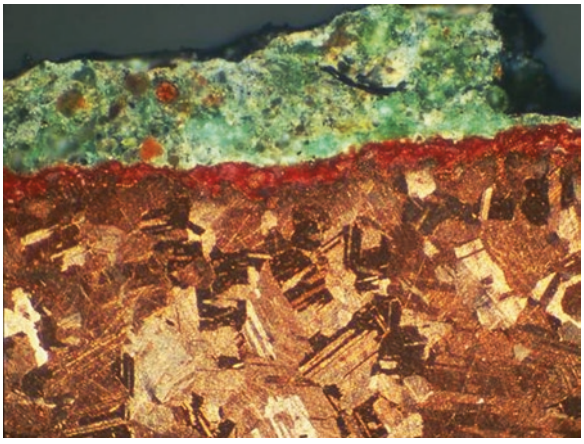

Fig. 6.6 One of five very important ancient Greek copper plaques which preserve a very early form of the Greek language. The lettering is entirely preserved in the malachite and copper trihydroxychloride corrosion products on the thick crust here, which overlies a thin, bright red cuprite layer, before passing into the worked and annealed copper grains of the sheet copper below. Lightly etched in ferric chloride, magnification x160

detailed information on all of these corrosion products and their characteristics, see Scott [58].

The preservation of pseudomorphic detail on the metallic surface, as shown in Fig. 6.5 from an ancient Chinese mirror of the Warring States period [62], is a mineral pseudomorph of an almost perfect silk textile used as an interlayer in the Chinese bronze mirror. No organic material remains, but the structure has been preserved completely in malachite and azurite corrosion products [60, 61].

In some cases, often very important, corrosion may have completely altered the metallic surface to a mass of corrosion products, which is the case of copper alloys, such as the section from the Greek copper plaque shown in Fig. 6.6. The plaque

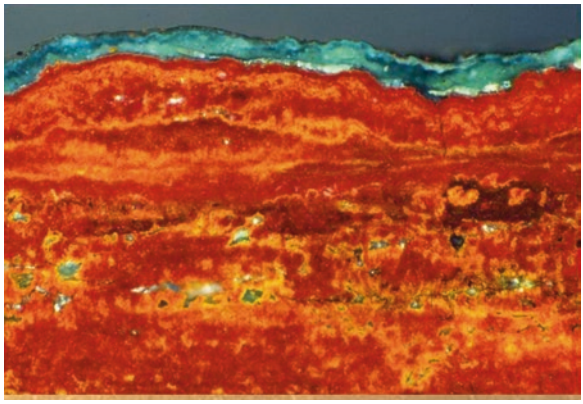

Fig. 6.7 Copper Dead Sea scrolls. Preserved lettering but completely mineralized copper sheet in this case, this preserves no metal whatever. Magnification x170

retains a surface in which letters can still actually be read, while the interior below the surface is covered with a complex corrosion crust [66]. Also the surfaces of the copper Dead Sea scrolls contain hammered lettering which can still be read [8, 58], while the matrix is completely converted to layers of cuprite which preserve little or nothing of the original metallic structure, as shown in Fig. 6.7.

There are many examples where the complete corrosion of archaeological metallic artefacts provides important structural information relating to corrosion events in the soil and how these impact the residual nature of the corroded matrix. A classic paper on the nature of the residual metallic matrix in the case of bronze alloys was that undertaken by Geilmann in [19]. Papers in which the nature of the corrosion can itself be used to link disparate museum artefacts together are exemplified by an example by Scott [56] on the examination of the patina and corrosion morphology of some Roman bronzes.

The Roman bronze statues of Togati, Roma and Venus (Demeter) and in the collection of the J. Paul Getty Museum were subject to a detailed technical study. Of particular interest are their unusual, mattes matte and finely preserved patinas, which closely parallel another bronze, the Nike, in the Cleveland Museum of Art. The bronzes, which date to AD 40–68, are described and analyzed, and an account of their corrosion is given, drawing on the work by Geilmann [19], who examined the corrosion of bronzes from sandy soils in Germany. The patinas of these objects contain substantial amounts of tin oxide and also display warty corrosion. It was postulated, and confirmed by analysis, that patinas of this kind should contain no chloride ions; thus, there are at least two types of warty corrosion of ancient bronzes. The first type, as here, is chemically stable and does not necessarily require strictly regulated humidity conditions. The second type of warty corrosion is related to the presence of chlorides, usually with an accumulation of cuprous chloride. The three bronzes studied here are closely related and are almost certainly from the same burial deposit, as evidenced by their associated soil and minerals. These materials were not completely cleaned from the surfaces of the bronzes, so essential information regarding their origin was preserved. Cleaning during conservation to a uniform "original surface" or "marker layer" would have removed this important evidence.

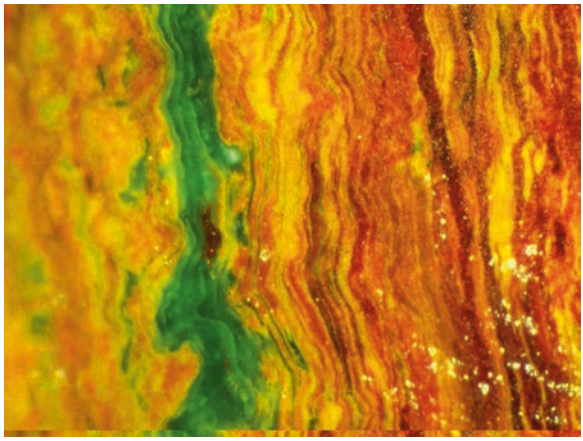

Fig. 6.8 Iranian toggle pin from the Middle Bronze Age, collection of Iran Bastan Museum, Iran. Total corrosion of the toggle pin has resulted in Liesegang rings in the corroded solid, which preserves no original microstructural detail. Unetched, magnification x 350

Robbiola and Portier [47] present a paper of wider significance which postulates a global approach to the authentication of ancient bronzes based on the characterization of the alloy-patina-environment system. Their work proposes a general framework for improving the practice of authentication of ancient bronze artefacts. It is shown that even if numerous technical and fundamental scientific improvements have overcome some of the limitations encountered in the characterization of materials, properties, metal and patina are always considered as independent systems. It is evidenced that authentication requires a global approach based on the investigation of the metallic materials-patina-close environment system. On this basis, the authors address the complex relationships between alloys, alteration (patinas) and environment (soil) and discuss the investigation of the consequence of decuprification (as a global phenomenon of bronze corrosion), taking into account the coupled interactions. An application from an example of a fake Chinese ding ritual vessel is then given.

The complete corrosion of some bronze artefacts creates complex layered structures which are caused by the slow interaction of corrosive solutions with the bronze alloy. Liesegang phenomena can then be observed in the corroded section if the growth features involve a determinative layered form as Fig. 6.8 illustrates.

6.1.1 Deliberately Oxidized or Corroded Surfaces

Oxidation techniques have been used to create surface films and colouration by light absorption, reflection or diffraction. A significant group of copper alloys, known in many different cultures of the Old World, was prepared by special patination techniques. In Egypt, the use of the black-patinated *hsmn km* alloy appears to be widespread, and Romans took the knowledge of the technique and applied it to produce the so-called Corinthian bronzes, which are known in Bronze Age Greek as kyanos and as *shakudo* in Japan from the twelfth century onwards [16, 39]. Most of these

alloys contain up to several percentages of gold and are combined with inlays of gold, silver or electrum [16, 41].

The black colour of these copper alloys is essentially an altered cuprite with some tenorite in which gold particles are finely dispersed and the lustrous black blue surface is mainly due to light absorption and diffuse reflection by the fine gold particles [39, 41]. Rare examples of this technique from the European Bronze Age are exclusively made of nearly pure copper, which were also black or dark brown in surface colouration, sometimes combined with gold inlays [5, 6, 53]. The analytical study of the Egyptian bronzes by La Niece and co-workers [33] showed that they were originally intended to be polychrome. Not only were the eyes, brows and nipples of some figures coloured but also regalia, clothing and jewellery. The range of materials and techniques included the well-known precious metal, glass and mineral inlays, as well as coloured alloys, patinated metal and applied pigments. Inlays may also have been patinated, particularly those produced in an arsenical copper alloy.

A range of other alloys were also employed using copper-silver alloys, *shibuichi*; *kuromido*, arsenic-copper alloy; *santoku*, a leaded tin bronze; and *shintyuu*, a leaded brass. These alloys could be used to create a whole range of colours including grey, grey-green and ranging from light to dark olive and earth browns. Imitation of Japanese alloys of *shakudo* or *shibuichi*, of long antiquity, led to a fashion for oxidized silver in France by the 1840s, and the fashion for oxidized silver surfaces continued up to the First World War [48].

Another technique employing oxidation to create blackened surfaces in high zinc alloys containing a small amount of copper was from ancient India, known as Bidriware. Analysis shows that the maximum copper content of such alloys was 10% but usually less than 5% with some lead [29, 31, 32]. The objects were cast and inlaid with silver, gold or brass. The final stage in the production of the black surface on the alloy is the use of a special local earth and ammonium chloride [31]. The earth is recommended to be taken from old palace walls and associated areas which are likely to be rich in the decayed products of urine, and therefore these agents are thought to be active in producing the blackened surface of the Bidriware but leaving the inlays unaffected [29].

Iron surfaces could be coloured by heating or chemically producing oxide layers appearing blue, brown or black in dependence of their thickness [67]. They can also be blackened by forcing a layer of flash rusting, followed by treatment with hydrogen gas to produce black velvet-like surfaces, referred to as bower-barffing [21].

6.2 Plating

6.2.1 Gilding

There is a progression in terms of surface coatings from the base metal to the overlying coating. For example, iron objects can be coated with copper, copper alloys with silver, silver with gold and gold with platinum. There are even examples of lead beads from the La Tolita culture of lead overlaid or inlaid with pieces of platinum [60, 61]. Gilding has probably been one of the most widespread plating technologies all over the ancient world. Gilding was applied to imitate solid gold, as a rare and valuable metal, and there are many cultures over the ancient world where gold coatings have been made, both over copper and silver alloys and, later, also over iron.

The early use of foil or leaf gilding may have involved a mechanical rather than metallurgical process, and examples are known from the beginning of the third millennium BC of silver nails covered with gold leaf from Tell Brak in Syria and of copper nails from Abu Shahrain, Iraq, from circa 2500 BC [42, p. 172; 43, p. 2]. Mechanical fixing or inlay techniques have been exclusively used in the Old World during the Bronze Age, and the technique has remained a common practice in all cultures up to modern times. An example from a tenth century AD context can be seen in a nose ornament from Ecuador in Fig. 6.9.

A real innovation and the first metallurgical gilding process is diffusion gilding, also called diffusion bonding, which is best known for gold and silver. Diffusion bonding has been first evidenced for an Elamite roundel from Iran, which is dated to the fourteenth/thirteenth century BC [42, p. 176; 43], but the technology must have been already well known at this time, as around one-third of the analyzed gold

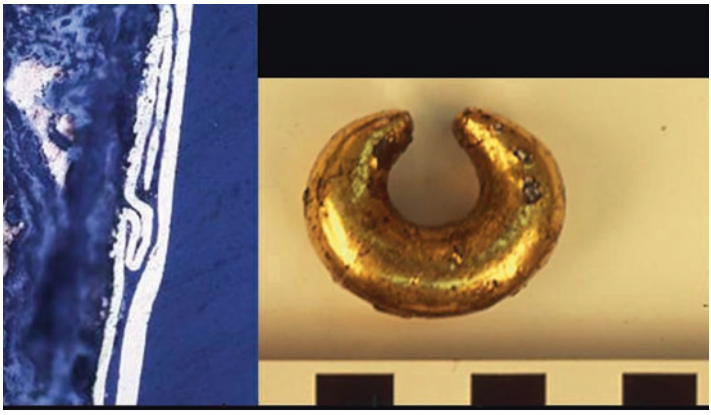

Fig. 6.9 Foil-gilded penannular nose ornament from the site of La Compania, Los Rios Province, Ecuador, from the tenth century AD secondary chimney urn burial. The section through part of the surface shows corroded copper beneath a typical gold foil covering where folds can be seen in the foil. Unetched, magnification on left is x75. Scale bar on the right is in centimetres

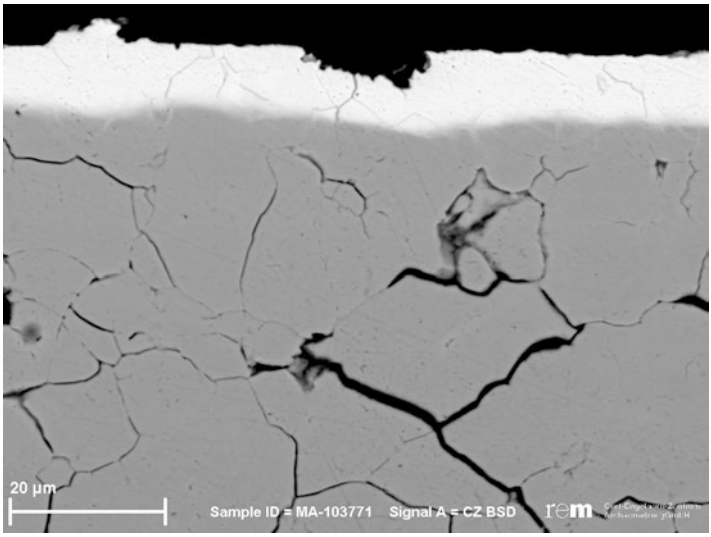

Fig. 6.10 SEM-BSE image of the intergranular fractured microstructure of a decorated silver quiver from the Royal tomb of Qatna in Syria shows a thin layer of gold, which is bond to the silver substrate by diffusion

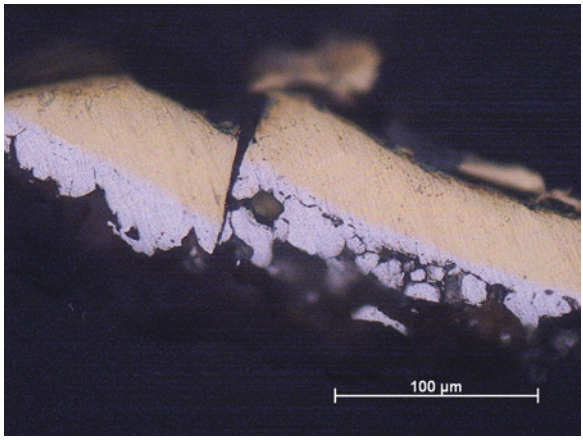

Fig. 6.11 Micrograph of the gilded silver foil from the head of a bronze rivet from the tomb of Asperg »Grafenbühl«, Germany, dated to around 500 BC

items from the Royal tomb of Qatna in Syria, dated to the early fourteenth century BC, are in fact gilded silver, as can be seen in Fig. 6.10.

Diffusion gilding is best documented for Greek and Etruscan items since the eighth/seventh century BC and must have entered Northern and Western Europe during the sixth century BC, when first examples can be proven (Fig. 6.11). Diffusion gilding has also been practised in Southeast Asia [49] and in South America.

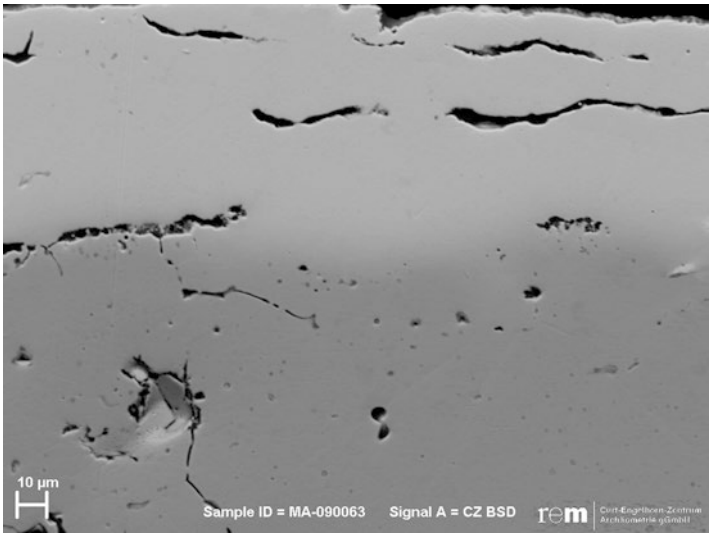

Fig. 6.12 SEM-BSE image of a foil and subsequent fusion-gilded silver spiral ring fragment from burial 4 in Prohear, Cambodia, dated to 44 BC to 51 AD, showing three superimposed gold layers and the zones of interdiffusion which are disrupted by cuprite inclusions and cavities

The clamping together of gold foil or gold leaf and silver to anneal the couple easily creates a diffusion bond between surface and substrate, as both metals are totally soluble in each other (Chap. 4). Since the diffusion coefficient D_{Ag} is greater than D_{Au}, the Kirkendall effect emerges by volume expansions on the slower diffusion component side which induce surface contour changes, optically evident through bubbles, which are significant for diffusion-bonded objects ([50, 59]). The micrographs of the cross section of diffusion-bonded items usually show strong bonded layers without any gaps, and an EDX line scans or element maps show the gradually decreasing gold and the increasing silver contents from the attached gold to the silver layer on the inside (see Schorer et al. [51], p. 206). The presence of copper can form copper oxide inclusions by inner oxidation, which locally prevent the bonding, as shown in Fig. 6.12.

Another important metallurgical technique is amalgam or fire gilding. Gold can be mixed with mercury to create a series of pasty amalgams. It was recognized early on that if a pasty mass of gold amalgam was spread over the surface of cleaned copper, and gently heated, that interdiffusion of mercury between the substrate and the gold layer would ensure a metallurgical bond [42]. Most of the mercury evaporates leaving a dull and porous surface, which must be rubbed and smoothed. The spongy gold surface of fire-gilded objects can often be seen in cross section shown in Fig. 6.13, especially in depressions, and is quite distinctive.

Amalgam gilding creates gold-mercury intermetallic phases, and traces of mercury can usually be detected by XRF analysis from the surface of such objects. The mercury amalgam technique came to dominate the gilding used in historic periods,

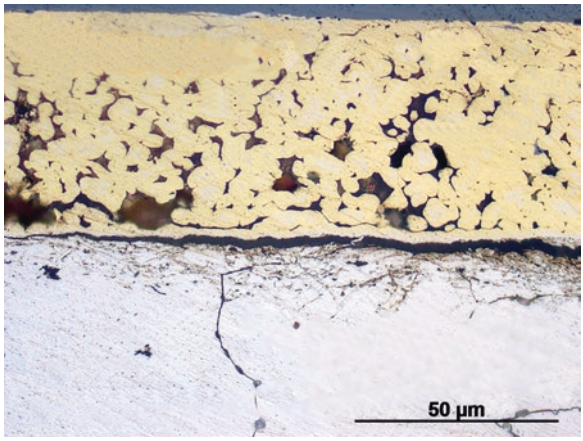

Fig. 6.13 A silver falcon brooch from the early medieval cemetery from Bedburg-Königshoven in the Rhineland, Germany, has a typical thick porous fire-gilded surface

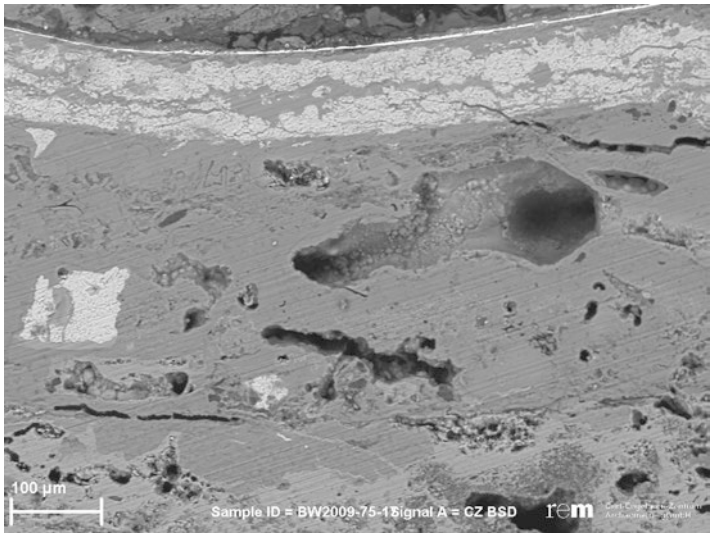

Fig. 6.14 SEM-BSE image shows the corroded iron disc of a cameo fibula from Mannheim-Seckenheim, dated to the early nineth century AD. The iron has been plated with a layer of copper and then fire gilded

but leaf and diffusion bonding were still extensively used. Mercury amalgam gilding probably originated in China, during the Warring States period [42, 43]. By the second century AD in the Old World, mercury amalgams were commonly used, but these were used surprisingly early in the Celtic world where knowledge of the technique goes back to the first century BC [22, p. 255; 34, 43]. Some rare earlier examples could indicate that amalgam gilding was known in Europe before this period (see Kallfass et al. [28]; Oddy [42]), if their dates are secure. Fire gilding of iron was also employed, as can be seen in Fig. 6.14.

Bronze Age fire-gilded objects such as a disc from Rathgall in Ireland and the metal-hilted sword recovered from the river Niers near Oedt in Westphalia (Germany) have been proven to be fakes or incorrectly dated (Craddock, personal communication; [54]). Certain regions of the ancient world, such as the entire continent of pre-Hispanic South America, never used amalgam gilding.

Yet another technique of surface treatment was reported for the first time by Bergsøe, following his examination of a number of gilded copper objects from the Esmeraldas-Tumaco area [11]. Some of the fish-hooks and needles from this area appear to have been made in a tumbaga alloy, followed by depletion gilding, but examination by Bergsøe of successive surface scrapings convinced him that the gradual decrease in gold content towards the centre of the object was a consequence of a fusion-gilding process, in which a piece of shaped copper was dipped into a molten gold-copper alloy. After dissolving the copper base of five gilded objects in dilute nitric acid, Bergsøe found the remaining scales to have a composition of 64.8% gold, 26.8% copper and 8.24% silver, an alloy with a liquidus of about 970 °C. The copper-base alloy averages a gold content of 2.1%, perhaps as a result of contamination or as a result of the reuse of scrap. Work by Scott [55] confirmed the existence of wash-gilded copper from both the Esmeraldas-Tumaco and Nariño areas. An example is shown in Fig. 6.15, which is a cross section through a fusion-gilded fish-hook from La Tolita. The thickness of the coating here is 180 microns and has been made in a gold-copper alloy of composition 26% gold, 2% silver and 72% copper.

There is a zone of interdiffusion of 35 microns. The liquidus temperature of the coating is 1080 °C, while the melting point of the copper base is 1100 °C. A delicate metallurgical operation must be conducted in order to affect this kind of surface coating. The porosity close to the underlying surface of the copper shows a series of pores which may be due to the Kirkendall shift, as the rate of diffusion of gold in copper is greater than the rate of diffusion of copper in gold. This can have the effect of creating porosity as the boundary as gold diffusion proceeds.

Gilding, mise en couleur, surface enrichment, depletion gilding and colouring are all used in various ways in the literature to describe the same event: the removal of

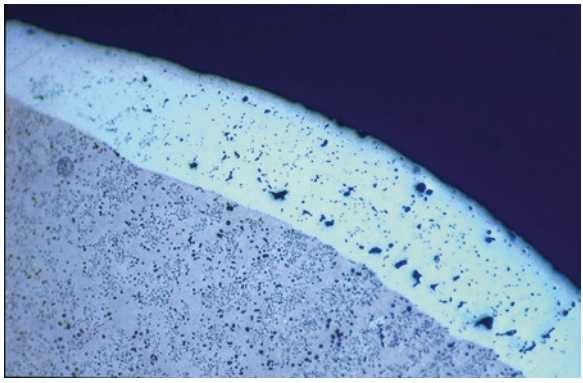

Fig. 6.15 Diffusion-bonded gold-copper alloy fusion coat over copper. Fish-hook from the site of La Tolita, Ecuador. A tour de force of diffusion bonding on a small object no more than 1.6 mm in diameter. Etched in ferric chloride, magnification x130

one or more constituents from a gold alloy to leave a surface enriched in gold which, on subsequent burnishing, gives the appearance that the whole object (or selected parts of the object) is golden in colour. The number of these descriptive terms used in various contexts has led to some confusion in the archaeological literature as to how they are to be applied. Lechtman [35] prefers the term depletion gilding to surface enrichment; she defines it as "The enrichment of a surface in gold by the removal of other alloying elements already present". Gold is a noble metal and highly resistant to corrosion in soils and atmospheres, because of its low chemical affinity for most elements and its high positive electrode potential. Gold alloys become increasingly susceptible to corrosion as the content of the less noble constituents rises. Tammann [69] found that the resistance of gold alloys to tarnish and corrosion at room temperature was not greatly affected, as long as the gold content of the resulting alloy was not below 50 atomic percentages (about 65 wt. %). For a general review, see Rapson and Groenewald [46]. Depletion gilding is a corrosion process, which is termed de-alloying in modern corrosion sciences. De-alloying is an electrochemical reaction that causes surface depletion effects in gold alloys by the selective dissolution of copper and silver from the solid solution leaving behind a porous residue of pure gold [14]. Due to the differences in the standard electrode potentials of silver and copper to gold, they dissolve anodically in most moist environments, and silver can also be removed by the reactivity of the halogens towards silver.

In contrast to other well-known de-alloying systems such as copper-zinc, there is no dissolution-redeposition mechanism, as gold usually does not undergo dissolution [14]. One would expect that the enrichment of gold on the surface could stop the corrosive attack, but further diffusion of the more reactive elements towards the surface and the gold away from the surface is proposed for the continuing of the leaching process [14, 18]. As surface alloying element's atoms were dissolved, the residual gold atoms reform into gold-rich islands so that fresh atoms were exposed layer by layer. As the corrosion proceeds, the surface reorders by island nucleation and growth; finally the islands grow into an interconnected structure resulting in a very thin epitaxial surface coating of gold. A typical island-and-channel morphology in the cross section of a tumbaga alloy from the Tairona area of Colombia reveals the general pattern of attack. The weak plant acids are able to continue their attack and alteration of the surface as the gold atoms rearrange themselves to create the channels seen in the photomicrograph below in Fig. 6.16.

The compositional contrast of the microstructure of a silver and gold alloy from Prohear in Cambodia clearly reveals the enrichment of gold along the channels (Fig. 6.17).

Surface enrichment techniques have been extensively used in ancient South America to change the surface composition of gold-copper or gold-silver-copper alloys [57]. This is especially so in Colombia where the great majority of metalwork was made in copper-gold alloys and there is ethnohistorical evidence for this kind of surface alteration as, for example, Fernández de Enciso, writing in 1519 of the Indians of Santa Marta, Department of Magdalena, an area of the Tairona culture: "…there is in possession of the Indians much gold and copper. There is also found much gilded copper. The Indians say that they gild the copper with a herb which is

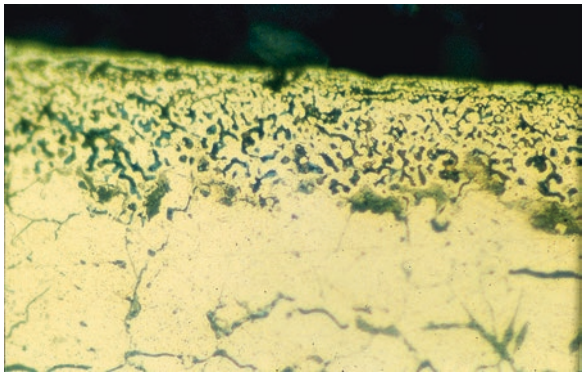

Fig. 6.16 Surface enrichment in gold has created this island and channel morphology in an ancient Colombian gold alloy from the Nariño area. The gold content at the surface rises to about 75–80%, while the bulk of the copper-gold-silver alloy has about 25% gold, 70% copper and 5% silver

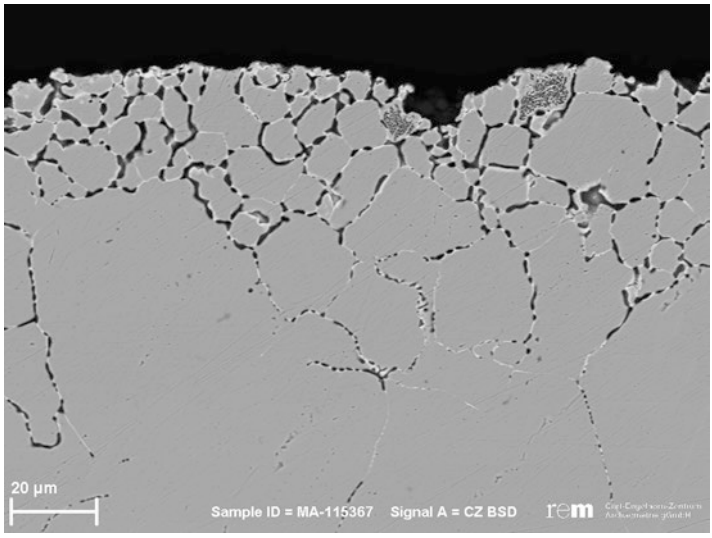

Fig. 6.17 Depleted surface of a spiral made of a silver and gold alloy with 63.5% silver and 36% gold from Prohear, Cambodia

in that land, crushed, and with the top taken off; and they wash the copper with it; and placed in the fire it assumes the colour of very fine gold, and changes in colour more or less according to whether they give it more or less of the herb…".

Depletion gilding is rarely documented for the Near East [43], but some examples are known from Southeast Asia [49], and evidence from England and from northwest France for the late Iron Age suggests deliberate surface treatment by goldsmiths to enhance the colour of the alloys [22, 34].

Electrochemical deposition of gold films from solution was reported by Lechtman [36] used as the gilding of some Moche period metalwork (0 AD–600 AD), from the site of Loma Negra, near the Peruvian-Ecuadorian border. Examination showed them to be of copper with very thin gold coatings of 0.5–2.0 micron thickness. The coatings were relatively uniform and covered all surfaces, and there was a solid-

Fig. 6.18 Electrochemically plated Vicus disc from ancient Peru. The underlying copper has a trace of gold content, but the thin, continuous gold covering can just be seen at this magnification. Etched in ferric chloride, magnification x80

state diffusion zone between the gold and copper showing that, at some stage, heating was carried out. There was no evidence of mercury gilding or the use of gold foil or leaf or of the flushing-on of molten gold. Lechtman suggested the use of an electrochemical replacement technique: identical coatings were produced in the laboratory using gold dissolved in aqueous solutions of NaCl + KNO_3 + K_2SO_4• $Al_2(SO_4)_3$•12H_2O. Gold can go into solution in this aqueous mixture in the form of the complex [$AuCl_4^-H^+$]•3H_2O. Sodium bicarbonate additions were made to bring the pH up to 9. Under these conditions cleaned copper sheet placed into the simmering solution became plated with gold. By dissolving silver in the same solution, it is possible to produce silver-plated copper. An example of an electrochemically plated ancient Peruvian dangle from the Vicus culture is shown in Fig. 6.18.

The electrochemical replacement technology has been reported exclusively from Peru and Ecuador for the early centuries AD so far [25, 57] and is a remarkable metallurgical achievement by the ancient pre-Hispanic cultures, at a time when the Western world had no knowledge of the procedure at all.

6.2.2 Silvering

The existence of silver-enriched copper-silver alloys is common. Fusion of silver or silver-copper alloys to the surface has been extensively employed in the Old World, especially by the Romans to fabricate silver-plated coins or decorative items [30, 70]. Where the base alloy was of copper, a layer of solder of a silver-copper alloy could be flowed over the surface, creating a eutectic alloy at the join. If the core was of iron, this soldering or fusion process could not be used, and the silver plating had to be carried out either by using a separate silver-copper hard solder or by soldering silver foil to the iron surface. Silver sheets were also soldered to copper alloys (Chap. 4).

In the binary alloy, the working and annealing to shape create copper oxidation (this also applies to copper-rich tumbagas), and the removal of scale and cleaning of

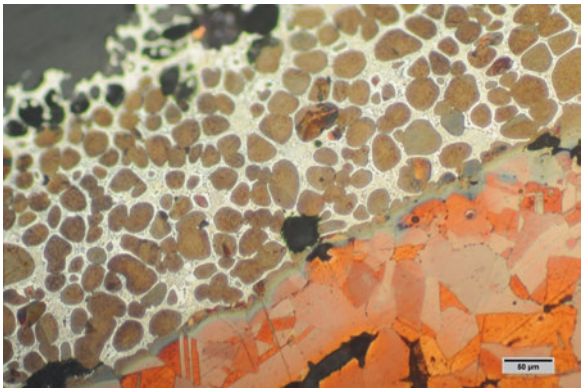

Fig. 6.19 Silvered penannular nose ornament from La Compania, Los Rios Province, Ecuador, from secondary chimney urn burial, the tenth century AD. Section shows the skilful, thick silver-copper alloy coating over the copper nose ring, which is then surface enriched in silver by depletion of copper, so that the entire nose ornament appears to be made in silver. Etched in potassium dichromate followed by colour etching to reveal the worked and annealed copper grains, magnification given on scale bar is 50 microns

the surface create a surface-enriched effect. It would not be necessary to employ the ferric salt and sodium chloride mixture in the surface treatment of these copper-silver alloys, since copper removal is all that is required. In the New World, silver-copper alloys are mainly found along the pacific littoral from Ecuador to Peru and in the Andean highlands (Meggers [38], pp. 133–8, 152, 163). They are also found in the Nariño area of Colombia.

These alloy surface alteration techniques employing silver can be very hard to characterize if metallographic examination cannot be carried out. An example is shown in Fig. 6.19, which is the cross section of a penannular silver nose ornament from Ecuador. Surface study with X-rays would only reveal a silver-copper alloy, as the coating is 100 microns thick. Metallographic examination shows that under the silver-copper alloy layer, which has been fusion-silvered to the surface, there is a pure copper interior which has been hammered and worked to shape the nose ornament before the silver-copper alloy of lower melting point was fused or flowed over the surface. This silver-copper alloy was then lightly worked and annealed, since some annealing twins can be seen in the alloy coating, and was then enriched in silver by pickling to clean and remove some of the copper from this binary alloy.

Silver plating on iron is much less common, but with introduction of coinage, iron-cored coin forgeries so-called *subferrati* appeared, which were coated with more valuable metals like silver [1, 70].

6.2.3 *Platinum Coatings*

The only culture of the ancient world to make use of platinum coatings was that of the Esmeralda-La Tolita Indians, along the Pacific littoral of Ecuador and Colombia [55, 60, 61]. Metallographic examination, shown in two examples below, reveals that two different techniques of platinum coating were employed. In one, shown on the upper section, a thin layer of platinum grains was applied to the surface and then heated with the blowpipe, slowly creating an interdiffusion zone between the unmelted platinum grains and the gold substrate. On burnishing, the platinum alloy surface (isoferroplatinum, as the platinum usually contains a small percentage of iron), will assume an interesting range of platinum colours, which in burial may be tinged with a slight blush of iron corrosion in the form of haematite. An example is shown in Fig. 6.20.

In the second type of platinum coating, a thin diffusion-bonded sheet of gold-platinum sintered alloy is made, which is then hammered and annealed to create a composite thin sheet. This gold-platinum sheet or foil is then hammered over the gold substrate and adhered by diffusion bonding. Metallography reveals this truly remarkable achievement of the La Tolita Indians. Figure 6.21 is from a small armlet or bangle in the collections of the National Museum of the American Indian, Washington, from La Tolita, which is part of a bimetallic finish used on this particular object. Here a layer of gold appears to have been applied to a gold-platinum sintered sheet beneath. The bimetallic finish is used in this object to create contrasting surface design in gold and gold-platinum.

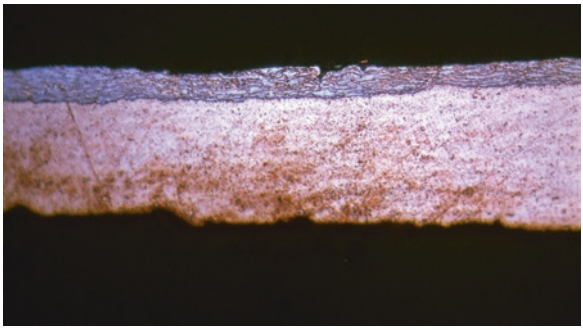

Fig. 6.20 Sophisticated platinum-plating technology from the Indians of La Tolita, Ecuador, from about 100 BC to early centuries AD. Here a separate, well-hammered gold-platinum composite foil has been made, and this foil is then diffusion bonded to the gold sheet beneath to make a platinum coating of some thickness. The silver content of the platinum-gold composite is not the same as the silver content of the gold sheet beneath, showing the separate origin of the two components. Etched in aqua regia, magnification x80

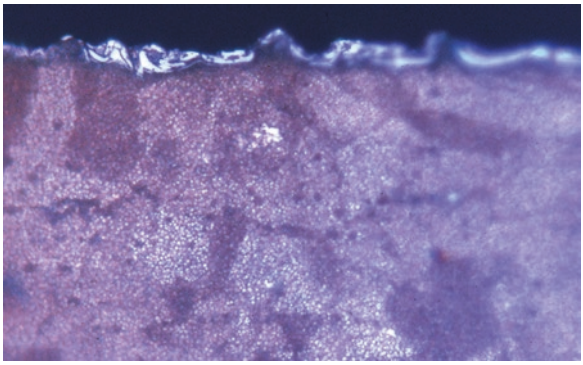

Fig. 6.21 Platinum plated dangle from La Tolita. Here tiny platinum laths have been applied to the surface of the finished object and then carefully heated with the blowpipe to create some interdiffusion. The platinum-iron native alloy produces a steel-grey surface colouration. Etched in aqua regia, magnification x680

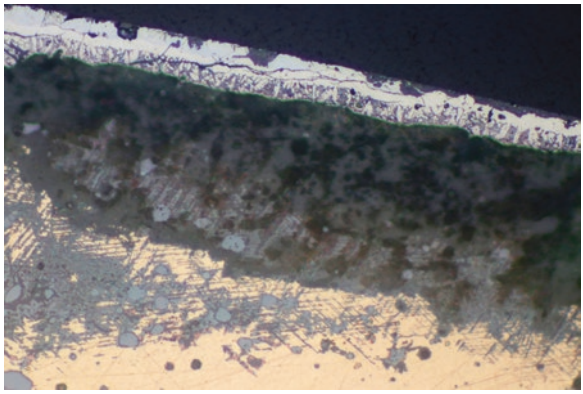

Fig. 6.22 Tinning on a Chinese belt buckle from the Tang Dynasty. The three layers of tinning which have formed by diffusion can just be seen, from small remnants of metallic tin to the eta phase and then the epsilon phase and the alpha + delta eutectoid phase. Unetched, magnification x240

6.2.4 Tinning

The history and technology of tinning copper alloys has been well described by Meeks [37], which should be consulted for detailed information. Tinning has been used to produce high-reflecting and corrosion-resistant surfaces, because tin is non-toxic, has a pleasant appearance and is a cheaper alternative to silvering. Tinning produces very thin layers and has also been used to imitate silver in coin forgeries [30]. Tin is usually applied in the liquid state, due to its low melting point, and therefore forms phases with the substrate alloy by solid-state diffusion [37]. Excess tin is rarely found on the surface of tinned copper alloys, but all the intermetallic compounds η, ε and δ, as well as the eutectoid, are (Fig. 6.22). The η-phase Cu_6Sn_5 is common. Surface layers of eutectoid can also form by inverse segregation; either

an accident of casting or deliberately encouraged by manipulation of the casting conditions has been responsible for tin-enriched surfaces on Bronze Age implements and Chinese artefacts and has generated a considerable literature. In order to investigate these surface alterations in detail, metallography is essential.

The tinning of iron is principally a protective coating; as unalloyed iron and steel readily stains and rusts, it has to be coated or serviced. While blades have to be consistently polished and oiled, wrought irons have usually been black annealed or coated.

6.2.5 Copper Plating on Iron

Copper alloy plating on iron is a particular technology from the Iron Age to modern times, and a number of techniques had been evolved (see Ankner and Hummel [2]; Corfield [15]). The first method involves the use of a sheet copper metal, which is wrapped around the iron leaving flanges which are then tightly held together by striking from either side or just fixed into a notch [40]. The copper plating could also be applied by hammering on to the prepared surface of the iron which could be roughened to form a physical bond with the plated surface. This technique has widely been applied in Europe for the substantial plating of silver and copper alloys on the base terminals of belt fittings, stirrups or sword hilts from the early medieval to high medieval period. It is also possible to apply copper alloys simply by dipping the iron object into a molten copper alloy, but fusion plating of copper alloys was widely used for practical reasons. The technique has been actually described by Theophilus as part of the manufacturing process of barrel padlocks: “Now make an alloy of two parts of copper and a third of tin and crush it to a powder with a hammer in an iron pot; then burn some gold, add a little salt to it, mix it with water, smear it all around and sprinkle the powder around it. When it is dry, smear the mixture around it again more thickly and put it on live coals. Then carefully cover it all around with charcoal let it cool by itself and wash it and this way you can braze anything of iron that you want but it cannot be gilded in any other way” [24]. Corfield [15] has pointed out the improvement of protection against corrosion, but the joining by brazing seems to be much more relevant, as mostly small and thin pieces are joined, which are difficult to forge weld, because of the fast overheating and the high burn-off. In the early Iron Age, these joins, induced by technological reasons, were skilfully used for individual decorative plating [17], but later on the brazing alloys were adopted to cover the hole object in the most cases (see Ankner and Hummel [2]; Corfield [15]).

Figure 6.23 shows a sample from some unspecified rings from Assur, which are ostensibly copper plated, but most probably just brazed to join the parts together. Plating iron with copper alloys might also have an economical background to save the higher-prized metal. Early examples are bronze-plated iron bowls from Voulokaliva near Halos in Greece, dated to the end of the ninth and the beginning of

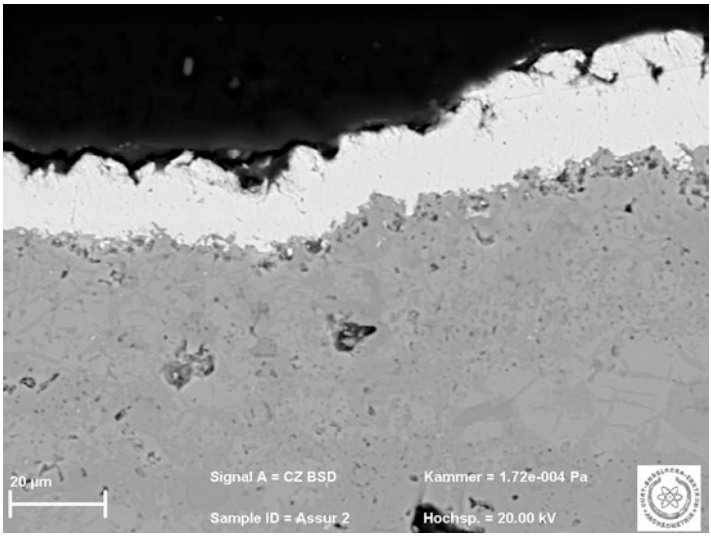

Fig. 6.23 SEM-BSE image of a cross section from an iron ring from Assur. A layer of copper covers the whole surface and has fulfilled all cavities

the seventh century BC [3], but like silver, copper-plated iron-cored coins had been produced to imitate real copper-alloyed coins (e.g. Haubner and Strobl [23]).

References

1. Anheuser, K.: Silver-plated-on-iron Roman coins. In: Oddy, A., Cowell, M. (eds.) Metallurgy in Numismatics 4 Royal Numismatic Society Special Publication 30, pp. 134–146. Royal Numismatic Society, London (1998)
2. Ankner, D., Hummel, F.: Kupferlote bzw. Verkupferung auf Eisen. Arbeitsblätter für Restauratoren. **18**(2), 196–206 (1985)
3. Asderaki, E., Rehren, T., Malakasioti, Z.: Bronze-plated iron bowls from Early Iron Age central Greece. In: Moreau, J.F., Auger, R., Chabot, J., Herzog, A. (eds.) Proceedings of the 36th International Symposium on Archaeometry in 2–6 May 2006, Quebec City, Canada, pp. 383–390 (2009)
4. Baas Becking, L.G.M., Kaplan, I.R., Moore, D.: Limits of the natural environment in terms of pH and oxidation-reduction potentials. J. Geol. **68**(3), 243–284 (1960)
5. Berger, D., Schwab, R., Wunderlich, C.-H.: Technologische Untersuchungen zu bronzezeitlichen Metallziertechniken nördlich der Alpen vor dem Hintergrund des Hortfundes von Nebra. In: Meller, H., Bertemes, F. (eds.) Der Griff nach den Sternen. Wie Europas Eliten zu Macht und Reichtum kamen, pp. 751–777. Tagungen des Landesmuseums für Vorgeschichte Halle Band 05/II, Halle (2010)
6. Berger, D., Hunger, K., Bolliger-Schreyer, S., Grolimund, D., Hartmann, S., Hovind, J., Müller, F., Lehmann, E.H., Vontobel, P., Wörle, M.: New insights into early bronze age damascene technique north of the Alps. Antiqu. J. **93**, 25–53 (2013)
7. Berthelot, M.P.E.: Sur l'altération lente des objects de cuivre, au sein de la terre et dans les musées. Compte Rendus Hebdomadaires des Séances de l'Académie des Sciences. **118**, 768–770 (1994)

8. Bertholon, R.L., Blengino, G.-M.J.M., Durand, E.: De nouvelles approaches de la lecture du rouleau de cuivre de Qunran: re-restauration minimale, radiographie-x et traitement d'image, moulage et galvanoplastie. In: Colloque sur la conservation et restauration des biens culturels. Association des restaurateurs d'art et d'archéologie de formation universitaire (ARAAFU), Paris, pp. 295–300 (1995)
9. Born, H.: Multi-coloured antique bronze statues. In: LaNiece, S., Craddock, P. (eds.) Metal Plating and Patination, pp. 10–20. Butterworth-Heinemann, Oxford (1993)
10. Bosi, C., Garagnani, G.L., Imbeni, V., Martini, C., Mazzeo, R., Poli, G.: Unalloyed copper inclusions in ancient bronze artefacts. J. Mater. Sci. **37**(20), 4285–4298 (2002)
11. Bray, W.: The techniques of gilding and surface-enrichment in pre-Hispanic American metallurgy. In: La Niece, S., Craddock, P. (eds.) Metal Plating and Patination, pp. 182–192. Butterworth and Heinemann, Oxford (1993)
12. Brown, B.F., Burnett, H.C., Chase, W.T., Goodway, M., Kruger, J., Pourbaix, M.: Corrosion and Metal Artifacts – A Dialog Between Conservators and Archaeologists and Corrosion Scientists. National Bureau of Standards Special Publication 479, Houston, TX (1977)
13. Chase, W.T.: Chinese bronzes: casting, finishing, patination and corrosion. In: Scott, D.A., Podany, J., Considine, B.B. (eds.) Ancient and Historic Metals, pp. 85–115. Conservation and Scientific Research, Marina del Rey (1994)
14. Corcoran, S.G.: Effects of metallurgical variables on Dealloying corrosion. In: Cramer, S.D., Covino, B.S. (eds.) Corrosion: Fundamentals, Testing, and Protection ASM Handbook 13A, pp. 287–293. ASM International, Materials Park (2003)
15. Corfield, M.: Copper plating on iron. In: La Niece, S., Craddock, P.T. (eds.) Metal Plating and Patination, pp. 276–283. Butterworth and Heinemann, Oxford (1993)
16. Craddock, P.T., Giumlia-Mair, A.: Hsmn-km, Corinthian bronze, shakudo: black patinated bronze in the ancient world. In: La Niece, S., Craddock, P.T. (eds.) Metal Plating and Patination: Cultural, Technical and Historical Developments, pp. 101–110. Butterworth-Heinemann, London (1993)
17. Eichhorn, P., Rollig, H., Schwarz, U., Urbon, B., Zwicker, U.: Untersuchungen über die Hallstattzeitliche Technik für Bronzeeinlagen in Eisen. Fundberichte aus Baden-Württemberg. **1**, 293–312 (1974)
18. Forty, A.J.: Micromorphological studies of the corrosion of gold alloys. Gold Bull. **14**(1), 25–35 (1981)
19. Geilmann, v.W.: Verwitterung von Bronzen im Sandboden. Angew. Chem. **68**, 201–212 (1956)
20. Gettens, R.J.: The Corrosion Products of Metal Antiquities, Smithsonian Report for 1963, pp. 547–568 (1964)
21. Goodway, M.: Patination of Iron by bower – barfing. In: La Niece, S., Craddock, P.T. (eds.) Metal Plating and Patination, pp. 155–160. Butterworth and Heinemann, Oxford (1993)
22. Gruel, K., Leclerc, G., Nieto-Pelletier, S., Barrandon, J.-N., Blet-Lemarquand, M., Gratuze, B.: Les monnaies gauloises de l'Orne, de la Mayenne et de la Sarthe, approches typologique, analytique et territoriale. In: Barral, P., Dedet, B., Delrieu, F., Giraud, P., Le Goff, I., Marion, S., Villard-Le-Tiec, A. (eds.) L'Âge de fer en Basse-Normandie. Annales littéraires de l'Université de Franche-Comté 883, Besançon, pp. 247–260 (2011)
23. Haubner, R., Strobl, S.: Copper-coated Roman coins – Subferrati. Pract. Metallogr. **53**(5), 273–294 (2016)
24. Hawthorne, J.G., Smith, C.S.: On Divers Arts: the Foremost Medieval Treatise on Painting, Glassmaking and Metalwork. University of Chicago Press, Chicago (1963)
25. Hörz, G., Kallfass, M.: The treasure of gold and silver artifacts from the Royal Tombs of Sipán, Peru – a study on the Moche metalworking techniques. Mater. Charact. **45**(4–5), 391–419 (2000)
26. Hughes, M.: Artificial patination. In: La Niece, S., Craddock, P.T. (eds.) Metal Plating and Patination, pp. 1–18. Butterworth and Heinemann, Oxford (1993)
27. Hughes, R., Rowe, M.: The Colouring, Bronzing and Patination of Metals. The Crafts Council, London (1982)
28. Kallfass, M., Paul, J., Jehn, H.: Investigations on the Embrittlement of an antique Roman silver bowl. Pract. Metallogr. **2**, 317–323 (1985)

29. Stronge, S.: Bidri ware of India. In: La Niece, S., Craddock, P.T. (eds.) Metal Plating and Patination, pp. 135–147. Butterworth-Heineman, Oxford (1993a)
30. La Niece, S.: Technology of silver-plated coin forgeries. In: Archibald, M.M., Cowell, M. (eds.) Metallurgy in Numismatics 3. Royal Numismatic Society Special Publication 24, pp. 227–236. Royal Numismatic Society, London (1993b)
31. La Niece, S.: Bidri ware and its black patina. In: Srinivasan, S., Ranganathan, S., Giumlia-Mair, A. (eds.) Metals and Civilizations. Proceedings of the International Conference Beginning of the Use of Metals and Alloys (BUMA VII), Bangalore, pp. 185–190 (2015)
32. La Niece, S., Martin, G.: The technical examination of bidri ware. Stud. Conserv. **32**, 97–101 (1987)
33. La Niece, S., Shearman, F., Taylor, J., Simps, A.: Polychromy and Egyptian bronze: new evidence for artificial coloration. Stud. Conserv. **47**(2), 95–108 (2002)
34. La Niece, S., Farley, J., Nigel Meeks, N., Joy, J.: Gold in Iron Age Britain. In: Schwab, R., Milcent, P.-Y., Armbruster, B., Pernicka, E. (eds.) Iron Age Gold in Celtic Europe. Forschungen zur Archäometrie und Altertumswissenschaft 6, pp. 407–429. Verlag Marie Leidorf, Rahden/Westf (2018)
35. Lechtman, H.N.: Ancient methods of gilding silver: examples from the old and new worlds. In: Brill, R.B. (ed.) Science and Archaeology, pp. 2–30. Massachusetts Institute of Technology, Cambridge, MA (1971)
36. Lechtman, H.N.: A pre-Columbian technique for electrochemical replacement of gold and silver on copper objects. J. Metals. **41**, 154–160 (1979)
37. Meeks, N.: Surface characterization of tinned bronze, and high tin bronze. In: La Niece, S., Craddock, P.T. (eds.) Metal Plating and Patination, pp. 247–275. Butterworth and Heinemann, Oxford (1993)
38. Meggers, B.J.: Ecuador, Ancient Peoples and Places. Thaínes and Hudson, London (1966)
39. Murakami, R.: Japanese traditional alloys. In: La Niece, S., Craddock, P.T. (eds.) Metal Plating and Patination: Cultural, Technical and Historical Developments, pp. 85–94. Butterworth-Heinemann, London (1993)
40. Mutz, A.: Ein römischer Kesselbügel als Unikum. Schweißtechnik. **62**(9), 263–266 (1972)
41. Notis, M.R.: The Japanese Alloy Shakudo: its history and its patination. In: Maddin, R. (ed.) The Beginning of the Use of Metals and Alloys, pp. 315–327. MIT Press, Cambridge, MA (1988)
42. Oddy, W.A.: Gilding of metals in the old world. In: La Niece, S., Craddock, P.T. (eds.) Metal Plating and Patination, pp. 171–181. Butterworth and Heinemann, Oxford (1993)
43. Oddy, W.A.: A history of gilding with particular reference to statuary. In: Drayman-Weisser, T. (ed.) Gilded Metals: History, Technology and Conservation, pp. 1–19. Archetype, London (2000)
44. Pliny the Elder: Natural History, 10 vols, trans. H. Rackham. Harvard University Press/William Heinemann, Cambridge/Harvard/London (1979)
45. Plutarch: Plutarch's Moralia, vol 5., trans F. C. Babbitt 351C-438E, pp. 264–265. Harvard University Press; London, William Heinemann, Cambridge (1984)
46. Rapson, W.S., Groenewald, T.: Gold Usage. Academic, London (1978)
47. Robbiola, L., Portier, R.: A global approach to the authentication of ancient bronzes based on the characterization of the alloy-patina-environment system. J. Cult. Herit. **7**, 1–12 (2006)
48. Rudoe, J.: Oxidized silver in the 19th century: the documentary evidence. In: La Niece, S., Craddock, P.T. (eds.) Metal Plating and Patination, pp. 161–170. Butterworth and Heinemann, Oxford (1993)
49. Schlosser, S., Reinecke, A., Schwab, R., Pernicka, E., Sonetra, S., Laychour, V.: Early Cambodian gold and silver from Prohear: composition, trace elements and gilding. J. Archaeol. Sci. **39**(9), 2877–2887 (2012)
50. Schorer, B., Schwab, R.: Neue Untersuchungen zu Vergoldungstechniken in der jüngeren Hallstattzeit. Restaurierung und Archäologie. **6**, 57–69 (2013)
51. Schorer, B., Leusch, V., Schwab, R.: New insights into Hallstatt gold from Southwest Germany: technological aspects and material analyses. In: Schwab, R., Milcent, P.-Y., Armbruster,

B., Pernicka, E. (eds.) Iron Age Gold in Celtic Europe, Forschungen zur Archäometrie und Altertumswissenschaft 6, pp 181–254. Marie Leidorf Verlag, Rahden/Westf. (2018)
52. Schwab, R., Haustein, M., Lockhoff, N., Pernicka, E.: The art of Benin: authentic or faked? In: Degrigny, C., van Langh, R., Joosten, I., Ankersmit, B. (eds.) METAL 07 Volume 1. Proceedings of the Interim Meeting of the ICOM-CC Metal WG Amsterdam. 17–21 September 2007, pp. 91–95, Amsterdam (2007)
53. Schwab, R., Ullén, I., Wunderlich, C.-H.: A sword from Vreta Kloster, and black patinated bronze in early bronze age Europe. J. Nordic Archaeol. Sci. **17**, 27–35 (2010a)
54. Schwab, R., Willer, F., Meinel, D., Schmauder, M., Pernicka, E.: The sword from the Niers: a note to European bronze age brass and fire gilding. Hist. Metall. **44**(1), 1–9 (2010b)
55. Scott, D.A.: Pre-Hispanic Colombian Metallurgy: studies of some gold and platinum alloys. In: PhD thesis University of London (1982)
56. Scott, D.A.: An examination of the patina and corrosion morphology of some Roman bronzes. J. Am. Inst. Conserv. **33**, 1–23 (1994)
57. Scott, D.A.: A review of gilding technique in ancient South America. In: Drayman-Weisser, T. (ed.) Gilded Metals: History, Technology and Conservation, pp. 203–222. Archetype, London (2000)
58. Scott, D.A.: Copper and Bronze in Art: Corrosion, Colorants Conservation. The Getty Press, Los Angeles (2002)
59. Scott, D.A.: Gold and platinum metallurgy of La Tolita: a metalworking Centre of the Pacific lowlands of Ecuador. In: Perea, A., Montero Ruiz, I., Garcia-Vuelta, O. (eds.) Tecnologia del oro antiguo: Europa y America. Anejos de Archivo Espanol de Arqueologia 32, pp. 63–82. Ministry of Culture, Madrid (2004)
60. Scott, D.A.: The La Tolita-Tumaco culture: master metalsmiths in gold and platinum. Lat. Am. Antiq. **27**, 122–145 (2011a)
61. Scott, D.A.: Chinese bronze mirrors in the Cotsen collection: the virtual and the real. In: von Falkenhausen, L. (ed.) The Cotsen Collection of Chinese Bronze Mirrors 2. Monumenta Archaeologica 25, pp. 198–234. Cotsen Institute of Archaeology, Los Angeles (2011b).
62. Scott, D.A.: Some decorative techniques and corrosion on Chinese bronze mirrors in the Cotsen collection. In: Jett, P., McCarthy, B. Douglas, J.G. (eds.) Scientific Research on Ancient Asian Metallurgy, Proceedings of the Fifth Forbes Symposium at the Freer Gallery of art, pp 52–62. Archetype Publications, London (2012)
63. Scott, D.A.: The use of metallographic and metallurgical investigation methods in the preservation of metallic heritage artefacts. In: Dillmann, P., Watkinson, D., Angelini, E., Adriaens, A. (eds.) Corrosion and Conservation of Cultural Heritage Metallic Artefacts European Federation of Corrosion Publications 65, pp. 82–100. Elsevier, Oxford (2014a)
64. Scott, D.A.: The metallography of colour. Stud. Conserv. **59**, 107–117 (2014b)
65. Scott, D.A.: Metallography and microstructure of metallic artifacts. In: Roberts, B., Thornton, C. (eds.) Archaeometallurgy in Global Perspective: Methods and Syntheses, pp. 67–89, Springer, Amsterdam (2014c)
66. Scott, D.A.: Physical and chemical examination of the copper plaques. In: Woodard, R.D. (ed.) The Textualization of the Greek Alphabet, pp. 107–118. Cambridge University Press, New York (2014d)
67. Scott, D.A., Eggert, G.: Iron and Steel in Art: Corrosion, Colorants, Conservation. Archetype Publications, London (2009)
68. Smith, C.S.: Historical notes on the colouring of metals. In: Bishay, A. (ed.) Recent Advances in the Science and Technology of Materials 3, pp. 157–167. Second Cairo Solid State Conference, New York/London (1974)
69. Tammann, G.: Die chemischen und galvanischen Eigenschaften von Mischkristallreihen und ihre Atomverteilung ein Beitrag zur Kenntnis der Legierungen. Z. Anorg. Allg. Chem. **107**, 1–239 (1919)
70. Zwicker, U., Oddy, A.W., La Niece, S.: Roman techniques of manufacturing silver plated coins pages. In: La Niece, S., Craddock, P.T. (eds.) Metal Plating and Patination, pp. 223–246. Butterworth and Heinemann, Oxford (1993)

Etching Solutions

This section deals with etching solutions that can be used for archaeological metals. Further details regarding etchants can be found in the literature referred to in Chap. 3. The listing below is therefore very selective and represents the etchants which have been found useful in the experience of the authors.

As regards the solvents used in etching solutions, water (H_2O) should be distilled water, and ethanol (C_2H_6O) should be anhydrous (99%) or not less than 95% alcohol. All chemicals refer to common commercially available concentrated laboratory grade substances and must be handled with care and in accordance to laboratory safety regulations currently in force in the laboratories concerned. The manufacturers of these chemicals also provide safety data sheets which can be consulted for further information regarding storage, handling and use.

Before etching, ensure that the sample is as scratch-free as possible and that the surface is free of oil, water or ethanol staining, as these will all interfere with the correct etching of the sample. Some samples are liable to be stained on etching due to the presence of different phases, holes or interdendritic porosity. In such cases the sample should be carefully washed in ethanol after etching and dried as thoroughly as possible to prevent excessive staining. Samples can be repolished, cleaned in ethanol and then dried and re-etched. This is often advisable if the finish is less than desired on the final polishing and first etching.

For etching the sample can be held in a pair of tongs, of which there are many different types available. Make sure that there is enough room in the etching tray, often a crystallizing dish, for the sample diameter and the tongs to be immersed into the etching solution. Use gentle agitation if possible while etching to avoid stagnant conditions and uneven etching. Samples after etching can be stored in an efficient desiccator or simply repolished and dried if exceptionally valuable. Samples with etched surfaces will continue to corrode, and in the case of iron artefacts, this can be severe with filiform corrosion of exposed surfaces being a common phenomenon. Sound metallographic principle dictates that all specimens should be examined in the unetched state before proceeding to etching. This is partly because etching may

D. A. Scott, R. Schwab, *Metallography in Archaeology and Art*, Cultural Heritage Science, https://doi.org/10.1007/978-3-030-11265-3

dissolve out any non-metallic inclusions or adversely affect the examination of patina and corrosion which can be essential in authenticity determinations.

Health and Safety

Observe all health and safety regulations pertaining to the country in which you are working.

Many etchants, such as nital, are only partially stable and tend to alter over time in their bottle. Make up small quantities of etchants if just for your own use, as this not only ensures that the etchants are fresh but also saves money on chemical supplies. Many of the preparations described here are poisonous or have to be used in a fume hood, depending on local regulations.

Etchants for Iron, Steel and Cast Iron

Nital 95–99 ml ethanol and 1–5 ml nitric acid. The 2% solution is the most common. Nital is the most useful general etchant for most iron alloys. The strength of the nital solution tends to vary over time, and if no etching appears in a reasonable time frame, the worker can try adding a few drops of nitric acid to the solution to increase acid strength.

Picral 100 ml ethanol and 2–4 g picric acid. The 4% solution (saturated) is the most common. Picral is a very useful etchant for iron and carbon steels. Often used for iron and heat-treated steels, pearlite and martensite. Cementite is stained a light yellow. This can be very useful in distinguishing ferrite from cementite. Nital and picral can be used mixed in a 1:1 proportion.

Oberhoffer's Reagent 500 ml distilled water, 500 ml ethanol, 50 ml hydrochloric acid, 30 g ferric chloride, 1 g copper chloride and 0.5 g stannous chloride. After etching the section should be rinsed in a 4:1 mixture of ethanol and hydrochloric acid. Useful for steels in segregation studies such as arsenic segregation.

Heyn's Reagent 40 ml distilled water and 40 g copper (II) ammonium chloride. Copper precipitates must be wiped from the surface with distilled water or washed off with distilled water from a wash bottle. Useful for phosphorus segregation in steels.

Klemm's Reagent I 50 ml stock solution of saturated aqueous sodium thiosulphate and 1 g potassium metabisulphite. Useful for some colour etching of ferrite and for phosphorus segregation in cast steels and cast iron.

Baumann's Print Solution 100 ml distilled water and 5 ml sulphuric acid. Silver bromide paper is saturated with the solution and firmly pressed against the specimen surface. After 1–5 min, rinse and fix with a solution of 6 g sodium thiosulphate in 100 ml distilled water. Wash and dry. Useful for verification, arrangement and distribution of iron and manganese sulphide inclusions.

Beraha's CdS Reagent 100 ml distilled water, 24 g sodium thiosulphate, 3 g citric acid and 2 g cadmium chloride. Use for 20–40 s. Used as a tint etchant for iron and carbon steels. Ferrite is stained brown or violet. Carbides, phosphides and nitrides may be only lightly stained. With Beraha's reagent, ferrite is coloured, but cementite is not, so that both proeutectoid cementite and cementite in pearlite are in strong contrast to the ferrite, which can make even thin films of cementite easily visible.

Beraha's HCl Reagent I 100 ml stock solution of Beraha I and 1 g potassium bisulphite. Colour etchant for heat-treated steels.

Alkaline Sodium Picrate 2 g picric acid, 25 g sodium hydroxide and 100 ml distilled water. This solution is useful for distinguishing between iron carbide and ferrite in steels. Solution can be heated to boiling but is best used at 50°–70 °C for 10 min or longer if required. The cementite is darkened by this reagent, while ferrite is unaffected. Etching in this solution may provide a good indication of pearlite lamellae spacing.

Beaujard's Reagent 20 g sodium bisulphate and 100 ml distilled water. It is often a good idea to etch in nital for 2–4 s beforehand. Beaujard's reagent can then be used for 10–25 s: the surface should be very carefully washed and dried; otherwise, the deposited surface film will be disturbed. The reagent produces good contrast between ferrite grains and between lightly tempered martensite and ferrite, as well as delineating cementite networks. The reagent works by depositing a complex oxide-sulphide-sulphate film on the metal surface, in various shades of brown.

Dimethylglyoxime Nickel Test Some ancient steels contain nickel as an important impurity. A simple test is to take a nickel print by pressing a blotting paper soaked in dimethylglyoxime against the polished section when the nickel-rich areas are revealed by brown staining on the blotting paper.

Vilella's Reagent 1 g picric acid, 100 ml ethanol and 5 ml hydrochloric acid. A reagent that can be used to reveal clearly the needles of plate martensite. It is useful for exposing the austenitic grain size of quenched and tempered steels if this feature is at all discernible.

Sodium Metabisulphite 100 ml distilled water and 1 g sodium metabisulphite. Colour etchant for heat-treated steels to colour martensite.

Etchants for Copper and Copper Alloys

Acidified Potassium Dichromate 80–100 ml water, 5–8 ml sulphuric acid, 2–10 g potassium dichromate, 4 ml sodium chloride (saturated solution) or a drop hydrochloric acid added just before using.

Ammonium Hydroxide/Hydrogen Peroxide 50 ml distilled water, 50 ml ammonium hydroxide and 10–50 ml hydrogen peroxide. Make up and use fresh only. Adding larger amounts of hydrogen peroxide creates better grain contrast, and adding less hydrogen peroxide creates better grain boundary etching. Can be used with benefit on a number of different alloy types.

Aqueous Ferric Chloride 100 ml distilled water, 5–50 ml hydrochloric acid and 5–25 g ferric chloride. Produces grain contrast, very useful for all copper alloys, etching time from a few seconds to 60 s with 3–5 s being common. The authors prefer to use alcoholic ferric chloride as aqueous solution etches fast and often stains.

Alcoholic Ferric Chloride 240 ml ethanol, 60 ml hydrochloric acid and 20 g ferric chloride. This is the most common etchant used by the authors.

Aqueous Ammonium Persulphate 200 ml distilled water and 20 g ammonium persulphate. Produces grain contrast. Must be use fresh; will not keep.

Acidified Ammonium Persulphate 100 ml distilled water, 10 g ammonium persulphate and 5 ml hydrochloric acid. Helpful etchant for copper-nickel alloys.

Beraha's Lead Thiosulphate Etchant 12 g sodium thiosulphate, 1.2 g lead acetate and 1.5 g citric acid in 50 ml distilled water. Colours grains depending upon their orientation and contrasts α/β-brasses. Can be used after ammonium persulphate pre-etch.

Beraha's Selenic Acid Reagent 300 ml ethanol, 2 ml hydrochloric acid and 0.5 ml selenic acid. Colours grains depending upon their orientation and contrasts α/β--brasses. Can be used after ammonium persulphate pre-etch.

Klemm's Reagent II 100 ml stock solution of saturated sodium thiosulphate and 5 g potassium metabisulphite. Immerse for revealing segregations in cast and worked copper alloys.

Klemm's Reagent III 20–40 g potassium metabisulphite, 100 distilled water and 11 ml stock solution. Colours grains depending upon their orientation. Intermetallics are not etched, and segregations become clearly visible.

Potassium Ferricyanide 5 g potassium ferricyanide and 100 ml distilled water. This etchant can be used to darken some precipitates such as Cu_3P which may coexist with the alpha+ delta eutectoid. Cu_3P can be seen as a purple shade against the very pale blue of the delta phase in bronzes. After etching in alcoholic ferric chloride, this distinction is lost. Some difficulties may be overcome by using a relatively high amount of aqueous ammonia in the final polish.

Etchants for Gold Alloys

Ammonium Persulphate/Potassium Cyanide 100 ml distilled water, 10 g ammonium persulphate and 10 g potassium cyanide. Very useful for gold alloys. Sometimes good results can be obtained after a brief etch/clean in a 10% persulphate pre-etch. The most common problem is etch pitting with this etchant, which can be hard to eliminate.

Aqua Regia 40 ml nitric acid and 60 ml hydrochloric acid. Used for a few seconds or up to 1 min. Use fresh. Aqua regia is a strong oxidizing solution and highly corrosive. In most alloys it provides grain contrast.

Hydrogen Peroxide/Iron (III) Chloride 100 ml distilled water, 100 ml hydrogen peroxide and 32 g ferric chloride. Sometimes useful for variable gold jewellery alloys and Au-Cu-Ag alloys.

Etchants for Silver Alloys

Acidified Potassium Dichromate 10 ml sulphuric acid; 100 ml potassium dichromate, saturated in water; and 2 ml sodium chloride (saturated solution). Dilute 1:9 with distilled water before use and swab with cotton wool. Can also be used without the sulphuric acid addition.

50 ml ammonium hydroxide and 20 ml hydrogen peroxide. Must be used fresh. Immerse for up to 60 s.

25 ml ammonium hydroxide, 25 ml water and 50 ml hydrogen peroxide. For silver-copper alloys. Add peroxide last, use fresh, and sample can be etched for up to 45 s.

Ammonium Persulphate/Potassium Cyanide 100 ml distilled water, 10 g ammonium persulphate and 10 g potassium cyanide. Also useful for gold alloys (see above).

Etchants for Tin Alloys

Ammonium Polysulphide A saturated aqueous solution of ammonium polysulphide. Use for 20–30 min. Wipe off with cotton wool after etching. Can be used for all types of tin alloys. Nital or picral can also be used (see etchants for iron, steel and cast iron).

Taff's Reagent 60 ml ethanol, 30 ml distilled water, 5 ml hydrochloric acid and 2 g ferric chloride. Add one drop of hydrogen peroxide to solution before use. For pure tin and tin-bismuth alloys.

100 ml ethanol and 2–10 ml hydrochloric acid. For pure tin and alloy. Immerse for 1–5 min.

Klemm's Reagent II 50 ml saturated aqueous sodium thiosulphate and 5 g potassium metabisulphite. Immerse for 60–90 s for grain colouration.

Etchants for Zinc Alloys

Zinc alloys are difficult to prepare mechanically. Fake microstructures are common because deformation is difficult to prevent.

Palmerton's Reagent 100 ml distilled water, 20 g chromic oxide, 1.5 g sodium sulphate (anhydrous) or 3.5 g sodium sulphate, hydrated. Can be used for seconds or minutes.

100 ml distilled water and 10 g sodium hydroxide. Can be used for pure zinc and zinc-copper alloys, immersed for 5–15 s.

100 ml ethanol and 5 ml hydrochloric acid. For zinc samples, can be immersed for several seconds.

Klemm's Reagent I 50 ml saturated aqueous sodium thiosulphate and 1 g potassium metabisulphite. Immerse sample for about 30 s.

Etchants for Lead Alloys

If difficulty is experienced in the preparation of lead alloys, a good technique is to try finishing the polishing with fine alumina powder or use etch-polish techniques.

Glycerol Etchant 84 ml glycerol, 8 ml glacial acetic acid,

100 ml ethanol and 1–5 ml nitric acid. Use fresh only. Gives grain boundary contrast. Nital can also be used (see etchants for iron, steel and cast iron).

80 ml water, 15 ml acetic acid and 25 ml nitric acid. For lead and lead-tin alloys. Use fresh for several seconds up to minutes.

Glacial Acetic Acid 15 ml glacial acetic acid and 20 ml nitric acid. Useful for lead solders and Pb-Sn alloys.

Colour Metallography

As compared with conventional etching, colour metallographic methods enhance contrast with interference layers produced by evaporation, by sputtering or by chemical deposition for colour effects (see Chap. 3). It is sometimes useful to investigate the application of colour metallography to ancient metallic object specimens to enhance the visual appreciation of microstructural features. One of the potential advantages to interference film metallography is that coring and segregation may be revealed when conventional metallographic techniques fail. Further colour etching solutions and details concerning the techniques which may be employed can be found in the literature referred to in Chap. 3.

Some of the useful recipes are set out below and in the list of etchants. For colour etching different strengths of Klemm's reagent are the most useful. The stock solution of Klemm's reagents is a cold-saturated sodium thiosulphate solution of approximately 1 kg sodium thiosulphate in 300 ml distilled water, which can be stored without limit. The etchants themselves have to be made fresh every time it is used, by the addition of a few grams of sodium metabisulphite (see above). After immersion etching, you can cover the beaker tightly, or pour the solution into a tightly closed bottle, and keep reusing it for nearly a month – until crystals start precipitating. The stock solution can be taken, and new water can be repeatedly added till the salt will go back into solution. Pre-etching with standard general-purpose etchants such as 10% aqueous potassium peroxydisulphate is often useful but not generally required.

For Beraha's lead sulphide or cadmium sulphide solutions, the conditions of use are more exacting and have to be followed carefully. The chemicals must be dissolved in the order given. After the sodium thiosulphate is dissolved, the lead acetate (or cadmium acetate) is added and allowed to attempt to dissolve. Beraha says that you have to let it go into solution before adding the citric acid, but that does not happen. After about 30 min of stirring, add the citric acid. The solution is then placed in a dark bottle and placed in a dark closed cabinet to age for 24 h before use. This solution will easily last for about 6 months before it starts to change colour and

D. A. Scott, R. Schwab, *Metallography in Archaeology and Art*, Cultural Heritage Science, https://doi.org/10.1007/978-3-030-11265-3

is exhausted. It could probably be kept between uses at a temperature of 10–15 °C, but it should be allowed to warm to 25 °C before use. The more common laboratory approach is to mix a stock solution, e.g. 500 ml, of aqueous saturated sodium thiosulphate. Pre-etching is often useful but not generally required.

Beraha's etchants with hydrochloric acid require individual stock solutions and the addition of a few grams of potassium bisulphite before use. The stock solution for Beraha's reagent I is 24 g ammonium difluoride, 1000 ml distilled water and 200 ml hydrochloric acid. The stock solution for Beraha's reagent II is 48 g ammonium difluoride, 800 ml distilled water and 400 ml hydrochloric acid and 50 g ammonium difluoride, 600 ml distilled water and 400 ml hydrochloric acid for Beraha's reagent III.

A Glossary of Terms and Definitions

Acicular structures Non-equilibrium substructure that may possess an elongated or needle-shaped microstructure.

Age-hardening The process of hardening and strengthening of alloys spontaneously or over time at ambient conditions by the precipitation of dispersed particles from a supersaturated solid solution. For the ageing of carbonsteels, see *tempering*.

Allotropy Ability of some elements to change their crystal structure in dependence of temperature or pressure.

Alloy A combination of two or more metallic components. The term alloying suggests that the mixture was deliberate.

Alpha2 phase In ironmeteorites this is a variation of the kamacite crystals, which are the alpha phase in the iron-nickel system. The phase designation means that the crystals are a variation on the usual alpha phase (which here is kamacite).

Alpha brass An alloy of copper and zinc with no more than 38% zinc, usually less than 32% zinc, consisting of a single phase, the copper-rich α_{Cu} solid solution.

Amalgam An alloy of mercury with other metals, which can be liquid, pasty or solid, depending on the proportion of mercury. Mercury may form an amalgam with gold, silver, tin, zinc, lead, copper and most other metals. The microstructure of these amalgams may be complex.

Amalgam gilding Process used for gilding of copper, silver or iron. Gold becomes pasty when mixed with mercury and can be applied to the surface. Gentle heating drives off most of the mercury. Mercury can also be rubbed onto the cleaned substrate surface followed by attachment of gold leaf or foil.

Annealing Process of heat treatment carried out on a metal or alloy, usually to soften the material after cold-working to allow further deformation or to eliminate residual stress. Can be further elaborated as stress-relief anneal, solid solution anneal, normalizing.

Annealing twins Twins that are formed during recrystallization in certain face-centred cubic and also in few body-centred cubic metals. They appear in two

D. A. Scott, R. Schwab, *Metallography in Archaeology and Art*, Cultural Heritage Science, https://doi.org/10.1007/978-3-030-11265-3

parallel straight lines across the grain after etching and result from atomic displacements. Twins have a special mirror image orientation relationship to the matrix lattice.

Anode Electrode of an electrolytic cell at which oxidation occurs. In an electrochemical reaction, the anode is the component of a system that usually corrodes.

Austenite Iron undergoes a phase transition between 911° and 1394 °C, from bcc iron to the face-centred cubic (fcc) configuration of gamma iron, called austenite. Austenite can dissolve considerably more carbon, up to 2.03% by weight at 1146 °C.

Bainite Generally a metastable non-lamellar aggregate of ferrite and carbides formed below martensitic start temperatures and above eutectoid decomposition to pearlite. In some nonferrous alloys, microstructures similar to bainite occur.

Bidri Specific Indian zinc alloys, finished by surface treatment to colour it black and often inlaid with silver. The alloys contain high amounts of zinc with small amounts of copper and some lead.

Bloom A semisolid iron extraction process in which a mass of smelted iron and iron slag is produced in the bloomery process. The bloom must be refined by reheating and forging to squeeze out the slag and weld the iron particles to enable a consolidated iron bar.

Body-centred cubic (bcc) A unit cell in which atoms are arranged at the corners of a cube with one atom in the centre of the cube. Bcc metals are strong and tough and can accommodate small atoms within the lattice.

Brass An alloy of copper and zinc, usually with copper as the major alloying element and with zinc up to 40% by weight. Early alloys were binary alloys containing 90–70% copper and 10–30% zinc. The colour of brass changes with increasing zinc content from a rich copper red through pale yellow to white as the zinc increases.

Brazing Joining of metals together with a filler alloy which melts above 425 °C. Modern brazing alloys are usually copper-zinc alloys to which silver is added and therefore often called silver solders. In ancient time copper and copper alloys, silver-gold, copper-silver and the silver-gold-copper alloys were used for brazing operations on iron, copper alloys and precious metals in particular.

Bronze In historical usage, bronze is essentially an alloy of copper and tin. In modern nomenclature, the term bronze includes all copper alloys, which do not have zinc or nickel as the major alloying element, and the composition of the alloy must be specified.

Brinell hardness A static hardness test that uses a small steel ball indenter. This method has become less common but does allow some comparison with the results from the Vickers scale, as well as other scales used more for industrial purposes such as the Rockwell scale.

Carburization Process of increasing the surface concentration of carbon in iron by solid-state diffusion, by heating austenitized iron together with carbonaceous matter such as wood charcoal or horn shavings to produce carbon monoxide gas that is adsorbed by the metal (see also case-hardening).

Case-hardening Synonym for carburization and other diffusional surface treatments but usually involves also subsequent heat treatments like quenching and following tempering of the adsorbed layers.

Casting Fabrication process of pouring metal into moulds of desired shape. After solidification the metal should assume the shape of the mould. The simplest forms are open moulds that are uncovered at the time of casting, but more complex forms have been used from the beginning (see moulds and lost-wax casting).

Casting-on A process of making a cast part attached to an already existing object or component. In antiquity, a lost-wax addition, made by creating a small mould around part of an object and casting on metal directly to it. Often used for dagger handles or repair or construction of large bronze figures.

Cast iron An iron-carbon alloy that usually contains 2–4% carbon. Generally divided into three groups. Grey cast iron in which free carbon occurs as flakes of graphite. It has excellent casting properties and can be machined. White cast iron in which all of the carbon is taken up as cementite and as pearlite. These irons are usually hard and brittle. Malleable cast irons are usually obtained by heat treatment of white cast irons, in the white heart process, for example, a certain amount of carbon is removed from the surface by oxidation.

Cathode Electrode of an electrolytic cell at which reduction takes the place. In many corrosion processes, the cathodic regions are protected during corrosion, while anodic regions are dissolved and electrons flow towards the cathode.

Cementation This term has several meanings in ancient metallurgy. Cementation of gold alloys with salt in a crucible may remove silver leaving pure gold behind. Brass has been made by interdiffusion of zinc vapour to metallic copper, called cementation process. Carbonaceous material may be used to cover wrought iron, which is then heated, so that the carbon can diffuse into the structure (see carburization and case-hardening).

Cementite Hard and brittle iron carbide that crystallizes in the orthorhombic system with the chemical formula Fe_3C containing about 6.6% carbon.

Chasing Non-cutting but plastic deforming metalworking by the use of chasing tools, often of brass, bronze or wrought iron. Softer metals like gold can also be enchased by tools made of antler, wood or bone. Unlike engraving, metal is distorted around the chased design and residual stress is not removed.

Close-packed hexagonal (cph) Close-packed hexagonal metals with a repeating sequence of atoms as ABABABAB. The unit lattice has a hexagonal prism structure with one atom at each corner, one in the centre of the bottom and top faces and three in the centre of the prism. Metals of cph structure tend to be brittle such as cadmium, cobalt, titanium and zinc.

Coherent precipitation Precipitation of fine particles of a second phase, with an orientation that continues the lattice of the matrix. They are usually not large enough to resolve and therefore imperceptible by optical microscopy.

Cold-working Plastic deformation of a metal at a temperature low enough to cause permanent strain hardening. The treatment usually consists of rolling, hammering or drawing at room temperature when the hardness and tensile strength are

increased with the amount of cold-work, but the ductility and impact strength are reduced.

Columnar Long column-like grains that can form when a pure metal is cast into a mould. Also seen in electrotyped copper.

Continuous precipitation The formation of precipitates or inclusions from a supersaturated solid solution, distributed uniformly through the grains themselves. They grow by long-range diffusion without recrystallization of the matrix.

Coring Segregation of an alloy on the successive freezing to the solid. Zones are formed, especially in dendritic castings, in which a continuous series of small changes in composition occurs as the dendrite is formed. Especially common, in ancient cast bronzes and cast silver-copper alloys. Coring is accentuated in alloys with a wide separation between liquidus and solidus curves.

Crimping Mechanical joint between two pieces of metal in which they are deformed to shape an overlap or attachment.

Cupel A porous ceramic, usually made from bone ash or a mixture of bone ash with lime. The cupel is used to melt small amount of precious metals, usually silver to separate the lead. In the extraction of lead from silver, the oxidized lead is absorbed into the cupel leaving a button of silver behind. The cupel can then be broken and smelted to recover the lead.

Cupellation A two-stage process applied to extract precious metals, usually silver. Silver can be recovered from argentiferous ores or from debased silver alloys by the addition of lead, which can later be removed by oxidizing the lead in a cupel or in a special furnace, the so-called cupellation hearth.

Cupro-nickel Alloys containing copper and nickel usually from 15% to 70% nickel but in ancient alloys often with less nickel than this. Alloys with about 25% nickel are now used for coinage metals.

Dendritic Crystals formed during solidification and shaped like the branches of a tree. Dendrites are common in cast alloys and may look like an intersecting snowflake pattern.

Depletion gilding Surface enrichment with gold by removal of one or more base components. Commonly used in ancient South America for the gilding of tumbaga alloys or gold-silver-copper alloys by removing copper from the outer surfaces by pickling.

Depletion silvering Silver-copper alloys usually develop a scale when worked and annealed. Removing oxide scale enriches the surface in silver creating a depleted copper zone and making the alloy silver in colour.

Diffusion The migration of one alloy or metal into another. Interdiffusion also occurs with the second metal migrating into the first. Usually heat is required for this process to occur.

Diffusion bonding Bonding or joining of two metals by heating them together. Each will diffuse into the other at different rates creating a strong and permanent metallurgical bond.

Diffusion coefficient The diffusivity D describes the rate of movement of a substance into material. Its value depends on factors like temperature, concentration or crystal structure and is given as an SI unit of square metres per second (m^2/s).

Discontinuous precipitation The formation of precipitates or inclusions from a supersaturated solid solution, laid down at grain boundaries, often by a process of ageing. They grow by short-range diffusion with the recrystallization of the matrix.

Dislocation Defects in the crystal structure of a metal that allow movement of planes or atoms within the lattice. Edge and screw dislocations are two common types.

Dislocation entanglement The density of dislocations increases on working the metal until dislocation entanglement is reached. At this point the metal is brittle, and no further movement can occur. Annealing will restore working properties.

Drawing The act of pulling a wire through a draw plate of hard material to reduce the cross section dimension, with a corresponding increase in length of the wire.

Ductility The ability of a metal to undergo plastic deformation to a certain extend without fracture, especially during drawing.

Electrochemical corrosion Corrosion of a metal in which anodic and cathodic reactions result in metallic dissolution. The most common form of corrosion of buried or marine metals.

Electrochemical replacement plating Electroless plating technology used in ancient Peru as a gilding technique producing layers of extraordinary thinness. Cleaned copper will exchange with gold solutions to form a thin gold surface as the copper is corroded away.

Electrum Naturally occurring or deliberate produced alloys of gold and silver, usually white or pale silvery in colour and containing about 40% silver.

Engraving Cutting metalwork with a sharp graver to remove metal from a surface for decoration. Gravers must be harder than the base metal but also tough to prevent breaking the edge.

Epsilon phase In iron meteorites this is derived from the carbide phase with has the formula $Fe_{2\text{-}3}C$. This is a hexagonal close-packed phase in the iron-carbon system, seen in iron meteorites.

Equilibrium diagram A synonym for a phase diagram or constitutional diagram.

Equilibrium structures Microstructures that represented full equilibrium phases predicted from the phase diagram. In ancient metals the microstructures are usually far from equilibrium.

Equiaxed grain Individual crystal of equal dimensions or properties in all directions. The equiaxed grains are ideally hexagonal in form.

Eutectic The eutectic is a fixed composition in binary alloys with the lowest melting point. The eutectic reaction converts one liquid phase directly into two distinct solid phases upon cooling and the microstructure consists of an intermixture of two or more solid phases.

Eutectoid Decomposition from a solid solution into a finely dispersed mixture of two or more solid phases upon undercooling creates a microstructure called the eutectoid. The eutectoid point is fixed in binary alloys and the morphology may resemble the eutectic.

Fahlore Old German miner's term used for a variety of complex sulphide minerals such as tennantite ($Cu_{12}As_4S_{13}$) and tetrahedrite ($Cu_3Sb_4S_{13}$), chatted with copper ores.

Fayalite An iron silicate (Fe_2SiO_4) which melts at about 1205 °C crystallizes in the orthorhombic system and belongs to the olivin group. Fayalite is the predominant mineralogical constituent of ancient slag. Its name is derived from Fayal Island, which is of volcanic origin and where it has first been observed.

Ferrite Body-centred cubic modification of iron at room temperature, also called alpha iron (α_{Fe}).

Face-centred cubic (fcc) In this lattice system that is an atom at each corner of a cube and an atom at the centre of the cube faces. Face-centred cubic metals tend to be soft and easily worked such as silver, gold, copper, lead and platinum.

Forge welding Basic blacksmithing technology to combine different pieces of iron by heating them to white heat and hammering them to effect an interfacial bond. It is comparable to modern pressure welding.

Fusion gilding A process used in ancient South America, especially Ecuador, for the gilding of copper alloys by dipping or fusion of molten gold alloys to the surface resulting in thick gold alloy coatings. May also be used to create silver alloy coatings over copper.

Gama-hada Japanese decorative technique making use of immiscible metals such as silver or silver-copper alloy droplets on iron.

German silver One synonym for alloys of copper, nickel, and zinc, usually consisting of 52–80% copper, 5–35% nickel and 10–35% zinc. This alloy was formerly used for many decorative purposes as a cheap substitute for silver, since it does not readily tarnish and is also of silvery hue.

Gilded Covering of a less noble metal or non-metal either totally or partially with gold.

Gold leaf Leaf in ancient technology is rare. The term is reserved for gold less than 1 micron thick.

Gold foil Any gold sheet greater than 1 micron thick.

Grain Single crystal with a polygonal shape within a polycrystalline metal or alloy. The interface between two grains, the grain boundary separates areas of the same structure but different orientation.

Grain boundary segregation Also known as grain boundary precipitation, as mostly non-metallic or intermetallic compounds precipitate preferentially at the interfaces because of their higher energy state.

Granulation Usually refers to tiny gold grains attached to an object with a specific solder, made in situ by reduction of a copper salt with organic glue or by use of diffusion bonding of the gold grains.

Graphite An allotropic form of carbon, occurring in the trigonal system as grey, soft, lustrous plates. It is the form of carbon found in steels and cast irons and usually occurs in grey cast irons as thin flakes or nodules.

Grey cast iron Cast iron with a grey fracture. The fracture colour is indicative that the cast iron contains free carbon as graphite.

Gunmetal Copper alloys which may have different compositions, but usually an alloy of copper, tin and zinc.

Hardness Resistance of a material to plastic deformation. Hardness testing is usually performed by the indentation of specified test specimen.

Hard soldering An alternative term for the use of a brazing alloy for joining, as opposed to the use of soft solders.

Hot-working Deformation of metals or alloys above their recrystallization temperature.

Hypereutectic alloy Alloys including a eutectic and having an excess of the solute. The microstructure may contain some eutectic and primary dendrites of the solute.

Hypereutectoid alloy Alloys including eutectoid decomposition and having an excess of the solute. The microstructure may show some proeutectoid precipitations of the solute with some eutectoid.

Hypoeutectic alloy Alloys including a eutectic and having an excess of the solvent. The microstructure may contain some eutectic and primary dendrites of the solvent.

Hypoeutectoid alloy Alloys including eutectoid decomposition and having an excess of the solvent. The microstructure may show some proeutectoid precipitations of the solvent with some eutectoid.

Intaglio The process of engraving or removing metal to create a design. The depression so formed may be filled with niello, glass or enamel.

Interstitial solid solution Some elements (H, C, N) with small atom sizes may occupy lattice spaces between the atoms of a solvent without causing too great a distortion of the original lattice structure.

Kamacite An important constituent of iron meteorites. It is the α(Fe,Ni) phase, an alloy of iron and nickel, usually in the proportions of 90:10 to 95:5 although impurities such as cobalt or carbon may be present. It is a major constituent of iron meteorites (octahedrite and hexahedrite types). In the octahedrites it is found in bands together with taenite, forming Widmanstätten patterns. In hexahedrites, fine parallel lines called Neumann lines are often seen, which are evidence for structural deformation of adjacent kamacite plates due to shock from impacts.

Karat Traditional term used to express the degree of purity or fineness of gold. The fineness of alloyed gold can be expressed in the number of parts of gold that are contained in 24 parts of the alloy or by parts per thousand. For example, 18 karat gold contains 18/20 parts of gold and is 75% gold or 750 parts fine, while pure gold is 24 karat or 1000 parts fine.

Kirkendall effect Phenomenon that can be observed at the interdiffusion of two components having different diffusion coefficients D. Due to the difference in diffusion rate, voids are formed at the boundary interface on the side of the faster component, while the side of the lower component will expand by volume

Leaf gilding Mechanical covering with gold by the application of gold leaf or gold foil. Sometimes held mechanically by roughing the surface or by an organic adhesive.

Ledeburite Name applied to the cementite-austenite eutectic at 4.3% carbon which forms at 1148 °C. During cooling the austenite in the eutectic may transform into a mixture of cementite and pearlite.

Liquidus The line on a binary phase diagram that shows the temperature at which solidification begins upon cooling from the melt or finish melting during heating. In a ternary diagram the liquidus is a surface not a line.

Lost-wax casting Casting metal from a wax model. The object to be made is shaped in wax, either solid or hollow, and is covered in a clay mould. When the wax is molten out, the space can be filled with molten metal, usually bronze or brass.

Martensite Often used for the hard, needlelike component of quenchedsteels, but more generally any needlelike transformation product of a quenched alloy. The most common in ancient materials is martensite in quenched steels or martensite in the beta-quenched bronzes.

Martensitic transformation Spontaneous diffusion less phase change by rapid cooling of specific alloys, like carbon steels or high-tin bronze.

Mechanical twinning Plastic deformation of individual crystals produced by mechanical strain alone, which exhibits changes in orientation of the distorted crystal planes. Twinning occurs in metals with CPH structure such as zinc or bcc metals such as iron.

Meteoritic iron Iron from outer space. Usually an alloy of iron and nickel. Small amounts of cobalt and manganese are typical. Some early exploitation made use of meteoric iron. The iron comes in many different types, the most common being the octahedrites and the hexahedrites.

Moulds Hollow forms made of clay, sand, stone or metal to give molten metals a particular shape. Moulds made of wood and antler have been used for casting tin and lead, while shell of cuttlefish for precious metals is also evidenced. Open moulds are the simplest use of casting into an open-shaped depression in clay or stone. Piece moulds are made of two or more pieces in stone, bronze or clay. Hollow cast objects are usually piece moulds with false cores modelled in clay (see also lost-wax casting).

Neumann bands These are mechanical twins in iron alloys after deformation by a sudden impact. They can often be seen in ancient iron artefacts. In meteorites, they can be found as a series of fine pattern lines seen in cross sections of many hexahedrite iron meteorites and some octahedrites in the kamacite phase.

Nitriding The hardening of steels due to nitrogen content that may result in nitrides or carbon nitrides being formed in the alloy, usually of acicular shape.

Pattern-welding Ancient blacksmithing process of ornamenting a metal surface with a specific pattern by welding different irons and steels together. Forge-welded composite rods of iron and steel can be twisted and combined with other composite rods to produce complex manifold pattern after grinding, polishing and probably final treatment with acids.

Pearlite A fine mixture of ferrite and cementite found in steels. The eutectoid, pearlite, will be complete when the carbon content reaches 0.8%.

Peritectic Reaction of a solid phase with a liquid of a different composition to create a new solid phase by cooling to the peritectic temperature. The new phase

may consume all of the liquid to form a totally new solid. An example is the beta phase in the bronze system.

Peritectoid Solid-state reaction in which two solid phases in a binary system react to form a new solid phase. A peritectoid reaction occurs in the bronze system, for example, in which at 65% copper, a reaction between Cu_3Sn and the solid solution gamma produces a new phase, Cu_4Sn at about 580 °C.

Pewter Ancient pewter is an alloy of lead and tin, much used in Roman times. The poisonous nature of lead has resulted in the replacement of lead with antimony, although antimony is also inadvisable in high amounts for utensils. Pewter in antiquity may consist of 60–80% tin and 40–20% lead, while modern pewter may be 15–30% copper, 5–10% antimony and 87–94% tin.

Phase A component in a heterogeneous system having a homogeneous chemical composition and uniform physical properties.

Phase diagram A diagram with axes of temperature and composition describing the different phases that may occur in an alloy with change in either composition or temperature. A binary phase diagram consists of two components on each end of the horizontal axe versus the temperature on the vertical axe. A ternary diagram consists of three components plotted on a triangle, representing each the horizontal axe of a binary diagram, while the temperature is plotted perpendicular to composition triangles.

Piece mould A mould taken from a model that may be assembled in a number of pieces before being used for sloshing wax over the mould interior for lost-wax copies of a master model. Such techniques were common in the Renaissance.

Plessite A fine mixture, a eutectoid, between kamacite and taenite (qv), the alpha and gamma phase of the iron-nickel system. It is found in the octahedrite meteorites, and many morphological varieties are known to occur. It is a meteorite texture consisting of a fine-grained mixture of the minerals kamacite and taenite found in the octahedrite iron meteorites. Some varieties are acicular plessite, black or type II plessite, comb plessite, net plessite, pearlitic plessite and spheroidized plessite.

Polycrystalline Consisting of many individual crystalline grains. Most metal are polycrystalline solids.

Polygonal Many-sided. Some grain shapes may be polygonal.

Prill In the extraction of copper from primitive smelts, the metal is produced as small droplets or particles in a slaggy matrix. These small metallic particles are called prills which often are extracted by breaking up the melted product and salting the metal. In a crucible process trails all small droplets of metal adhering to the crucible lining.

Pseudomorphic The replacement in the corrosion process of one material with corrosion products of another that mimics the form of the replaced product. Pseudomorphic replacement of organic materials is common on iron and can occur with copper alloys and silver-copper alloys as well.

Puddled iron Process to refine pig iron by stirring the liquid iron with long rods (paddle) to bring all iron into contact with the hot air to oxidize as much impurities as possible. The technology has been developed in England during the eigh-

teenth century and spread all over Europe in the nineteenth century. It has finally given up at the beginning of the twentieth century because of the introduction of the Thomas process.

Quenching The act of quickly cooling a metal or alloy by plunging it into a cold liquid like water, oil or brine to supress equilibrium decomposition. The quenching of steel refers to the production of martensite and bainite to harden a tool or weapon. Quenching of nonferrous alloy is used to avoid embrittlement during cold-work. The quenching of gold alloys is to suppress ordering reactions, while silver-copper alloys or bronzes are quenched to prevent eutectic and eutectoid decomposition, respectively.

Repousse Working from the back of the metal, often using the slight relief of a chased design on the front. The metal is then displaced by hammering, usually on a soft support such as pitch, so as to create raised designs on the front.

Riveting Joining of metal sheet by small metal pegs passing through the sheet and being hammered down.

Safidruy Islamic term for high-tin bronzes, often white in colour.

Shakudo Japanese term for the deliberate use and manufacture of coloured gold-copper alloys.

Shibuichi Japanese term for decorative silver-copper alloys often worked and annealed, to create decorative surfaces when coloured by chemical etching or staining.

Sinking A technique in which a vessel can be produced by hammering from the inside. The sheet metal is hammered either on the flat surface of an anvil or more commonly hammered into a shallow concave depression in the anvil. Also called blocking or hollowing.

Slag A relict of pyrotechnical processes like smelting or processing metals, consisting basically of silicates and metal oxides. Slag can contain metallic prills, charcoal and undecomposed ore minerals. Slag can be entirely glassy like early blast furnace slag, but most ancient slag is a mixture of high-temperature minerals like fayalite, glassy components and secondary minerals from the weathering of the slag.

Slag stringers Small pieces of slag that have become incorporated into the metal and are then strung out as small elongated ribbons as a result of working the metal to shape it.

Slip planes Dislocated crystallographic planes in which slip occurs due to plastic deformation. Slipping can only occur in certain crystal planes and can only move in specific directions. Due to the different atomic arrangements in the distinct crystal systems, dislocations move along a given system. Especially fcc metals may show a fine series of parallel lines called slip bands, because of their 12 slip systems.

Slush casting Method of casting in which metal is often spun or agitated in the mould so that a thin shell is formed. More common in ancient and historic metalwork is slush wax work in which wax is slush cast over a piece mould interior before investment.

Soft solders A term predominantly applied to lead-tin alloys used in ancient soldering. The upper limit of the melting range of modern solders is about 425 °C, but ancient solders melt at about 130–260 °C.

Solid solution A relative homogenous crystalline phase of different elements which share the lattice of a matrix metal. Substitutional and interstitial solid solutions are possible.

Solidus The line in the phase diagram that separates the pasty stage of the alloy, usually a mixture of solid and liquid, from the completely solid alloy below the temperature of the solidus line. The solidus temperature may be different at different alloy compositions, depending on the type of the phase diagram.

Sorbite An obsolete term for very fine pearlite produced by the decomposition of martensite by tempering or insufficient quenching.

Speculum A name sometimes applied to Roman or bronze mirrors containing a high percentage of tin. Historic speculum may contain about 67% copper and 33% tin. Ancient mirrors made use of similar alloys often of beta bronze composition and up to about 24% tin.

Spinning Turning metals on a lathe followed by depression of metal while in motion.

Stamping Plastic deformation of metal by a hard die, often used for assay purposes.

Steel A malleable alloy of iron and carbon that contains about 0.1–1.9% carbon. The carbon is present as cementite, usually as a component of pearlite.

Sterling silver A common coinage binary alloy of 92.5% silver and 7.5% copper.

Strain hardening A synonym for work hardening.

Strain lines Same as slip lines.

Striking A method of making coins and medals. The impression is cut in negative in a very hard material, and this die is then placed over the coin blank and given a heavy blow, thus compressing the metal of the blank into the recesses of the die.

Taenite An important phase constituent of iron meteorites; it is (gamma) γ (Fe, Ni), a solid solution alloy of iron and nickel. The amount of nickel present in this phase varies from about 20% up to 65%. In octahedrites (a class of meteorites), it is found in bands interleaved with kamacite, making the well-known Widmanstätten pattern, whereas in ataxites, it is the dominant constituent. In octahedrites a fine intermixture with kamacite can occur, which is called plessite.

Tempering A heat treatment that is usually applied to steels in which some of the hardness is removed by heating at moderate temperatures from 452 to 650 °C depending on the type of tempering required. Tempered martensite decomposes and forms fine particles of iron carbides.

Tinning The operation of coating a base metal with tin. The coating may be obtained by hot dipping into molten tin or by wiping the molten tin over the surface of the object.

Troostite An obsolete term for very fine pearlite, not resolvable by optical microscopy. It is produced by the decomposition of martensite by tempering or insufficient quenching and is sometimes synonymous with bainite. Nodular troostite is very characteristic for steels not cooled quickly enough to form martensite.

Tumbaga Collective name given in ancient South America to the alloys of copper and gold, of wide range of composition and colour.

Tutenag Copper-zinc-nickel alloy of silvery colour, imported from China to Europe in the eighteenth to nineteenth century AD.

TTT diagrams Time-temperature-transformation diagrams most useful in considering the nature of the quenched microstructure to be found in steels and high-tin bronzes. The quenching rate and composition results in a different series of TTT diagrams that are commonly used to investigate transformation effects on components found during the quenching of alloys.

Vickers hardness A static hardness test that uses a pyramid-shaped diamond indenter having an angle of 136 degrees between the faces. The loading can be used for microhardness measurements for all materials. It is one of the most useful hardness testing scales.

Weld A term used to describe a joint made between two metals made by the heating and joining the separate parts with no solder applied. Ancient welds were often made in precious metals, such as gold and silver and in the joining of iron components, especially in the fabrication of wrought iron.

White cast iron Cast iron with a whitefracture due to the presence of the carbon in the cast iron as cementite rather than free graphite.

Widmanstätten structure A very characteristic type of structure that forms when a new solid phase is produced from a parent solid phase as plates or laths along certain crystallographic planes of the original crystals. The structure is associated with many meteoric irons and with changes upon cooling in worked iron and many nonferrous alloys.

Wootz A kind of steel, made in small crucibles in ancient India and often of hypereutectoid steel with a very low slag content. This cast steel was widely used for the manufacture of sword blades and other quality products.

Work hardening Increase of hardening by plastic deformation.

Wrought The process of hammering or deforming a metal or alloy, as opposed to casting.

Wrought iron Malleable**i**ron that has been produced from the bloomery process and has been consolidated by hammering and annealing into a wrought product. Wrought iron usually contains slag stringers that have been elongated and flattened in the process of working from the bloom.

Index

D. A. Scott, R. Schwab, *Metallography in Archaeology and Art*, Cultural Heritage Science, https://doi.org/10.1007/978-3-030-11265-3

C